



2008

SYNTHESIS AND STRUCTURE-PROPERTY STUDIES OF ORGANIC MATERIALS CONTAINING FLUORINATED AND NON-FLUORINATED # SYSTEMS (SMALL MOLECULES AND POLYMERS)

Yongfeng Wang
University of Kentucky, ywangb@uky.edu

[Right click to open a feedback form in a new tab to let us know how this document benefits you.](#)

Recommended Citation

Wang, Yongfeng, "SYNTHESIS AND STRUCTURE-PROPERTY STUDIES OF ORGANIC MATERIALS CONTAINING FLUORINATED AND NON-FLUORINATED # SYSTEMS (SMALL MOLECULES AND POLYMERS)" (2008). *University of Kentucky Doctoral Dissertations*. 593.
https://uknowledge.uky.edu/gradschool_diss/593

This Dissertation is brought to you for free and open access by the Graduate School at UKnowledge. It has been accepted for inclusion in University of Kentucky Doctoral Dissertations by an authorized administrator of UKnowledge. For more information, please contact UKnowledge@lsv.uky.edu.

ABSTRACT OF DISSERTATION

Yongfeng Wang

The Graduate School
University of Kentucky

2008

SYNTHESIS AND STRUCTURE-PROPERTY STUDIES OF ORGANIC
MATERIALS CONTAINING FLUORINATED AND NON-FLUORINATED π
SYSTEMS (SMALL MOLECULES AND POLYMERS)

ABSTRACT OF DISSERTATION

A dissertation submitted in partial fulfillment of the
requirements for the degree of Doctor of Philosophy in the
College of Arts and Science
at the University of Kentucky

By
Yongfeng Wang

Lexington, Kentucky

Director: Dr. Mark D. Watson, Professor of Chemistry

Lexington, Kentucky

2008

Copyright © Yongfeng Wang 2008

ABSTRACT OF DISSERTATION

SYNTHESIS AND STRUCTURE-PROPERTY STUDIES OF ORGANIC MATERIALS CONTAINING FLUORINATED AND NON-FLUORINATED π SYSTEMS (SMALL MOLECULES AND POLYMERS)

Organic electronic materials have high potential in consumer electronics. Challenges facing materials chemists include development of efficient synthetic methodologies and control over interrelated molecular self-assembly and (opto) electronic properties. The body of this work focuses on preparing and investigating the self-assembly of potential organic semiconductors comprised of polymers and small molecules containing thiophenes and fluorinated arenes.

New synthetic methodology is reported which exploits S_NAr reactions of fluorinated aromatics to form various thiophene-containing conjugated polymers. The catalyst system of CsF and 18-crown-6 is easily removed by extraction and the sole side-product fluorotrimethylsilane is volatile, yielding polymers with high as-synthesized purity and high molecular weight. Efficient synthetic routes relying heavily on S_NAr reactions are also established to prepare small-molecule fluorinated polycyclics and benzodichalcogenophene derivatives.

The self-assembly of all polymers and small molecules reported herein are engineered via: (1) intermolecular interactions between fluorinated and non-fluorinated π -systems, (2) inter- and intramolecular interactions between fluorine atoms and thienyl sulfur atoms, as well as in some cases (3) space-filling demands of other substituents like alkyl side-chains. A key outcome of the polymer work is proof of the hypothesis that the conjugated backbones of polymers containing head-to-head 3,3'-dialkyl-bithiophene units can be forced into coplanarity due to enhanced π -stacking in the solid state, with some possible contribution from attractive intramolecular S-F interactions. For fluorinated polycyclics, two antiparallel triangular arrangements of fluorine and sulfur atoms are incorporated into lath-shaped small molecules to form extensive networks of edge-to-edge interactions, which in turn lead to 2D face-to-face π -stacking. A series of benzodichalcogenophene derivatives are designed to have coplanar ring systems and slipped π -stacking arising from intramolecular S-F close contacts and intermolecular π - π F interactions.

Finally, (opto) electronic properties are manipulated using the design principles included above. Copolymers of 3,3'-alkylbithiophenes with perfluorobenzene display

reduced solid-state optical band gaps as a consequence of their mode of self-assembly. CF_3 substituents are used to decrease (optical) energy gap and decrease the LUMO levels of fluorinated polycyclics and benzodichalcogenophenes (BDT(Se)). Other substituents attached to the BDT core are used to further alter the energy levels.

KEY WORDS: Organic electronic materials; nucleophilic aromatic substitution; perfluoroarene; supramolecular engineering; self assembly.

Yongfeng Wang
Student's signature

03/21/2008
Date

SYNTHESIS AND STRUCTURE-PROPERTY STUDIES OF ORGANIC
MATERIALS CONTAINING FLUORINATED AND NON-FLUORINATED π
SYSTEMS (SMALL MOLECULES AND POLYMERS)

By

Yongfeng Wang

Dr. Mark D. Watson

Director of Dissertation

Dr. Robert B. Grossman

Director of Graduate Studies

03/21/2008

Date

DISSERTATION

Yongfeng Wang

The Graduate School
University of Kentucky
Lexington
2008

SYNTHESIS AND STRUCTURE-PROPERTY STUDIES OF ORGANIC
MATERIALS CONTAINING FLUORINATED AND NON-FLUORINATED π
SYSTEMS (SMALL MOLECULES AND POLYMERS)

DISSERTATION

A dissertation submitted in partial fulfillment of the
requirements for the degree of Doctor of Philosophy in the
College of Arts and Science
at the University of Kentucky

By
Yongfeng Wang

Lexington, Kentucky

Director: Dr. Mark D. Watson, Professor of Chemistry

Lexington, Kentucky

2008

Copyright © Yongfeng Wang 2008

Dedicated to

My wife and my best friend

Jianing Yang

and my beloved parents, parents-in-law and sister

Mr. Hongxing Wang

Mrs. Jihua Li

Mr. Qibai Yang

Mrs. Shuxia Chen

Mrs. Yongli Wang

ACKNOWLEDGEMENTS

For the completion of my PhD and my dissertation I have to appreciate so many people around me for their help.

First, I send my deepest gratitude and sincerest thanks to my advisor and chair of my committee Dr. Mark D. Watson for giving me this opportunity to join his group and work with him. He is a kind of role model for me who really knows how to work with his students and his colleagues. He demonstrates a scientific attitude and abundant scientific knowledge and possesses a humorous and nice nature of personality. He not only taught me vital hands-on laboratory techniques but also trained me how to become an independent and creative scientist. He helped me to overcome a steep language barrier when I came to the USA, encouraged me to face some personal difficulties during my PhD period and trusted me to be somewhat unofficial lab manager to train new group members. He gave me so much freedom to do what I want to do in my research. At the same time, he also has an open-door policy where I have easy access to him for advice and where open two-way communication is encouraged. He has created a very supportive and comfortable working environment where I can perform to my best level.

Second, I would like to thank my other committee members Dr. John Anthony, Dr. John Selegue and Dr. Zachary Hilt, and outside examiner Dr. Barbara Knutson, who took their time to review my dissertation and gave me so many suggestions and comments. Especially, I should appreciate Dr. John Anthony for his patience and advice whenever I approached him for advice over the years.

Third, I want to thank Dr. Sean Parkin, Mr. John Layton, Dr. Jack Goodman and Dr. Johannes Gierschner (University of Mons-Hainaut, Belgium) for their help with X-ray diffraction, NMR, mass spectrometry and theoretical calculations respectively.

Fourth, I would like to thank all the members of the Watson lab, both past and present: Don Cho, Kathy Beckner, Tanmoy Dutta, Xugang Guo, Manindar Kaur, Arawwaladon Liyanage, Mark Seger, James Robinson and Megan Lang. I had a pleasant time working with them in the lab for these last five years.

Last but more importantly, I wish to express my gratitude to my parents, Hongxing Wang and Jihua Li, who always strongly support me, love me and take pride in me. Without their encouragement, understanding and support I can not sail through my

grown-up and study period. I should also send my deepest thanks and my true love to my wife and friend Jianing Yang. Now I can say that it is the only thing I did right and never regret that I met her and married her. Whenever I am depressed or happy, she always stands by me and gives me support and encouragement. Because of her, I had more motivation and drive to work and study in the past five years in the USA; because of her, I am enjoying life everyday; because of her, I cherish more in the future. I am lucky to have wonderful parents-in law, Qibai Yang and Shuxia Chen. Thank you for your love, trust and support. I should send my thanks to my elder sister Yongli Wang as well who always supports me and encourages me.

I will have a new start of my life soon. At this time I want to thank all of you again to help me and support me in the past and I will remember all of you forever.

TABLE OF CONTENTS

CHAPTER 1 INTRODUCTION	1
1.1 Organic electronic materials	1
1.1.1 Organic thin film transistors	1
1.1.2 Problems and challenges.....	3
1.1.3 Design rules and materials	4
1.2 Conducting polymers: polythiophene	10
1.2.1 Electrochemical polymerization	12
1.2.2 Chemical Polymerization.....	12
1.3 Aromatic interactions and self assembly	16
1.3.1 Aromatic interactions.....	16
1.3.2 Self assembly of conjugated polymers	21
1.4 Orientation and reactivity in nucleophilic substitution of polyfluoroaromatic compounds	23
1.5 Thesis of this work.....	26
CHAPTER 2 SYNTHESIS AND CHARACTERIZATION OF ALTERNATING THIOPHENE AND PIF COPOLYMERS	27
2.1 Introduction.....	27
2.2 Synthesis of alternating 3,4-dialkoxythiophene and perfluoroarene copolymers.....	33
2.3 Synthesis of alternating 3,3-Dihexyl-3,4-dihydro-2 <i>H</i> -thieno[3,4- <i>b</i>][1,4]dioxepine [ProDOT(Hx) ₂] and C ₆ F ₄ copolymer.....	41
2.4 Synthesis of alternating 3,3',4,4'-tetrabutoxy-2,2'-bithiophene and C ₆ F ₄ copolymer .	44

2.5 Synthesis of alternating 4,8-dialkyl/dialkoxy benzodithiophene and C ₆ F ₄ copolymers	46
2.6 Synthesis of alternating 3,3'-dialkyl-2,2'-bithiophene and C ₆ F ₄ copolymers and their nonfluorinated counterparts	48
2.6.1. Introduction.....	48
2.6.2. Synthesis of fluorinated copolymers.....	52
2.6.3. Synthesis of nonfluorinated copolymers.....	54
2.7 Synthesis of alternating 3,3'-dialkoxy-2,2'-bithiophene and C ₆ F ₄ copolymers	55
2.8 Synthesis of alternating 3,3'-dialkyl-2,2'-bithiophene and C ₆ F ₄ copolymers by oxidative polymerization	57
2.9 Polymer Characterization.....	59
2.9.1 Yields, GPC and DSC analysis.....	59
2.9.2 Optical properties in solution and in solid state.....	61
2.9.3 Supramolecular arrangement of polymers in the solid state as revealed by wide angle xray diffraction (WAXD).....	71
2.10 Conclusions.....	77
 CHAPTER 3 SYNTHESIS AND CHARACTERIZATION OF HIGHLY FLUORINATED BENZOBISBENZOTHIOPHENES (BBBT).....	79
3.1 Introduction.....	79
3.2 Syntheses of highly fluorinated benzobisbenzothiophenes (BBBT)	83
3.2.1 Syntheses of compounds 3-15a,b.....	83
3.2.2 Synthesis of compound 3-19.....	85
3.2.3 Syntheses of compounds 3-24a,b.....	86
3.2.4 Functionalization of compound 3-24a	88
3.3 Crystal structures of highly fluorinated BBBTs 3-15a and b, 3-19, 3-24a and b and 3-25	89

3.4 UV-Vis spectra and cyclic voltammetry	93
3.5 Conclusion and outlook	98
CHAPTER 4 SYNTHESIS AND CHARACTERIZATION OF BENZODICALCOGENOPHENES FUNCTIONALIZED WITH FLUORINATED AROMATICS	
	100
4.1 Introduction.....	100
4.2 Synthesis of perfluoroarene-substituted benzodichalcogenophene compounds.....	102
4.3 Crystal structures of compounds 4-14 through 4-25.....	105
4.4 Optoelectronic properties of BDT(Se) derivatives	110
4.5 Thermal properties of BDT(Se) derivatives	118
4.6 Conclusions.....	119
CHAPTER 5 CONCLUSION AND OUTLOOK.....	
	121
5.1 Conclusion	121
5.2. Outlook	124
CHAPTER 6 EXPERIMENTAL SECTION.....	
	128
6.1 Materials and methods	128
6.2 Syntheses.....	129
REFERENCES	185
VITA	201

LIST OF TABLES

Table 2. 1 Pd content and resistance before and after removal of Pd residue ¹⁰⁴	28
Table 2. 2 Properties of polymers	60
Table 2. 3 Data collected from diffraction patterns in Figure 2. 36.....	73
Table 3. 1 Yields of mono-and di-pentafluorophenylation of 3-14 during optimization studies ^{c, d}	85
Table 3. 2 Electrochemical data , estimated HOMO and LUMO levels and UV-Vis Data of 3-15a, 3-15b, 3-19, 3-24a, 3-26 and 3-5	94
Table 3. 3 Energetic positions of the frontier orbitals, bandgap E_{H-L} , vertical transition energy $E_{vert}(S1)$ and oscillator strength $f(S1)$ of the lowest electronic transition.	97
Table 4. 1 Pitch and roll angles ($\angle P$ and $\angle R$) for BDT(Se) derivatives	105
Table 4. 2 Electrochemical, UV-Vis and emission data for 4-14-4-25	112
Table 4. 3 Differential scanning calorimetry (DSC) data of compounds 4-14-4-25	119

LIST OF FIGURES

Figure 1. 1 Schematic structures of OTFT devices: top-contact structure (left) and bottom contact structure (right).....	2
Figure 1. 2 Structure of F ₁₆ CuPc 1-1.	5
Figure 1. 3 Structures of TCNQ, TCNNQ and DCMT.....	6
Figure 1. 4 Structures of oligothiophene derivatives.....	7
Figure 1. 5 Structures of acene derivatives.....	8
Figure 1. 6 Structures of NTCDA, NTCDI, NTCDI-R, PTCDA and PTCDI-R.....	10
Figure 1. 7 Representative structures of conjugated polymers.....	11
Figure 1. 8 Representative structures of some classes of conjugated polymers.....	11
Figure 1. 9 Possible mechanism of electrochemical polymerization of thiophene and derivatives. ⁴¹	12
Figure 1. 10 Synthesis of regioirregular/random poly(3-alkyl thiophene).	13
Figure 1. 11 Three possible coupling diads from coupling 3-alkyl thiophene.	14
Figure 1. 12 Synthesis of regioregular poly(3-alkylthiophene).	15
Figure 1. 13 Some other organometallic routes for thiophene copolymer synthesis: Sonogashira coupling (top) ⁵³ , Suzuki coupling ⁵⁴ and Stille coupling (bottom) ⁵⁵	16
Figure 1. 14 slip-stacked arrangement (TIPS-pentacene ⁵⁷ , left); herringbone (T-shape) (benzene ⁵⁸ , middle); herringbone-like (pentacene ⁵⁹ , right).	17
Figure 1. 15 Definition of pitch angle, roll angle and interplanar distance. ⁵⁶ Left: view along the short molecular axis of a “pitched” π -stack; Right: view along the long molecular axis of a “rolled” π -stack. $\angle P$ = pitch angle, $\angle R$ = roll angle.....	17
Figure 1. 16 Structures of 1-20, 1-21 and 1-22. ⁶²	18
Figure 1. 17 Structures and crystal packing of rubrene 1-23 (top) ⁶⁶ and 9,10-bis(methylthio)anthracene 1-24 (bottom) ⁶⁵	19
Figure 1. 18 Published ⁷¹ structures of a) 1,4-bis(phenylethynyl)-benzene 1-25 and b) 1,4-bis(pentafluorophenylethynyl)benzene 1-26; along with c) crystal packing of 1-25; d) crystal packing of 1-26; e) crystal packing of 1-25 and 1-26 complex (2:1).....	20
Figure 1. 19 a) Structure of permethoxylated hexa-peri-hexabenzocoronene 1-27 ⁷² ; b) crystal packing of 1-27; c) crystal packing of the complex of 1-27 and C ₆ F ₆ (1:2).	21

Figure 1. 20 Crystal structures of thiophene derivatives with HH linkages: 1-28 ⁷⁷ , 1-29 ⁷⁸ , 1-30 ⁷⁹ and 1-31 ⁸⁰	22
Figure 1. 21 Schematic of lamellar and π -stacking for alky-substituted rigid-rod polymers. a) interdigitated structure model; b) tilted structure model.	23
Figure 1. 22 a) Stabilizing fluorine atom beta to carbanionic center; b) destabilizing fluorine atom directly attached to a carbanionic center; c) ion-dipole interaction activating ortho position to nucleophilic attack.	24
Figure 1. 23 Preferred orientation of nucleophilic attack on hexafluorobenzene (top) and octafluoronaphthalene (bottom). pp = pseudopara, pm = pseudometa.	25
Figure 1. 24 a) NH ₂ group activating meta position to nucleophilic attack; b) CF ₃ group activating para position to nucleophilic attack; c) ring nitrogen activating para position to nucleophilic attack.	26
Figure 2. 1 Structures of polymer PBTTT and PQT-12.	28
Figure 2. 2 Synthesis of alternating 3-dodecylthiophene-C ₆ F ₄ copolymer.....	30
Figure 2. 3 Mechanism of the trifluoromethylation reaction between a carbonyl compound and trimethyl(trifluoromethyl)silane. ¹¹⁶	31
Figure 2. 4 General scheme for the disclosed synthesis of alternating thiophene- π F copolymers, together with the generic structures of the monomers investigated. The fluoride source may be CsF.	32
Figure 2. 5 Synthesis of tetrafluoropyridynyl acetylenes.	33
Figure 2. 6 Synthesis of alternating thiophene- π F copolymers.	35
Figure 2. 7 ¹⁹ F, ¹ H, and ¹³ C NMR spectra of polymer 2-1a in CDCl ₃	36
Figure 2. 8 ¹⁹ F and ¹ H NMR of polymer 2-2 in C ₂ D ₂ Cl ₄	37
Figure 2. 9 Model reactions to elucidate reactivity.....	39
Figure 2. 10 ¹ H and ¹⁹ F NMR of oligomers 2-10 in CDCl ₃	40
Figure 2. 11 Synthesis of alternating ProDOT(Hx ₂)-C ₆ F ₄ copolymer.....	42
Figure 2. 12 ¹⁹ F (top) , ¹ H (middle) and ¹³ C (bottom) NMR spectra of polymer 2-19 in CDCl ₃	43
Figure 2. 13 Synthesis of alternating 3,3',4,4'-tetrabutoxy-2,2'-bithiophene-C ₆ F ₄ copolymer.	44

Figure 2. 14 Resonance structures of the intermediate for compound 2-21a undergoing ipso-substitution (protodesilylation).....	46
Figure 2. 15 ¹ H (top) and ¹⁹ F (bottom) NMR spectra of polymer 2-22 in CDCl ₃	46
Figure 2. 16 Synthesis of alternating 4,8-dialkyl/dialkoxy benzodithiophene -C ₆ F ₄ copolymers.....	48
Figure 2. 17 Structures of polymer 2-27 and 2-28.....	50
Figure 2. 18 X-ray crystal structure of compound 2-29, ¹⁴⁴ showing relevant intramolecular contacts (middle) and a view down molecular short axis (bottom).....	51
Figure 2. 19 Synthesis of alternating 3,3'-dialkyl-2,2'-bithiophene-C ₆ F ₄ copolymers.	52
Figure 2. 20 ¹ H (top) and ¹⁹ F (bottom) NMR spectra of polymer 2-33a in C ₂ D ₂ Cl ₄	54
Figure 2. 21. Synthesis of non-fluorinated copolymers 2-37.....	54
Figure 2. 22 Synthesis of alternating 3,3'-dialkoxy-2,2'-bithiophene-C ₆ F ₄ copolymers 2-42.....	56
Figure 2. 23 Synthesis of fluorinated copolymers 2-44.....	57
Figure 2. 24 ¹ H (top) and ¹⁹ F (bottom) NMR spectra of polymer 2-44b in C ₂ D ₂ Cl ₄	58
Figure 2. 25 Structures of polymers.....	59
Figure 2. 26 Color photographs of polymers (left: solid under ambient light; middle: solution under ambient light; right: solution under irradiation at 366 nm).....	61
Figure 2. 27 Solution UV-Vis spectra of the fluorinated polymers (THF, 10 ⁻⁵ M).....	62
Figure 2. 28 Solution PL spectra of the fluorinated polymers (THF, 10 ⁻⁷ -10 ⁻⁸ M).....	63
Figure 2. 29 Solution (10 ⁻⁵ M, THF) and solid state UV-Vis absorption spectra of polymers 2-33.	64
Figure 2. 30 Solution (THF, 10 ⁻⁷ -10 ⁻⁸ M) and solid-state PL spectra of polymers 2-33...	65
Figure 2. 31 Solution (THF, 10 ⁻⁵ M) and solid-state absorption spectra of polymers 2-33a/b and 2-37a/b.	67
Figure 2. 32 Solution (THF, 10 ⁻⁷ -10 ⁻⁸ M) and solid-state PL spectra of polymers 2-33a/b and 2-37a/b.....	67
Figure 2. 33 Solid-state absorption spectra of polymers 2-33a/b measured at RT before and after annealing at the indicated temperatures. Top: 2-33a, bottom: 2-33b.	68

Figure 2. 34 Solid-state PL spectra of polymers 2-33a/b measured at RT before and after annealing at the indicated temperatures. Top: 2-33a, bottom: 2-33b. Note: $T_m=140^\circ\text{C}$ (2-33a), $T_m=183^\circ\text{C}$ (2-33b).....	69
Figure 2. 35 Schematic illustration of the fiber alignment by a mini extruder, 2D WAXD pattern of an aligned fiber and packing of polymers. a) home-built fiber extruder and 2D WAXD pattern of the aligned fiber; b) lamellar packing and π stacking of polymers.....	71
Figure 2. 36 Characteristic 2D WAXD patterns of 2-33a (a), 2-33b (b), 2-33c (c), 2-37a (d), 2-37b (e), 2-44a (f), 2-44b (g) and 2-22 (h).	72
Figure 2. 37 Models showing the orientation of backbone rings relative to the π -stacking axis: (A) backbones orthogonal to and (B) tilted relative to π -stacking axis.....	75
Figure 3. 1 Published isomeric thienoacenes. Only compounds 3-2 were produced separately as pure isomers.	80
Figure 3. 2 Published ¹⁶² cascade reaction leading to thienoacenes.	80
Figure 3. 3 Published synthesis of regioisomerically pure benzobisbenzothiophene 3-5 (BBBT). ¹⁶⁴	81
Figure 3. 4 Structures of compound 3-6 ¹⁶⁶ , 3-7 ¹⁶⁷ , 3-8 ¹⁶⁸ , 3-9 ¹⁶⁹ , 3-10 ¹⁷⁰ and 3-11.....	81
Figure 3. 5 Close contacts between S and F in octafluorodibenzothiophene 3-12. ¹⁷²	83
Figure 3. 6 Synthesis of highly fluorinated BBBTs 3-15.	84
Figure 3. 7 Synthesis of fluorinated BBBT 3-19.....	86
Figure 3. 8 Synthesis of highly fluorinated BBBTs 3-24 with alkyl chains.	87
Figure 3. 9 ¹⁹ F NMR spectra for preparation of 3-24b from 3-23b.	88
Figure 3. 10 Functionalization of compound 3-24a.	88
Figure 3. 11 Crystal packing diagrams for (a) 3-5, ¹⁶⁴ (b) 3-19, (c) 3-15a, (d) 3-15b, (e) 3-24a, (f) 3-25, (g) 3-24b.	92
Figure 3. 12 Cyclic voltammograms (left, vs Fc/Fc ⁺) and Osteryoung square wave voltammograms (right, vs Fc/Fc ⁺ , $E_{1/2}=0.60\text{ V}$, which is the largest peak set to 0 mV) of compounds 3-15a (a), 3-15b (b), 3-19 (c), 3-24a (d) and 3-26 (e).	96
Figure 3. 13 Solution absorption spectra of compounds 3-15a, 3-15b and 3-19. (10^{-6}M THF).....	97

Figure 3. 14 Illustration of the different “lateral” and “terminal” positions considered during computational studies.....	97
Figure 3. 15 Calculated absorption spectra (in units of oscillator strength) for 3-15a, 3-15b and 3-19, representing the pure (vertical) electronic transitions, broadened by a Lorentzian.....	98
Figure 3. 16 Synthetic scheme of 3-27 and 3-28 with long alkyl solubilizing groups.	99
Figure 4. 1 Published π -extended heteroarenes containing chalcogenophenes.....	101
Figure 4. 2 Structures of some n-type materials with electron-withdrawing groups as terminal groups.....	102
Figure 4. 3 Synthetic schemes of compounds 4-14 – 4-25.....	104
Figure 4. 4 Crystal packing diagrams. Left: view along short molecular axis; right: view along long molecular axis (except 4-14 and 4-30 ⁹⁷).....	109
Figure 4. 5 Solution absorption (10 ⁻⁵ M THF) and photoluminescence (PL) (10 ⁻⁶ M, THF) spectra of compounds 4-14-4-25.	111
Figure 4. 6 Cyclic voltammograms (left, vs Fc/Fc ⁺) and Osteryoung square wave voltammogram (right, vs Fc/Fc ⁺ , large peak set to 0 V) of compounds 4-14 (a), 4-15 (b), 4-16 (c), 4-17 (d), 4-18 (e), 4-19 (f), 4-20 (g), 4-21 (h), 4-22 (i), 4-23 (j), 4-24 (k), 4-25 (l).....	116
Figure 5. 1 Example proposed synthesis of dendrimers.....	125
Figure 5. 2 Proposed regioregular copolymers of bithienothiophene copolymers B and C.	126
Figure 5. 3 Retrosynthesis of polymers B and C shown in Figure 5. 1.....	127
Figure 5. 4 Synthetic scheme of D with different solubilizing groups.....	127
Figure 6. 1 ¹ H (top) and ¹⁹ F (bottom) NMR (130°C, C ₂ D ₂ Cl ₄) spectra of compound 3-15a.	168
Figure 6. 2 ¹ H (top) and ¹⁹ F (bottom) NMR (75°C, CDCl ₃) spectra of compound 3-15b.	169
Figure 6. 3 ¹ H (top) and ¹⁹ F (bottom) NMR (r.t., CDCl ₃) spectra of compound 3-19....	170

Figure 6. 4 ^1H (top) and ^{19}F (bottom) NMR (50°C, CDCl_3) spectra of compound 3-24a.	171
Figure 6. 5 ^1H (top) and ^{19}F (bottom) NMR (r.t., CDCl_3) spectra of compound 3-24b..	172
Figure 6. 6 ^1H (top) and ^{19}F (bottom) NMR (120°C, $\text{C}_2\text{D}_2\text{Cl}_4$) spectra of compound 4-14.	173
Figure 6. 7 ^1H (top) and ^{19}F (bottom) NMR (120°C, $\text{C}_2\text{D}_2\text{Cl}_4$) spectra of compound 4-15.	174
Figure 6. 8 ^1H (top) and ^{19}F (bottom) NMR (120°C, $\text{C}_2\text{D}_2\text{Cl}_4$) spectra of compound 4-16.	175
Figure 6. 9 ^1H (top) and ^{19}F (bottom) NMR (120°C, $\text{C}_2\text{D}_2\text{Cl}_4$) spectra of compound 4-17.	176
Figure 6. 10 ^1H (top) and ^{19}F (bottom) NMR (r.t., CDCl_3) spectra of compound 4-18..	177
Figure 6. 11 ^1H (top) and ^{19}F (bottom) NMR (r.t., CDCl_3) spectra of compound 4-19..	178
Figure 6. 12 ^1H (top) and ^{19}F (bottom) NMR (r.t., CDCl_3) spectra of compound 4-20..	179
Figure 6. 13 ^1H (top) and ^{19}F (bottom) NMR (r.t., CDCl_3) spectra of compound 4-21..	180
Figure 6. 14 ^1H (top) and ^{19}F (bottom) NMR (r.t., $\text{C}_2\text{D}_2\text{Cl}_4$) spectra of compound 4-22.	181
Figure 6. 15 ^1H (top) and ^{19}F (bottom) NMR (r.t., CDCl_3) spectra of compound 4-23..	182
Figure 6. 16 ^1H (top) and ^{19}F (bottom) NMR (130°C, $\text{C}_2\text{D}_2\text{Cl}_4$) spectra of compound 4-24.	183
Figure 6. 17 ^1H (top) and ^{19}F (bottom) NMR (100°C, $\text{C}_2\text{D}_2\text{Cl}_4$) spectra of compound 4-25.	184

Chapter 1 Introduction

While no device studies are reported in this body of work, the ultimate goal is to expand our abilities as materials chemists to prepare and understand the self-assembly of materials which can function in organic electronic devices. Therefore, this chapter will provide some background concerning various important aspects of the broad field of organic electronic materials. After providing a brief introduction to organic field effect transistors, some background is provided for subjects of particular relevance to this body of work including different classes of n-type organic semiconductors, conjugated polymers and their synthesis, control over the self-assembly of π -electron systems, and synthetic utility of S_NAr reactions of highly fluorinated aromatics.

1.1 Organic electronic materials

1.1.1 Organic thin film transistors

Ever since the first field-effect transistors (FETs) with active components consisting of organic polymer¹ and small molecule² semiconductors were reported, there has been remarkable progress in the development of organic thin film transistors (TFTs). Due to easy processability (low temperature), light weight, flexibility and compatibility with flexible substrates, organic thin film transistors may rival commercial amorphous silicon TFTs in low-performance devices such as radio frequency identification (RF-ID) tags^{3,4}, pixel switching elements in active matrix flat panel displays^{5,6}, electronic paper, and smart cards.

Organic thin film transistors can be classified into two broad types: p-type and n-type. TFTs based on p-type semiconductors conduct holes or cations (the charge carrier) and achieve the “on” state when the gate voltage is negative, while those based on n-type semiconductors conduct electrons or anions (the charge carrier) and turn on with positive gate bias. In recent years it has been suggested on the basis of theoretical considerations⁷ and measurements of highly pure molecular crystals⁸ and polymers⁹, that generally organic conjugated (macro)molecules are intrinsically both good electron conductors and hole conductors. In practice the reasons that most organic semiconductors are p-type

or/and the mobility of electrons are much lower than hole mobility in the same material under a given electric field are due to some other extrinsic factors (i.e., the nature of the electrodes, the dielectric layer in transistors, and the environment) which are actually responsible for the type of transport. Thus it may not be appropriate to speak of p-type or n-type materials, but one should rather refer to observed p-channel or n-channel behaviors of complete devices based on those materials.

Commonly, there are two types of configurations to construct thin film transistors: top-contact and bottom contact. **(Figure 1. 1)** For both configurations, the organic thin film semiconductor is placed on the gate/dielectric layer and contacted with source and drain electrodes. The difference is that for the top-contact devices, source and drain electrodes are deposited on the top of the organic film, while for the bottom-contact, this deposition is reversed. For n-type semiconductors, when a sufficient positive gate bias (V_G) relative to the source drain is applied, a layer of accumulated negative charge is formed at the interface between organic film and dielectric layer. Under the applied drain voltage (V_D), the source-drain current (I) then develops (the device is “on”). For p-type semiconductors, when a sufficient negative V_G is applied, the HOMO level will be resonant with the Fermi levels of electrodes and holes will be injected from electrode to HOMO. The source-drain current will develop with applied V_D .

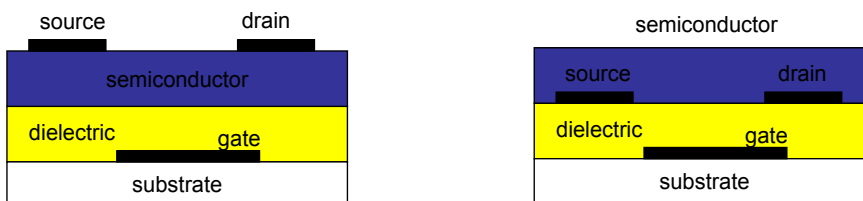


Figure 1. 1 Schematic structures of OTFT devices: top-contact structure (left) and bottom contact structure (right).

Three critical parameters are employed to evaluate the device performance of FETs: the charge carrier mobility (μ), the on/off current ratio ($I_{\text{on/off}}$) and the threshold voltage (V_{th}). The charge carrier mobility with units of $\text{cm}^2/(\text{Vs})$ is a quantity relating the drift velocity of charge carriers to the applied electric field across a material. The on/off current ratio can be defined as the ratio between the source-drain currents during the “on” and “off” states. Threshold voltage is defined as the voltage at which the transistor turns

from “off” to “on”. If OTFTs are to compete directly with amorphous Si:H TFTs, the former should provide field effect mobility $\mu \geq 1 \text{cm}^2 \text{V}^{-1} \text{s}^{-1}$, and $I_{\text{on/off}} \geq 10^6$ at a maximum operating voltage of about 15 V or less because amorphous Si:H, used as drives in LCDs, typically demonstrates these properties.

1.1.2 Problems and challenges

As mentioned above, p-type behavior is observed much more commonly in devices constructed from most organic semiconductors, that is, the application of a negative voltage on the gate electrode results in the formation of an accumulation layer of positive hole carriers. The reversed phenomena - n-type behavior with the positive gate voltage- is not as commonly observed.

There are three possible reasons why n-type behavior is less commonly observed. First, it is difficult to match the work function of source-drain electrodes with the LUMO of semiconductors. As a consequence electron injection is not easily achieved. When gold electrodes are typically used, hole injection is much easier for p-type transistors due to the close match between the work function of gold (4.8-5.1 eV) and HOMO energy levels of organic semiconductors (4.8-5.3 eV). However, the relatively large HOMO-LUMO gap of more than 1.5-2 eV makes a big mismatch between the work function of gold and the LUMOs of organic materials and results in tough electron injection. Low work function electrodes such as calcium, magnesium or aluminum have been evaluated to match the LUMO level and n-type behavior has been observed^{10, 11}, but they are unstable and easily oxidized by air. Second, the organic anions (electrons) which are accumulated with the application of positive gate voltage are easily complexed or reduced by water and oxygen in the air.¹² Third, intrinsically the electron and hole mobilities should be relatively equal.⁸ However, electrons are more easily trapped by impurities (hydroxyl and carbonyl groups) in the semiconductor or at semiconductor-dielectric interface.¹³ When a good interface between the semiconductor and dielectric layer is obtained by using dielectrics without OH groups^{9-11, 14}, e.g. SiO₂ surfaces with passivated silanol groups⁹, n-type behavior has been observed more easily.

1.1.3 Design rules and materials

In the past decade many efforts have been dedicated to develop n-type organic semiconductors. To function as n-type organic semiconductors, the materials should display the following characteristics:¹⁵

(1) *Conjugated π -electron systems*. Charge carriers are more easily injected into conjugated molecules than saturated molecules. Afterwards injected charge carriers are quickly delocalized along π orbitals and transported intra- and intermolecularly.

(2) *High electron affinity about 3.0-4.0 eV*. With higher electron affinity, LUMO levels can be decreased to thereby align well with the work function of electrodes and thus electron injection from electrode into semiconductors becomes more facile. Also high electron affinity can increase the stability of semiconductors to adventitious impurities such as atmospheric air and water.

(3) *Highly ordered in the solid state*. When compared to their inorganic counterparts, e.g. classical covalent semiconductors such as Si, organic materials present basic differences. For example, silicon exists as a three-dimensional network solid, held together by covalent silicon-silicon single bonds with bond strength 76 kcal/mol. Thus silicon forms isotropic solids with 3-dimensional conductivity and resultantly the films do not require controlling the molecular assembly. However, organic molecules are held in contact by much weaker forces. Further, anisotropic bulk self-assembly of conjugated π -systems, with their commonly flat shapes, generally leads to reduced dimensionality/increased directionality of charge transport. This provides many challenges/opportunities for materials chemists to design molecules which will assemble with good intermolecular orbital and thus electronic overlap resulting from highly ordered assembly in the solid state to achieve efficient charge transport.

To date, several n-type candidates have been reported. An efficient way to achieve n-type behavior is to functionalize p-type molecular frames (naphthalene, perylene, sexithiophene, pentacene) with strongly electron-withdrawing groups (cyano, perfluoroalkyl, fluorine, carbonyl, diimide). In the following, the classification of n-type semiconductors will be reviewed on the basis of molecular frames: phthalocyanine, fullerene, oligothiophene, naphthalene and perylene etc.

1. Phthalocyanine derivatives

In 1990 Guiliaud, Sadoun and Maitrot fabricated thin-film n-type semiconductors from two rare-earth phthalocyanines Pc_2Lu and Pc_2Tm . The best results were obtained using Si_3N_4 modified oxidized silicon wafers, with the mobility of 2×10^{-4} and $1.4 \times 10^{-3} \text{ cm}^2\text{V}^{-1}\text{s}^{-1}$ respectively for Pc_2Lu and Pc_2Tm .¹⁶ In 1998 Bao, Lovinger and Brown demonstrated that n-type transistors based on hexadecafluorinated copperphthalocyanine (F_{16}CuPc **1-1**) provided a field-effect mobility of $0.03 \text{ cm}^2\text{V}^{-1}\text{s}^{-1}$ and an on/off ratio of about 5×10^4 at the deposition temperature of 125°C .¹⁷ (**Figure 1. 2**) After storage in open air for more than half a year, neither mobility nor on/off ratio substantially changed.

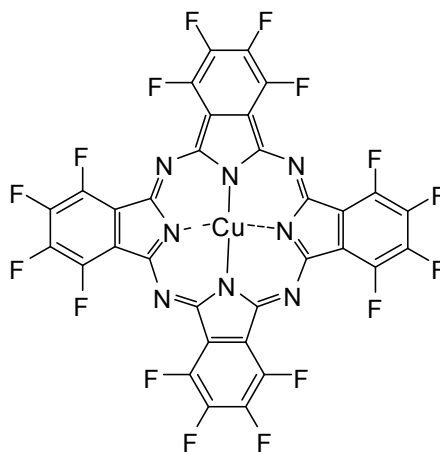


Figure 1. 2 Structure of F_{16}CuPc **1-1**.

2. Fullerene derivatives

In 1995, Haddon and coworkers reported n-type C_{60} thin-film-transistors having mobilities of 0.08 and $0.3 \text{ cm}^2\text{V}^{-1}\text{s}^{-1}$ and threshold voltages of 15 and -2.7V for devices prepared on untreated substrates and substrates treated with tetrakis(dimethylamino)ethylene (TDAE), respectively in ultrahigh vacuum. They attributed this improvement after TDAE treatment to the doped interface resulting from charge transfer complexes formed at the C_{60} /substrate interface which might reduce the barrier between gold electrode and C_{60} and increase the band bending.¹⁸ Kobayashi, Takenobu and Mori reported in 2003 that C_{60} thin film transistors fabricated by molecular-beam deposition showed mobilities of $0.5 \text{ cm}^2\text{V}^{-1}\text{s}^{-1}$, comparable to that of C_{60} single crystals ($0.5 \pm 0.2 \text{ cm}^2\text{V}^{-1}\text{s}^{-1}$ measured by the time-of-flight technique)¹⁹, and

current on/off ratios of more than 10^8 under a high vacuum without exposure to air.²⁰ Horiuchi and coworkers reported an air stable n-type thin film transistor from C₆₀ covered by an alumina insulating layer with $0.1 \text{ cm}^2\text{V}^{-1}\text{s}^{-1}$ mobility, the performance of which did not degrade after more than 30 days in open air.²¹

3. TCNQ derivatives

Tetracyanoquinodimethane **1-2** (TCNQ) and related derivatives (**Figure 1. 3**) have shown n-type behavior. In 1994 Brown and coworkers observed n-type behavior in metal-insulator-semiconductor field-effect transistors (MISFETs) based on TCNQ doped by tetrathiofulvalene (TTF) as active semiconducting material. These devices displayed maximum mobility of $3 \times 10^{-5} \text{ cm}^2\text{V}^{-1}\text{s}^{-1}$ and on/off ratio of four to over 450 upon exposure to air.²² In 1996 Katz et al. reported TCNNQ (**1-3**)-based FETs with electron mobilities of $3 \times 10^{-3} \text{ cm}^2\text{V}^{-1}\text{s}^{-1}$, higher than TCNQ without intentional doping and with greater stability in air.²³ In 2002 Frisbie et al fabricated n-type TFTs based on quinodimethane-substituted terthiophene **1-4** (DCMT), the electron mobility of which was 0.005 and $0.002 \text{ cm}^2\text{V}^{-1}\text{s}^{-1}$ for vapor-deposited and solution-deposited films respectively.²⁴ The quinoidal character of DCMT results in a reduced HOMO-LUMO gap compared to unsubstituted terthiophene. In addition, DCMT has low reduction potential and forms face-to-face slipped π -stacks in the solid state, which may come together to favor (electron) transport. After more carefully growing DCMT films on bottom-contact FETs, they achieved electron mobility of $0.2 \text{ cm}^2\text{V}^{-1}\text{s}^{-1}$, threshold voltage of -15V and on/off current ratio of more than 10^6 , close to benchmark p-type materials.²⁵

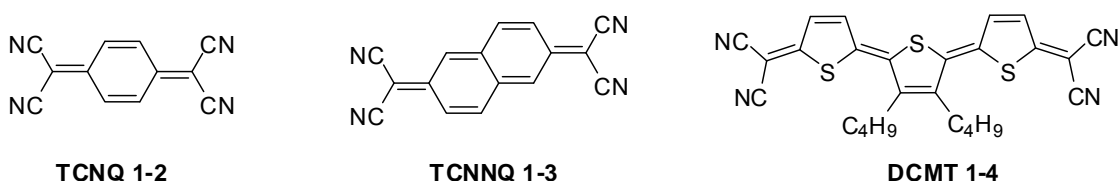


Figure 1. 3 Structures of TCNQ, TCNNQ and DCMT.

4. Oligothiophene derivatives

In 2000 Tobin Marks et al. reported the first n-type thin film transistors from sexithiophene by introducing perfluoroalkyl chains at the α,ω positions. Measurements

were executed on top-contact TFTs, fabricated by depositing the compound DFH-6T **1-5** onto the pretreated SiO₂ surface held at a temperature of 80-100°C, yielding mobilities as high as 0.02 cm²V⁻¹s⁻¹ and on/off ratio of 10⁵.²⁶ Later they increased the electron mobility to 0.22 cm²V⁻¹s⁻¹ and an on/off ratio to 10⁶ for n-type organic semiconductor with DFH-4T **1-6** as semiconducting layer.²⁷ Aside from introducing perfluoroalkyl chains, this team also incorporated fluoroaryl fragments into the oligothiophene frameworks to achieve n-type semiconductors. Of four such structures shown at the bottom of **Figure 1. 4**, only the α,ω- pentafluorophenyl capped quaterthiophene **1-7** (FTTTF) demonstrated n-type behavior, with electron mobility of 0.08 cm²V⁻¹s⁻¹, while those fabricated from fluoroarene-embedded oligothiophenes (TFTTFT **1-8** and TTFFTT **1-9**) showed p-type behavior.²⁸ In 2005 Tobin Marks and his coworkers also functionalized oligothiophene with perfluoroalkyl carbonyl groups. OFETs were constructed from compound DFHCO-4T (**1-10**) having electron mobility of 0.6 cm²V⁻¹s⁻¹, which was the highest electron mobility reported for an oligothiophene thin film transistor.²⁹

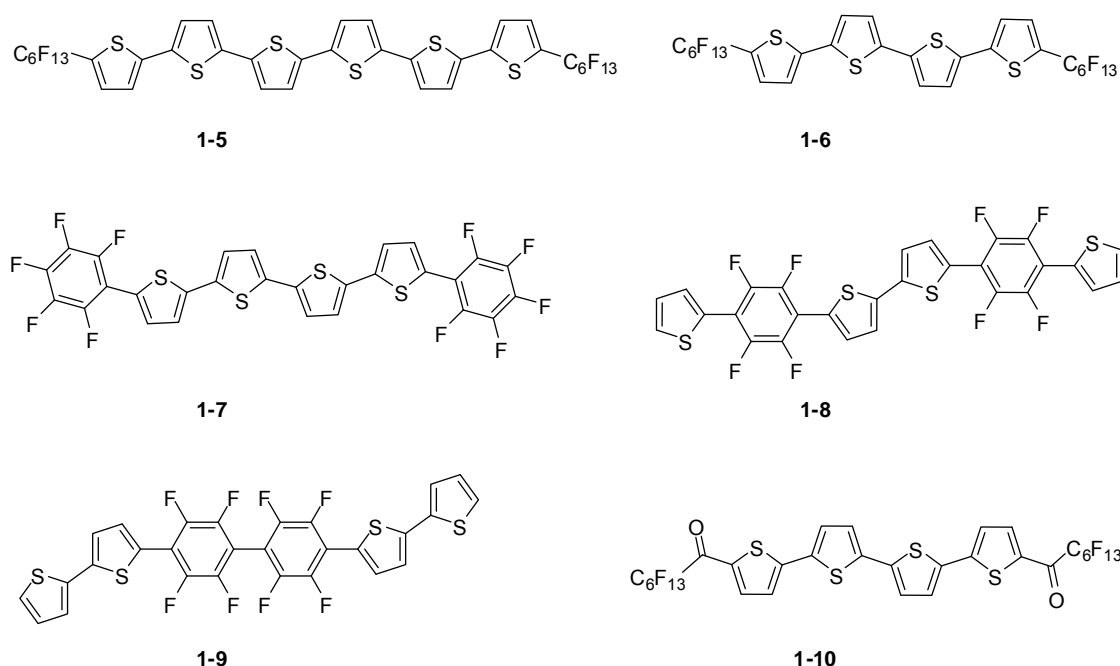


Figure 1. 4 Structures of oligothiophene derivatives.

5. Acene derivatives

In 2004 Suzuki and his coworkers reported electron mobility of $0.11 \text{ cm}^2\text{V}^{-1}\text{s}^{-1}$ and on/off ratio of 10^5 (in vacuo without exposure to air), from top-contact OFETs constructed from perfluoropentacene **1-11** evaporated onto OTS-modified SiO_2/Si at the substrate temperature of 50°C .³⁰ They also fabricated ambipolar OFETs with pentacene and perfluoropentacene using top-contact geometry, which have the mobility of $0.024 \text{ cm}^2\text{V}^{-1}\text{s}^{-1}$ for n-channel operation and $0.035 \text{ cm}^2\text{V}^{-1}\text{s}^{-1}$ for p-channel operation. Later they optimized their OFET fabrication to achieve electron mobility of $0.22 \text{ cm}^2\text{V}^{-1}\text{s}^{-1}$ and a good on/off current ratio of 10^5 .³¹ An ambipolar device combining pentacene and perfluoropentacene can have high electron and hole mobilities of 0.042 and $0.041 \text{ cm}^2\text{V}^{-1}\text{s}^{-1}$ respectively. Yamashita et al. introduced electron-accepting groups, that is, 4-trifluoromethylphenyl, to the termini of anthracene (**1-12**) by Suzuki coupling.³² The first n-type anthracene-based OFET was fabricated from this material, having electron mobility of 3.4×10^{-3} and on/off ratio of 10. Takimiya et al. also modified high-performance p-type materials by introducing strong electron-accepting groups (CN, CF_3) into the attached phenyl.³³ The OFETs built with the modified 4-trifluoromethylphenyl-functionalized benzodithiophene (BDT) or benzodiselenophene (BDS) (**1-13**) produced electron mobilities of 0.044 and $0.10 \text{ cm}^2\text{V}^{-1}\text{s}^{-1}$ at the substrate temperature of 60°C , respectively. Newly synthesized fluorinated BDT derivatives are the subject of Chapter 4 of this document.

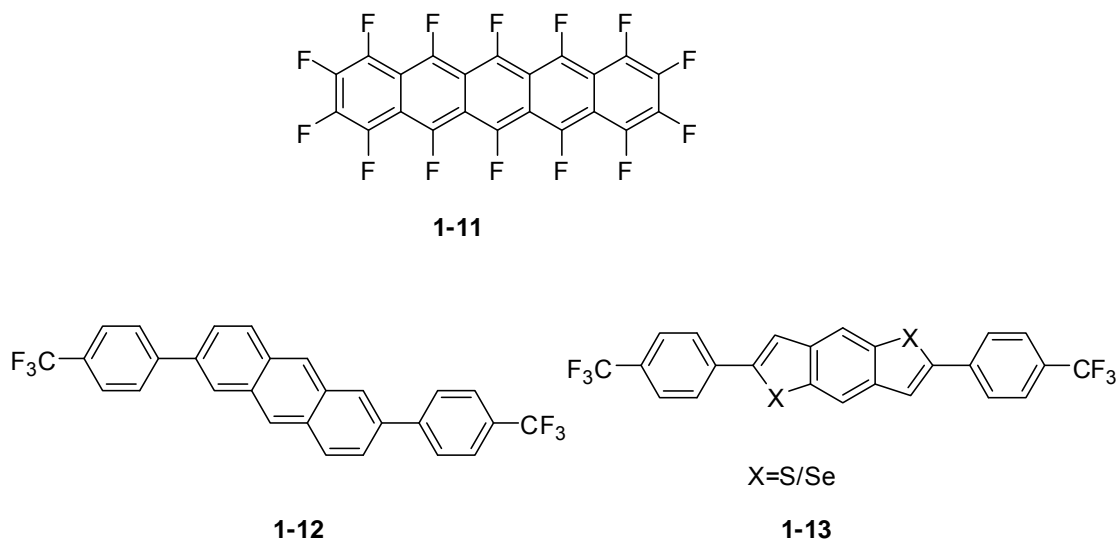


Figure 1. 5 Structures of acene derivatives.

6. Naphthalene and perylene derivatives

Some of the most impressive work on the development of n-type semiconductors so far has focused on the introduction of electron-accepting groups such as dianhydride and diimide onto naphthalene and perylene frameworks. (Figure 1. 6) In 1996 Katz and his coworkers built OFETs from NTCDA (**1-14**) and NTCDI (**1-15**) at a substrate temperature of 55°C in vacuum, achieving electron mobilities of 10^{-3} and 10^{-4} $\text{cm}^2\text{V}^{-1}\text{s}^{-1}$, respectively.²³ Later, they also reported that N-substituted NTCDI derivatives were used to fabricate OFETs.³⁴ A mobility of 0.1 $\text{cm}^2\text{V}^{-1}\text{s}^{-1}$ and on/off ratio with 10^5 for **1-16a** were recorded for operation in air after deposition at 70°C. The mobility of **1-16b** was 0.01 $\text{cm}^2\text{V}^{-1}\text{s}^{-1}$ when deposited at 25-50°C, and showed an on/off ratio of 4×10^4 . Interestingly, compound **1-16c** showed no FET activity in air, but displayed a mobility of 0.16 $\text{cm}^2\text{V}^{-1}\text{s}^{-1}$ after being held under reduced pressure for 4 days. They proposed that the denser packing of fluorinated chains for compounds **1-16a** and **1-16b** compared to alkyl chains of **1-16c** can somehow preclude the permeation of oxygen and water into the channel region of the active components. In addition, the electron-withdrawing features of fluorinated chains could possibly stabilize the injected electrons against environmental traps. However, more recent studies³⁵ suggest that perfluoralkyl chains attached to the imide nitrogens have little effect on the energy levels, and therefore these chains most likely enhance stability entirely by forming a protective barrier.

In 1997 Katz et al. observed n-type behavior in the directions along the PDCDA (**1-17**) molecular planes within crystals, with electron mobility of 10^{-5} - 10^{-4} $\text{cm}^2\text{V}^{-1}\text{s}^{-1}$ in vacuo.³⁶ In 2000 Zuilhof et al. measured the mobilities of N-C₁₈-PDCDI (**1-18a**) by the pulse-radiolysis time-resolved microwave technique, and found mobilities of 0.1 $\text{cm}^2\text{V}^{-1}\text{s}^{-1}$ in the liquid crystalline phase, and 0.2 $\text{cm}^2\text{V}^{-1}\text{s}^{-1}$ in the crystalline phase.³⁷ They ascribed the high charge carrier mobility to a very stable columnar arrangement of closely packed perylene cores in both the crystalline solid and liquid crystalline phases. Later, Malenfant et al. (IBM) deposited N-C₈-PDCDI (**1-18b**) films onto substrates at 50°C to fabricate n-type OFET devices, which had mobilities of up to 0.6 $\text{cm}^2\text{V}^{-1}\text{s}^{-1}$ and current on/off ratio of more than 10^5 .³⁸ The high mobility was attributed to high order obtained through the self-assembly process driven by interdigitation of the alkyl chain

substituents. Tobin Marks and his coworkers constructed OFETs from compounds **1-19a,b**, which displayed mobilities of 0.10 and 0.64 $\text{cm}^2 \text{V}^{-1} \text{s}^{-1}$ and on/off ratio of 10^5 and 10^4 under ambient atmosphere for **1-19a** and **b**, respectively.³⁹ The good charge transport properties were proposed to arise from considerable intermolecular π - π overlap with minimum interplanar spacing of 3.40Å. The ambient stability resulted from electron-withdrawing fluorinated chains, which again promote close packing through fluorocarbon self-segregation which provides a steric barrier to oxygen and moisture.

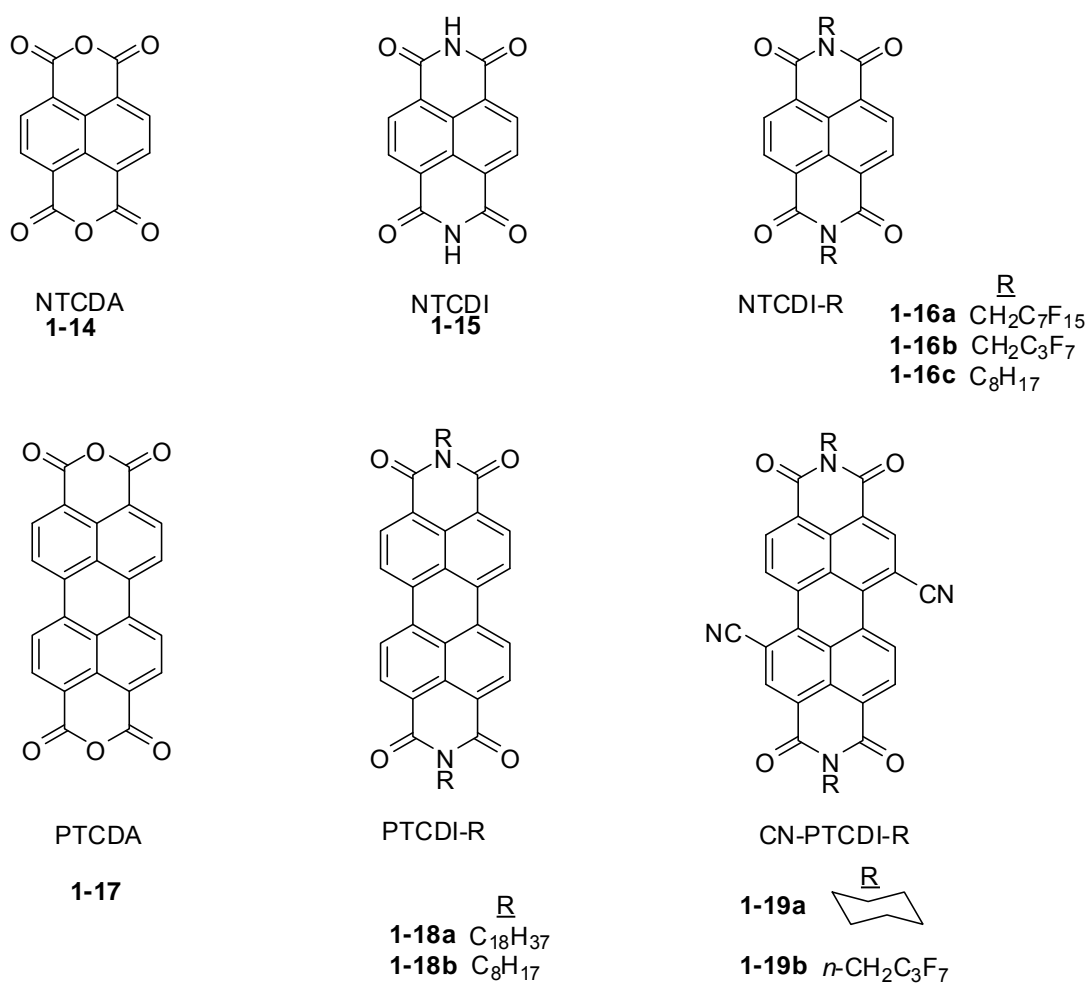


Figure 1. 6 Structures of NTCDA, NTCDI, NTCDI-R, PTCDA and PTCDI-R.

1.2 Conducting polymers: polythiophene

Conjugated polymers, also known as conducting polymers (CPs), most commonly are distinguished by a framework of alternating σ - and π -bonds, as well as electron lone pairs. (Figure 1. 7) However, electrons that constitute the π -bonds can be delocalized over “large” distances along the polymer backbones.

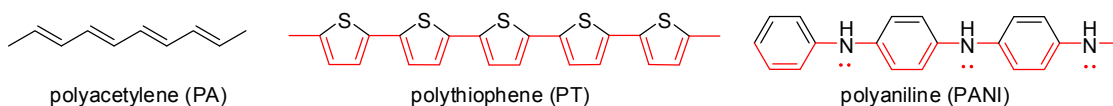


Figure 1. 7 Representative structures of conjugated polymers.

The science of conducting polymers has advanced very rapidly over the last 30 years, ever since the first report of metallic conductivities in doped polyacetylene by Shirakawa, Heeger and MacDiarmid in 1977.^{40, 41} Afterwards some novel conjugated polymers/copolymers have been synthesized, containing different structural frameworks based on aromatic, heteroaromatic, vinylic and acetylenic π -systems. (Figure 1. 8) Among these numerous CPs, poly(thiophene) (PT) has rapidly become the subject of considerable interest due to its good electrical properties together with its structural versatility, which led to multiple developments aimed at applications such as thin film transistors, light emitting diodes, solar cells etc.

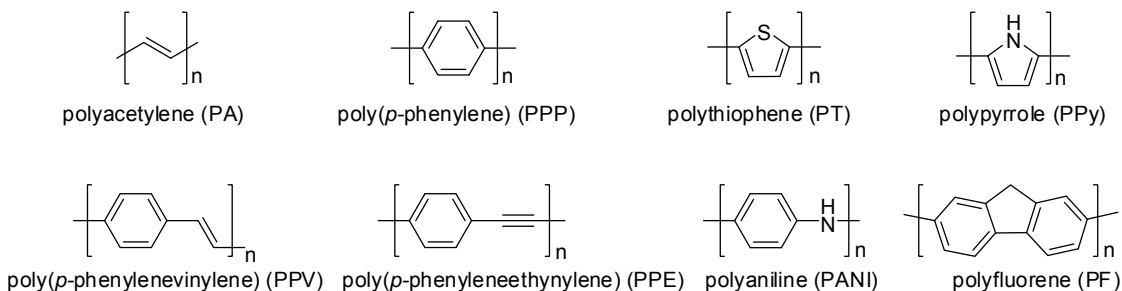


Figure 1. 8 Representative structures of some classes of conjugated polymers.

To date, thiophene-containing homo-/co-polymers have been synthesized via a variety of methods. Those methods can be classified into two main types: electrochemical and chemical method, which will be described in the following.

1.2.1 Electrochemical polymerization

Several mechanisms of the electropolymerization of five-membered heterocycle have been proposed, the most reasonable and acceptable one of which is shown in **Figure 1. 9**, derived from that of pyrrole electropolymerization.⁴² The electropolymerization features a succession of reactions as follows: 1) electrochemical formation of radical cation from the monomer; 2) chemical coupling of two radicals to produce a dihydrodimer dication; 3) deprotonation of the dihydrodimer dication to form dimer. The same process proceeds to form trimer, tetramer, pentamer until the polymer or oligomer can not dissolve in the electrolyte solution and deposits onto the electrode surface. Electrochemical polymerization is known to produce high purity polymers. This technique, however, can result in polymers with regioirregularity when employing monomers with lower symmetry (e.g. unsymmetrically substituted) and very wide molecular weight distributions.

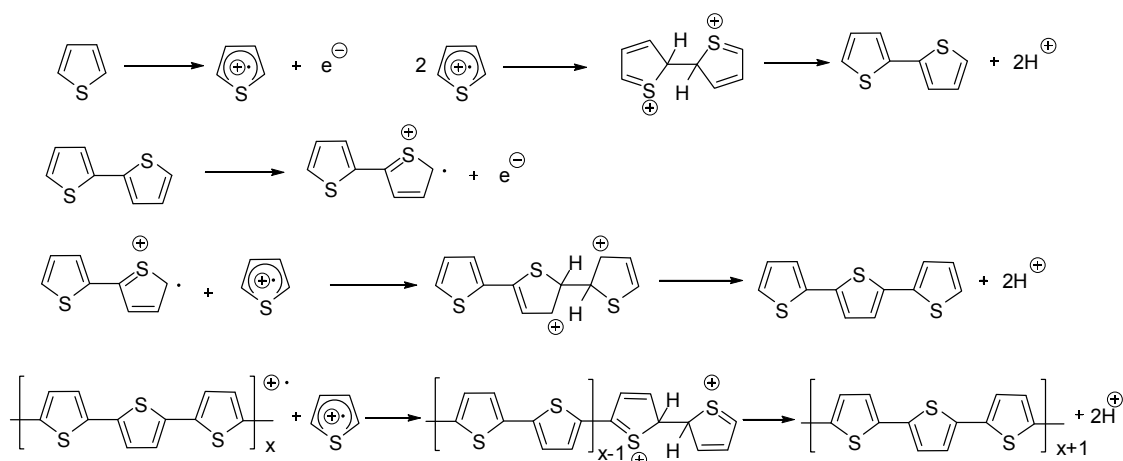


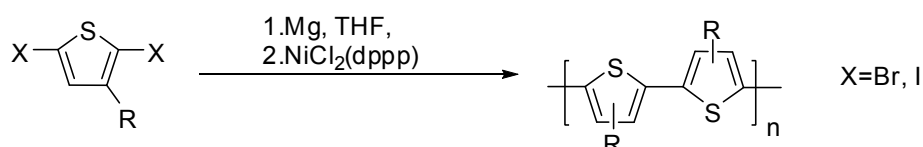
Figure 1. 9 Possible mechanism of electrochemical polymerization of thiophene and derivatives.⁴²

1.2.2 Chemical Polymerization

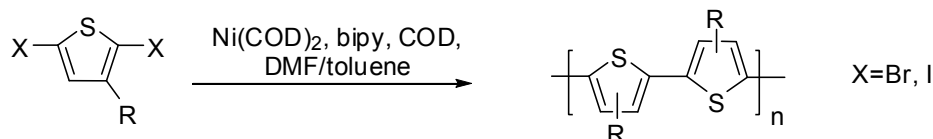
Commonly there are three main routes to synthesize the regioirregular soluble poly(3-alkylthiophene)s: Oxidative coupling, Yamamoto coupling and Kumada coupling. (Figure 1. 10) For Kumada coupling, 2,5-dihalo thiophenes are reacted with stoichiometric magnesium in THF to generate a mixture of Grignard species and then

polymer is obtained by halo-Grignard coupling under $\text{NiCl}_2(\text{dppp})$ catalysis.^{43, 44} The obtained regioirregular polymer is 2,5-linked, not 2,4-linked. For Yamamoto coupling, dehalogenative polycondensation of 2,5-dihalo-3-alkylthiophene with zerovalent nickel complexes, typically a mixture of bis(1,5-cyclooctadiene)nickel(0) ($\text{Ni}(\text{cod})_2$) and neutral ligand L (e.g., bipy), affords π -conjugated poly(3-alkylthiophene)s in high yields at 25-100°C.^{45, 46} This method produces polymer with a high content of head-head linkages (~ 60-70%). See **Figure 1. 11** for definition of head-to-head and other regiochemical relationships. This moderate regioselectivity arises from more efficient oxidative addition of C5-X than C2-X to the Ni(0) complex for steric reasons. As to the oxidative coupling method with FeCl_3 , materials prepared by this method commonly have molecular weights ranging from $M_n = 30\text{k}$ to 300k and with polydispersities ranging from 1.3 to 5 and regioregularity of 80% head-to-tail.⁴⁷ This polymerization proceeds through a radical mechanism rather than radical cation mechanism. The FeCl_3 has to be solid as active oxidant which is the case when CHCl_3 is used as a solvent in which FeCl_3 is only partially soluble. Considering all factors, an excess of FeCl_3 (about 4 eq) is required.⁴⁸ The polymers obtained by chemical synthesis of poly(3-alkylthiophene) usually contain some impurities to some extent which will affect device performance in organic electronics.⁴⁹

Kumada coupling method



Yamamoto coupling method



Oxidative coupling method

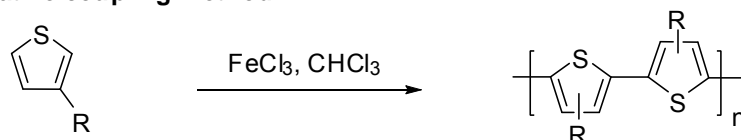


Figure 1. 10 Synthesis of regioirregular/random poly(3-alkyl thiophene).

Although the above three chemical methods for polythiophene synthesis can eliminate 2,4 linkages, they can not regiochemically control couplings between adjacent thiophene rings. Since 3-alkylthiophene is not a symmetrical molecule, there are three possible regiochemical couplings: HH, HT and TT. (**Figure 1. 11**) So far three methods have been developed to prepare regioregular polythiophene. (**Figure 1. 12**) McCullough et al. used lithium diisopropylamine (LDA), a significantly hindered base, to confine the lithiation at the 5-position of the thiophene rings, followed by transmetalation reaction with $\text{MgBr}_2 \cdot \text{Et}_2\text{O}$ to obtain regioselectively metallated monomer. These monomers are then homocoupled under transition-metal catalysis. The resulting polymers are characterized by a HT coupling of more than 93%.⁵⁰ Rieke and his coworkers employed Rieke zinc (Zn^*) to undergo oxidative addition to the C-Br bond primarily at the 5-position of 2,5-dibromo-3-alkylthiophene to afford 2-bromo-5-(bromozincio)-3-alkylthiophene which was polymerized under the catalysis by $\text{NiCl}_2(\text{dppp})$ to regioregular poly(3-alkylthiophene) with more than 97% head-tail coupling.^{51, 52} Wudl used a HH-dimer of alkylthiophene (3,3'-dialkyl-2,2'-bithiophene) to yield a regiochemically defined polymer, namely a HHTT coupled PAT.⁵³

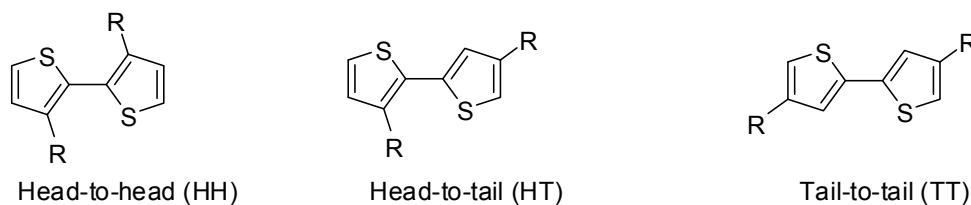
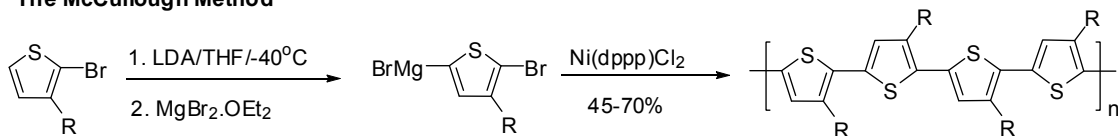
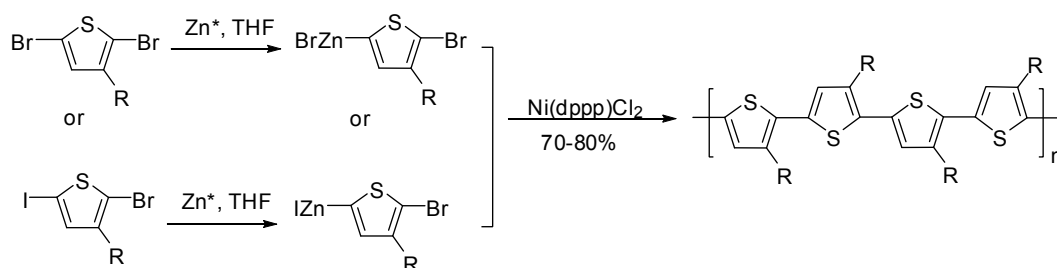


Figure 1. 11 Three possible coupling diads from coupling 3-alkyl thiophene.

The McCullough Method



The Rieke Method



The Wudl Method

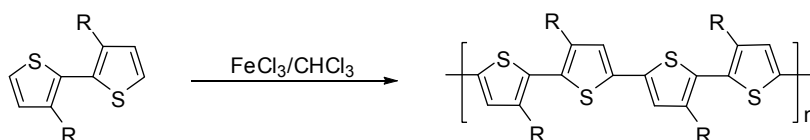


Figure 1. 12 Synthesis of regioregular poly(3-alkylthiophene).

In addition to the above described chemical methods for homopolymer synthesis, some other organometallic routes have been exploited to prepare thiophene copolymers, such as Sonogashira⁵⁴, Suzuki⁵⁵, Stille cross-couplings⁵⁶, etc. (Figure 1. 13). They have higher versatility with respect to the nonorganometallic methods and easier realization of more complex molecular structures required in many electronic and optoelectronic applications.

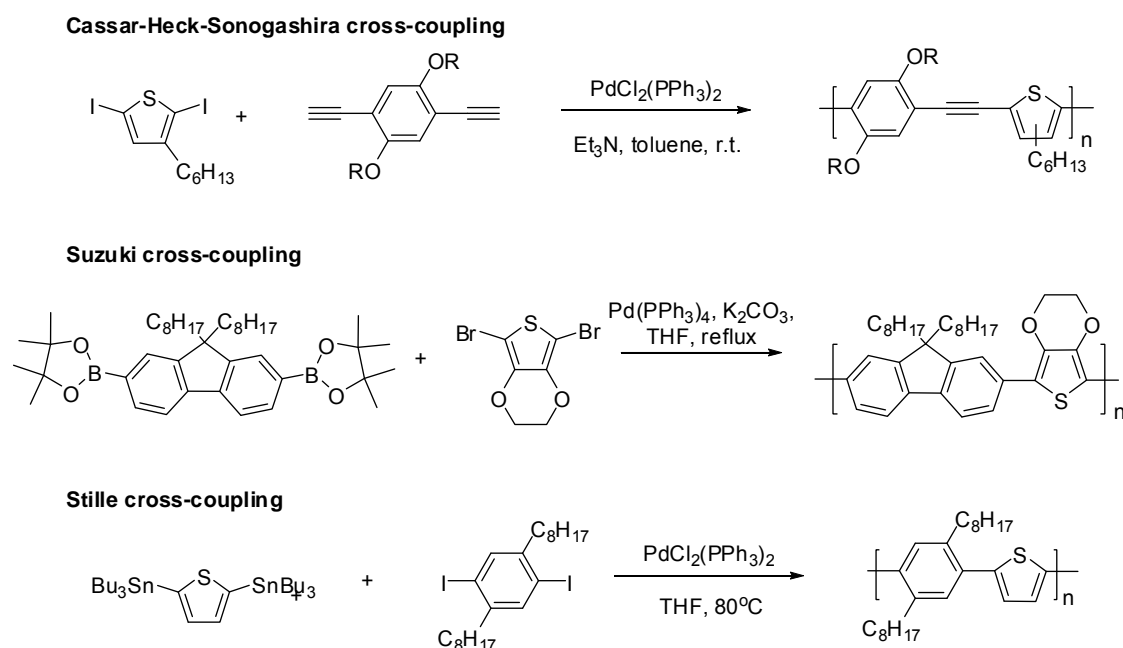


Figure 1. 13 Some other organometallic routes for thiophene copolymer synthesis: Sonogashira coupling (top)⁵⁴, Suzuki coupling⁵⁵ and Stille coupling (bottom)⁵⁶.

1.3 Aromatic interactions and self assembly

1.3.1 Aromatic interactions

Aromatic interactions (π - π interactions, C-H- π interactions) are so important in such diverse areas as molecular recognition processes associated with DNA and proteins, high-performance materials, electronic circuits and devices. The two most predominant types of aromatic interactions involve stacked arrangements (face to face, **Figure 1. 14** left) and herringbone-like configurations (edge to face, **Figure 1. 14** right), the extreme of which being the herringbone-T-shaped arrangement of aromatic planes (**Figure 1. 14**, middle). Face-to-face stacking with complete overlap (eclipsed) of neighbors within a π -stack is not favored energetically. The slipped stacked arrangement can be described by two terms: pitch angle ($\angle P$) and roll angle ($\angle R$).⁵⁷ Pictorial descriptions of pitch and roll are provided in **Figure 1. 15**. Pitch describes the regular, repeating displacement of successive neighbors within a π -stack along their long molecular axes. Roll is the corresponding displacement along the short molecular axes. Large overlap can be achieved when molecules have smaller pitch and roll angle.

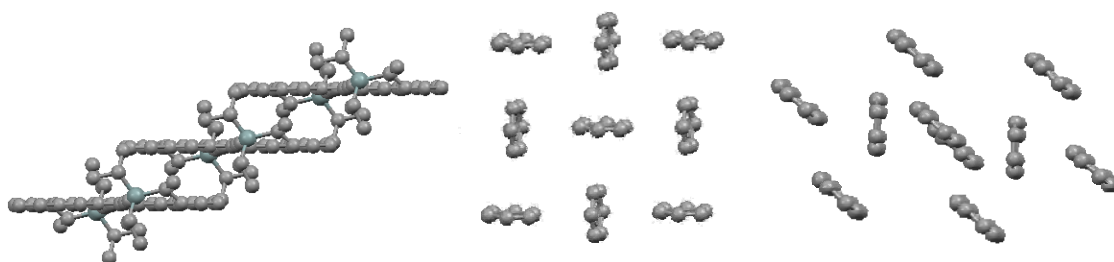


Figure 1. 14 slip-stacked arrangement (TIPS-pentacene⁵⁸, left); herringbone (T-shape) (benzene⁵⁹, middle); herringbone-like (pentacene⁶⁰, right).

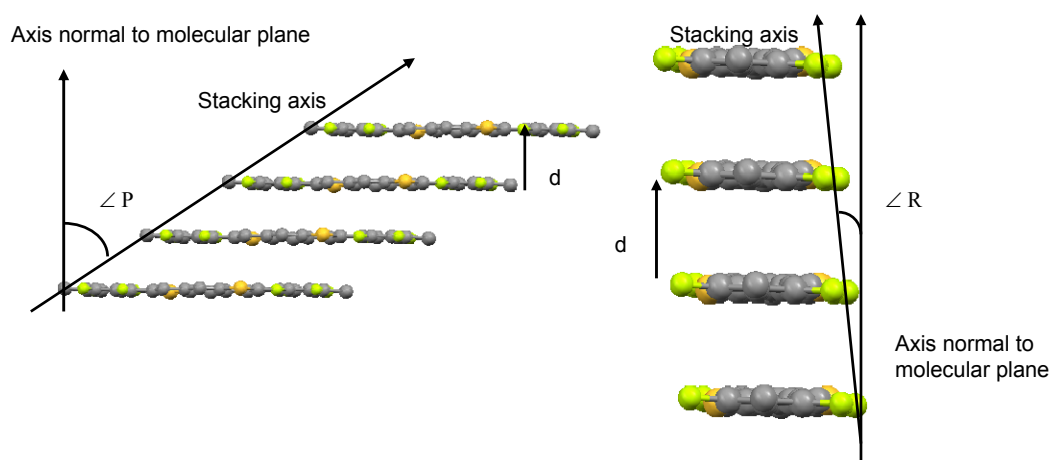


Figure 1. 15 Definition of pitch angle, roll angle and interplanar distance.⁵⁷ Left: view along the short molecular axis of a “pitched” π -stack; Right: view along the long molecular axis of a “rolled” π -stack. $\angle P$ = pitch angle, $\angle R$ = roll angle.

Experimental and computational studies^{61, 62} suggest that face-to-face packing can enhance the semiconducting properties because the intermolecular electronic overlap can be maximized to facilitate charge transport. There are various means to favor face-to-face at the expense of edge-to-face packing. One of the methods is to increase the ratio of C to H atoms, which is especially suitable for disc-like molecules. For example, benzene and anthracene (C/H ratios 1.00 and 1.40) adopt the herringbone and sandwich herringbone packing motifs, respectively, while **1-20**, **1-21** and **1-22** (C/H ratios 2.11, 2.11, 1.75) adopt face-to-face stacked packing motifs with extensive C-C contacts.⁶³ (**Figure 1. 16**) Another method to favor face-to-face packing is to introduce side chains or substituents around the periphery of the conjugated core system. Bao and her coworkers reported that

the introduction of chlorine atoms to the 5 and 11 positions of tetracene altered the molecular packing from herringbone to face-to-face, yielding single crystal hole mobility of $1.6 \text{ cm}^2\text{V}^{-1}\text{s}^{-1}$.⁶⁴ Anthony functionalized pentacene at its peri positions with relatively bulky silyl acetylene groups to preclude the herringbone packing motif and adopt the face-to-face π - π packing motif. It was found that the size of substituents significantly affect the molecular packing in the solid state. If the diameter of trialkyl silyl group is smaller than half the length of pentacene moiety (TES), the molecules assemble to one-dimensional face-to-face π -stacks. If the diameter of alkynyl groups is close to half the length of pentacene (TIPS), the molecules crystallize into two-dimensional face-to-face π -stacks resembling a brick wall.⁶⁵ Kobayashi et al. reported that chalcogen-chalcogen interactions between methylchalcogen groups (OCH_3 , SCH_3 and TeCH_3) at the 9,10 positions of anthracene play an important role in controlling the molecular packing.⁶⁶ The anthracene with OCH_3 groups has no O-O interaction and therefore is arranged in a herringbone packing motif similar to anthracene. On the other hand chalcogen-chalcogen interactions seem to exist between pendant SCH_3 (**1-24**) and TeCH_3 groups which contribute to face-to-face π - π slipped-stacking. (**Figure 1. 17**) It is also reported that phenyl groups at the 5,6,11,12 positions of tetracene **1-23** (rubrene) force face-to-face π - π slipped-stacking in the solid state⁶⁷, yielding single crystals with hole mobility up to $20 \text{ cm}^2\text{V}^{-1}\text{s}^{-1}$.^{68, 69} (**Figure 1. 17**)

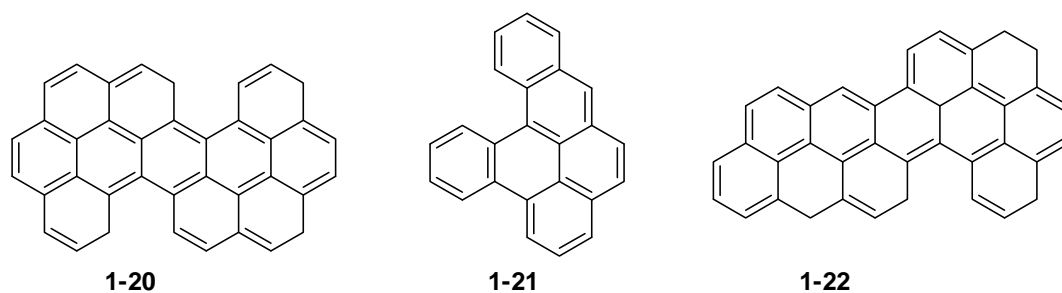


Figure 1. 16 Structures of **1-20**, **1-21** and **1-22**.⁶³

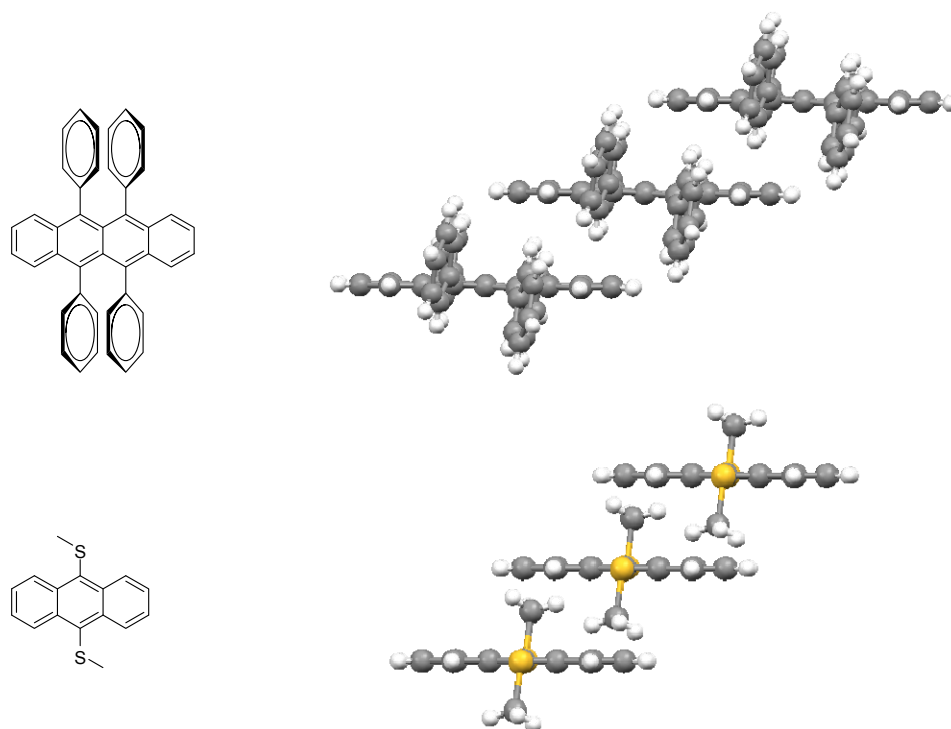


Figure 1. 17 Structures and crystal packing of rubrene **1-23** (top)⁶⁷ and 9,10-bis(methylthio)anthracene **1-24** (bottom)⁶⁶.

Alternatively to all the structural design features above, others have used attractive interactions between electron- rich and -poor arenes to favor face-to-face packing. In this area arene-perfluoroarene interactions have been employed regularly to drive molecular packing to the face-to-face π - π packing motif. In 1960 Patrick and Prosser reported that benzene (mp 5.5°C) and hexafluorobenzene (mp 4°C) form a 1:1 complex with a melting point of 24°C.⁷⁰ The increased melting point corresponds to the formation of attractive forces leading to face-to-face packing and therefore the strong interaction of benzene and hexafluorobenzene caused by the large but opposite in sign quadrupole moments. Since that time, the interaction between fluorinated and non-fluorinated π -systems (π - π F) has been exploited extensively in crystal engineering. In 1998 Grubbs et al. used face-to-face interaction of phenyl-perfluorophenyl groups to force crystallization of stilbene derivatives to set the stage for topochemical [2+2] photodimerization and photopolymerization of olefinic compounds.⁷¹ Todd Marder reported that the co-crystals of 1,4-bis(phenylethynyl)benzene and its perfluorinated analogue adopt face-to-face π - π

stacking arising from arene and perfluoroarene interaction, in contrast to the respective herringbone and nonstacked layer arrangements found in crystals of pure 1,4-bis(phenylethynyl)-benzene and its perfluorinated analogue.⁷² (**Figure 1. 18**) Application of these interactions to crystal engineering is quite broad in scope and tolerates even gross mismatch in identities/sizes of the π and π F partners. Muellen et al. reported that hexafluorobenzene (C_6F_6) is included into a cocrystal with permethoxylated hexa-*peri*-hexabenzocoronene **1-27** (permethoxylated HBC), a strongly twisted graphene molecule, changing the packing of the HBC from herringbone to face-to-face motif even without any π - π overlap between HBCs.⁷³ (**Figure 1. 19**) This change is caused by the electrostatic interaction between electron-rich permethoxylated HBC and electron-poor C_6F_6 .

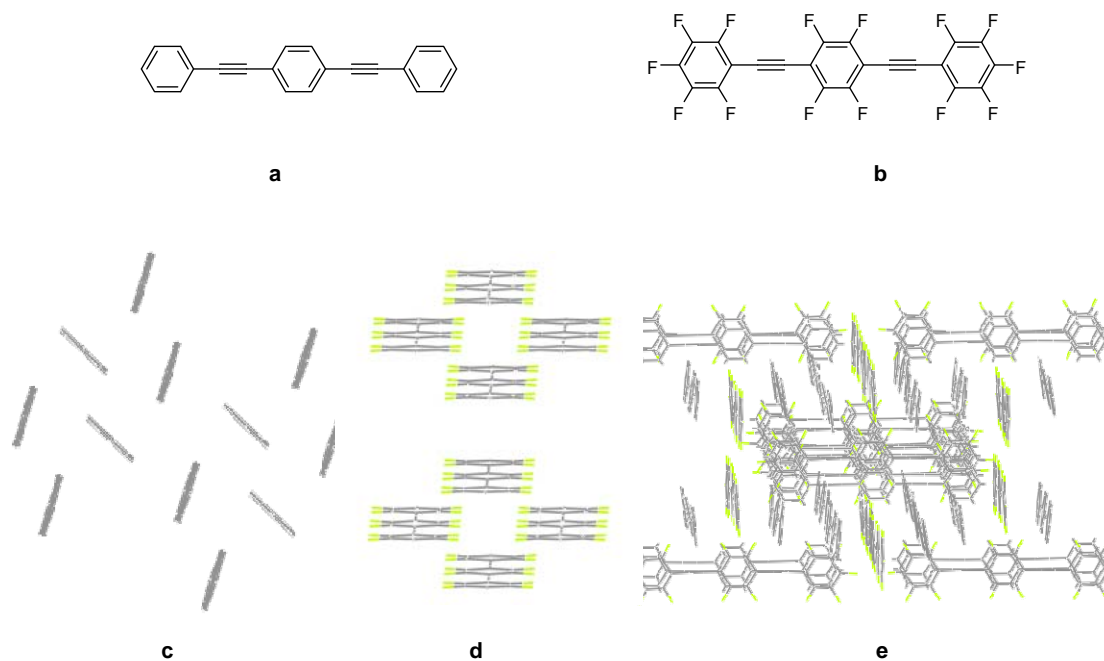


Figure 1. 18 Published⁷² structures of a) 1,4-bis(phenylethynyl)-benzene **1-25** and b) 1,4-bis(pentafluorophenylethynyl)benzene **1-26**; along with c) crystal packing of **1-25**; d) crystal packing of **1-26**; e) crystal packing of **1-25** and **1-26** complex (2:1).

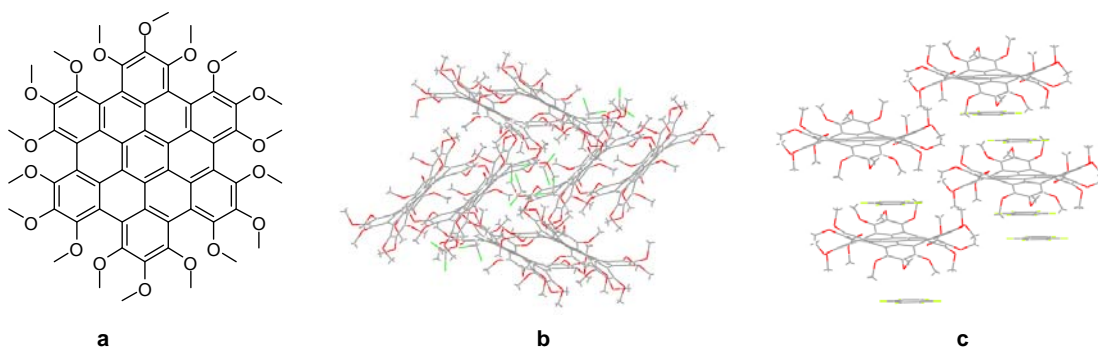


Figure 1. 19 a) Structure of permethoxylated hexa-*peri*-hexabenzocoronene **1-27**⁷³; b) crystal packing of **1-27**; c) crystal packing of the complex of **1-27** and C₆F₆ (1:2).

1.3.2 Self assembly of conjugated polymers

As mentioned above, semiconducting polymers have a wide range of potential applications in the field of organic electronics such as flat panel displays and photovoltaic cells. It is believed that molecular ordering in the solid state is critical for device performance. Highly ordered materials are required for thin film transistors with high carrier mobility.⁷⁴⁻⁷⁶ On the other hand, less ordered or totally amorphous materials are desirable for sensors and light emitting diodes.⁷⁷

Regioregularity can significantly influence the molecular ordering in the solid state and therefore affect the device performance. There are three possible regioisomeric dyads formed by coupling 3-alkylthiophene monomers at their 2,5-positions: HH, HT and TT as shown in **Figure 1. 11**. Usually if polymer contains more than 90% of one of these dyads, it is denoted as regioregular, otherwise irregioregular. Highly regioregular polymers can have a high degree of backbone coplanarity in the solid state and maximize the intermolecular electronic coupling which can lead to high charge carrier mobilities. The common belief described repeatedly in the literature is that if molecules incorporate some head-to-head coupling, two nearest alkyl substituents will sterically repel each other and so cause the polymer backbone to be twisted out of the planarity. However, whether the backbone is coplanar or not is more critically related to regularity of the spacing of the side chains along the backbone, and that this spacing be commensurate with the space-filling demands of a planarized backbone. Irregularity in the side-chain spacing, or incommensurate space-filling requirements of the side chains and a planarized, closely

π -stacked backbone will cause twisting of the backbone and/or disrupt ordered packing. (**Figure 1. 20**) There are many crystallographic examples which support this argument: HH linkages do not inherently limit conjugation nor disrupt packing, but instead the arrangement in the end is dependant on the overall space-filling demands of the whole molecule. For example, compound **1-28**⁷⁸ with HH coupling is fully planarized while compound **1-29**⁷⁹ is not. Electrostatic interactions between substituents and the thienyl sulfur atoms are also important. Compound **1-30**⁸⁰ with methoxy substituents is planarized while compound **1-31**⁸¹ with ester substituents is twisted. Therefore it is not reasonable to conclude that HH coupling will lead to the deviation from planarity for molecules.

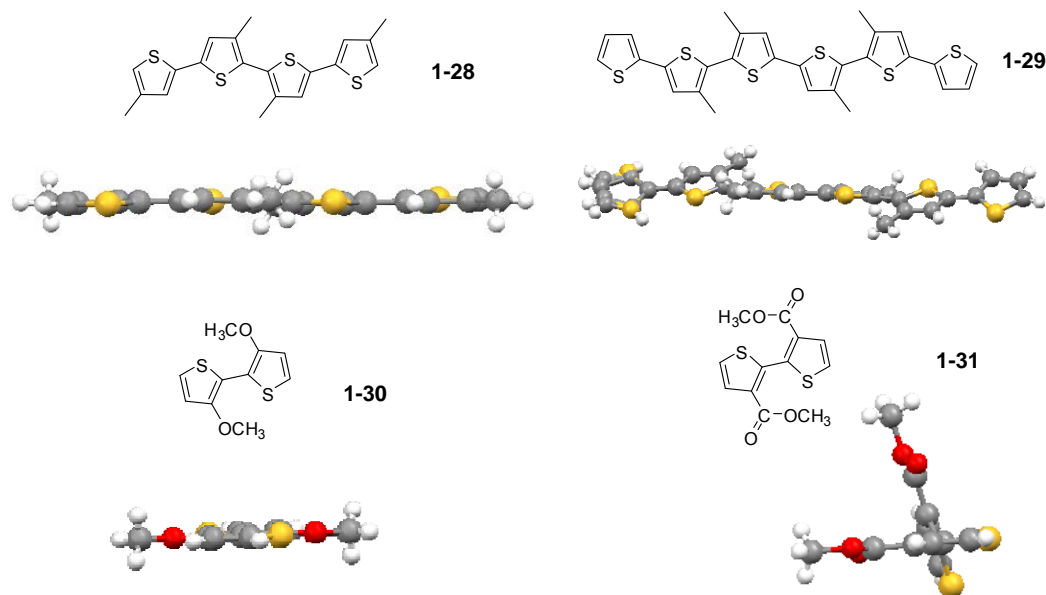


Figure 1. 20 Crystal structures of thiophene derivatives with HH linkages: **1-28**⁷⁸, **1-29**⁷⁹, **1-30**⁸⁰ and **1-31**⁸¹.

Alkyl side chains incorporated into conjugated polymers not only can increase the solubility and processability while maintaining the electroactive nature, but also affect molecular ordering in the solid state and hence bulk electronic properties. The nanophase separation between π -conjugated backbones and alkyl side chains leads to lamellar structures and certainly provides some significant contribution to the drive towards π -stacked motifs (in a similar manner to substituents on small molecules). This structure makes the bulk electronic structure highly anisotropic. Charge carrier transport can be

maximized along two dimensions (polymer backbone and π -stacking axis), while charge carrier transport is very poor along the other dimension (lamellar packing). Higher mobility can be achieved in FETs when lamellar packing is normal and the π -stacking axes are parallel to the substrate. It is believed that FET charge-carrier mobility is limited by interchain transport not by intrachain transport.⁷⁶ Therefore many researchers have employed various methods to induce close π - π stacking such as electrostatic interaction between electron-rich and electron-poor moieties in the backbone⁸² and charge transfer complexes^{83, 84}. Two packing models of the alkyl side chains are proposed to form lamellar packing.⁸⁵⁻⁸⁷ First, the side chains may extend in the same plane as the polymer backbones and interdigitate each other (**Figure 1. 21a**). Alternately, the side chains tilt away from lamellar layers with no interdigitation (**Figure 1. 21b**). One may imagine a number of states intermediate between these.

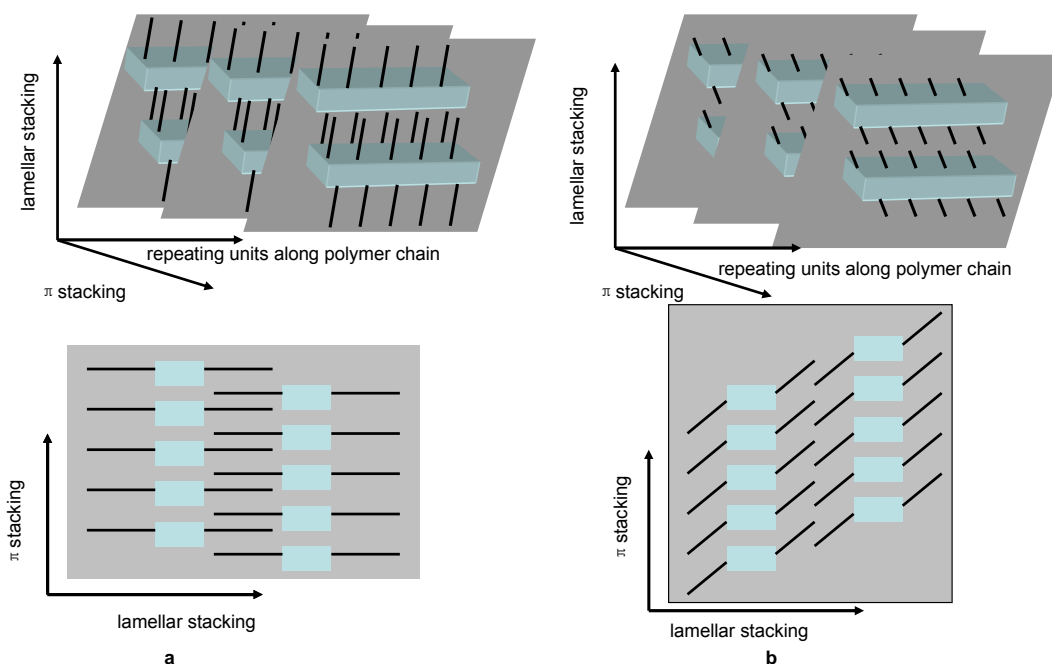


Figure 1. 21 Schematic of lamellar and π -stacking for alky-substituted rigid-rod polymers. a) interdigitated structure model; b) tilted structure model.

1.4 Orientation and reactivity in nucleophilic substitution of polyfluoroaromatic compounds

S_NAr reactions of polyfluoroaromatics were heavily relied upon to prepare all the new materials reported here, and therefore some basic principles of this chemistry should be described. Perfluorinated aromatic compounds are reactive substrates for nucleophilic attack.⁸⁸ The orientation of nucleophilic aromatic substitution about polyfluorinated aromatics already carrying other substituents is relatively well understood. The generalization is that fluorine atoms ortho or meta to the site of nucleophilic attack are activating, whereas para-fluorine atoms are slightly deactivating. The activating and deactivating effect of fluorine atoms have been studied and explained extensively.⁸⁹⁻⁹¹ A fluorine atom beta to a carbanion center (**Figure 1. 22a**) is strongly carbanion-stabilizing due to the inductive electron-withdrawing effect of fluorine. On the other hand, fluorine substituents destabilize a directly adjacent carbanionic center (**Figure 1. 22b**) due to electron-electron repulsion (high electron density about fluorine and short C-F bond). The activating effect of ortho fluorine atoms in the case of **c** is attributed to ion dipole interaction, an initial-state effect, making the carbon under nucleophilic attack more electron-deficient and more easily approachable by the nucleophile. (**Figure 1. 22**)

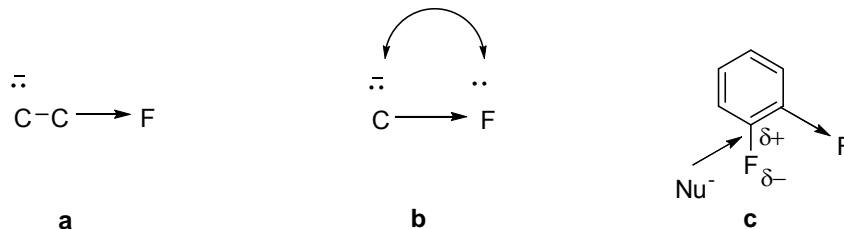


Figure 1. 22 a) Stabilizing fluorine atom beta to carbanionic center; b) destabilizing fluorine atom directly attached to a carbanionic center; c) ion-dipole interaction activating ortho position to nucleophilic attack.

The orientation of nucleophilic attack on polyfluoroaromatics is directed by a maximum of activating fluorine atoms (ortho and meta) and minimum of deactivating fluorine atoms (para). This generalization can also be applied to other aromatics such as octafluoronaphthalene where the number of activating fluorines (ortho, meta, pseudo-ortho and pseudo-meta) should be maximized and the number of deactivating fluorines (para and pseudo-para) should be minimized.⁹² (**Figure 1. 23**) Powerful

electron-donating groups (NH_2 , or O^-) which can destabilize the transition state (electron-pair repulsion) will increase the *meta* substitution^{93,94} and electron-withdrawing groups (ring nitrogen or CF_3) which can stabilize the transition state will increase the *para* substitution.⁹⁵ (**Figure 1. 24**)

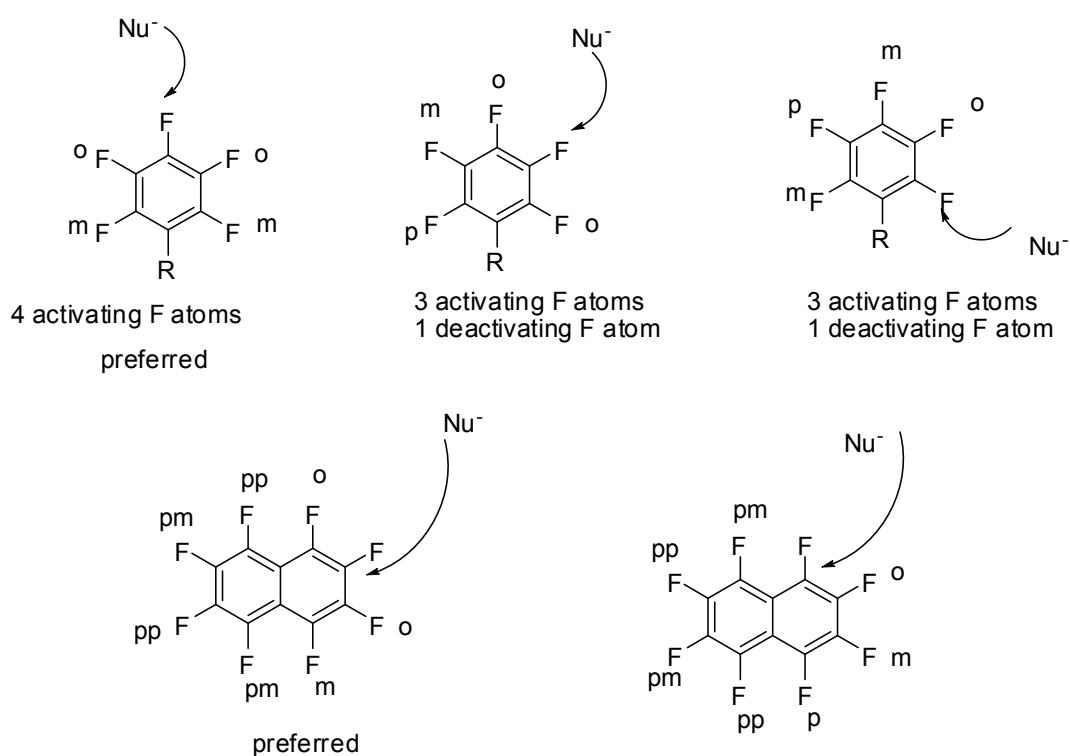


Figure 1. 23 Preferred orientation of nucleophilic attack on hexafluorobenzene (top) and octafluoronaphthalene (bottom). *pp* = pseudopara, *pm* = pseudometata.

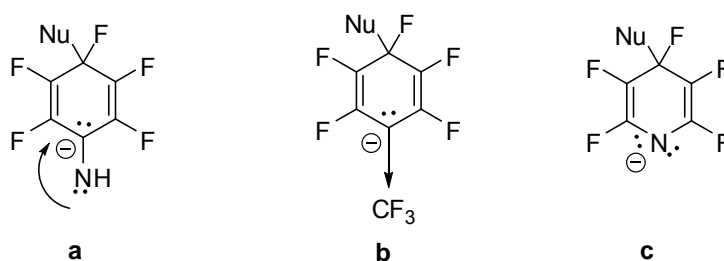


Figure 1. 24 a) NH₂ group activating *meta* position to nucleophilic attack; b) CF₃ group activating *para* position to nucleophilic attack; c) ring nitrogen activating *para* position to nucleophilic attack.

1.5 Thesis of this work

The remainder of this dissertation is divided into three chapters describing the results of three independent but interrelated research projects centered on the synthesis, supramolecular engineering, and structure-property studies of 3 different classes of fluorinated organic electronic materials. These are thiophene-based CPs (Chapter 2), extended fused polycyclics based on the benzothiophene scaffold (Chapter 3) and functionalized benzodithiophenes (Chapter 4). Common unifying themes are:

1. Synthetic methodology development exploiting S_NAr reactions of fluorinated aromatics to form the various conjugated frameworks;
2. Control of self-assembly via intermolecular interactions between fluorinated and non-fluorinated π -systems, inter- and intramolecular interactions between fluorine atoms and thienyl sulfur atoms, as well as in some cases space-filling demands of other substituents like alkyl side-chains;
3. Control over (opto)electronic properties using the design principles included in theme 2 above.

The effects of molecular design on self-assembly are elucidated by x-ray crystallography (small molecules) and wide-angle x-ray diffraction (polymers). Thermal properties are investigated by differential scanning calorimetry. (Opto) electronic properties are studied by cyclic voltammetry and UV-Vis absorption and photoluminescence spectroscopy. The thesis is entirely based on these themes and does not involve electronic device studies.

Chapter 2 Synthesis and characterization of alternating thiophene and π F copolymers

2.1 Introduction

The science of conducting polymers has advanced very rapidly over the last 30 years, ever since the first report of metallic conductivities in doped polyacetylene by Shirakawa, Heeger and MacDiarmid in 1977.⁴⁰ Among the numerous CPs, poly(3-alkylthiophene)s (P3AT) are among the most studied as organic electronic materials,^{82, 96-102} especially for applications in thin film transistors. However, the relatively low ionization potentials (IP) of P3ATs make them easily doped by atmospheric oxygen which can lead to rapidly degrading FET performance in air. This poor stability in air could require costly device production in inert atmosphere and encapsulation, which defeats one of the main purposes of pursuing organic electronics: potential lower cost alternatives to inorganic semiconductors.

However, the rich chemistry of thiophenes allows the material chemist the ability to overcome these challenges. Heeney et al (Merck) incorporated relatively highly electron-localizing thieno[3,2-b]thiophene into the backbone of polymer PBTTT (**Figure 2. 1**) to increase IP (0.3 eV greater than for P3AT).⁷⁵ FETs prepared from PBTTT provided good performance ($\mu_{\text{FET}} = 0.2\text{-}0.6 \text{ cm}^2\text{V}^{-1}\text{s}^{-1}$ and $I_{\text{on/off}} \geq 10^6$) and showed good stability to low humidity (4%) air. A series of the most detailed collaborative studies of the nature of PBTTT film morphology followed. Atomic force microscopy (AFM) characterization of the film surface showed well-defined terraces resembling those seen in films from crystalline small molecules. Combining these results with a series of other studies, including x-ray diffraction and polarized spectroscopy, these researchers have made the clearest case for the importance of side-chain spacing along the polymer backbone. It seems completely reasonable that increasing the spacing between the side chains, due to the unsubstituted rings, allows interdigitation of side-chains from neighboring polymer chains. This translates to overall higher order and performance. Ong et al took a somewhat related approach to both increase IP (0.1 eV greater than for P3ATs) and increase solid-state order by incorporating unsubstituted bithiophene units

into polymer PQT. A TFT device fabricated from PQT showed mobilities of up to $0.14\text{cm}^2\text{V}^{-1}\text{s}^{-1}$ and on/off ratio of over 10^7 under ambient conditions.⁷⁴

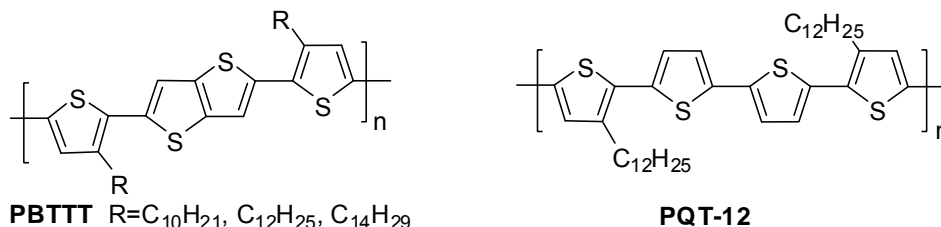


Figure 2. 1 Structures of polymer **PBTTT** and **PQT-12**.

Thiophenes are covalently entrained at their 2,5-positions within these materials most commonly by transition-metal-catalyzed coupling¹⁰³ or (electro)chemical oxidative polymerization.¹⁰⁴ The limited means by which conjugated polymers can be purified may leave behind residues from catalysts and reactive functionalities, which may have a detrimental effect on thin film device performance,^{105, 106} as well as intrinsic chemical defects arising from side reactions. Krebs clearly demonstrated that Pd nanoparticles formed from Pd catalysts are deleterious to the electronic properties of a series of different polymers produced by palladium catalyzed coupling. After greatly decreasing the content of Pd nanoparticles from a PPV (Poly(phenylenevinylene)), a PPE (Poly(phenyleneethynylene)) and a PAT (Poly(alkylthiophene)), by complexation with N,N-diethylphenylazothioformamide, resistivities of all three polymers greatly increased.¹⁰⁵ (**Table 2. 1**) As revealed above, high-performance FETs based on conjugated polymers are coming into reach despite these drawbacks. However, energy- and time-intensive purification is required (e.g. repeated extended soxhlet extraction with a series of solvents). If all other factors were equal, selection of synthetic methodology could be reduced to choosing which associated trace defects/impurities minimally impact targeted properties.

Table 2. 1 Pd content and resistance before and after removal of Pd residue¹⁰⁵

polymer	Pd content before/after(ppm)	Resistance before/after (kΩ)
PPV	17860/<0.1	0.10/30
PPE	268/<0.1	0.03/45

There were several targets and associated hypotheses identified at the onset of the projects described in this chapter:

1. Target: Design and implement alternative transition-metal-free methods to prepare thiophene-containing polymers, thereby reducing material costs and effort required to purify the products
2. Hypothesis: High molecular polymers might be prepared by the reaction of appropriate nucleophiles with perfluoroarenes
3. Target: Begin to evaluate the scope of this polymerization method by preparing a series of different polymers from different thiophene monomers with differing electronic and steric properties.
4. Hypothesis: The reactivity of the nucleophilic monomers, and therefore the purity and molecular weight of the resulting polymers, will vary depending on the chemical identity of the monomers
5. Target: Engineer the properties of the polymers by varying nature of the backbones and the substituents
6. Hypothesis: The presence or absence of fluorine substituents will dictate solid-state ordering via intramolecular (S-F atoms) and/or intermolecular (electron-rich and -poor units) interactions, along with the nature of side chains. This can include forcing planarization of conjugated polymer backbones that would otherwise be twisted without fluorination.

Regioselective fluoride-displacement reactions⁸⁸ undergone by perfluorinated π -systems (π F) provide unique opportunities to prepare conjugated polymers with minimal reagents/catalysts. Reactions between chalcogenide nucleophiles and π F's have been exploited to make alternating copolymers,¹⁰⁷⁻¹⁰⁹ but few carbon-carbon bond-forming polymerizations are reported. Notable examples are oligomers and polymers obtained via reaction of π F's with metalated ferrocenes¹¹⁰ or indene,¹¹¹ and small molecules from lithiated thiophenes/benzenes.^{82, 112, 113}

In the initial stages of the work described herein, several attempts were made to prepare alternating thiophene-perfluoroarene copolymers by reaction of 2,5-lithio-3-alkyl

thiophene with hexafluorobenzene. (**Figure 2. 2**) Only sticky, colorless to pale yellow low molecular weight oligomers were produced. ^{19}F NMR spectra were most complicated, indicating that the products were not well-defined, arising from the difficulty to obtain perfect stoichiometry between 3-dodecylthiophene and *n*-BuLi and poor regioselectivity of the reaction of bis-lithiated thiophenes toward C_6F_6 . Thereafter, the search began for environmentally stable and easily handled nucleophilic thiophenes, which may be activated in situ preferably, and even more preferred if the activator could be used in catalytic amounts.

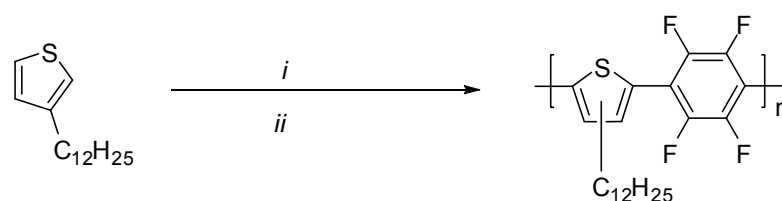


Figure 2. 2 Synthesis of alternating 3-dodecylthiophene- C_6F_4 copolymer. *i*: *n*-BuLi, TMEDA, hexane; *ii*: C_6F_6 .

Shreeve reported substitution of fluoride substituents from perfluoroaromatic substrates by nucleophiles derived from $\text{Me}_3\text{SiOCH}_2\text{R}_f$, $\text{Me}_3\text{SiOC}_6\text{F}_5$, or $\text{Me}_3\text{SiOC}_6\text{F}_4\text{X}$ ($\text{X} = \text{H}, \text{NO}_2, \text{CN}, \text{CF}_3$) under catalysis by fluoride anion, in which the nucleophilicity of the ether group is markedly enhanced by the formation of the strong silicon-fluorine bond (~ 142 kcal/mol) found in the volatile trimethylsilyl fluoride byproduct.¹¹⁴⁻¹¹⁶ Silicon-assisted perfluoroalkylation has become a useful method for transferring “ R_f ” groups to electrophiles under mild reaction conditions.^{117, 118} The mechanism is outlined below in **Figure 2. 3**. In this case, fluoride ion is required only as an initiator to initially form nucleophilic pentacoordinate silicate ions. After the first catalytic cycle, the reaction becomes autocatalytic with alkoxide anion intermediates serving to activate carbon-silicon bonds.

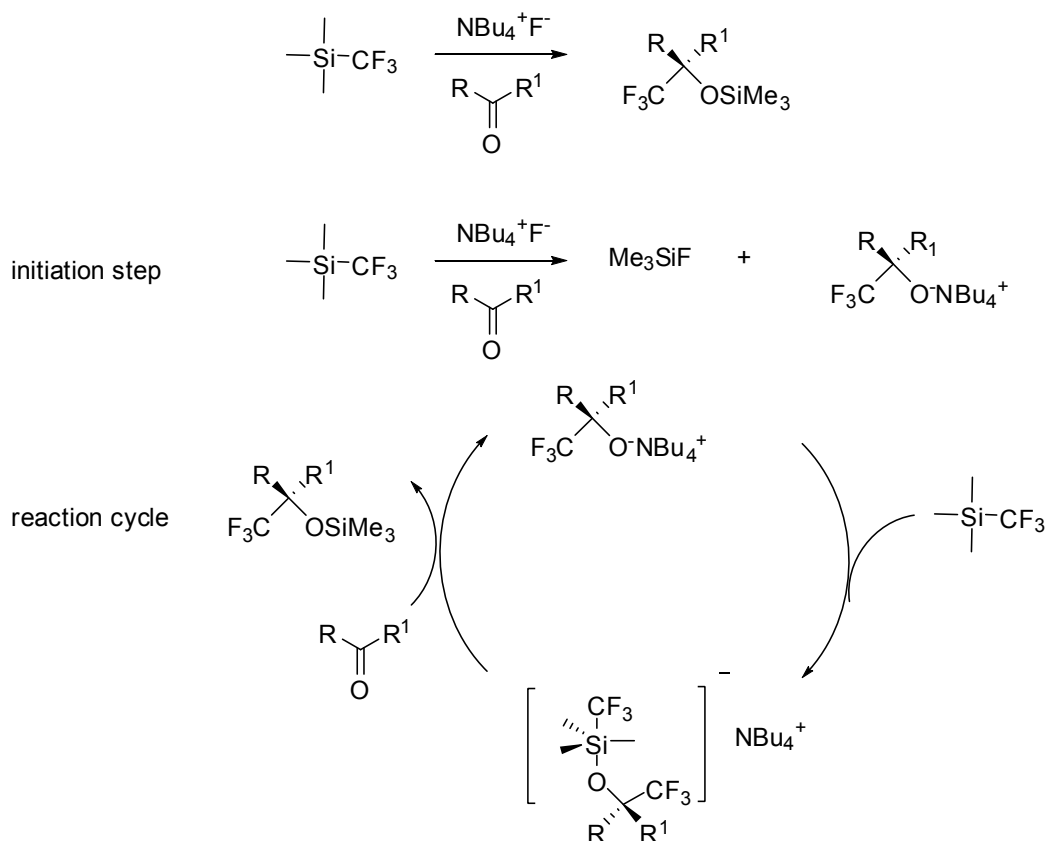


Figure 2. 3 Mechanism of the trifluoromethylation reaction between a carbonyl compound and trimethyl(trifluoromethyl)silane.¹¹⁷

This chapter describes preliminary investigations into exploiting the known fluoride activation of silicon-carbon bonds toward electrophiles, described above, to prepare a series of thiophene-containing copolymers with perfluorinated arenes. (**Figure 2. 4**) The coupling reaction occurs between highly fluorinated π -electron systems and silyl-functionalized monomers, in which the silicon group is attached to sp^2 -hybridized carbons (thiophene derivatives). The bonds connecting the TMS groups to the 2,5-positions of thiophene can indeed be activated and induced to react with perfluorarenes. With each new bond-formation, the reagent which induces the reaction (fluoride ion) is regenerated. The reaction therefore proceeds to high yields producing high-molecular weight polymers, requiring only a minute (catalytic) amount of fluoride additive. Chemically pure polymers are produced with well-defined end-groups. However, the degree of chemical perfection depends on the chemical nature of monomers

and reaction conditions. ^1H and ^{19}F NMR characterization shows low percentages of chemical defects, but only time and device studies will show whether these defects will affect device performance. There are no doubt only very low levels of extrinsic impurities in the as-synthesized polymers because the fluoride ion source and the sole side product (TMSF, a gas) are very easily removed by washing with water and evaporation, respectively. The reaction is a highly attractive alternative to transition-metal-catalyzed reactions which currently dominate the field.

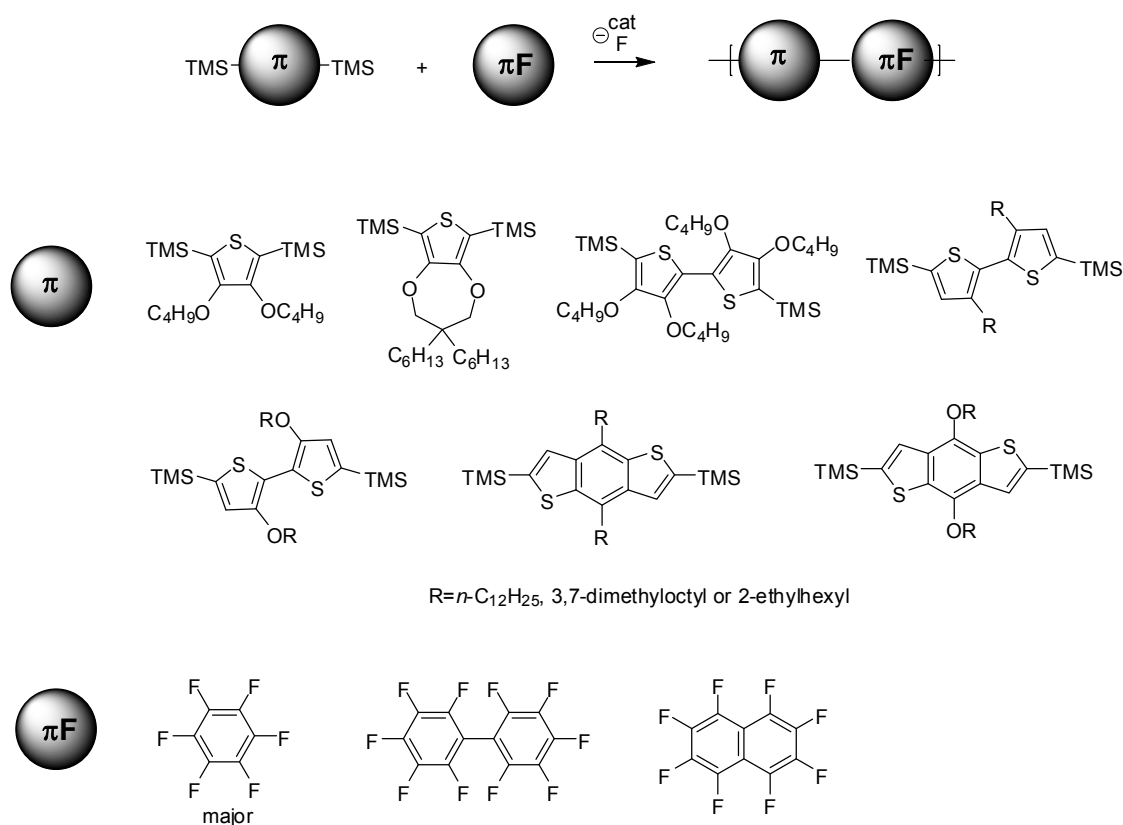


Figure 2. 4 General scheme for the disclosed synthesis of alternating thiophene- πF copolymers, together with the generic structures of the monomers investigated. The fluoride source may be CsF.

After first publication of this methodology it was discovered that we were not the first to form bonds between π - and πF units by this chemistry. There are reports of the reaction of pentafluoropyridine with aryl trimethylsilylacetylene, catalyzed by CsF or KF. (3 mole excess per TMS group).¹¹⁹ (**Figure 2. 5**) Surprisingly, these researchers always

used molar excesses of fluoride, despite that the reaction requires only catalytic amounts of fluoride, as confirmed by others in our group.

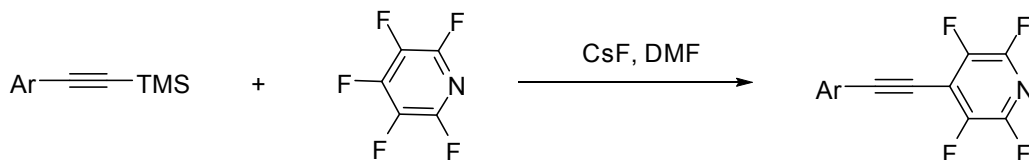


Figure 2. 5 Synthesis of tetrafluoropyridynyl acetylenes.

The first part of this chapter will describe the preparation of a series of polymers from thiophene monomers with differing steric and electronic nature (**Figure 2. 4**). All 13 monomers were prepared by (modified) published procedures, except the monomer bearing propylenedioxy substituents, which was prepared in one step from 3,3-dihexyl-3,4-dihydro-2H-thieno[3,4-b][1,4]dioxepine (ProDOT(Hx₂)), provided by the group of Prof. John R. Reynolds (University of Florida). The reason for choosing this series of monomers can be divided into two parts: 1) investigate the scope of this polymerization chemistry, and 2) engineer the properties of the polymers by varying the nature of the thiophene substituents.

The second half of this chapter will describe structure-property studies to compare the effects of repeat unit structure on self-assembly and (opto) electronic properties. Properties were studied by x-ray crystallography or fiber XRD (polymers), UV-Vis absorption and photoluminescence (PL) spectroscopy. The electronic and optical properties of these copolymers can be manipulated by varying the substituents and backbones and controlling self-assembly of the polymer chains in the solid state. The series of monomers shown in **Figure 2. 4** are arranged in order of decreasing steric repulsion predicted to exist between pendant groups along the resulting polymer backbones.

2.2 Synthesis of alternating 3,4-dialkoxythiophene and perfluoroarene copolymers

Here the above methodology was developed employing perfluoroarenes as electrophiles and 2,5- bis(trimethylsilyl)thiophenes as the silyl-functionalized, masked nucleophiles. The incorporation of alkyl or alkoxy groups prevents undesired α , β - and β ,

β -couplings within the polymer backbone and improves solubility. Additionally, alkoxy substituents increase the electron density of aromatic systems and thus polymer oxidation potentials. Taken together with the expected backbone torsion caused by repulsion between pendant oxygen and fluoride atoms, these polymers are designed to be amorphous blue-emitting solids. Thiophene monomers with substituents at the 3,4-positions were also employed to eliminate any issues with regioregularity of monomer incorporation within the polymer backbones. **(Figure 2. 6)** The bromine atoms of 3,4-dibromothiophene were exchanged for methoxy groups in a methanol/sodium methoxide medium, assisted by CuO and a catalytic amount of KI in 75% yield. Treatment of 3,4-dimethoxythiophene with 4 equivalents of *n*-butanol in the presence of 10% of *p*-toluenesulfonic acid (PTSA) in toluene at 80°C gave 3,4-dibutoxythiophene (**2-4**) in 64% yield after purification by column chromatography. 3,4-dialkoxythiophene is deprotonated at the 2 and 5 positions with *n*-BuLi in hexane:DME at 0°C and quenched with trimethylchloride (TMSCl) to produce compound **2-5** in 91% yield.

Copolymerization with various π F's was initiated at 80°C with fluoride ion as catalyst, 18-crown-6 as co-catalyst and toluene as solvent. Fluoride ion is regenerated with each C-C bond formed. In principle, the only constituents of the reaction mixture should be target polymer, solvent, fluorotrimethylsilane (bp =16°C), and the water-extractable initiator system. Therefore, the polymers may be purified by washing with water and evaporation, respectively.

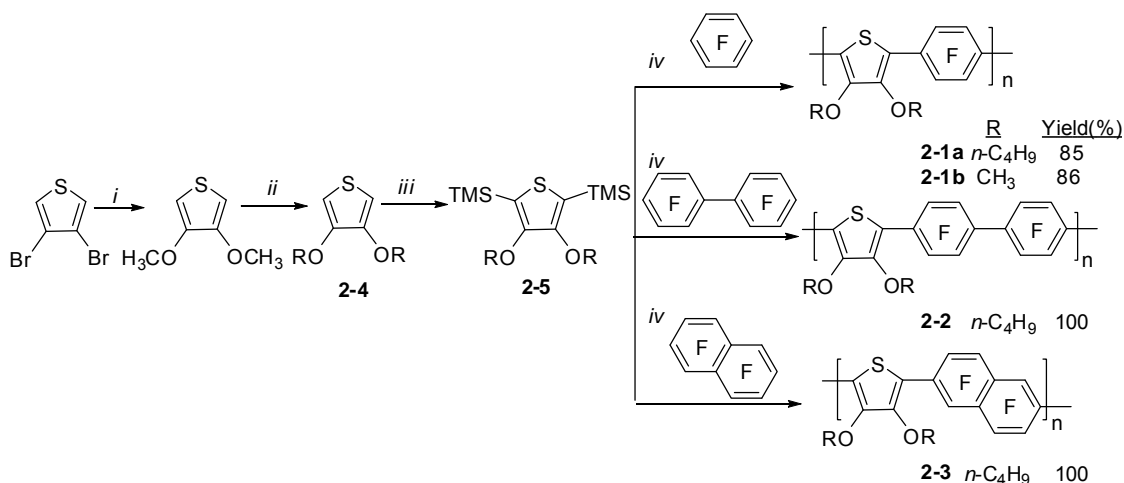


Figure 2. 6 Synthesis of alternating thiophene- π F copolymers. *i*: NaOCH₃, CH₃OH, CuO/KI, reflux, 75%; *ii*: *n*-butanol, PTSA, 80°C, 64%; *iii*: a) *n*-BuLi, hexane/DME, 0°C; b) TMSCl, 0°C, then r.t., 91%; *iv*: 0.1 eq CsF, 0.2 eq 18-crown-6, toluene, 80°C.

¹H, ¹³C, and ¹⁹F NMR spectra for **2-1a** and **2-2** indicate high chemical purity, in accordance with the structures in **Figure 2. 6** (see **Figure 2. 7** and **Figure 2. 8** for full spectra). Polymer **2-2** is defect-free within detection limits. The absence of detectable defects for polymer **2-2** indicates that perfluorobiphenyl is reactive only at the 4,4'-positions under these conditions. Small signals in the ¹⁹F spectrum of **2-1a** indicate ortho/meta linkages or branching with estimated concentration $\leq 1/53$ repeat units (1 defect/106 rings).

Similar to small-molecule products resulting from reaction of other nucleophiles with perfluoronaphthalene,⁸⁸ polymer **2-3** is significantly less regiopure. ¹⁹F NMR shows three major signals corresponding to the symmetry depicted in **Figure 2. 6**, along with seven smaller signals arising from end-groups. There are three additional small signals, most likely from 2,7-substitution about naphthalene (~7% based on relative integrals). NMR indicates that the end-groups are almost exclusively monosubstituted π F residues for polymers **2-3**. These polymers are therefore telechelic macromonomers, which might be end-functionalized via fluoride displacement by other nucleophiles.

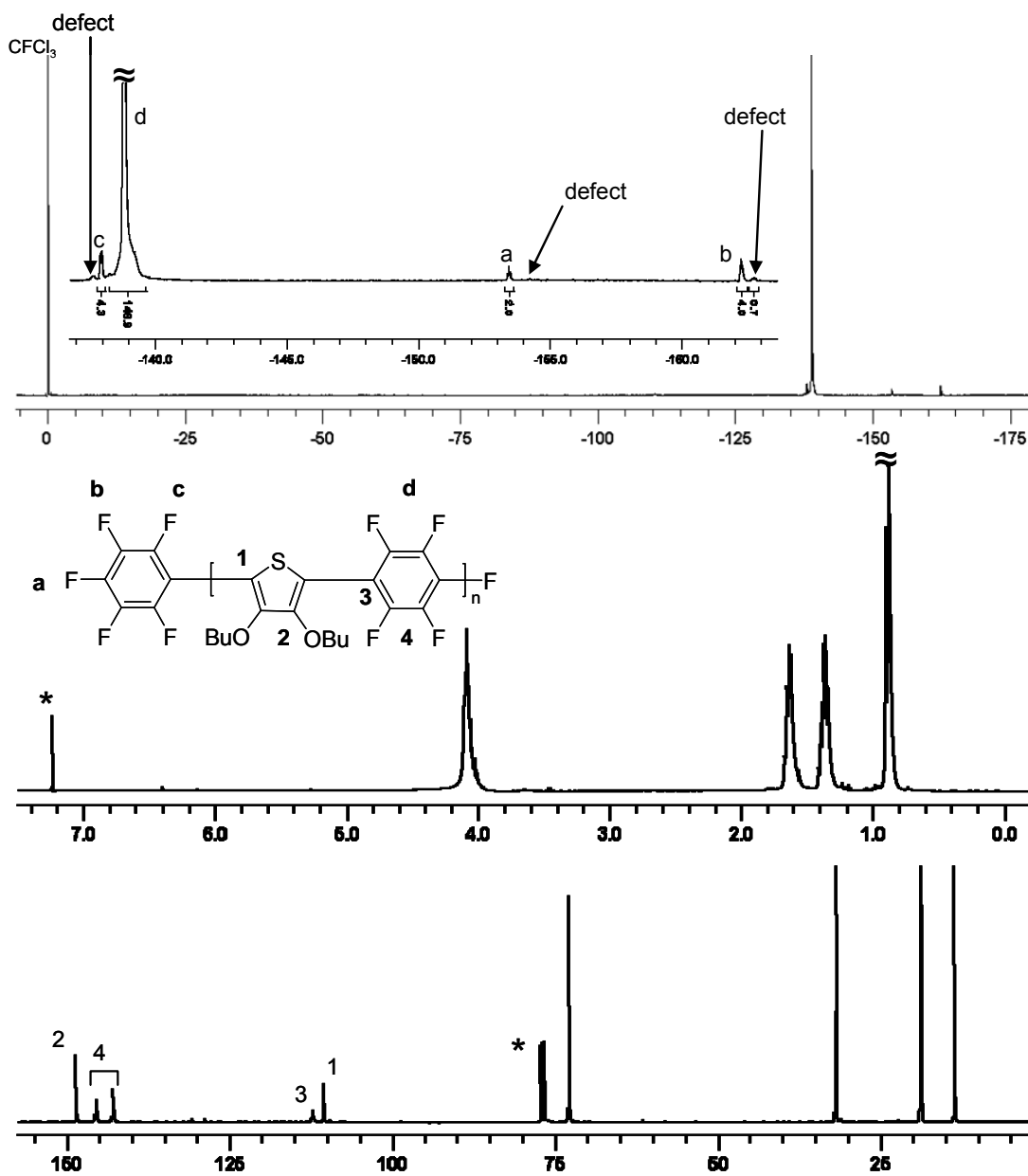


Figure 2. ¹⁹F, ¹H, and ¹³C NMR spectra of polymer **2-1a** in CDCl₃. Number average degree of polymerization calculated from ¹⁹F NMR is $P_n = (146.9F/4F) \approx 37$, or 74 aromatic rings ($M_n \approx 14$ kDa), in good agreement with GPC data ($M_n = 28$ kDa, versus polystyrene), which typically overestimates by a factor of 2. *(H)DCCl₃ solvent/reference.

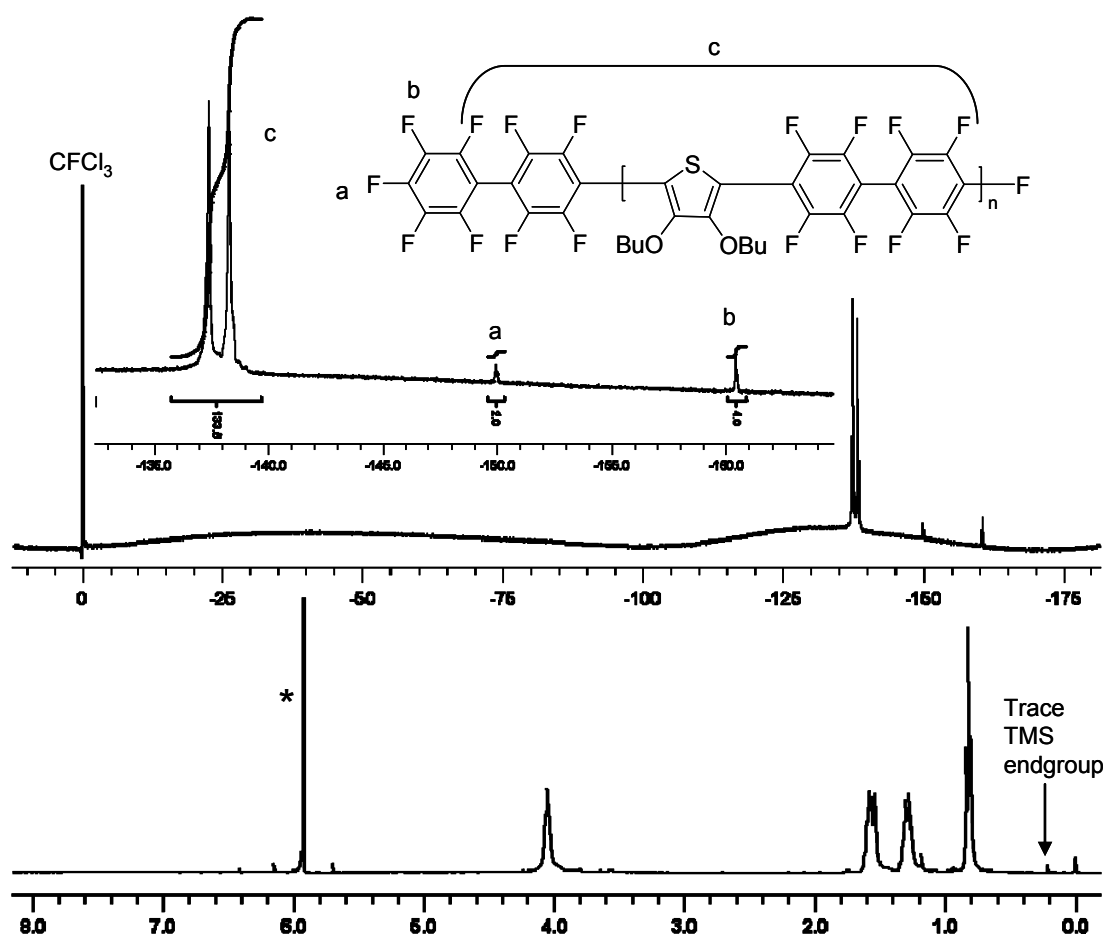


Figure 2. 8 ^{19}F and ^1H NMR of polymer **2-2** in $\text{C}_2\text{D}_2\text{Cl}_4$. Number average degree of polymerization calculated from ^{19}F NMR is $P_n = (133.5\text{F}/8\text{F}) \approx 17$, or 51 aromatic rings ($M_n \approx 8.7$ kDa), in good agreement with GPC data ($M_n = 17$ kDa, versus polystyrene), which typically overestimates by a factor of 2. * ($\text{H})\text{D}_2\text{C}_2\text{Cl}_4$ solvent/reference.

The end-groups are defined because the πF monomer was added in excess. This stoichiometric imbalance should have led to lower than observed degrees of polymerization (P_n) according to the Carothers equation [$P_n = (1 + r)/(1 - r)$, where r is the ratio of limiting to excess monomer]. For polymer **2-1a**, the employed 20% molar excess of C_6F_6 should provide $P_n \approx 11$ ($M_n \approx 4$ kDa). The difference between measured (28 kDa) and predicted M_n far exceeds the typical 2-fold overestimation by gel permeation chromatography for semirigid polymers. Further, exact stoichiometry led to solvent-swallowable but insoluble gels. This indicates that the average functionality of C_6F_6

under these conditions is >2 , i.e., on average, slightly more than two reactive C-F bonds per molecule. This should lead to higher than predicted P_n , branching, and gelation, the last of which can be suppressed via stoichiometric imbalance.

In any case, the Carothers equation assumes equal reactivity of all functional groups, and therefore it cannot apply here. Deviation from Carothers equation has been reported for polymerizations in which all functional groups do not have the same reactivity.^{120, 121} Most substituents activate the para position of pentafluorobenzenes toward further substitution.⁸⁸ The first and second attacks on C_6F_6 should occur with different rates.

The 2- and 5-positions of the thiophenes should also have variable reactivity in this scheme. These polymerizations must proceed through anionic intermediate(s), i.e., pentacoordinate silicate anions,¹¹⁷ whether or not desilylation to a formal carbanion intermediate precedes C-C bond formation. Therefore, reactivity at the thienyl 5-position should change significantly after an electron-donating TMS group at the 2-position is replaced by an electron-withdrawing πF group.

The model studies in **Figure 2. 9** delineate functional group reactivity during the polymerizations. The well-defined nature of this chemistry is also supported by the mass balance for each model reaction, which is excellent, given that the products were isolated by chromatography. Compound **2-6** provided details beyond those involved in the related polymerization. Nearly 50% conversion to oligomers **2-8** through **2-10** requires that the thiophenes gain a second nucleophilic site. A reasonable scenario is proton transfer to fluoride-activated **2-6** from **2-7** (C_6F_5 lowers pK_a), also accounting for approximately eqimolar production of **2-4**. Fluoride is lost in this step but can be regenerated when the new anion of **2-7** reacts with other πF 's to form the higher oligomers. The low P_n (**Figure 2. 10**) of the oligomers results from gross imbalance in stoichiometry between C_6F_6 and *bifunctional* thiophenes formed in situ by proton-transfer. A similar outcome was observed by others during the reaction of 2-lithio-thiophene with tetrafluoroethylene: higher thienylene-vinylene oligomers were formed.¹²²

To avoid proton-transfer chemistry, the 5-position was blocked with a methyl group (**2-12**). To our surprise, the ratio of isolated **2-13** and **2-14** indicates that the first and second attacks on C_6F_6 proceed with essentially the same rate. Most groups attached to a pentafluorobenzene direct further substitution to the para-position, and contrary to our

results, also accelerate reaction. On the other hand, the high isolated yield of **2-16** upon reaction of equimolar amounts of **2-5** with **2-13** shows that conversion of the second TMS group of **2-5** is markedly more rapid than that of the first. For that reason, ~43% of **2-5** was recovered, separately, as unreacted starting material and monodesilylated product **2-6**. Since the amount of desilylation was approximated by the amount of CsF employed (~10%) and desilylation is minimal during the related polymerizations, **2-6** was likely formed during aqueous workup. The remaining **2-5** and **2-13** were converted to an inseparable mixture of **2-15a,b**, thereby accounting for nearly complete mass balance. It is unclear at this point why we obtain degrees of polymerization higher than predicted by Carothers equation, when using an excess of C₆F₆. If the second reactive group of a given monomer becomes more reactive after the first group has been converted, i.e. the first reaction of that monomer is the rate-limiting step, then it can be expected that a stoichiometric excess of that monomer will enhance the degree of polymerization over practical reaction times. However, in this case, it is the thiophene monomer that produces the more reactive intermediate.

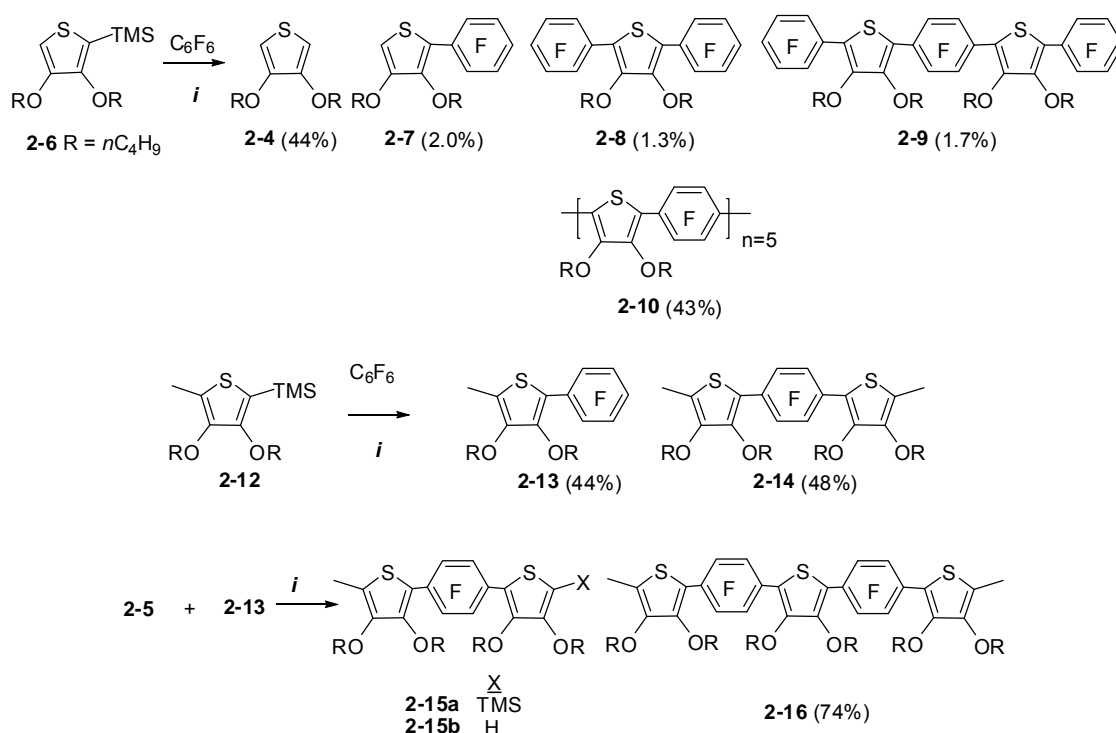


Figure 2. 9 Model reactions to elucidate reactivity. *i*: 0.1 equiv CsF, 0.2 equiv 18-crown-6, toluene, 80 °C. (%)= isolated yields. Yield for **2-16** based on **2-13**.

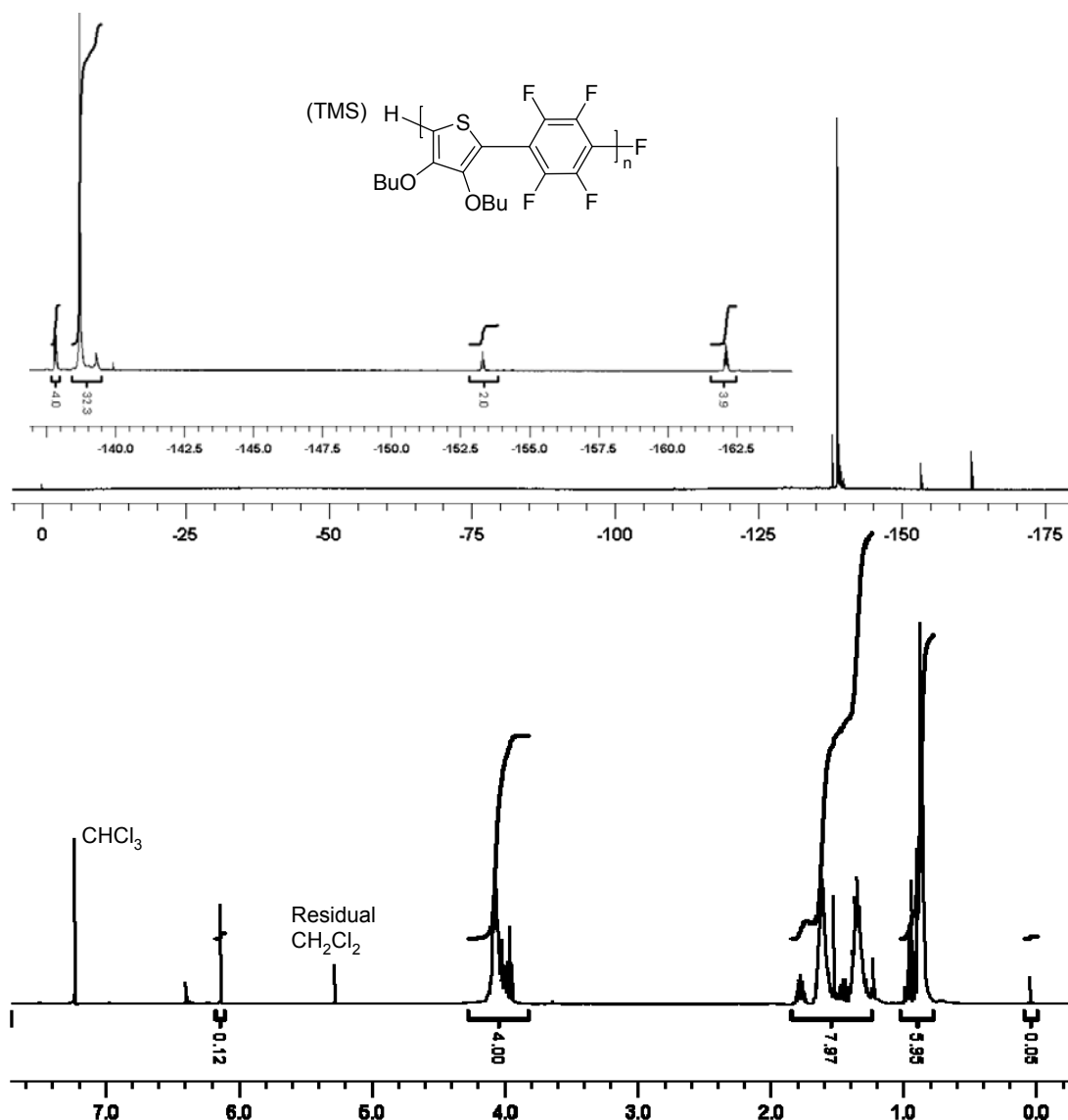


Figure 2. 10 ^1H and ^{19}F NMR of oligomers **2-10** in CDCl_3 . Compare to spectra of analogous higher polymer **2-1a** in **Figure 2. 7** above. ^1H spectrum appears complicated due to low molecular weight (signals from end groups). Number average degree of polymerization, calculated from the ratio of end-groups to repeating units (sums from both ^1H and ^{19}F NMR spectra), for oligomers **2-10** is $P_n \approx 5.3$. This corresponds to $M_n \approx 2$ kDa, in good agreement with GPC data (4.3kDa, versus polystyrene), which typically overestimates by a factor of 2 but we note that this overestimation decreases with decreasing nominal molecular weight.

These reactions contrast the reported behavior of silyl thiophenes during fluoride-activated palladium-catalyzed Hiyama coupling,^{123, 124} during which the thienyl groups are expelled from the catalytic cycle following proteodesilylation. We have, however, found that stoichiometric CsF and a palladium catalyst can indeed lead to moderately successful Hiyama coupling between silyl thiophenes and iodobenzene (~40% conversion, not shown). The fluoride source may be crucial.

2.3 Synthesis of alternating 3,3-Dihexyl-3,4-dihydro-2*H*-thieno[3,4-*b*][1,4]dioxepine [ProDOT(Hx)₂] and C₆F₄ copolymer

In regard to the polymers **2-1** through **2-3**, both 3 and 4 positions of thiophene moieties are substituted, and steric repulsion between pendant alkoxy groups and fluorides should cause significant twisting along the backbone in the polymers. Blocking the 3- and 4-positions of thiophene with an alkylenedioxy group yields a highly electron-rich fused heterocycle, 3,4-alkylenedioxythiophene, where the alkylenedioxy bridge may slightly diminish steric repulsion between thiophene and fluorinated aromatic units relative to 3,4-dialkoxy groups.¹²⁵ So the dialkylated 3,4-propylenedioxythiophene (ProDOT-R₂) was chosen to incorporate into polymer backbones, and its longer alkyl groups should increase solubility of polymers in organic solvents.

As shown in **Figure 2. 11**, monomer **2-18** was synthesized in high yield by bis-lithiation of compound **2-17**, provided by the group of John Reynolds (University of Florida), with *n*-BuLi and quenching with TMSCl. Polymer **2-19** was prepared via the same methodology as employed for polymers **2-1** through **2-3**. The product polymer was purified by extraction with deionized water and precipitation into methanol to remove inorganic impurities and low molecular weight oligomers. Polymer **2-19** was obtained in quantitative yield as a bright yellow solid that was easily soluble in THF, toluene, chloroform, and methylene chloride.

Moderately high molecular weight was obtained only when the temperature was at least 110°C and the ratio of C₆F₆ and **2-18** was 1.0. The latter point indicates that all functional groups have equal reactivity throughout the polymerization. This stands in contrast to the polymerizations with 3,4-dialkoxythiophenes described above. It is no

surprise that the differing electronic nature of the ProDOT monomer alters its chemical reactivity. The restricted dihedral angles between the oxygen lone pairs and the thiophene ring alter the electron donating/withdrawing ability of the pendant alkoxy groups. Therefore the reactivity of the carbon-silicon bonds and likely the activating/directing effect of the thiophene ring on the C₆F₅ end groups of growing polymer chains are different than in the case of 3,4-dialkoxythiophenes.

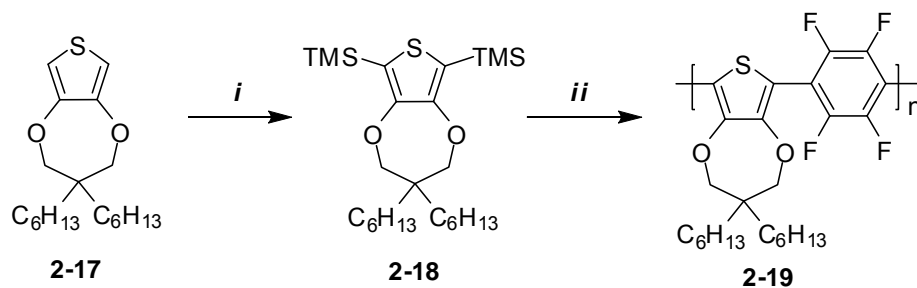


Figure 2. 11 Synthesis of alternating ProDOT(Hx₂)-C₆F₄ copolymer. *i*: a) *n*-BuLi, hexane/DME, 0°C; b) TMSCl, 0°C, then r.t., 96%; *ii*: 0.1 eq CsF, 0.2 eq 18-crown-6, C₆F₆, toluene, 110°C, 100%.

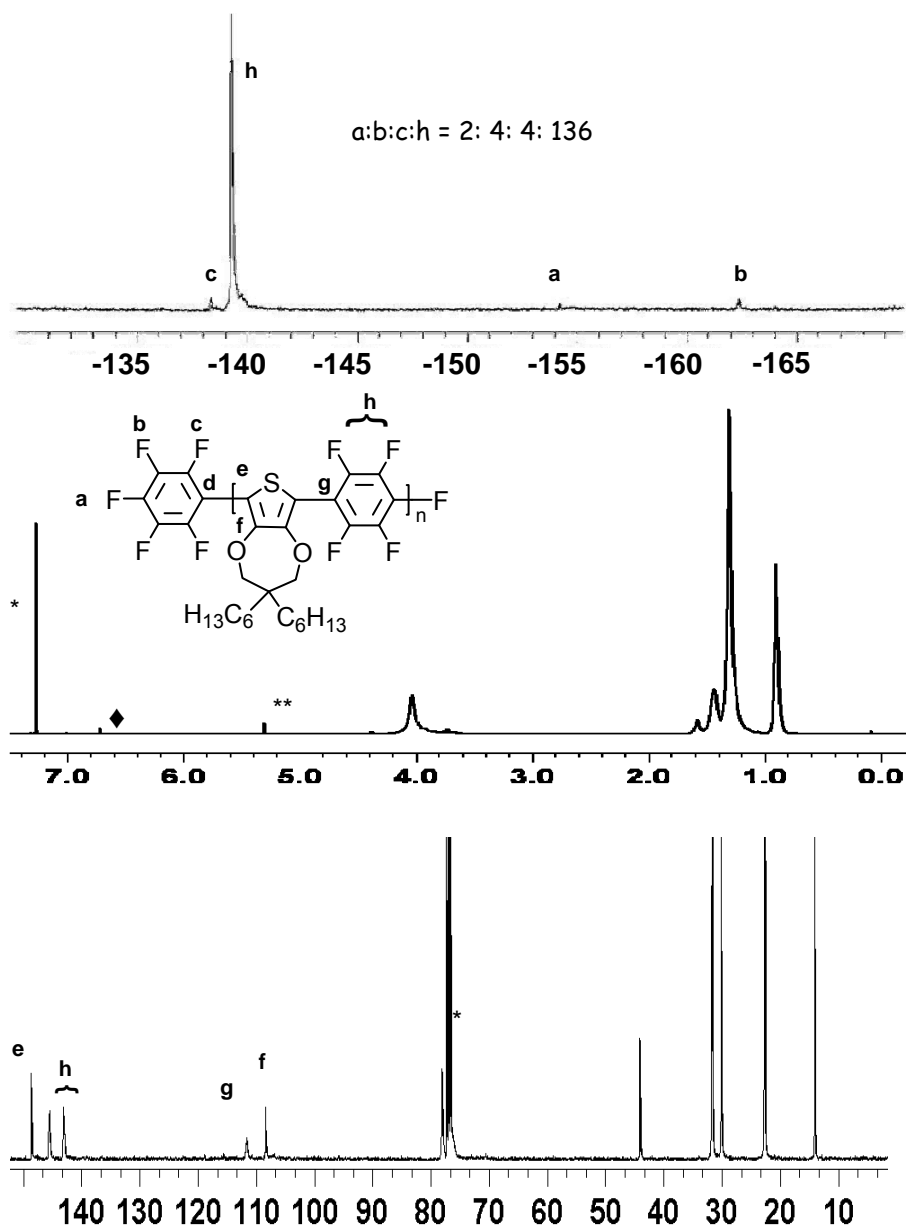


Figure 2.12 ¹⁹F (top) , ¹H (middle) and ¹³C (bottom) NMR spectra of polymer **2-19** in CDCl₃. Number average degree of polymerization calculated from ¹⁹F NMR is $P_n = (136F/4F) \approx 34$, or 68 aromatic rings ($M_n \approx 17$ kDa), in good agreement with GPC data ($M_n = 35$ kDa, versus polystyrene), which typically overestimates by a factor of 2. *(H)DCCl₃ solvent/reference, **CH₂Cl₂ residue and ♦ProDOT end group.

¹⁹F, ¹H and ¹³C NMR spectra for **2-19** indicate high chemical purity, in accordance

with the structure shown in **Figure 2. 11** (see **Figure 2. 12** for full spectra). ^{19}F NMR (**Figure 2. 12**, top) showed one major signal corresponding to 1,2,4,5-tetrafluorobenzenes of the repeating unit, along with three smaller signals arising from end-groups. The ^1H NMR spectrum (**Figure 2. 12**, middle) showed a very small signal from the ProDOT end group which must arise from a low degree of protodesilylation. The signals arising from carbons connected to fluorine in the polymer backbone were split into a doublet of multiplets by fluorine ($J_{\text{doublet}}=248\text{Hz}$). Number average degree of polymerization calculated from ^{19}F NMR is $P_n = (136\text{F}/4\text{F}) \approx 34$, or 68 aromatic rings ($M_n \approx 17$ kDa), in good agreement with GPC data ($M_n = 35\text{kDa}$, versus polystyrene), which typically overestimates by a factor of 2. The polydispersity is around 2.2 ($\text{PDI}=2.2$).

2.4 Synthesis of alternating 3,3',4,4'-tetrabutoxy-2,2'-bithiophene and C_6F_4 copolymer

As described above, steric repulsion between pendant alkoxy groups and fluorine atoms should cause significant twisting along the backbone in the polymers **2-1** through **2-3**, and **2-19**. We chose to also investigate 3,3',4,4'-tetrabutoxy-2,2'-bithiophene (**2-20**) to slightly increase conjugation along the polymer backbones, leading to a decrease in optical energy gap. While there will still be steric repulsion between pendant alkoxy and fluoride substituents, the two thiophene rings in each repeat unit should be able to become coplanar.

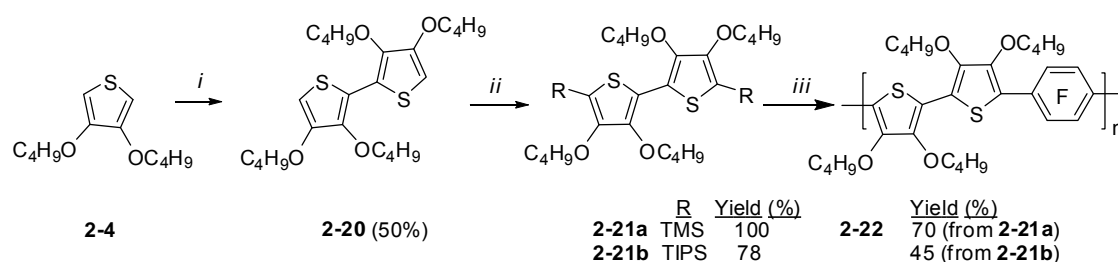


Figure 2. 13 Synthesis of alternating 3,3',4,4'-tetrabutoxy-2,2'-bithiophene- C_6F_4 copolymer. *i*: a). *n*-BuLi, THF, -78°C , b). CuCl_2 , -78°C then r.t.; *ii*: a). *n*-BuLi, THF, -78°C , b). TMSCl (**2-21a**)/TIPSCl (**2-21b**), -78°C then r.t.; *iii*: CsF, 18-crown-6, toluene, 80°C , using monomer **2-21a** and CsF, 18-crown-6, THF, 70°C , using monomer **2-21b**.

As shown in **Figure 2. 13**, 3,3',4,4'-tetrabutoxy- 2,2'-bithiophene (**2-20**) was

synthesized from 3,4-dibutoxythiophene via a metalation reaction followed by dimerization with CuCl_2 .¹²⁶⁻¹²⁸ Monomer **2-21a** was prepared from compound **2-20** by metalation with *n*-BuLi and reaction with TMSCl. Due to the large number of electron-donating substituents, **2-21a** is not stable towards aqueous acid or base, or even with silica gel, as it easily undergoes ipso-substitution (protodesilylation). The cation resulting from protonation of the 5(5') position can be highly delocalized as illustrated in **Figure 2. 14**. Therefore, monomer **2-21a** had to be isolated under strictly anhydrous conditions using Schlenk techniques. The reaction mixture was concentrated under argon, then the organic product was dissolved in 20mL hexane and 5mL CH_2Cl_2 and separated from inorganic salts via cannula filtration. To ensure quantitative conversion and eliminate the need for column chromatography, molar excesses of *n*-BuLi and TMSCl were employed. A yellow solid (**2-21a**) was obtained after evaporation of solvents under reduced pressure. Monomer **2-21b**, carrying triisopropyl silyl groups was much more stable and could be isolated in 78% yield following standard aqueous workup and column chromatography.

Polymer **2-22** was prepared with the same methodology as illustrated for polymers **2-1** through **2-3** using CsF and 18-crown-6 as catalyst system and toluene as solvent at 80°C. Interestingly, monomer **2-21b** is completely unreactive in toluene, but polymer **2-22** may be obtained from monomer **2-21b** if THF is used as solvent. Monomer **2-21a** is reactive in either solvent. This mirrors the reactivity of various silyl compounds towards protodesilylation as a function of the steric bulk of the silane. This difference in reactivity opens the possibility for selective reaction at the two “ends” of a monomer carrying TMS and TIPS groups. This selectivity could possibly be exploited for step-wise buildup of well-defined oligomers, including dendrimers if multifunctional monomers (branching units) are employed that are functionalized with TMS and TIPS groups.

Polymer **2-22** was obtained in high chemical purity which can be seen from ^1H and ^{19}F NMR spectra (**Figure 2. 15**) and moderately high molecular weights ($M_n = 20\text{kDa}$, PDI = 2.14 from monomer **2-21a** and $M_n = 15\text{kDa}$, PDI = 1.81 from monomer **2-21b**). Polymer **2-22** is a greenish yellow solid which is readily soluble in common organic solvents such as THF, chloroform, 1,1,2,2-tetrachloroethane and toluene.

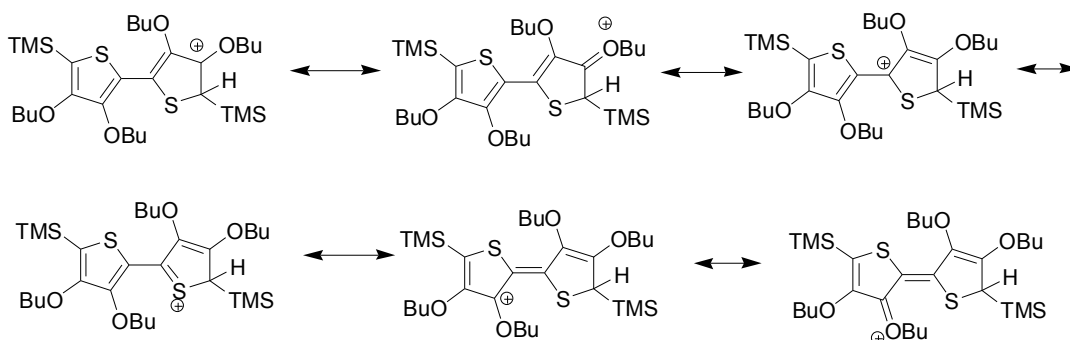


Figure 2. 14 Resonance structures of the intermediate for compound **2-21a** undergoing ipso-substitution (protodesilylation).

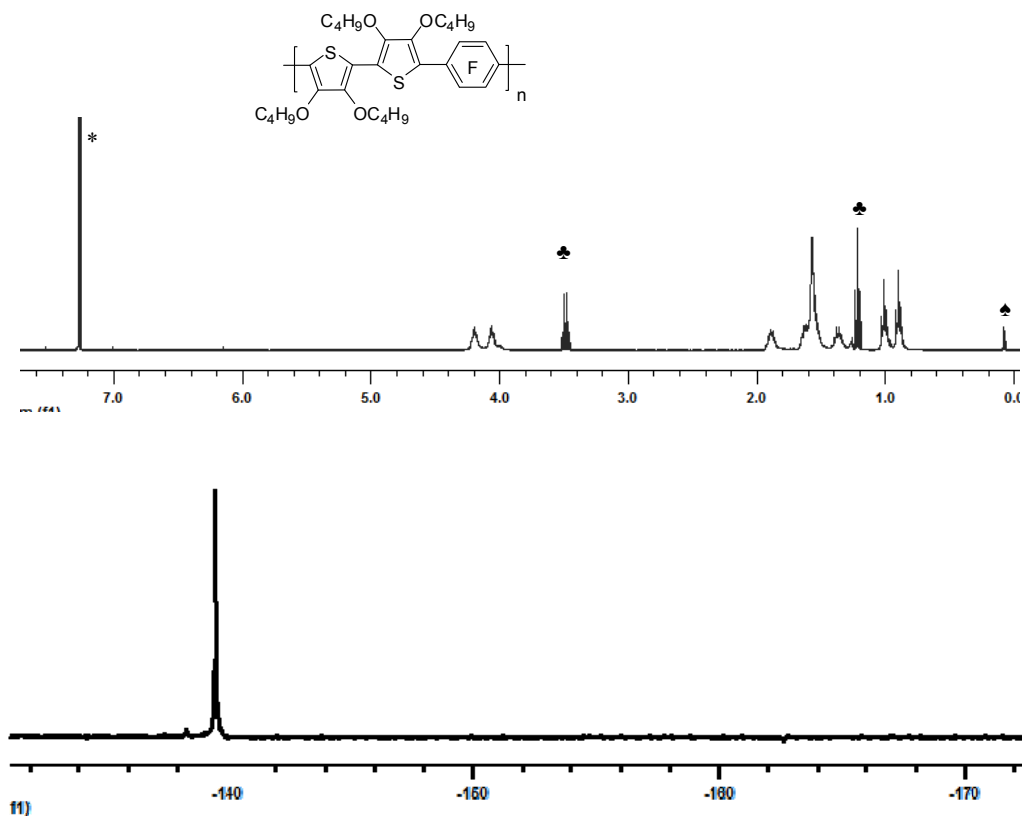


Figure 2. 15 ¹H (top) and ¹⁹F (bottom) NMR spectra of polymer **2-22** in CDCl₃. *(H)DCCl₃ solvent/reference, ♣ ether residue and ♠ silicone grease.

2.5 Synthesis of alternating 4,8-dialkyl/dialkoxy benzodithiophene and C₆F₄ copolymers

Self-organization in many solution-processed, semiconducting conjugated polymers

results in complex microstructures: ordered microcrystalline domains within an amorphous matrix. Charge transport is usually limited by the most difficult hopping processes and is therefore dominated by the disordered matrix, resulting in low charge carrier mobilities.¹²⁹ Analysis of the FET performance of polymer semiconductors shows that polymer regioregularity is crucial to establishing high crystalline order which is necessary for achieving high mobility.⁷⁴⁻⁷⁶ To diminish torsion/increase planarization and therefore conjugation along the polymer backbone, thiophene containing monomers without substituents in the 3-position were investigated. Benzodithiophene (BDT) units have recently been incorporated into (co)polymers¹³⁰ showing high conductivity when doped and into simply-substituted small molecules⁹⁸ with good field-effect mobility. Therefore we chose to study 4,8-Dialkyl/dialkoxy benzothiophene-based monomers (**2-24**) which unify several potentially beneficial properties: 1) an inherent structural symmetry which allows them to be linked at the C-2 and C-6 positions without regiochemical variability generally associated with the use of polymer semiconductors for OTFT fabrication, 2) location of substituents at the C-4 and C-8 positions should completely eliminate steric/electronic repulsion between them and the fluoride substituents, 3) the completely planar monomer could lead to enhanced π - π stacking order for efficient charge carrier transport to afford high FET mobility,^{131, 132} 4) electron-richness should enhance intermolecular interactions with electron-accepting perfluoroarenes.¹³³

Unfortunately, only very low molecular weight oligomers (**2-26**) could be obtained from monomers **2-25**. Due to time limitations, optimization of this polymerization will have to be carried by others in the future.

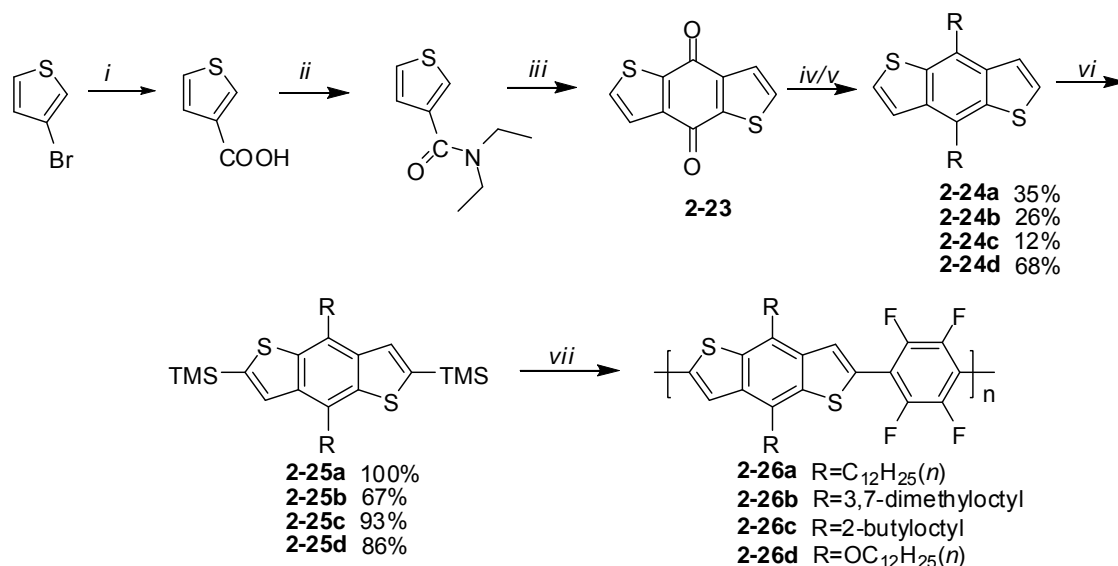


Figure 2. 16 Synthesis of alternating 4,8-dialkyl/dialkoxy benzodithiophene -C₆F₄ copolymers. *i*: *n*-BuLi, ether, -78°C, CO₂, 48%; *ii*: a). SOCl₂, CHCl₃, reflux, b). diethyl amine, 0°C, 100%; *iii*: a). LDA, ether, -78°C, 57%, b) H₂O; *iv*: for **2-24a-2-24c** a). RMgBr, THF, 70°C, b). SnCl₂; *v*: for **2-24d** a). Zn, NaOH in the mixture of ethanol and water, reflux, b). *p*-CH₃C₆H₄SO₂-OR, reflux; *vi*: a). *n*-BuLi, THF, -78°C, b). TMSCl; *vii*: CsF, 18-crown-6, toluene, 80°C.

2.6 Synthesis of alternating 3,3'-dialkyl-2,2'-bithiophene and C₆F₄ copolymers and their nonfluorinated counterparts

2.6.1. Introduction

For electronic devices, self-assembly of the polymer chains in the solid state can maximize charge transport within the bulk material, particularly through π -stacking and leading to optimized device performance.¹³⁴ Co-facial π -stacking can be achieved by (1) exploiting liquid crystal properties,¹³⁵ (2) creating larger π system,¹³⁶ (3) introducing the substituents to molecules that preclude edge-to-face interactions,⁶⁵ (4) exploiting attraction between electron-rich and -poor segments.^{83, 84, 96, 137, 138} Recently, attractive interactions between fluorinated (π F) and nonfluorinated (π) π -electron units provide fairly predictable control over supramolecular behavior, which has been most clearly demonstrated with small molecules.^{71, 139-142} In our group, the new methodology without

transition metals was developed to synthesize alternating copolymers between highly fluorinated π -electron systems and silyl-functionalized monomers. It can be expected that perfectly alternating structures should lead to enhanced π -stacking due to intermolecular π - π F interactions.

Alkyl substituents not only increase solubility of polymers, but can also tune electronic and optical properties. Reports of the effects of head-to-head bithiophene linkages on the solid-state properties of conjugated polymers are conflicting. It was reported that for poly(4,4''-dioctylterthiophene) containing 3,3'-dioctyl-2,2'-bithiophene (**2-27a**) (**Figure 2. 17**) there are head-head steric interactions between the pendant octyl chains on neighboring thiophene rings, which should result in a reduction in conjugation along the backbone.¹⁴³ In this same report, it was claimed that steric interactions were diminished in polymer **2-27b** because the repeating units contain only tail-tail linkages. We disagree with this assessment as there should be little difference, in terms of steric repulsion along the polymer backbones, between polymers **2-27a** and **2-27b**. Instead, the differences in electronic properties are more likely dictated by the packing of the side chains, which is likely different for these two polymers due to different side-chain spacing along the backbone.

However, for polymer poly[4,7-bis(4-octyl-2-thienyl)-2,1,3-benzothiadiazole] (**2-28b**) steric repulsion between the benzothiadiazole unit and thiophene side-chains influences the planarity and conjugation of the polymer chains more than that between the adjacent thiophene rings.¹⁴⁴ (**Figure 2. 17**) The polymer with head-to-head linkages (**2-28b**) displayed significantly reduced optical band gap compared to its analogue (**2-28a**) with tail-tail linkages. In addition, it was revealed by crystallographic studies that the C_6F_4 unit of the conjugated oligomer (**2-29**) is coplanar with the adjacent thiophene rings, and exhibits close H \cdots F and S \cdots F non-covalent intramolecular contacts.¹⁴⁵ (**Figure 2. 18**)

Therefore we chose to incorporate 3,3'-dialkyl-2,2'-bithiophene units into copolymers with C_6F_6 (**2-33**) (**Figure 2. 19**). We proposed that the rings along these copolymer backbones could be highly coplanar despite their head-to-head thiophene linkages. The coplanarity will be enforced by intermolecular attraction between thiophene and C_6F_4 units, as well as via intramolecular S-F and H-F interactions. The recently implemented design principles which greatly enhance order, device performance and stability that were

described at the outset of this chapter may all be met by these polymers. The side chains are more spaced out along the backbone to allow interdigitation, and the IP will likely be increased by the fluorine substituents. Polymers **2-33** were prepared with three different types of alkyl substituents in order to study the effect of steric bulk on solubility, and self-assembly. Their syntheses and those of non-fluorinated controls are described below.

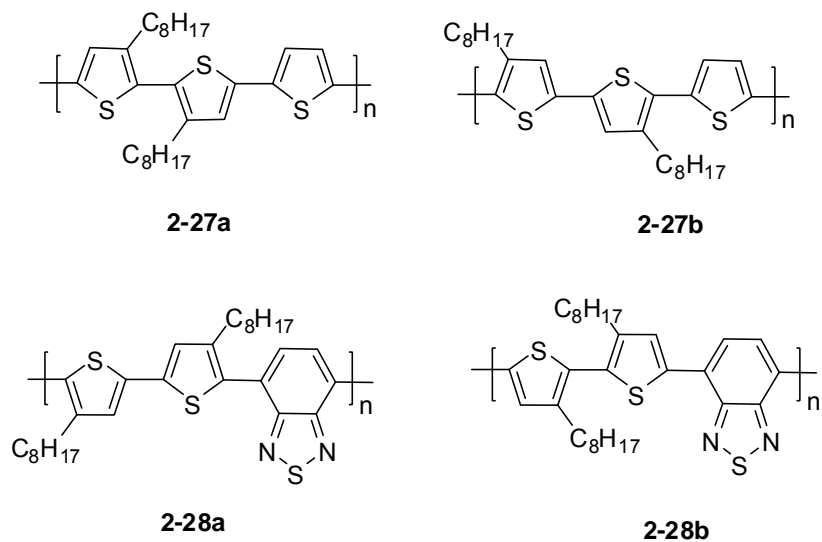


Figure 2. 17 Structures of polymer **2-27** and **2-28**.

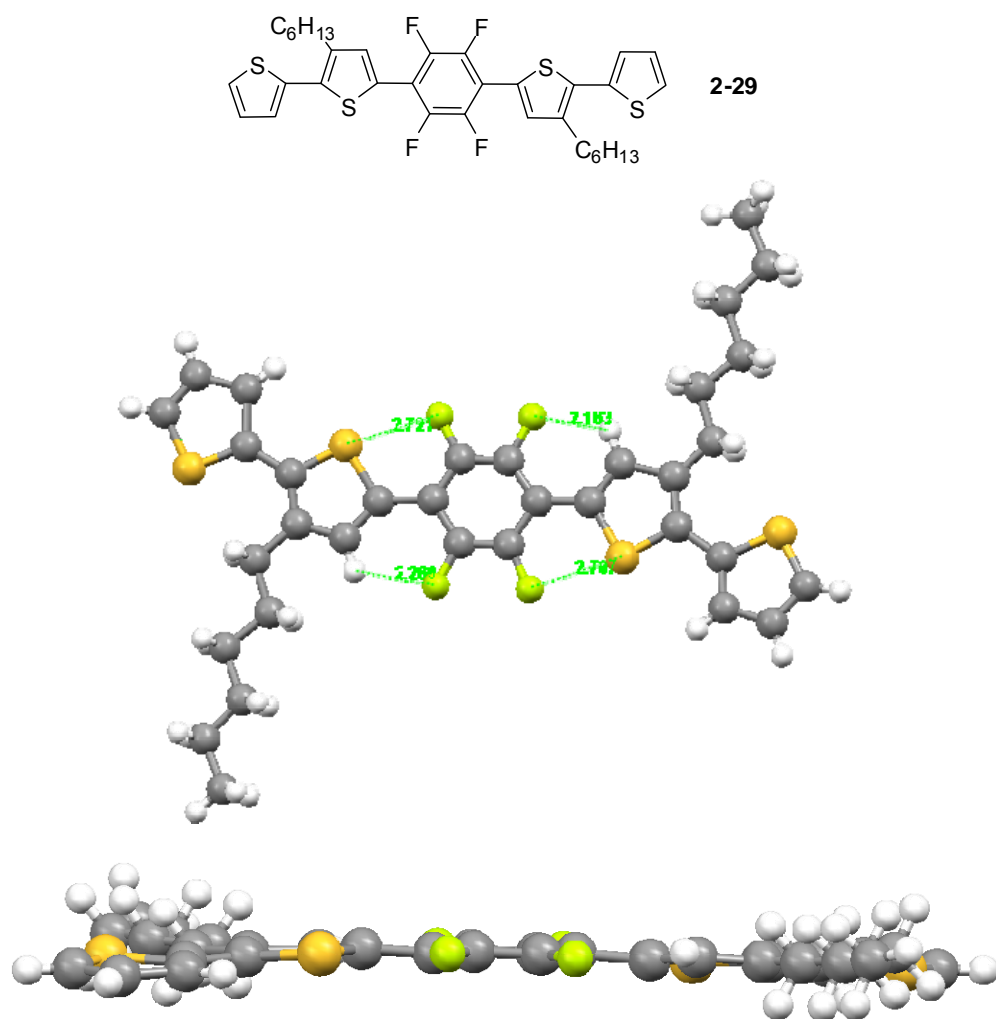


Figure 2. 18 X-ray crystal structure of compound **2-29**,¹⁴⁵ showing relevant intramolecular contacts (middle) and a view down molecular short axis (bottom).

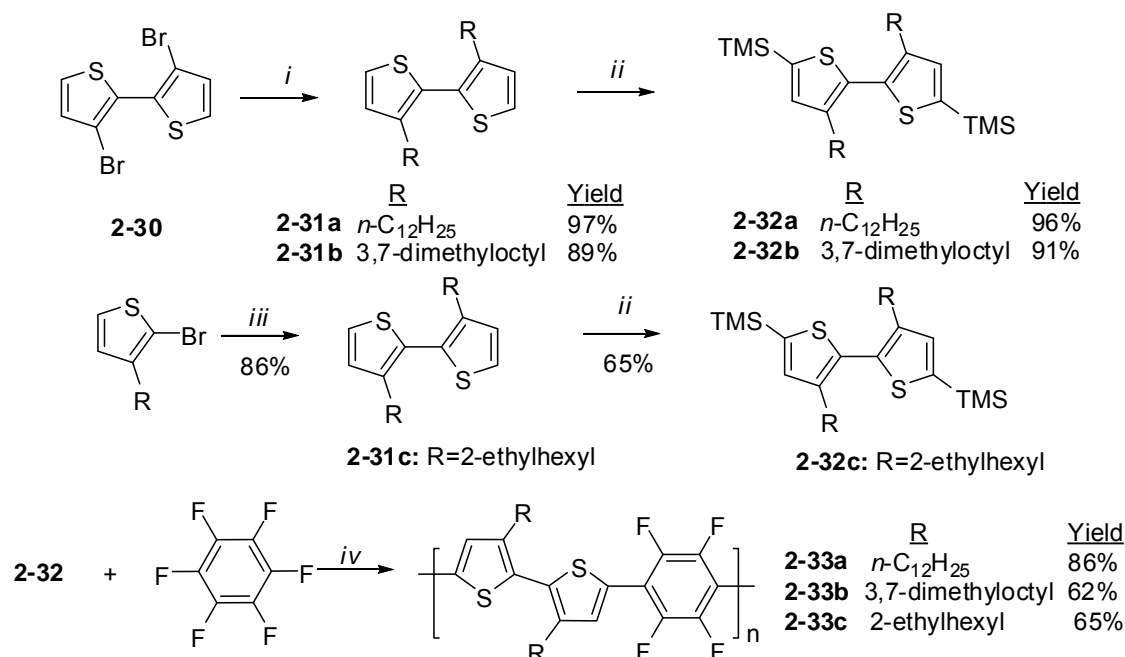


Figure 2. 19 Synthesis of alternating 3,3'-dialkyl-2,2'-bithiophene- C_6F_4 copolymers. *i*: RMgBr, ether, $\text{NiCl}_2(\text{dppp})$, reflux; *ii*: a). $n\text{-BuLi}$, TMEDA, hexane, 0°C for 0.5h then reflux for 2h, b). TMSCl, 0°C then r.t.; *iii*: $\text{Ni}(\text{COD})_2$, 2,2'-bipyridyl, COD, DMF, toluene, 80°C ; *iv*: CsF, 18-crown-6, toluene, 80°C .

2.6.2. Synthesis of fluorinated copolymers

The general synthetic routes towards bithiophene-containing monomers and fluorinated polymers are outlined in **Figure 2. 19**. Monomers were synthesized by two routes. **2-31a** and **2-31b** were prepared from 3,3'-dibromo-2,2'-bithiophene (**2-30**) by Kumada coupling reaction with dodecylmagnesium bromide or 3,7-dimethyloctyl magnesium bromide catalyzed by a Ni(II) complex. The preparation of **2-31c** was different because 2-bromo-3-(2-ethylhexyl)thiophene was available in-house. Thus the homocoupling of 2-bromo-3-(2-ethylhexyl)thiophene with zero-valent nickel, in the presence of cyclooctadiene and 2,2'-bipyridyl in the mixture of dimethylformamide and toluene, gave the product **2-31c** as a brown liquid in 86% yield. 3,3'-dialkyl-2,2'-bithiophene (**2-31**) was lithiated by $n\text{-BuLi}$ at low temperature and quenched with TMSCl to obtain monomers 3,3'-dialkyl-5,5'-bis(trimethylsilyl)-2,2'-bithiophene (**2-32**).

The polymers **2-33** were prepared with the same methodology as described above using CsF and 18-crown-6 as catalysts and toluene as solvent at 80°C. Polymers **2-33** were obtained in high chemical purity which can be seen from ¹H and ¹⁹F NMR spectra (see **Figure 2. 20** for **2-33a**) and high molecular weights ($M_n = 22\text{kDa}$, PDI = 2.09 for **2-33a**, $M_n = 20\text{kDa}$, PDI = 1.96 for **2-33b** and $M_n = 11\text{kDa}$, PDI = 2.1 for **2-33c**). Before beginning structure-property studies, there are immediately obvious differences between polymers **2-33a,b** and polymer **2-33c**, which carries the most bulky side-chains (greatest steric bulk in the vicinity of the polymer backbone). Polymers **2-33a** and **2-33b** were isolated as orange-to-red solids which were readily soluble, but only in hot common organic solvents such as THF, chloroform, 1,1,2,2,-tetrachloroethane and toluene, while **2-33c** was isolated as a yellow solid which was easily soluble in common organic solvents at room temperature.

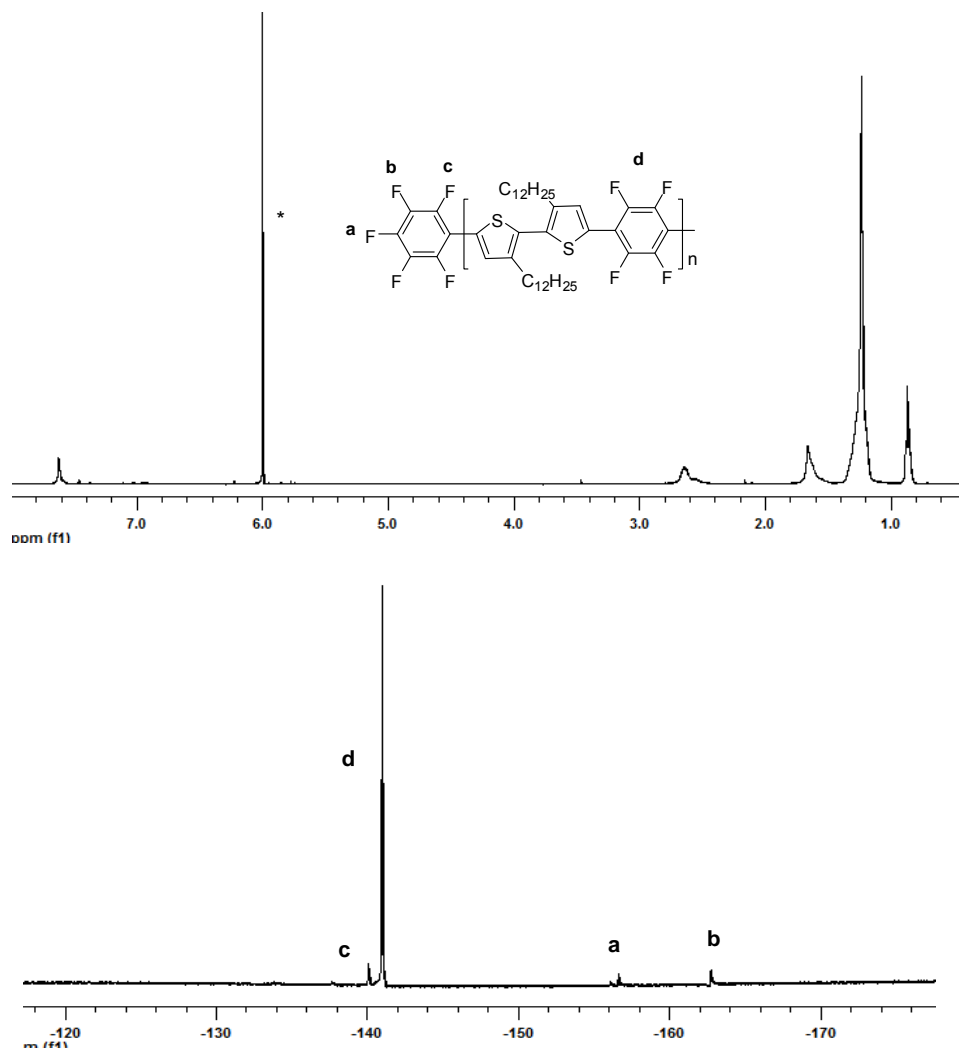


Figure 2. 20 ^1H (top) and ^{19}F (bottom) NMR spectra of polymer **2-33a** in $\text{C}_2\text{D}_2\text{Cl}_4$. * (H) $\text{C}_2\text{D}_2\text{Cl}_4$ solvent/reference.

2.6.3. Synthesis of nonfluorinated copolymers

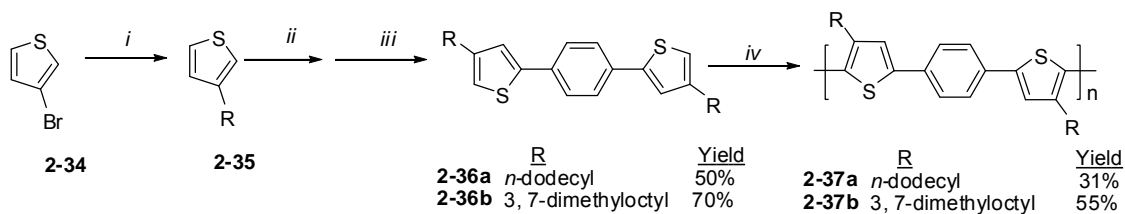


Figure 2. 21. Synthesis of non-fluorinated copolymers **2-37**. *i*: RMgBr , $\text{NiCl}_2(\text{dppp})$, ether; *ii*: a). LDA , THF , -78°C , 1h, b). ZnCl_2 , -78°C for 1h, r.t. for 1h; *iii*: $\text{Pd}(\text{PPh}_3)_4$,

THF, 1,4-dibromobenzene, 70°C for 48h; *iv*: FeCl₃, CHCl₃, 50°C for 48h (**2-37a**) or r.t. for 48h (**2-37b**).

To investigate the effect of fluorination on the properties of copolymers such as electrical and optical properties and self-assembly in the solid state, non-fluorinated versions **2-37** of copolymers **2-33** were synthesized as controls. (**Figure 2. 21**) 3-Alkyl thiophenes were synthesized from 3-bromo-thiophene through the Kumada coupling reaction. The synthesis of the monomers exploited the Negishi coupling reaction between organozinc chloride and halosubstituted compounds under the catalysis of palladium complex. 3-Alkylthiophenes were converted to (4-alkylthiophen-2-yl)zinc(II) chlorides via lithiation, followed by transmetalation reaction with anhydrous zinc chloride in THF. Lithium diisopropylamine (LDA), a significantly bulky base, was employed to selectively lithiate the 5-position of the thiophene rings. (4-Alkylthiophen-2-yl) zinc (II) chlorides were coupled with 1,4-dibromobenzene in THF catalyzed by tetrakis (triphenylphosphine) palladium (0) to afford monomers **2-36a** and **2-36b** in 50% and 70% respectively after purification. The polymers were obtained via FeCl₃ oxidative polymerization in chloroform at 50°C and 25°C for polymer **2-37a** and **2-37b** respectively. After being precipitated into methanol and dedoped with aqueous ammonium hydroxide, these polymers were obtained as brownish-yellow solids, suggesting inorganic residues. They were obtained as bright yellow solids after heating at 60°C in hexanes followed by passage through a short pad of silica gel.

2.7 Synthesis of alternating 3,3'-dialkoxy-2,2'-bithiophene and C₆F₄ copolymers

The exact analogues of polymers **2-33**, but carrying alkoxy side chains in place of alkyl chains were prepared for two reasons. Alkoxy side chains should increase the electron-richness of the thiophene units, perhaps leading to a greater tendency toward quinoidal character along the backbones, and lower optical energy due to intramolecular charge transfer between electron-rich and -poor segments.¹⁴⁶⁻¹⁴⁸ Thiophene polymers bearing alkoxy, instead of alkyl side chains, have been shown to display reduced optical energy gaps.^{149, 150} 3,3'-Dialkoxy-2,2'-bithiophene units, such as 3,3'-dipentyloxy-2,2'-bithiophene¹⁵¹ and 3,3'-dioctyloxy-2,2'-bithiophene¹⁵² although

containing a head-to-head linkage, crystallize with their thiophene rings in the same plane as evidenced by single X-ray structures and polymer analogues display optical properties which suggest coplanar backbones (relatively small optical energy gaps).^{151, 153, 154} It has been proposed that there is actually an electrostatic attraction between pendant oxygen atoms and thienyl sulfur atoms which may contribute to the drive towards backbone planarization.¹⁵⁵

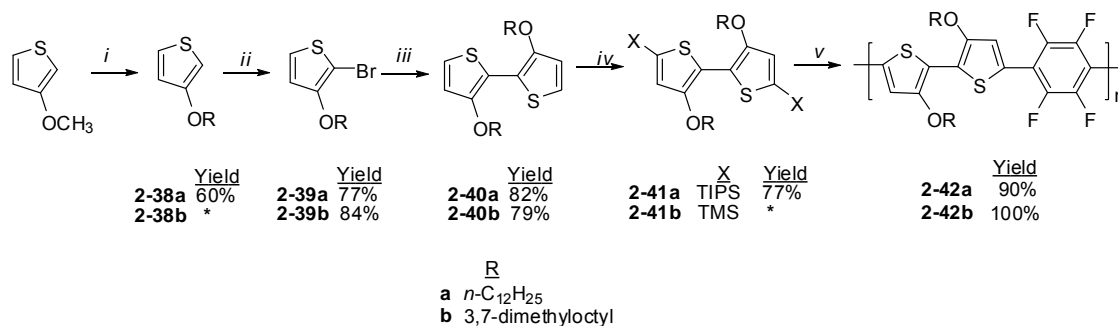


Figure 2. 22 Synthesis of alternating 3,3'-dialkoxy-2,2'-bithiophene-C₆F₄ copolymers **2-42**. *i*: ROH, PTSA, toluene, reflux; *ii*: NBS, DMF, 0°C; *iii*: Ni(COD)₂, 2,2'-bipyridyl, COD, DMF, toluene, 80°C; *iv*: a) *n*-BuLi, THF, 0°C, b) TMSCl/TIPSCl, 0°C; *v*: CsF, 18-crown-6, toluene, 80°C, for **2-42b** and CsF, 18-crown-6, THF, 70°C, for **2-42a**. The yield of **2-38b** was not calculated because it was not pure and purified further in the next step. The yield of **2-41b** was not calculated as it was sensitive to moisture.

The general synthetic routes towards 3,3'-dialkoxy-bithiophene monomers and fluorinated copolymers are outlined in **Figure 2. 22**. Compounds **2-40** were obtained from 3-methoxythiophene through transesterification with the corresponding alcohols under catalysis by PTSA, followed by bromination with NBS and Yamamoto coupling. 3,3'-dialkoxy-2,2'-bithiophenes (**2-40**) were lithiated by BuLi at low temperature and quenched with TIPSCl or TMSCl to obtain monomers **2-41a/41b**. Similar to the tetraalkoxy-bithiophene monomers **2-21**, monomer **2-41b** was not stable towards aqueous acid, base, and silica gel, due to high tendency to undergo ipso-substitution (protodesilylation). Monomer **2-41b** was likewise prepared using a large excess of *n*-BuLi and TMSCl to ensure complete conversion eliminating the need for chromatography, then separated from inorganic residues and volatile organic by cannula filtration and concentration under reduced pressure, respectively. Monomer **2-41a**,

bearing more bulky TIPS groups, was more stable and could be isolated in 77% yield following standard aqueous workup and column chromatography.

Polymer **2-42a** could be prepared via the same methodology as described above using CsF and 18-crown-6 as catalyst system and toluene as solvent at 80°C. Again similar to the tetraalkoxybithiophene monomers, monomer **2-41b**, was unreactive in toluene but could be copolymerized with C₆F₆ in the more polar THF. Due to limited time, only one attempt was made to prepare polymers **2-42a** and **2-42b**. Each was obtained with rather low molecular weight (approx 3kDa) as estimated by combined ¹H and ¹⁹F NMR end-group analysis. ¹H NMR spectra indicated a rather high number of protodesilylated thiophene end-groups, which could explain the relatively low degrees of polymerization. Despite their low molecular weight, oligomers **2-42a** and **2-42b** are deep purple (almost black) in the solid state suggesting relatively low optical energy gaps. These oligomers are only weakly fluorescent in the solid state, fluoresce orange in concentrated solution, but fluoresce yellow in very dilute solution, suggesting strong interactions between electron-rich and electron-poor parts in solution and the solid state.

2.8 Synthesis of alternating 3,3'-dialkyl-2,2'-bithiophene and C₆F₄ copolymers by oxidative polymerization

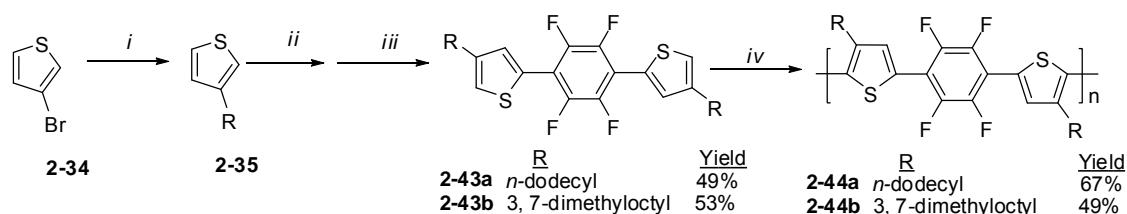


Figure 2. 23 Synthesis of fluorinated copolymers **2-44**. *i*: RMgBr, NiCl₂(dppp), ether; *ii*: a). LDA, THF, -78°C, 1h, b). ZnCl₂, -78°C for 1h, r.t. for 1h; *iii*: Pd(PPh₃)₄, THF, 1,4-dibromo-2,3,5,6-tetrafluorobenzene, 70°C for 48h; *iv*: FeCl₃, CHCl₃, 70°C for 48h (**2-44a**) or r.t. for 48h (**2-44b**).

Alternating 3,3'-dialkyl-2,2'-bithiophene-C₆F₄ copolymers **2-44** were prepared via oxidative polymerization alternatively in order to compare this standard methodology to our newly described method. The syntheses of the monomers **2-43** and polymers **2-44** were executed similar to those of monomers **2-36** and polymers **2-37**. Polymers **2-44**

were obtained in high chemical purity which can be seen from ^1H and ^{19}F NMR spectra (**Figure 2. 24**) and relatively high molecular weights ($M_n = 14\text{kDa}$, PDI = 2.55 for polymer **2-44a** and $M_n = 22\text{kDa}$, PDI = 2.78 for polymer **2-44b**). Polymers **2-44** are orange to deep red or dark brown solids, depending on isolation conditions. The dark brown color suggests residual iron impurities. This color can be removed after passing the polymers through a short pad of silica gel.

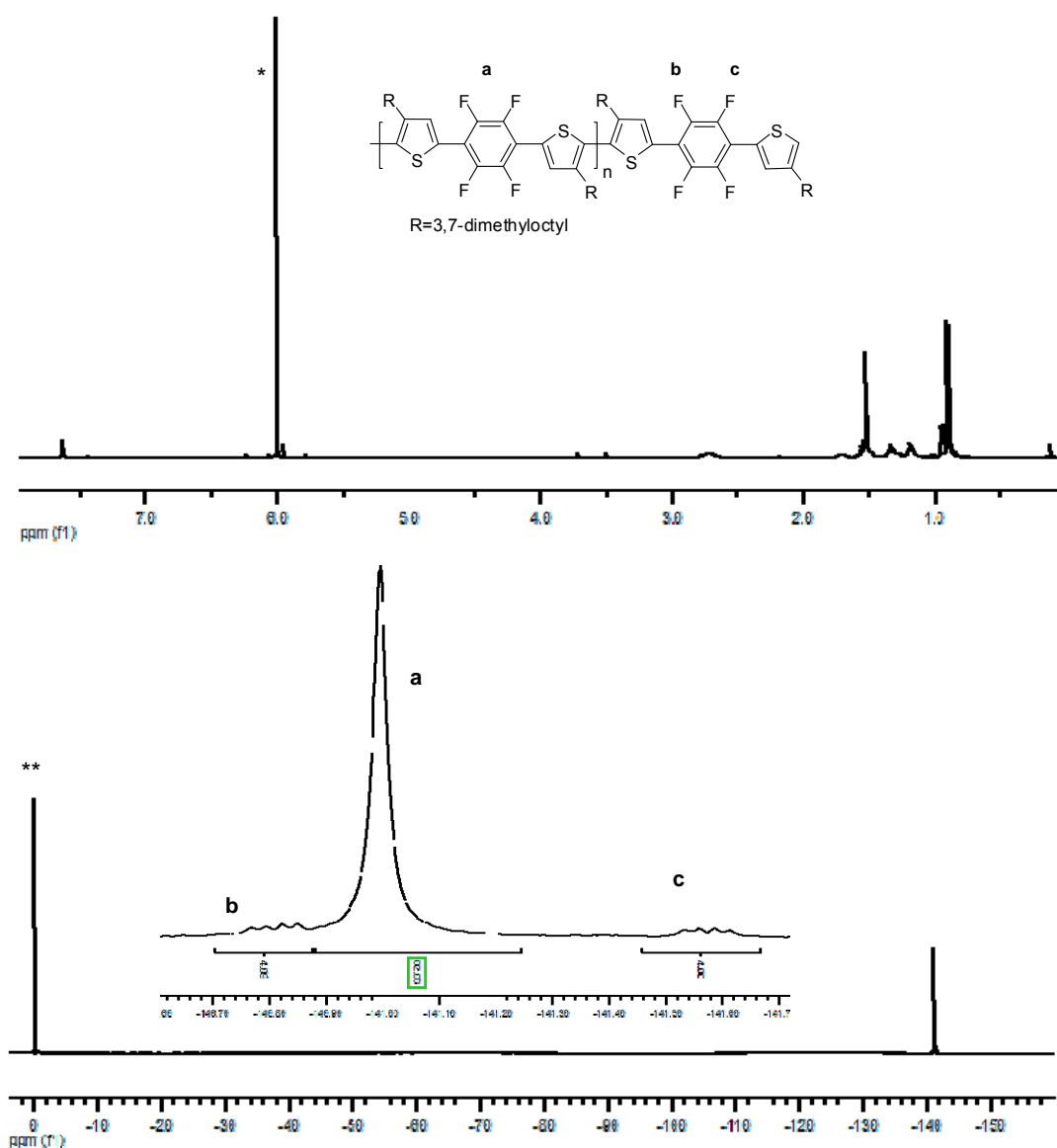


Figure 2. 24 ^1H (top) and ^{19}F (bottom) NMR spectra of polymer **2-44b** in $\text{C}_2\text{D}_2\text{Cl}_4$. Number average degree of polymerization calculated from ^{19}F NMR is $P_n = (82F/4F+2) \approx 22$, or 66 aromatic rings ($M_n \approx 13\text{ kDa}$), in good agreement with GPC data ($M_n = 22\text{kDa}$,

versus polystyrene), which typically overestimates by a factor of 2. *(H) D₂C₂Cl₄ solvent/reference and ** CCl₃F.

2.9 Polymer Characterization

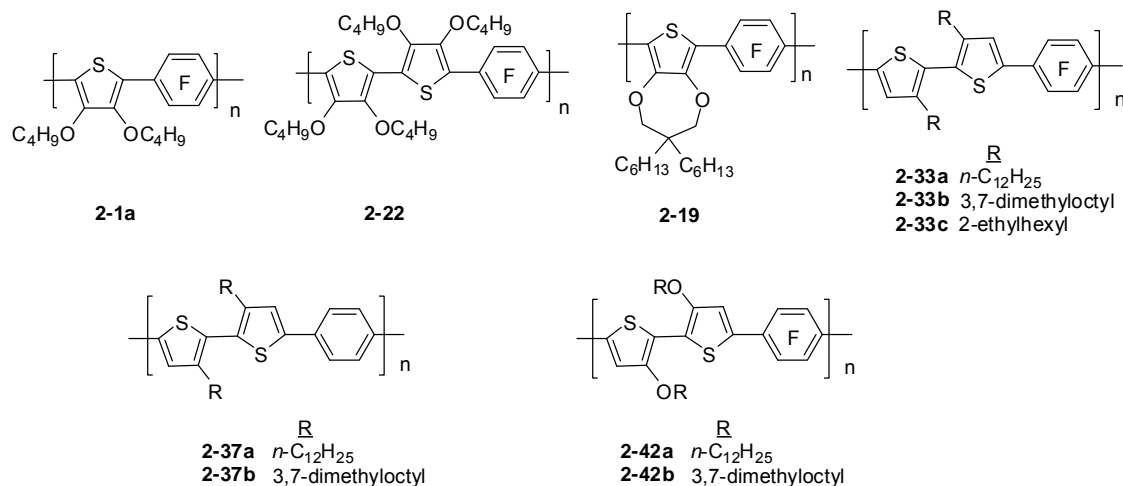


Figure 2. 25 Structures of polymers.

2.9.1 Yields, GPC and DSC analysis

The structures of polymers which have been characterized are collected in **Figure 2. 25**. The yields, molecular weight, optical data and melting points or glass transition temperatures of the polymers are listed in **Table 2. 2**. Most of the yields are good, while yields of **2-37a** and **2-37b** are somewhat moderate likely due to losses incurred during passage through a silica column to remove the iron residue. The molecular weights are moderately high for most polymers as determined by GPC using polystyrene standards. The molecular weights of **2-42a** and **2-42b** without optimizing reaction conditions are quite low, such that their actual molecular weights fell outside the calibration range of the employed GPC. NMR showed that they are only oligomers. Most polymers showed a glass transition or melting transition, observable as 2nd order (step change or change in slope) and 1st order transitions (minima) in DSC traces.

Table 2. 2 Properties of polymers

Polymer	yield (%)	M _n [PDI] ^a (kDa)	λ _{max} sol abs ^b /PL ^c (nm)	λ _{max} film ^g abs/PL (nm)	λ _{onset} (abs) sol/film (nm)	E _g ^h sol/film (eV)	T (°C)
2-1a	85	28[2.7]	334/370	-	380/-	3.26/-	57 ^d
2-19	100	35[2.2]	347/425	-	391/-	3.17/-	106 ^d
2-22	70	20[2.1]	395/476	412/500	444/-	2.79/-	210 ^e
2-33a	86	22[2.1]	377/485	470/625	437/567	2.84/2.19	140 ^e
2-33b	62	20[2.0]	380/486	470/625	437/569	2.84/2.18	183 ^e
2-33c	65	11[2.1]	377/477	390/544	434/464	2.86/2.67	23 ^d
2-37a	31	30[2.0]	388/486	401/505	443/494	2.80/2.51	52 ^d , 115 ^e
2-37b	55	47[1.6]	390/488	394/505	449/467	2.76/2.66	38 ^d
2-42a	90	f	501/568	524/685	645/-	1.92/-	-
2-42b	99	f	510/571	524/685	643/-	1.93/-	327 ^e
2-44a	67	14[2.55]	i	i	i	i	107 ^e , 149 ^e
2-44b	49	22[2.78]	j	j	j	j	212 ^e

^a GPC vs polystyrene standards. ^b 10⁻⁵ M THF. ^c 10⁻⁷ - 10⁻⁸ M THF. ^d DSC: 2nd order transition. ^e DSC: 1st order transition. ^f Low molecular weight (≤3 kDa) estimated from NMR end-group analysis. ^g spun-cast from toluene solution (1mg/mL). ^h E_g=1240/λ_{onset}. ⁱ same as **2-33a**. ^j same as **2-33b**.

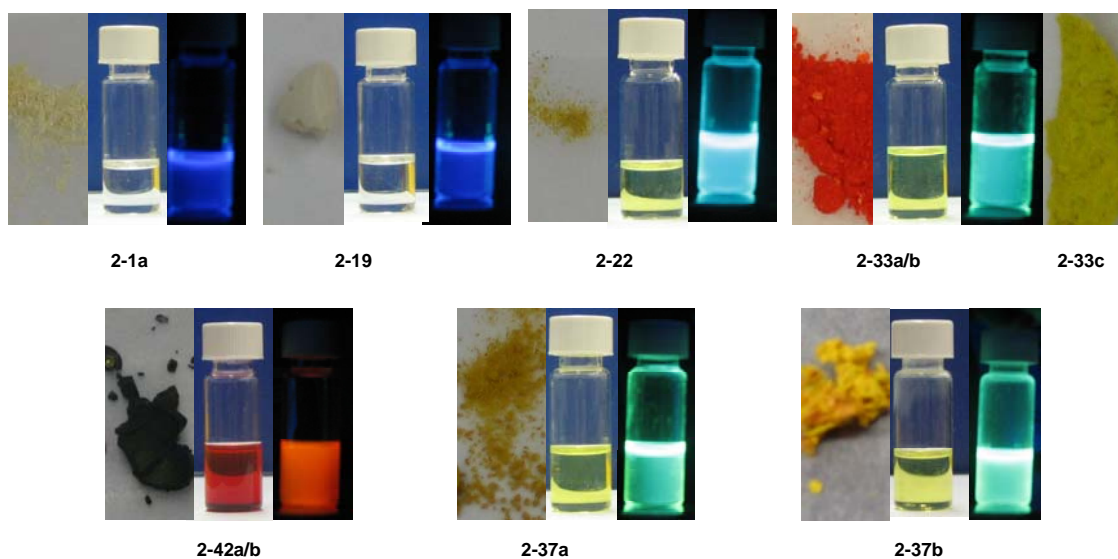


Figure 2. 26 Color photographs of polymers (left: solid under ambient light; middle: solution under ambient light; right: solution under irradiation at 366 nm).

2.9.2 Optical properties in solution and in solid state

Color photographs of polymers in the solid state and in solution under ambient light and UV light (366 nm) are shown in **Figure 2. 26**. Polymers **2-1a** and **2-19** are colorless in the solid state and in solution, and emit blue light in solution under UV irradiation. This is as expected because conjugation along the polymer backbones should be entirely disrupted due to substantial torsion between successive rings caused by steric/electronic repulsion between pendant alkoxy and fluorine substituents. Polymer **2-22** is yellow in the solid state and emits yellow light in solution due to a slightly lowered optical band gap corresponding to the possibility of the coplanarity of the bithiophene units. Conjugation is still however limited by backbone torsion due to steric repulsion between pendant alkoxy and fluoride substituents. Polymers **2-33a** and **2-33b** are orange to deep red in solid and green fluorescent in solution arising from extended conjugation and/or π -stacking as there is at most a limited steric hindrance to coplanarity of thiophene rings and fluorinated benzene rings, as was predicted. Non-fluorinated polymers **2-37a** and **2-37b** are also green fluorescent in solution, similar to **2-33a/b**, but are yellow in the solid state, suggesting a significantly higher optical energy gap associated with extensive conjugation-limiting torsion along their polymer backbones. Polymers **2-42a/b** even with

low molecular weights are dark-purple/black in the solid state and orange-red fluorescent in solution. We attribute these red-shifts, relative to polymers **2-33**, to a likely combination of greater backbone planarity and possible enhanced intra- and intermolecular donor-acceptor interactions.

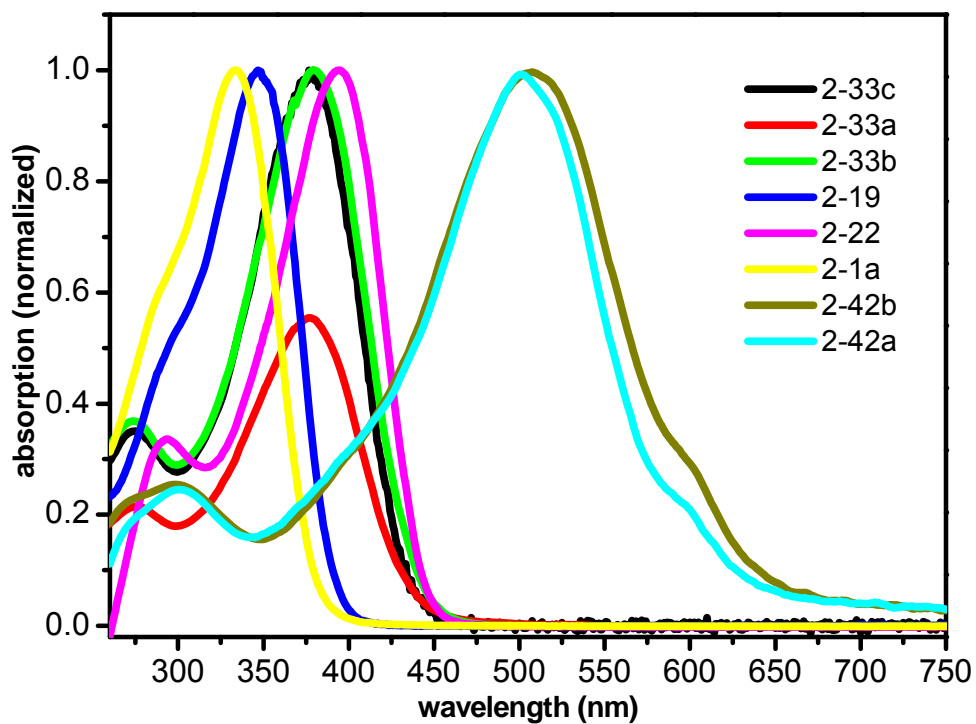


Figure 2.27 Solution UV-Vis spectra of the fluorinated polymers (THF, 10^{-5} M).

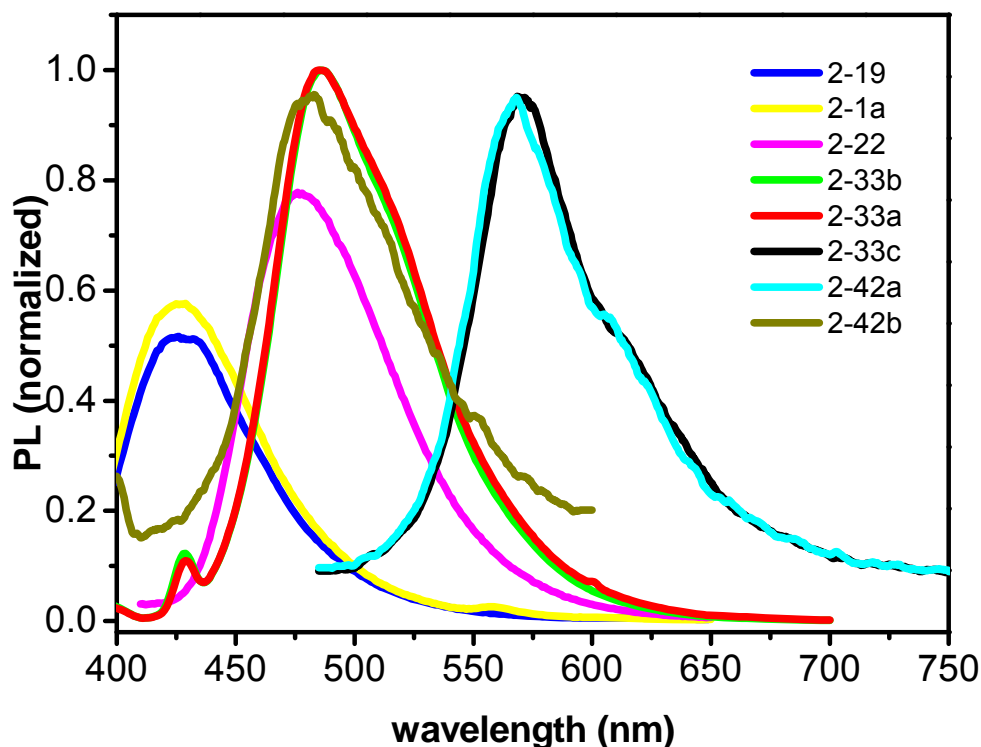


Figure 2.28 Solution PL spectra of the fluorinated polymers (THF, 10^{-7} - 10^{-8} M).

Solution UV-Vis absorption and PL spectra of all fluorinated copolymers are collected in **Figure 2.27** and **Figure 2.28**. Their peak maximum values are also included in **Table 2.2** along with optical energy gaps estimated from the onset of absorption ($E_g = 1240/\lambda_{\text{onset}}$). The UV-Vis absorption and PL maxima, as well as E_g , clearly depend on the structures of back bones and substituents. Compared with polymer **2-1a**, solution λ_{max} of all other fluorinated polymers are red-shifted, due to increased conjugation which in turn can be attributed to variably diminished steric/electronic repulsion. For polymer **2-19**, the absorption and PL λ_{max} are red shifted by 13nm and 55nm, respectively. As described above, this may be attributed to some small increase in conjugation between coplanar thiophene units. Steric/electronic repulsion is significantly reduced in polymers **2-33**, resulting in red shifts of 46nm and 110nm in the absorption and PL λ_{max} . The solution λ_{max} of polymers **2-42** is red-shifted by 120nm (absorption) and by 80-90nm (PL) **2-33** arising from the strong electron-donating effect of alkoxy groups, which are located such

that steric/electronic repulsion between substituents is minimized. The decreased steric hindrance of alkoxy groups relative to alkyl groups should also be considered.¹⁵¹

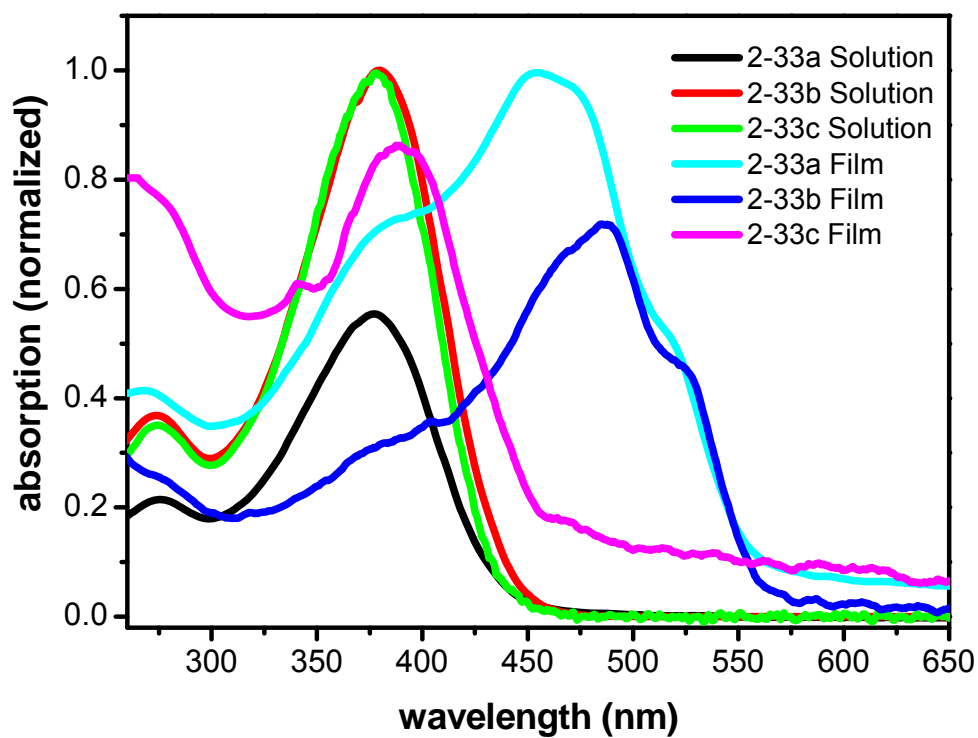


Figure 2. 29 Solution (10^{-5} M, THF) and solid state UV-Vis absorption spectra of polymers 2-33.

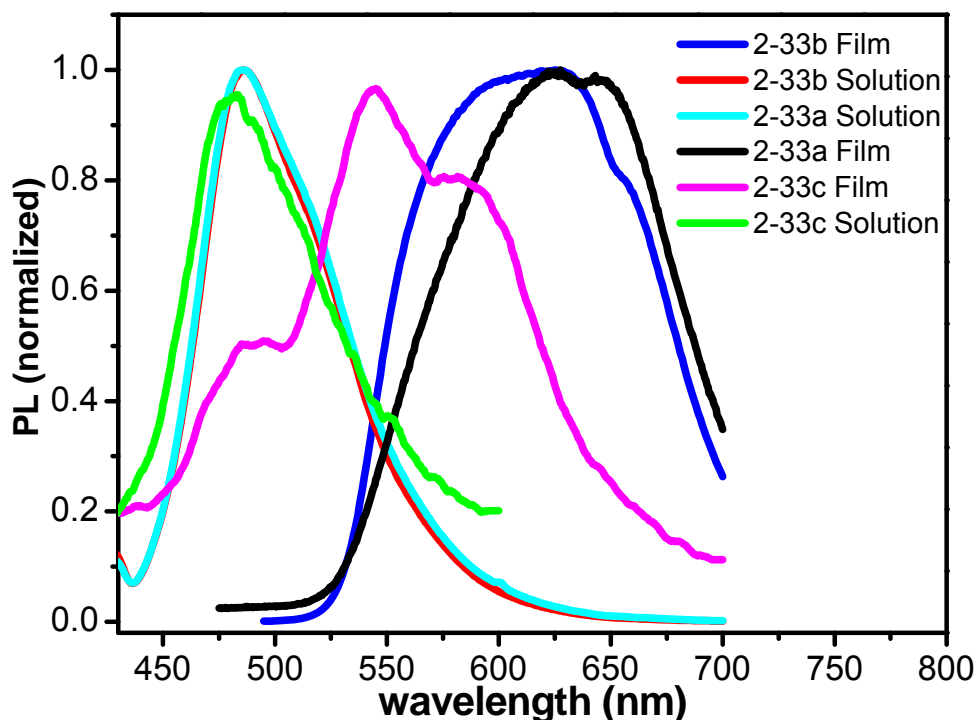


Figure 2.30 Solution (THF, 10^{-7} - 10^{-8} M) and solid-state PL spectra of polymers **2-33**.

For the series of copolymers **2-33** between perfluorobenzene and bithiophene derivatives carrying different alkyl substituents such as *n*-dodecyl, 3,7-dimethyloctyl and 2-ethylhexyl, the steric bulk of the alkyl substituents in the immediate vicinity of the polymer backbone significantly influences polymer self-assembly in the solid state and thus the optical properties. Films were spun-cast onto quartz plates from toluene (1mg/mL). The UV-Vis absorption and PL spectra in solution and in solid state are shown in **Figure 2.29** and **Figure 2.30**. The three polymers display almost identical, broad, featureless absorption ($\lambda_{\text{max}}=380\text{nm}$) and emission profiles ($\lambda_{\text{max}}=480\text{nm}$) in solution. In solution, there is no driving force for back-bone planarization and therefore the polymer conformations are represented by a broad thermal population with varying degrees of backbone torsion (essentially representing a very large number of different chromophores/fluorophores), resulting in broad featureless optical spectra independent of the identity of the side-chains. However, side chains will greatly affect polymer self-assembly in the solid state and thus cause significant differences in the absorption and emission spectra of polymers. The absorption and PL spectra of as-cast films from all

polymers **2-33** are red shifted relative to those in solution. For polymers **2-33a/33b** the absorption spectra are red shifted by 90nm ($\lambda_{\text{max}} = 470$ nm for both **2-33a** and **2-33b** in solid state) and PL spectra by 140nm ($\lambda_{\text{max}} = 625$ nm for both in solid state), while for polymer **2-33c** the absorption is red shifted by only 13nm ($\lambda_{\text{max}} = 390$ nm in solid state) and PL spectrum by 67nm ($\lambda_{\text{max}} = 544$ nm in solid state). The larger red-shifts for polymers **2-33a,b** can be attributed to back-bone planarization and or π -stacking in the solid state which in turn can be attributed to intramolecular S-F interactions, and/or intermolecular π - π F interactions. The bulkier 2-ethylhexyl side-chains precluded the planarization and or π -stacking, leading to much smaller red shifts for polymer **2-33c** than noted for polymers **2-33a/33b** upon going from solution to solid state. These differences are also reflected in the 2D WAXD patterns of extruded filaments to be described below. (**Figure 2. 36**)

The effect of fluorination on optical properties was also investigated. The solution and solid-state UV-Vis and PL spectra of fluorinated copolymers **2-33a,b** are compared to their non-fluorinated analogues **2-37a,b** in **Figure 2. 31** and **Figure 2. 32**. In solution, fluorine substituents have relatively little intrinsic effect on optical properties, as polymers **2-33** (fluorinated) and **2-37** (nonfluorinated) with the same side chains have very similar absorption and emission profiles. Unlike polymers **2-33**, the absorption and PL λ_{max} of polymers **2-37** undergo relatively small red-shifts on going from solution to solid state. That is, the backbones of polymers **2-37** remain highly twisted in the solid state. These results, taken together with diffraction results described below, conclusively show that introduction of fluorine substituents forces coplanarization of polymer backbones in the solid state, due to intra- and/or intermolecular interactions, dispelling any potential notion that HH linkages alone can govern planarity.

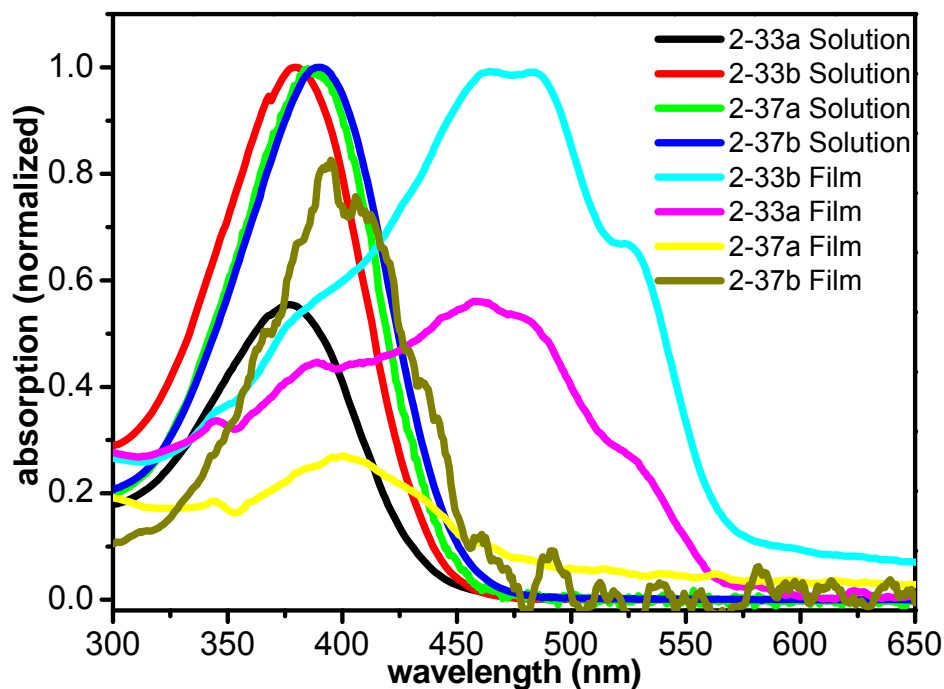


Figure 2. 31 Solution (THF, 10^{-5} M) and solid-state absorption spectra of polymers 2-33a/b and 2-37a/b.

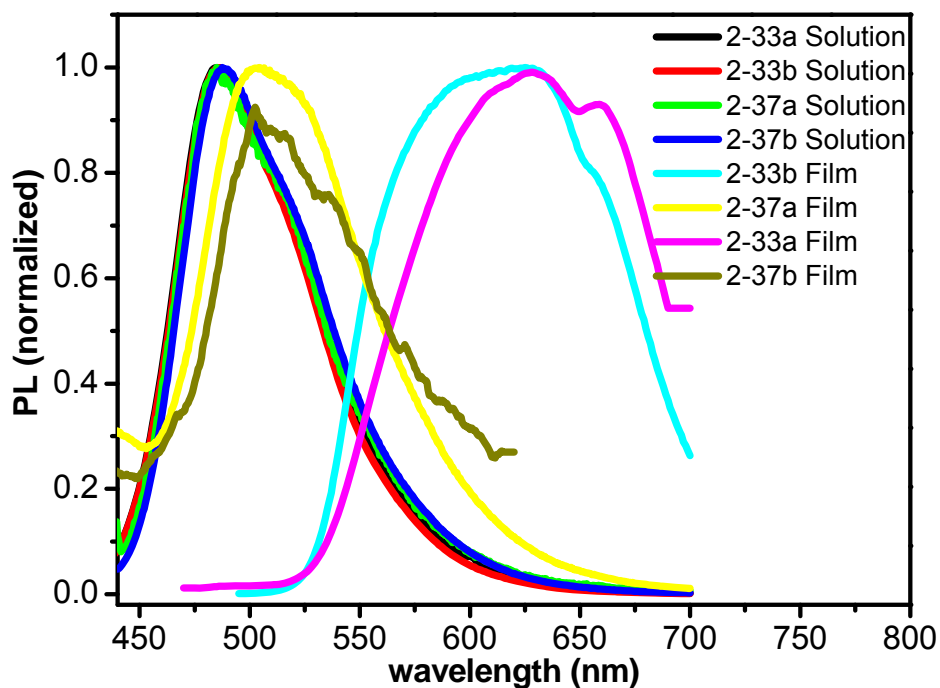


Figure 2. 32 Solution (THF, 10^{-7} - 10^{-8} M) and solid-state PL spectra of polymers 2-33a/b and 2-37a/b.

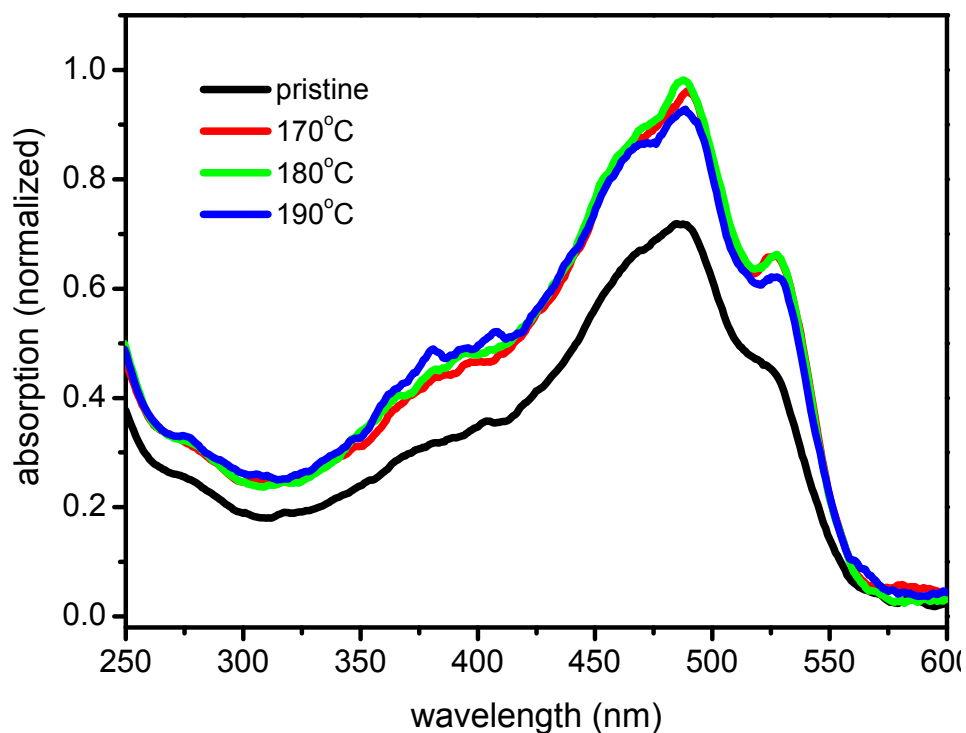
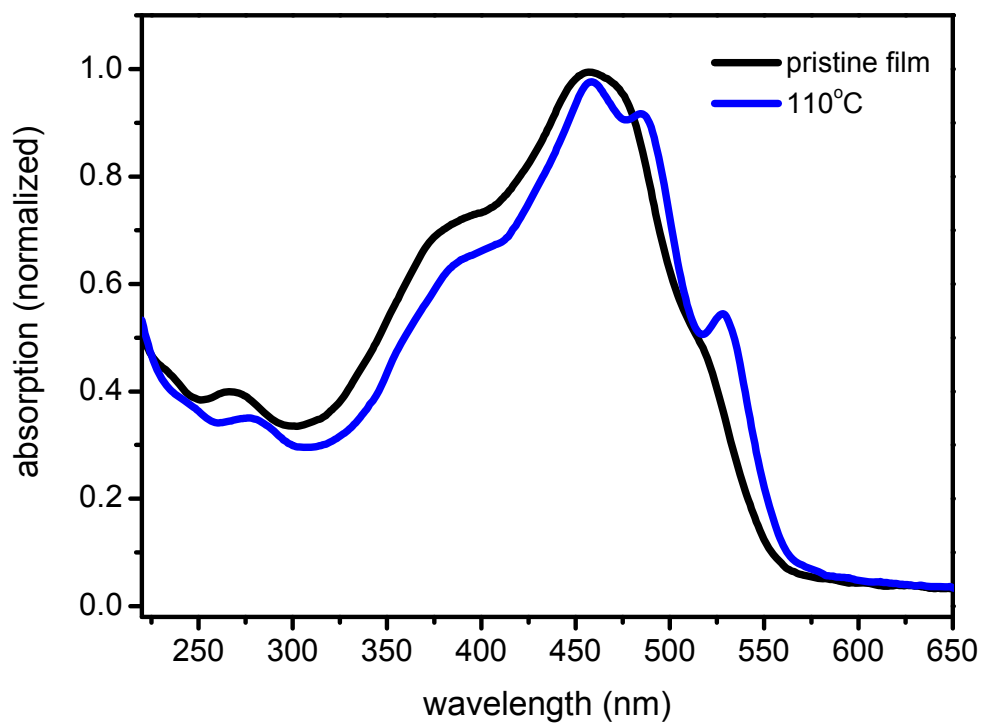


Figure 2. 33 Solid-state absorption spectra of polymers **2-33a/b** measured at RT before and after annealing at the indicated temperatures. Top: **2-33a**, bottom: **2-33b**.

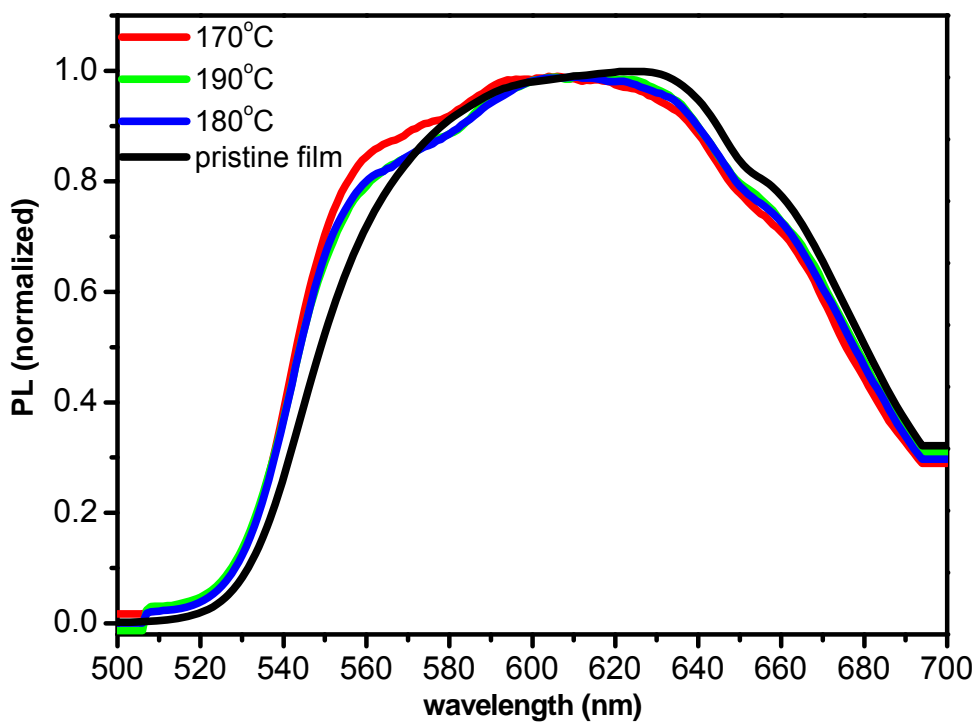
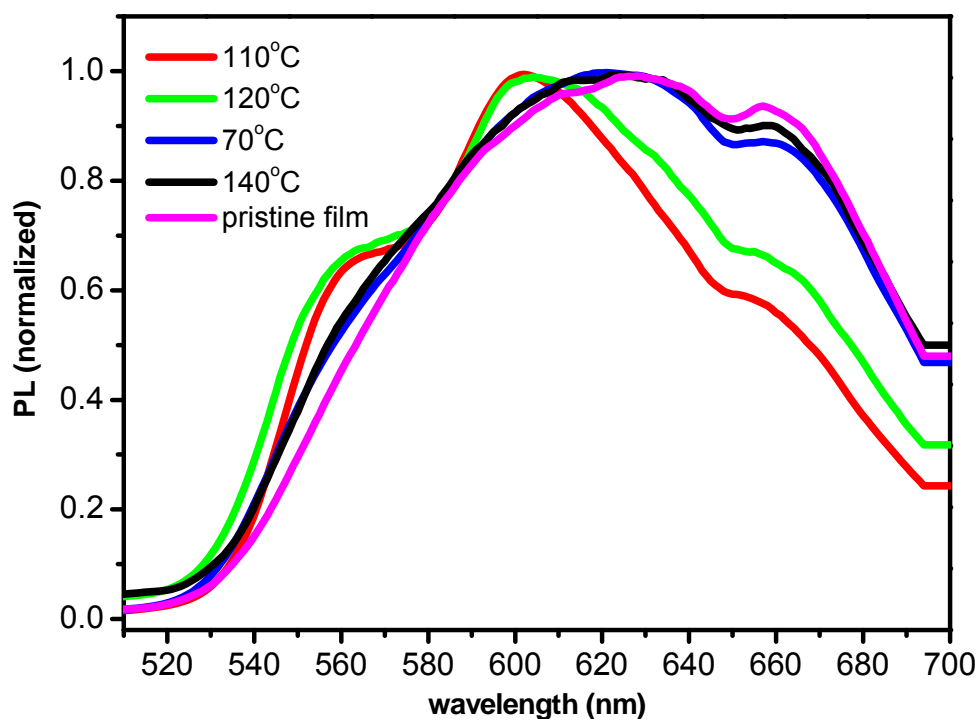


Figure 2. 34 Solid-state PL spectra of polymers **2-33a/b** measured at RT before and after annealing at the indicated temperatures. Top: **2-33a**, bottom: **2-33b**. Note: $T_m=140^\circ\text{C}$ (**2-33a**), $T_m=183^\circ\text{C}$ (**2-33b**).

Further information regarding the solid-state ordering of polymers **2-33a,b** was obtained by comparing absorption/PL spectra of thin films acquired before and after annealing near their 1st order (melting) transitions. (**Figure 2. 33** and **Figure 2. 34**) Annealing progressively closer to the melting temperatures results in increases in the fine structure of the spectra. This can be attributed to a narrowing of the population of states (decrease in variability of backbone torsion and π -stacking), effectively decreasing the number of different chromophores/fluorophores. This decrease in number of states corresponds to an increase in solid-state ordering. Annealing close to the melting temperature, without complete isotropization, provides sufficient thermal energy to allow disordered domains, kinetically trapped during solvent-casting, to reach equilibrium and become more ordered. While the spectra for polymers **2-33a** and **b** are very similar in terms of position of maxima after annealing, polymer **2-33a** appears to undergo greater changes. The origin of this different response to annealing will be revealed below by the results of WAXD studies.

2.9.3 Supramolecular arrangement of polymers in the solid state as revealed by wide angle xray diffraction (WAXD)

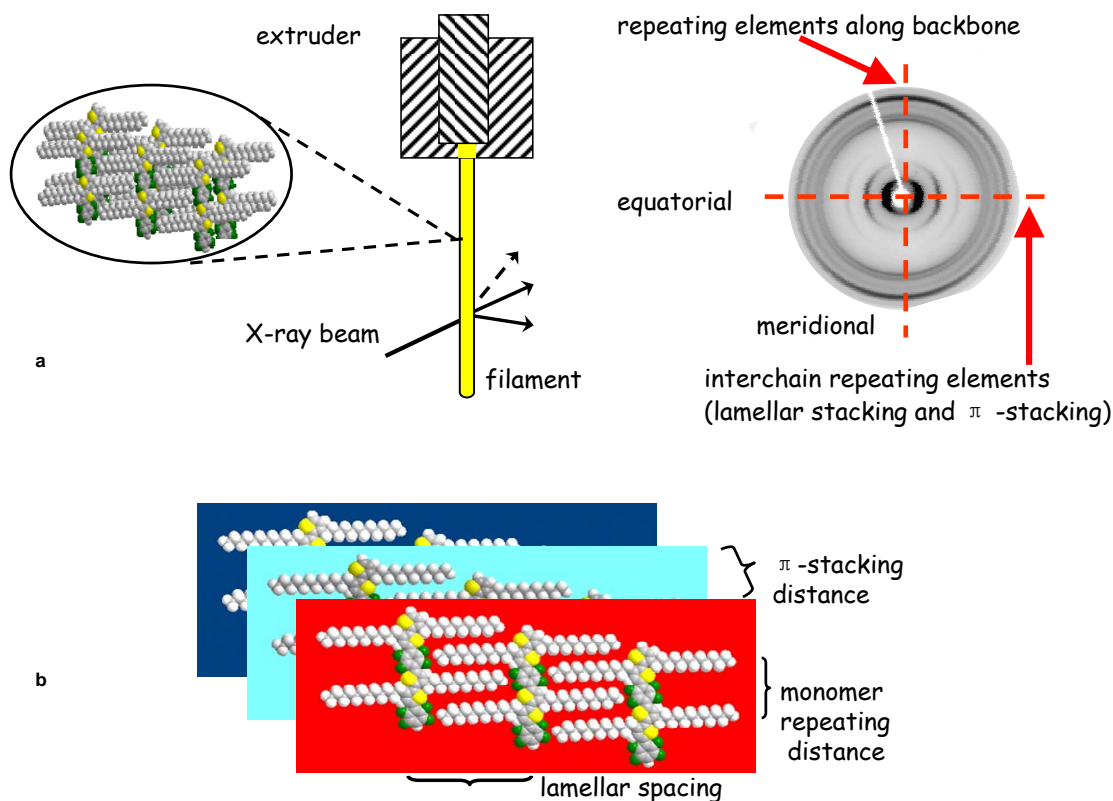


Figure 2. 35 Schematic illustration of the fiber alignment by a mini extruder, 2D WAXD pattern of an aligned fiber and packing of polymers. a) home-built fiber extruder and 2D WAXD pattern of the aligned fiber; b) lamellar packing and π stacking of polymers.

The supramolecular arrangement resulting from self-assembly of polymers **2-33** and **2-37** in the solid state was investigated by two-dimensional wide-angle X-ray scattering (2D-WAXD) from aligned fibers. The fibers were aligned by a home-built mini-extruder which is illustrated schematically in **Figure 2. 35a**. The polymer backbones were mechanically aligned by forcing bulk samples through a thermally equilibrated die (0.5 mm I.D) via a piston-operated extruder. The fiber samples were mounted perpendicular to the incident X-ray beam and diffracted x-rays were collected with an area detector. A representative 2D WAXD pattern is also shown in **Figure 2. 35a**. The order of these materials is much shorter range relative to crystalline small molecules, and therefore the

number of reflections is correspondingly much smaller. Aligning the polymers however greatly enhances interpretation of diffraction results relative to powder diffraction. Since the fibers are loaded vertically with respect to the incident X-ray beam, the meridional diffractions result from repeating elements along the backbone and the equatorial diffractions provide information about the interchain repeating elements including lamellar spacing and π -stacking. The lamellar spacing and π -stacking of planar conjugated polymers with simple linear alkyl side chains are defined in **Figure 2. 35b**.

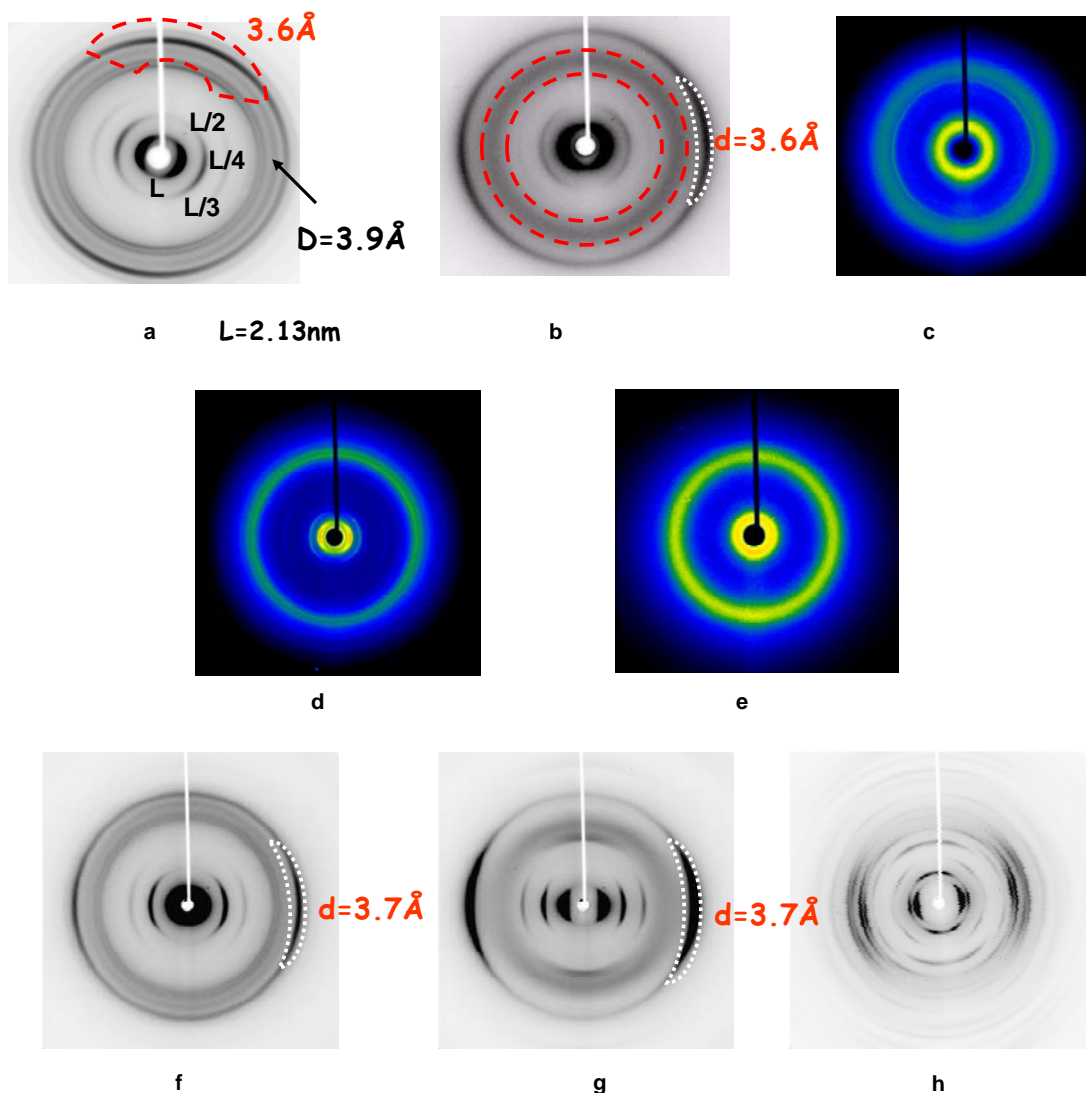


Figure 2. 36 Characteristic 2D WAXD patterns of **2-33a** (a), **2-33b** (b), **2-33c** (c), **2-37a** (d), **2-37b** (e), **2-44a** (f), **2-44b** (g) and **2-22** (h). Polymers **2-44a/b** have the same chemical structures as **2-33a/b**, but were synthesized via oxidative polymerization

(FeCl₃). Polymers **2-44a/b** were annealed at 20-30 degrees below their melting points. Unfortunately, the thermal histories of the fibers from **2-33a/b** were not recorded. Concentric red dashed circles in “b” enclose the diffuse halo resulting from isotropic diffraction of amorphous side chains, while white dashed arcs in “b”, “f” and “g” represent π -stacking.

Table 2. 3 Data collected from diffraction patterns in **Figure 2. 36**

polymer	Lamellar spacing	“d” or “D” ^a	Meridional	“halo”
	L, L/2, L/3 (Å)	π -spacing (Å)	maxima (Å)	(Å)
2-33a	20.16, 9.84, 6.52	3.94	4.59, 4.36, 3.66	-
2-33b	19.15, 9.75, 6.40	3.67	-	4.61
2-44a	20.41, 10.53, 6.91	3.72	-	-
2-44b	19.62, 9.88, 6.54	3.72	5.88	4.93

^a π -stacking distance, see **Figure 2. 37** for definition.

All relevant 2D WAXD diffractograms discussed below are collected in **Figure 2. 36** and relevant data extracted therefrom are collected in **Table 2. 3**. The diffraction pattern from polymer **2-22**, was not analyzed in detail but is shown as it contradicts predictions. It shows higher order reflections in all quadrants, including off-meridional ones indicating long-range 3-dimensional order. Based on the properties of polymer **2-1a**, it was expected that the highly twisted backbone of **2-22**, combined with limited or no π -stacking (based on solid-state abs-PL measurements) would correspond with an amorphous solid state. Somehow the highly twisted backbones can still pack efficiently in an order array.

Polymers **2-33a/b** and **2-44a/b** are identical but prepared by the new synthetic method described herein and by oxidative coupling, respectively. For the polymers **2-33a/b** (**Figure 2. 36 a and b**), there are series of equatorial reflections at smaller angles with relative d-spacings of L , $L/2$, $L/3$, etc., with intensities decreasing in that order. This indicates alternating, parallel zones of varying electron density corresponding to polymer

backbones separated by alkyl side chains (lamellar packing, with repeating distance = L). For polymer **2-33a**, there is a series of sharp reflections centered on the meridian, the most intense one at $d=3.6\text{\AA}$, corresponding to the spacings between ordered n -dodecyl side chains, while for polymer **2-33b** there is an isotropic halo centered around $d = 4.6\text{\AA}$ corresponding to the average spacing between carbon atoms of disordered side chains which fill the space between the rigid conjugated units. This difference in side-chain ordering is easily explained in that polymer **2-33b** carries racemic branched chains, which should resist crystallization. The lamellar spacing for **2-33a** is 20.2\AA , which is a few angstrom greater than the length of this polymer's dodecyl side chains, suggesting the side chains are interdigitated, but not fully. Despite the fact that the side chains of **2-33b** are shorter by 4 carbons, the lamellar spacing is only reduced by 1\AA . This suggests that the side chains are substantially less interdigitated, which may be justified due to their greater lateral demand for space (methyl branches and disordered state). For the polymer **2-33b**, there is an intense equatorial reflection centered at $d=3.6\text{\AA}$, which does not fit, either in intensity or d -spacing, into the series of diffraction maxima resulting from lamellar packing. This can be assigned to the π -stacking distance of the polymer backbones. This spacing is slightly less than that typically reported for thiophene based polymers (3.7\AA), which we ascribe to attractive π - π F interactions. Therefore a 2-dimensional unit cell describing the lateral packing of polymer chains can be assigned with sizes equal to " L " and " d " or " D " as defined in **Figure 2. 37**.

Polymer **2-33a** displays no reflections near $d = 3.6\text{\AA}$, but instead shows rather weak equatorial reflections at $d = 3.9\text{\AA}$, suggesting a larger π -stacking distance and relatively short range order along that dimension. However, the large red-shifts denoted above in the optical spectra of polymer **2-33a** upon going from solution to the solid state indicate that the polymer backbones are planarized and/or closely π -stacked. We therefore propose that the backbone rings of polymer **2-33a** are indeed closely π -stacked, but tilted relative to the stacking axes (see **Figure 2. 37B**). This is exactly analogous to "roll" defined in **Figure 1. 15** and the associated text in chapter 1. As the tilt angle increases, the measured distance increases despite a constant intermolecular distance separating backbone rings. Using simple trigonometry, and assuming that the π -stacking distance is similar for polymers **2-33a,b**, the angle (Φ) between the ring planes and the normal to the

stacking axes can be estimated from $\Phi = \arccos(d/D) = \arccos(3.6/3.9) = 23^\circ$. A model of such an arrangement of polymer chains was created and diffractograms from it simulated using Cerius2 software. The tilt angle Φ was varied in increments, each time recalculating the diffraction pattern. The simulated diffraction maxima arising from the distance “D” became progressively weaker with increasing angle Φ , thereby showing that the polymers may be well-ordered and closely π -stacked as suggested by abs/PL measurements, and still give rise to weak reflections. These exactly analogous differences were also observed in the diffraction patterns of alternating arene-perfluoroarene poly (phenylene ethynylenes) carrying the same branched and unbranched alkyl chains in our group.¹⁵⁶ It is important to note that both of polymers **2-33a/b** show strong reflections at $d = 3.6 \text{ \AA}$ in the powder x-ray diffraction. The x-y plots of diffraction intensity versus scattering angle obtained from much more common powder diffraction measurements would not have allowed to distinguish between their differing packing arrangements.

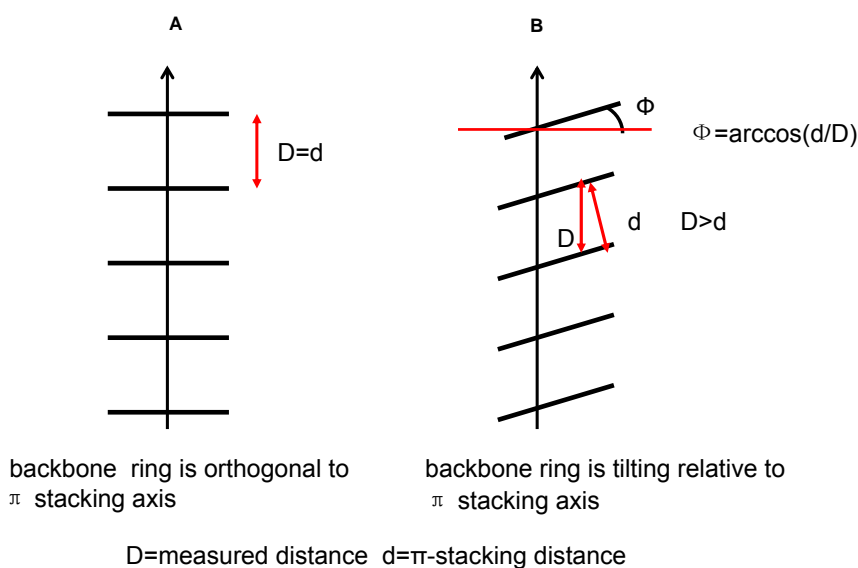


Figure 2.37 Models showing the orientation of backbone rings relative to the π -stacking axis: (A) backbones orthogonal to and (B) tilted relative to π -stacking axis.

Recall that polymers **2-44a/b** are identical in composition to **2-33a/b**, but were prepared by a traditional method. Polymer **2-44a** and **2-33a** have similar thermal properties, but the melting point of **2-44b** is 30°C higher than **2-33b** (Table 2.2 above). The diffractogram from an annealed **2-44b** fiber is very similar to **2-33b** with some

important exceptions. Easily visible meridional arcs appear at $d = 5.88 \text{ \AA}$. This is approximately $\frac{1}{2}$ the length of the polymer repeat unit, suggesting that face-to-face neighbors overlap with fluorinated rings overlying non-fluorinated rings. Both the highest order arc assigned to lamellar spacing and the one assigned to the π -stacking are increased in relative intensity compared to **2-33a**. The diffractogram of **2-44a** does not contain the low angle meridional arcs of **2-33a**. The diffraction arcs assignable to π -stacking indicate a closer d-spacing of 3.7 \AA . Taken all together, this suggests that **2-44a/b** are more highly ordered and/or pack more closely than **2-33a/b**. Unfortunately, these results can not be rigorously compared, as the thermal histories were not recorded of the fibers from **2-33a/b**. FET devices will be fabricated to see whether this difference will be translated to differences in electronic properties. There were no notable differences between the optical spectra of annealed films of polymers prepared by the two methods (**2-33a** vs **2-44a** or **2-33b** vs **2-44b**)

The differing degrees to which the solid-state absorption and PL spectra of polymers **2-33a** and **2-33b** undergo changes upon annealing can now be explained in terms of side-chain ordering. The liquid-like side-chains of polymer **2-33b** are simply space-filling spectators, which allow packing to be dominated by the main chains. The as-cast state of order more closely resembles the equilibrium state obtained upon annealing. However, the equilibrium state of polymer **2-33a** must involve more complex and cooperative ordering of main and side chains. This is less likely to be achieved during rapid solvent evaporation occurring during film casting. Therefore, the ordering of polymer **2-33a** undergoes greater changes upon annealing, which is reflected in the greater changes in its optical spectra.

The diffraction pattern from polymer **2-33c**, carrying 2-ethylhexyl side chains, differs greatly from the patterns obtained from polymers **2-33a,b**. There are just two radially symmetric reflections at intermediate and wide angle. There are no higher order reflections, indicating that there is not even short-range order. The diffuse ring at small angle corresponds to the average distance separating disordered main chains and the one at larger angle corresponds to the average spacing between disordered side chains. Polymer **2-33c** is therefore completely amorphous. The radial symmetry of these reflections indicates that even if the polymer was aligned during extrusion, the alignment

was lost prior to WAXD measurements. This is understandable as polymer **2-33c** has a glass transition centered at a temperature not much higher than room temperature. There is sufficient mobility in the disordered polymer that alignment will be lost at room temperature. The racemic 2-ethyl-hexyl side chains present significantly greater steric bulk in the vicinity of the polymer backbone, causing significant backbone torsion and disrupting ordering and precluding π -stacking. This again agrees with the solid-state optical measurements and the polymer's color (yellow versus orange to red for polymers **2-33a,b**). The increase in fine structure in the optical emission spectrum of polymer **2-33c** does not conflict with these results. Despite the fact that it is amorphous and somewhat mobile at room temperature, its mobility in the solid-state is surely reduced compared to in the solution. The transition from solution to solid-state is equivalent, in terms of mobility, to a decrease in temperature, which narrows the thermal population of differing states, thereby inducing some fine structure and likewise inducing a small red-shift.

Comparison of the diffraction patterns of fluorinated (**2-33b**) and non-fluorinated (**2-37b**) polymers carrying exactly identical 3,7-dimethyloctyl side chains is most revealing of the effect of fluorination on solid-state order. Recall that the optical spectra of polymer **2-33b** undergo significant red-shifts upon going from solution to solid state, while those of polymer **2-37b** are relatively unchanged. This suggests that nonfluorinated polymer **2-37b** does not become ordered, nor does it π -stack in the solid state. This is in perfect agreement with WAXD results. The WAXD pattern of **2-37b** likewise reveals that it is both completely amorphous and unoriented. This further agrees with DSC measurements, during which polymer **2-37b** undergoes only a glass transition (38°C), but no 1st-order transitions associated with ordered domains.

2.10 Conclusions

1. A new methodology without transition metals has been developed to synthesize commercially relevant thiophene-containing conjugated copolymers, in which the catalyst system of CsF and 18-crown-6 are facile to be removed by extraction to yield polymers with high purity and high molecular weight. The polymers are not completely defect-free and only time and device studies will reveal if there is any resulting

enhancement of device performance. Also the scope of this transition-metal-free polymer synthesis is likely to expand to a broad range of thiophene copolymers, based on the series of differing polymers prepared to date.

2. Model reactions reveal that the relationship between degree of polymerization and comonomer stoichiometry for this type of polymerization should deviate from that predicted by Carothers equation.

3. Optical properties can be tuned by manipulating the structures of backbones and side chains of polymers.

4. Fluorination can lead to significant red-shifts of optical transitions in the solid state.

5. The observed red-shifts result from planarization and/or π -stacking in the solid state as clearly demonstrated by WAXD measurements. These changes in turn arise either from attractive intramolecular S-F, or intermolecular π - π F interactions.

6. Optical properties critically depend on ordering and steric bulk of side-chains.

7. HH-linkages in thiophene (co)polymers do not inherently limit conjugation by causing backbone rings to twist out of plane.

Chapter 3 Synthesis and characterization of highly fluorinated benzobisbenzothiophenes (BBBT)

3.1 Introduction

Chalcogenoacenes are usually prepared via a range of reactions including transition-metal catalyzed couplings and/or electrophilic aromatic substitution. Some reported extended thienoacenes are shown in **Figure 3. 1**. Regioisomeric mixture **3-1** was prepared in eight steps starting from dibenzothiophene.¹⁵⁷ The importance of preparing regioisomerically pure materials has been demonstrated in some cases. Isomeric mixture **3-1** gave best performance ($\mu_{\text{FET}} = 0.15 \text{ cm}^2 \text{ V}^{-1} \text{ s}^{-1}$) when some fractionation occurred during device fabrication (sublimation). The two regiopure heteroacenes **3-2** were prepared separately, each in four steps, and showed OFET mobilities up to $0.12 \text{ cm}^2 \text{ V}^{-1} \text{ s}^{-1}$, with one of the isomers proving superior to the other.¹⁵⁸⁻¹⁶⁰ On the other hand, regioisomeric mixtures of anthradithiophenes **3-3** (ADT) provided good to excellent performance both in OFETs ($\mu_{\text{FET}} = 1 \text{ cm}^2 \text{ V}^{-1} \text{ s}^{-1}$)¹⁶¹ and solar cells.¹⁶² Of the three types of materials shown, ADT is the only one for which the molecular shape of the regioisomers is essentially the same, allowing essentially unperturbed cocrystallization. An important structural design feature is the steric bulk of the silyl groups, which dictates whether the molecules crystallize in 1-D or 2D slip π -stacks.

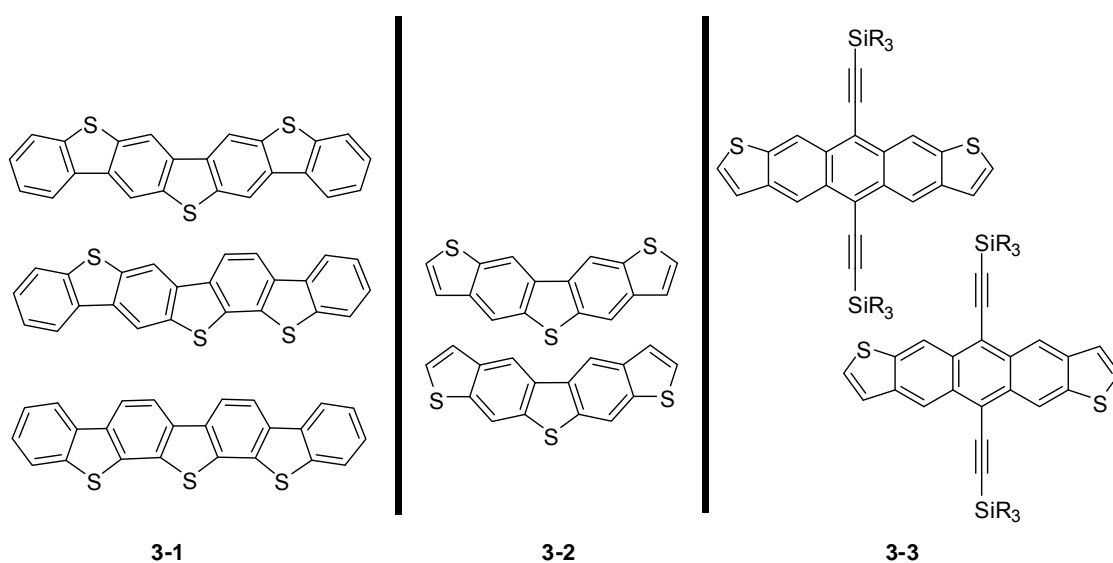


Figure 3. 1 Published isomeric thienoacenes. Only compounds **3-2** were produced separately as pure isomers.

Yamaguchi utilized elegant cascade reactions to prepare the α , ω -benzoterminated heteroacene **3-4** (**Figure 3. 2**).¹⁶³ Constructing nearly the entire long molecular edges from sulfur atoms served to enhance intermolecular π -overlap. OFET devices were constructed from **3-4** yielding mobilities $\sim 0.5 \text{ cm}^2 \text{ V}^{-1} \text{ s}^{-1}$ while those constructed from a selenium-containing analogue were $\sim 1.1 \text{ cm}^2 \text{ V}^{-1} \text{ s}^{-1}$.^{163, 164} This synthetic route does not allow for isomers.

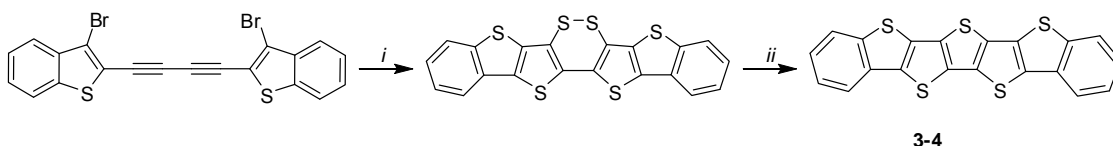


Figure 3. 2 Published¹⁶³ cascade reaction leading to thienoacenes. *i*: a) *t*-BuLi, 4eq, b) S, 4eq, c) [O], 68%; *ii*: Cu, Δ , 81%.

Near the end of the work described in this chapter, Takimiya et al reported a 5-step route (actually 7-steps including 2 steps to the starting material) (**Figure 3. 3**) to regioisomerically pure benzobisbenzothiophene **3-5** (BBBT).¹⁶⁵ A variety of reactions are used to form all the bonds which eventually form the polycyclic scaffold. It will be shown in this chapter that highly fluorinated BBBTs can be prepared in few laboratory steps exploiting the high reactivity of polyfluorinated aromatics towards nucleophiles.

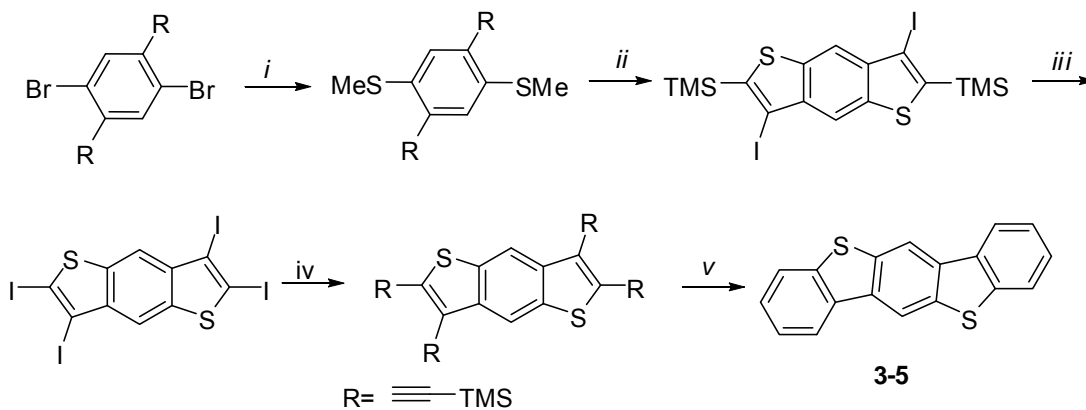


Figure 3. 3 Published synthesis of regioisomerically pure benzobisbenzothiophene **3-5** (BBBT).¹⁶⁵ *i*: a) *t*-BuLi, b) MeSSMe, 50%; *ii*: I₂, 89%; *iii*: ICl, 98%; *iv*: PdCl₂(PPh₃)₂, CuI, TMSA, 83%; *v*: Te, NaBH₄, 71%.

One of the many critical factors governing the performance of organic semiconductors is the mode in which they self-assemble to ordered arrays having extensive intermolecular orbital overlap.¹⁵ Some approaches to increase orbital overlap are a) increase the size of the π -system;¹³⁶ b) decorate the periphery with groups that preclude edge-to-face interactions;⁶⁵ c) enhance face-to-face interaction via attraction between electron-rich and -poor segments;^{28, 70} and d) construct peripheries from heteroatoms (e.g. compounds **3-1** through **3-5**, **Figure 3. 1**, **Figure 3. 2** and **Figure 3. 3** above).¹⁴¹

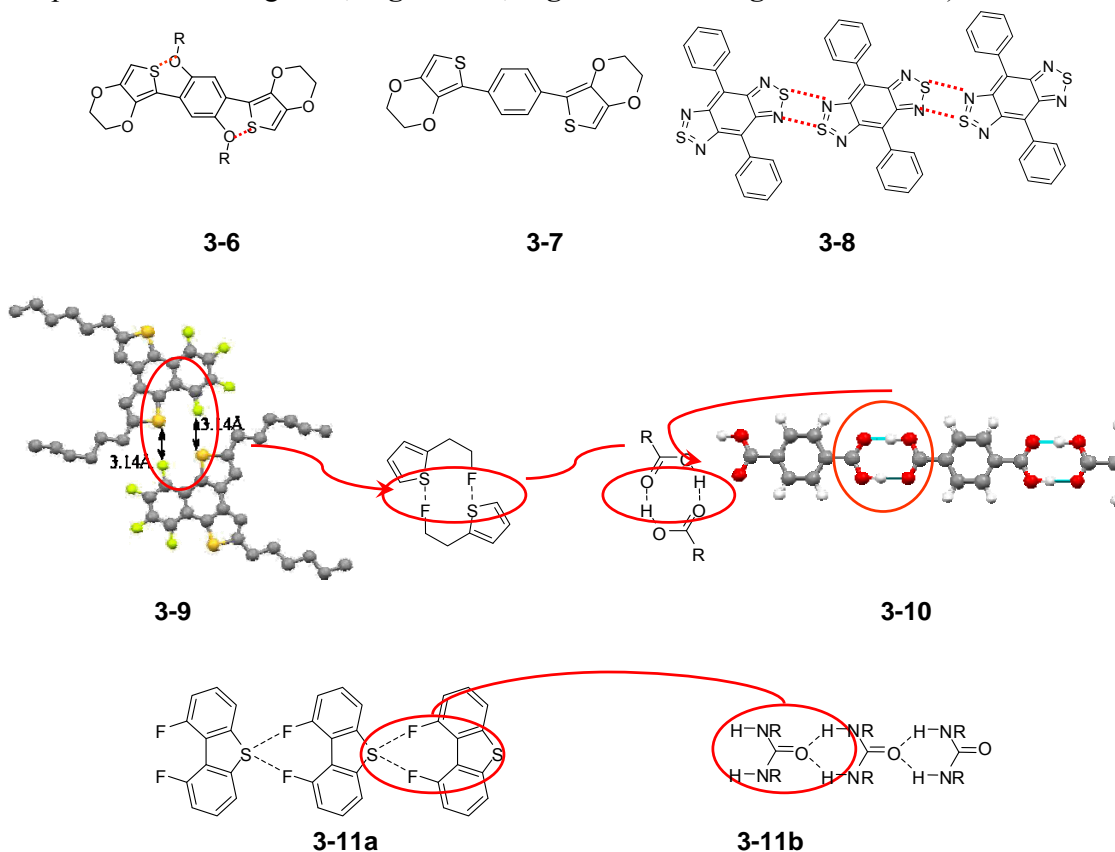


Figure 3. 4 Structures of compound **3-6**¹⁶⁶, **3-7**¹⁶⁷, **3-8**¹⁶⁸, **3-9**¹⁶⁹, **3-10**¹⁷⁰ and **3-11**. The edge-to-edge dimer of **3-9** is a partial packing diagram from the experimentally determined crystal structure.

Non-covalent intramolecular¹⁴⁵ and intermolecular interactions²⁸ have been often exploited to enforce coplanarity of ring systems in the solid state and to control relative orientations of rings within neighboring molecules. Reynolds reported that the aromatic rings of long-chain alkoxy-substituted BEDOT-B **3-6** are nearly coplanar with a torsion angle of only 6.8° due to intramolecular interactions through S-O contacts,¹⁶⁶ in contrast to its analogue bis(3,4-ethylenedioxythiophene) benzene (BEDOT-B) **3-7** without substituents on the central benzene ring.¹⁶⁷ The rings of **3-7** significantly deviate from coplanarity with torsion angle of 27.5°.

During crystallographic studies of various thienyl-sulfur containing fluorinated molecules prepared in our research group, various members have repeatedly noted close contacts between thienyl sulfur atoms and fluorine atoms. An example is the tetracyclic aromatic compound **3-9**¹⁶⁹ shown in **Figure 3. 4**. When the portions of the molecules enclosed by a red circle are considered alone, their relative antiparallel arrangement to the identical group in adjacent molecules may be compared to the dimeric assembly of carboxylic acids. More specifically, this is compared to the crystal packing of terephthalic acid **3-10** in the same figure.¹⁷⁰

A recent search of the Cambridge Structural Database reveals 99 structures with close contacts (less than sum of van der Waals radii) between organofluorine and thienyl sulfur atoms. This interaction may be merely electrostatic, as in the interaction of thienyl sulfur atoms with oxygen atoms¹⁵⁵ or may resemble that which imparts a rich supramolecular chemistry to chalcogenodiazoles, where nitrogen lone-pairs donate into nitrogen-chalcogen σ^* orbitals.¹⁷¹ For example, 4,8-diphenylbenzo[1,2-c:4,5-c']bis([1,2,5]thiadiazole) (**3-8**) forms ribbon structures due to intermolecular interactions through short S-N contacts as shown in **Figure 3. 4**.¹⁶⁸ Regardless of the specific nature of the S-F interaction, it would stand to reason that lath-shaped molecules bearing triangular arrangements of thienyl sulfur atoms and two fluorine atoms on opposite “sides” could crystallize into infinite sheets resembling urea self-assembly **3-11** (in analogy to comparing the arrangement of **3-9** to carboxylic acid dimerization **3-10**). Indeed, the crystal structure of octafluorodibenzothiophene **3-12** reveals two close contacts between every sulfur atom and two fluorine atoms.¹⁷² (**Figure 3. 5**) The BBT scaffold, if fully fluorinated, provides two such antiparallel triangular

F-S-F supramolecular synthons in one molecule. The remainder of this chapter will describe studies of such molecules demonstrating that the predicted edge-to-edge self-assembly is achieved through these S-F interactions. Additionally the facile expedient synthesis of fluorinated BBTs is described along with studies of the effect of fluorination on (opto)electronic properties.

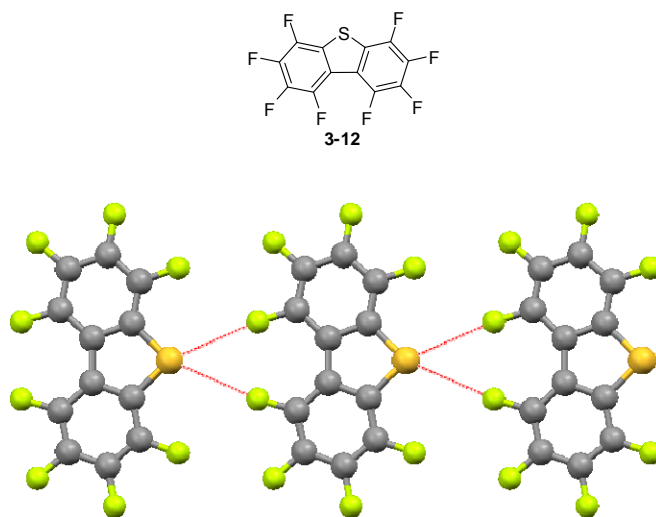


Figure 3. 5 Close contacts between S and F in octafluorodibenzothiophene **3-12**.¹⁷²

3.2 Syntheses of highly fluorinated benzobisbenzothiophenes (BBBT)

3.2.1 Syntheses of compounds 3-15a,b

The facile, efficient synthesis of highly fluorinated BBBT **3-15**, in just three laboratory steps from commercially available 1,2,4,5-tetrafluorobenzene is outlined here (**Figure 3. 6**). 1,4-bis(tert-butylthio)-2,5-difluorobenzene (**3-13**) was obtained as a byproduct of the synthesis of 1,2,4,5-tetrakis(t-butylthio)benzene for other purposes by aromatic nucleophilic substitution of 1,2,4,5-tetrafluorobenzene with excess sodium 2-methylpropane-2-thiolate. Therefore, the yield was not determined. Compound **3-13** was lithiated at its 3,6-positions via direct ortho-lithiation using 3 eq of freshly-prepared LDA at -78°C for 6 hours, and then used as a nucleophile to react with excess perfluoroarene to produce terphenylenes **3-14a,b** in 70-80% yield. These products were easily purified by sonication with methanol and 10% HCl. Conditions of lithiation of **3-13** were optimized using different lithiating reagents. (**Table 3. 1**). After addition of

C_6F_6 conversion to **3-14a** and **3-16** were estimated by GC-MS. These studies showed that with *n*-BuLi/TMEDA, *s*-BuLi/TMEDA, or *t*-BuLi, the major product is **3-16**. A commercial solution of LDA (Aldrich), produced **3-16** and **3-14a** in a 1:1 ratio. With 2.2 eq of LDA freshly prepared from *n*-BuLi and diisopropylamine, the ratio of **3-16** and **3-14a** is 1:5, and with 3 eq of freshly-made LDA, all of the resulting product is **3-14a**. These results agree with published reports indicating that LDA is the reagent of choice for aryl lithiation ortho to fluorine substituents.^{173, 174} If C_6F_6 was used as quenching reagent, a large excess (more than 20eq) should be used to prevent oligomer/polymer formation as most substituents can activate the para position of pentafluorobenzenes toward further substitution. However, a stoichiometric amount with C_7F_8 is sufficient since the first and only nucleophilic attack occurs para to the CF_3 group. Compounds **3-14** can be dealkylated with HF_4 ·ether complex¹⁷⁵ in toluene via Friedel-Crafts reaction (*t*-butyl group is transferred to the solvent toluene). The resulting thiophenols are deprotonated with potassium hydroxide and undergo ring closure via intramolecular S_NAr reaction to afford compounds **3-15a** and **b** as pale yellow solids in 60% and 90% yield respectively.

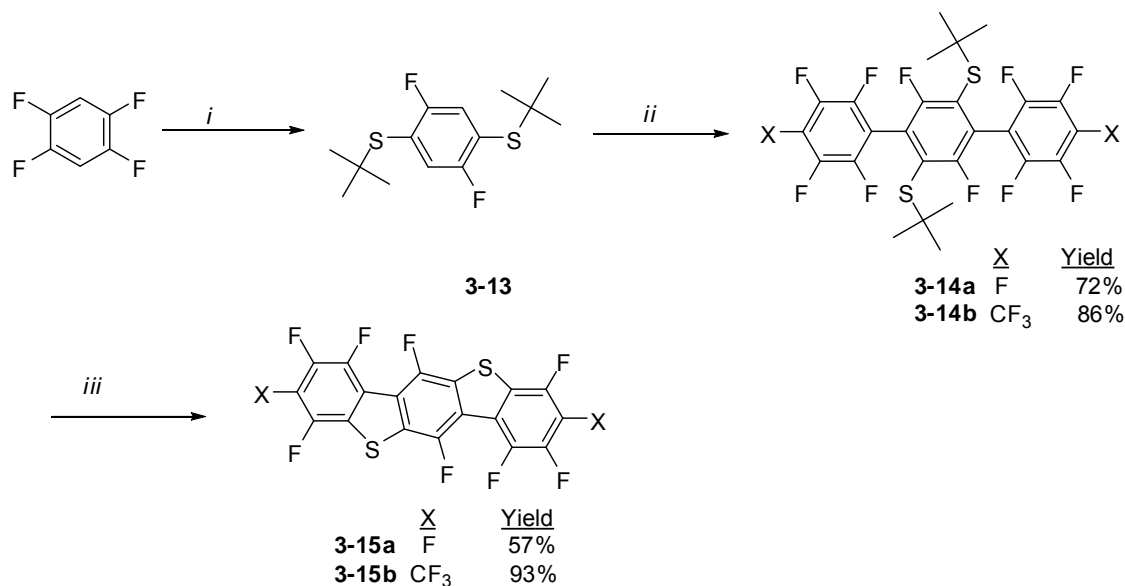
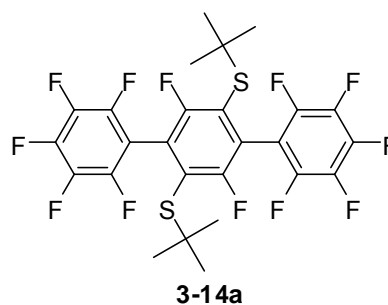
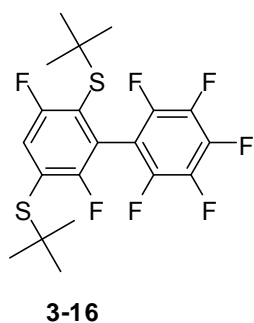


Figure 3. 6 Synthesis of highly fluorinated BBTs **3-15**. *i*: 2-methylpropane-2-thiol, NaH, DMF; *ii*: a). LDA, THF, $-78^\circ C$, b). C_6F_6 (**3-14a**), C_8F_8 (**3-14b**), $-78^\circ C$ then r.t.; *iii*: a). HF_4 ·ether (54 w%), $110^\circ C$, b). KOH, 18-crown-6, $110^\circ C$.

Table 3. 1 Yields of mono- and di-pentafluorophenylation of **3-13** during optimization studies ^{a, b}

	3-16	3-14a
	GC Yield	GC Yield
<i>n</i> -BuLi (2eq)+TMEDA	63%	37%
<i>s</i> -BuLi(2eq)+TMEDA	100%	No
<i>t</i> -BuLi(2eq)	100%	No
LDA ^c (2eq)	50%	50%
LDA ^d (2.2eq)	17%	83%
LDA ^d (3eq)	No	100%

^a All conditions identical except selection of lithiating system. ^b Yields are based on GC-MS. ^c From Aldrich. ^d Freshly made from *n*-BuLi and diisopropylamine at 0°C.



3.2.2 Synthesis of compound 3-19

Compound **3-19** was prepared as a control which is “missing” the central fluorine atoms, thereby partially truncating the F-S-F supramolecular synthon. (**Figure 3. 7**) 1,4-bis(tert-butylthio)-2,5-dibromobenzene **3-17** was prepared by aromatic nucleophilic substitution of 1,2,4,5-tetrabromobenzene with 2.1eq. *t*-BuSNa. Compound **3-17** underwent metal-halogen exchange with *n*-BuLi and the resulting nucleophilic dianion was quenched with a large excess of perfluorobenzene to provide **3-18** in 41% yield. Precursor **3-18** was selectively dealkylated by AlCl₃ in toluene¹⁷⁶ (transfer of *t*-butyl groups to solvent toluene similar to above synthesis of **3-15**) followed by deprotonation and cyclization to afford **3-19** as an off-white solid in 31% yield. Yields are relatively

low in this sequence as compound **3-19** was prepared merely as a control, with no optimization nor special care taken during isolations.

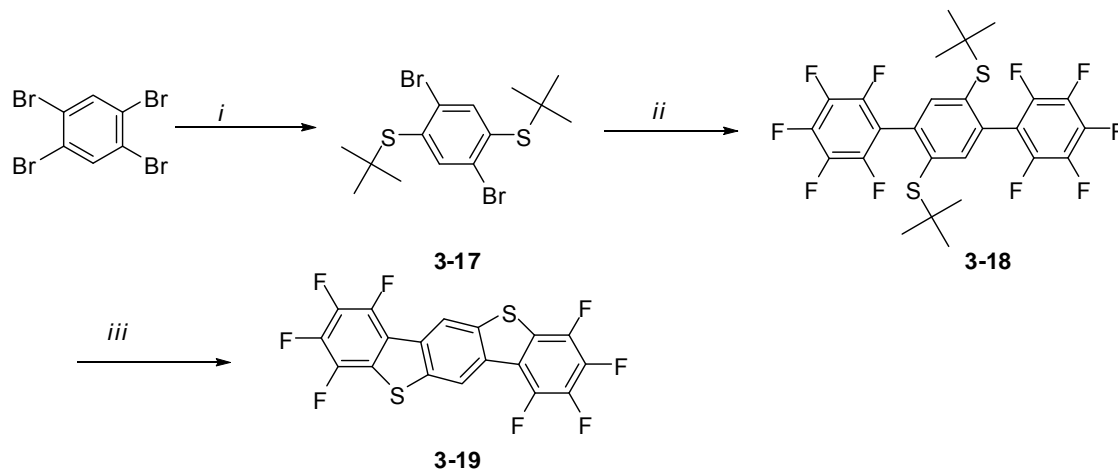


Figure 3. 7 Synthesis of fluorinated BBT **3-19**. *i*: *t*-BuSNa, DMF, 74%; *ii*: a). *n*-BuLi, 0°C, ether, b). C₆F₆, 0°C then r.t., 41%; *iii*: a). AlCl₃, toluene, r.t., b). KOH, 18-crown-6, r.t., 31%.

3.2.3 Syntheses of compounds **3-24a,b**

Alkyl chains (hexyl or dodecyl) were placed on the central benzene ring of fluorinated BBTs in order to increase solubility and to investigate their effect on self-assembly. BBTs **3-24** were prepared in five steps from 1, 4-dichlorobenzene in moderate-to-good yields. (**Figure 3. 8**) 1, 4-dialkylbenzenes **3-20** were prepared by Kumada coupling in the presence of NiCl₂[dppp]. Compounds **3-20** were then brominated with Br₂ and a catalytic amount of I₂ to obtain 1, 2, 4, 5-tetrabromo-3, 6-dialkybenzenes (**3-21**) quantitatively which then underwent nucleophilic aromatic substitution by isopropyl thiolate to yield 1, 4-dibromo-2, 5-dialkyl-3, 6-bis(isopropylthio)benzenes (**3-22**). The terphenylene precursors **3-23** were prepared by converting **3-22** to para-bis-metalates via halogen-lithium exchange and reacting with excess perfluoroarene. Finally the precursors **3-23** were dealkylated and underwent ring-closure to give the final rod molecules **3-24**¹⁷⁶ similar to the procedures described above.

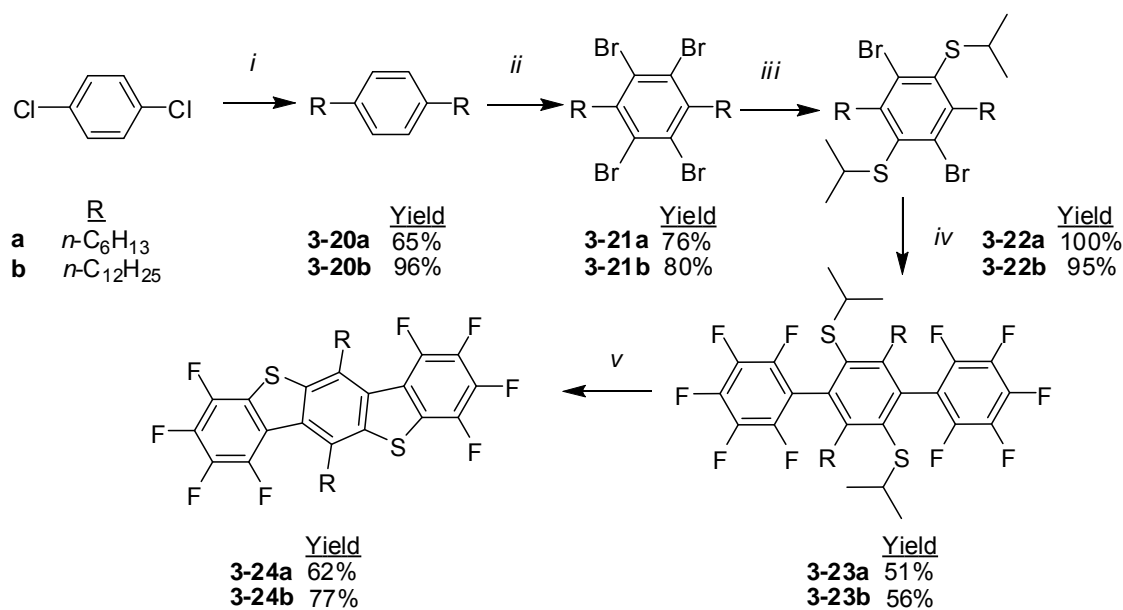


Figure 3. 8 Synthesis of highly fluorinated BBBTs **3-24** with alkyl chains. *i*: RMgBr, ether, NiCl₂[dppp], reflux; *ii*: Br₂, Cat. I₂, 0°C; *iii*: propane-2-thiol, NaH, DME, 50°C; *iv*: a). *t*-BuLi, ether, -78°C, b). C₆F₆, DME; *v*: a). AlCl₃, toluene, b). KOH, 18-crown-6.

A ¹⁹F NMR-scale reaction was conducted to monitor the conversion of **3-23b** to **3-24b** (**Figure 3. 9**). In ¹⁹F spectrum “a”, there are three multiplets corresponding to three types of fluorines in the pentafluorophenyl groups of starting material **3-23b**. After AlCl₃ was added, the solution became red. Spectra **b-e** were measured at different times. With respect to spectrum **a**, more signals continuously appear which arise from various sources such as compound **3-23b**, its derivatives with one and two iso-propyl groups removed, likely aluminum complexes of all these, etc. After overnight agitation, only three new signals are present in spectrum **e** corresponding to three types of fluorines in the fully dealkylated compound (**A**). Freshly-ground KOH and 18-crown-6 were added in one portion into the NMR tube. The solution immediately became yellow upon shaking. After another overnight period with agitation, four new signals appear in spectrum **f** corresponding to four types of fluorines in the final product **3-24b**, indicating the cleanliness of this two-step, one-pot conversion.

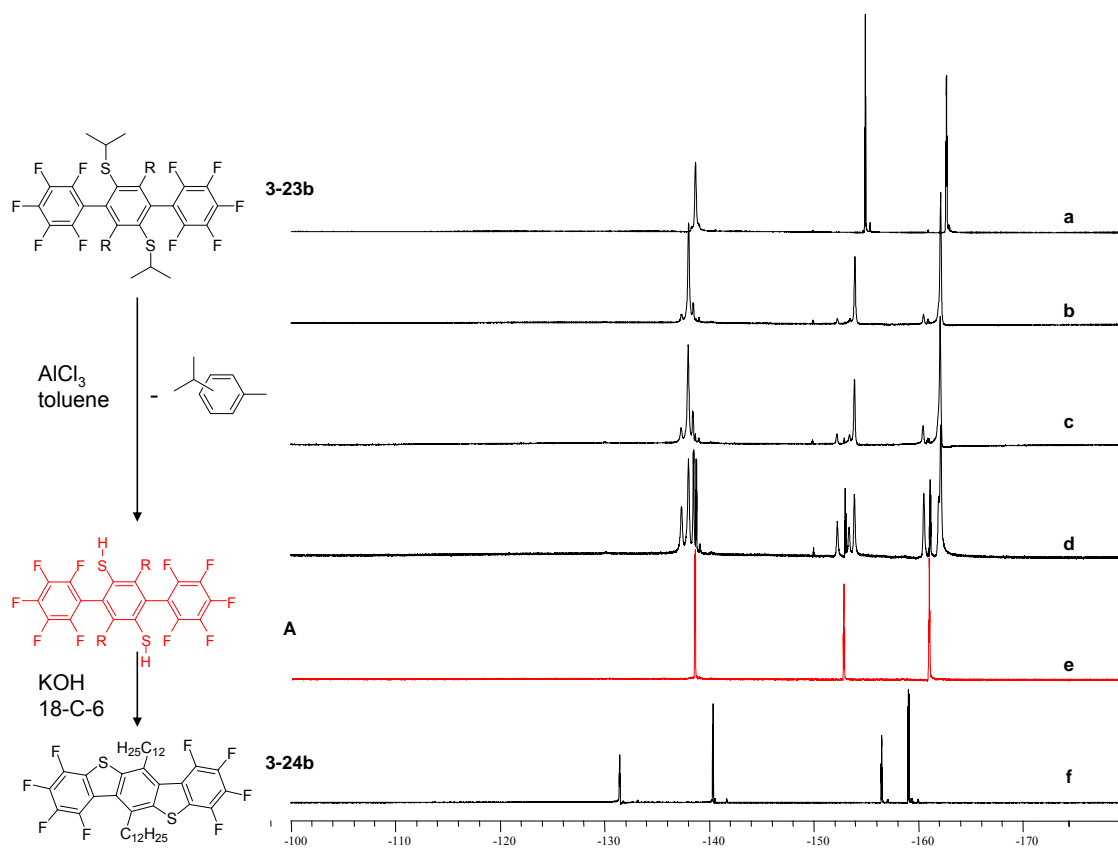


Figure 3. 9 ^{19}F NMR spectra for preparation of **3-24b** from **3-23b**.

3.2.4 Functionalization of compound **3-24a**

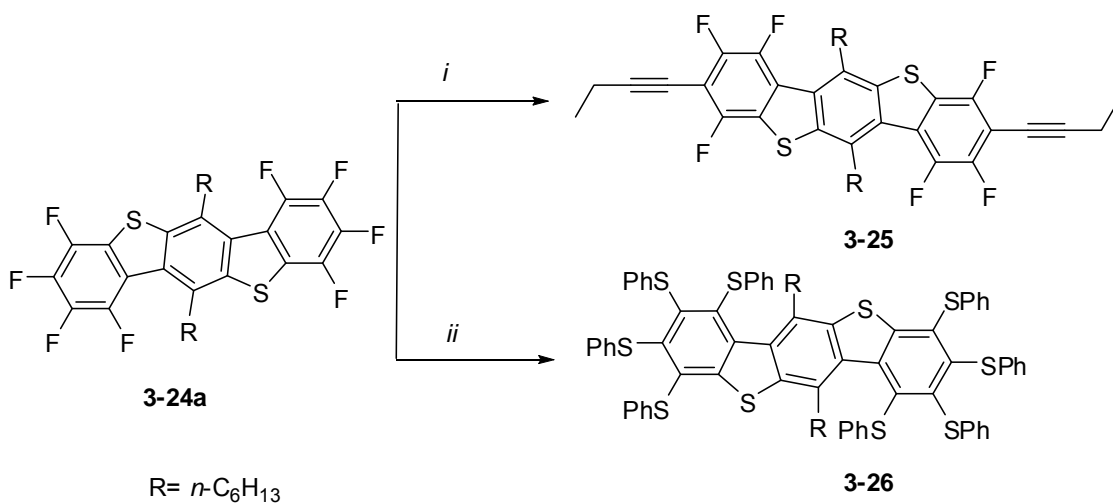


Figure 3. 10 Functionalization of compound **3-24a**. *i*. Butynyllithium, THF, r.t., 31%; *ii*. benzenethiol, NaOH, DMF, 53%.

Highly fluorinated BBTs can also serve as building blocks via substitution of select or all fluorine atoms. The preliminary examples shown in **Figure 3. 10** are each the result of a single unoptimized trial. The regioselectivities of partial substitution reactions are a function of the nucleophile and the relative directing abilities of the sulfur- and carbon-centered substituents. The butynyl anion nucleophile will replace fluorines at the positions meta to sulfur atoms because the carbon-centered substituent is more efficient to stabilize an adjacent carbanionic center than sulfur-centered substituent in the Meisenheimer complex.¹⁷⁷ The actual selectivity of this reaction is not yet determined, as a substantial portion of the reaction mixture was accidentally lost during purification. Therefore compound **3-25** was isolated in 31% yield. It is a potential substrate for alkyne metathesis. As expected based on reports^{178, 179} of other perthiolated π -systems, the reduction wave onset of **3-26** is approximately 200mV more positive than its precursor **3-24a** (**Table 3. 2**).

3.3 Crystal structures of highly fluorinated BBTs 3-15a and b, 3-19, 3-24a and b and 3-25

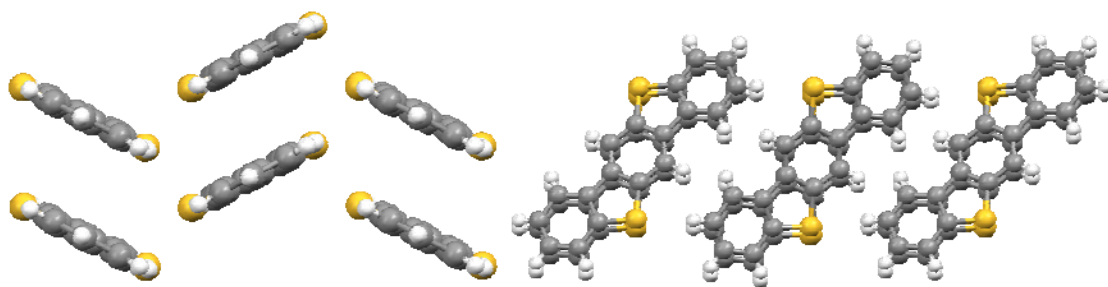
Single-crystal x-ray analyses revealed that all BBTs **3-15a,b**, **3-19**, and **3-24a,b** form slip stacks with face-to-face orientation. With the exception of **3-24a**, all assemble with S-F close contacts. Partial packing diagrams are included in **Figure 3. 11** along with that of the published nonfluorinated parent **3-5** for comparison.¹⁶⁵ BBT **3-5** packs in a typical herringbone-like arrangement with edge-to-face interactions along its long edges.

Derivatives **3-15a,b** crystallize with predicted full edge-to-edge arrangements with eight S-F close contacts per molecule. BBT **3-15b** assembles to sheets with all unsaturated atoms lying in perfectly parallel planes while the molecular planes of **3-15a** tilt slightly against similar planes containing the molecular centroids. Both fully fluorinated BBTs form slip π -stacks along two dimensions, a feature which has been shown to improve FET performance.¹⁸⁰⁻¹⁸² For **3-15a**, one π -stacking axis is defined by 10 close contacts per molecule (6 C-C, 4 C-S), and the other by two S-S close contacts. The average face-to-face (atom-to-plane) distance is 3.34 Å. For **3-15b**, π -overlap is minimal and defined along each of two dimensions by 4 C-S interatomic distances (3.51

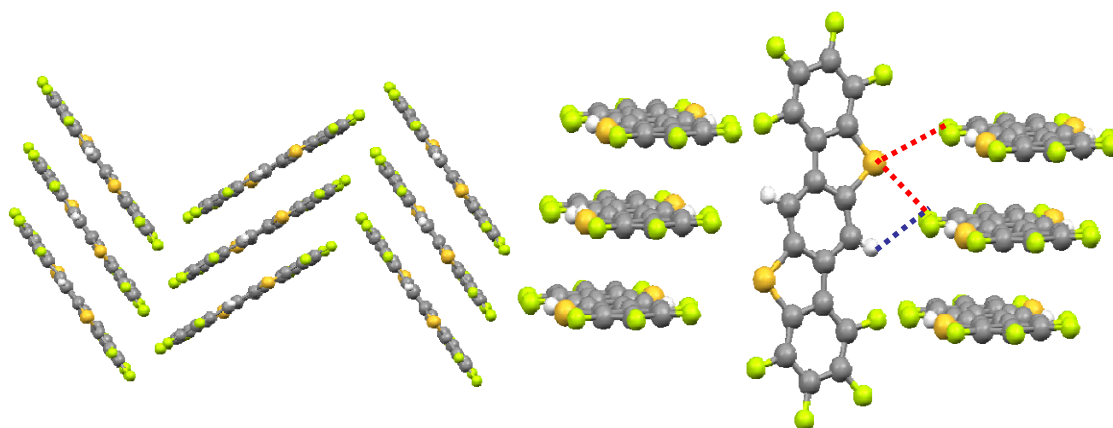
Å) which approximate the sum of the vdW radii of carbon and sulfur. The interplanar distance is exceptionally small (3.2Å), similar to that reported³⁰ for perfluoropentacene and likewise attributed to electrostatic attraction. The large slip along the short molecular axis may also contribute. Whether recrystallized via vapor sublimation¹⁸³ or from solution, **3-15b** forms very thin, “large” flexible plates.

While BBTs **3-24a,b** lack central fluorine atoms to complete the F-S-F edge-to-edge interactions, their bulky side chains preclude edge-to-face interactions along their long edges. The side-chains of **3-19**, **3-24a**, and **3-25** also expand the π -stacking distance (3.40-3.45 Å) relative to the other BBTs.

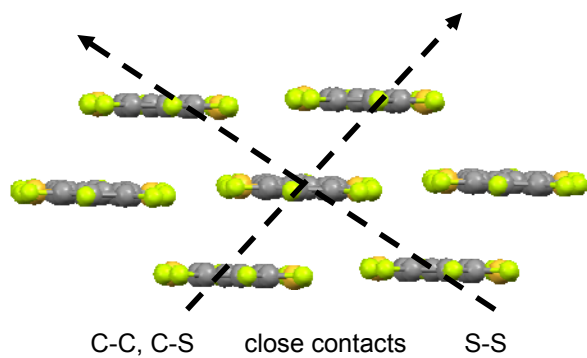
BBBT **3-19**, X = H, serves as a control. It is fully fluorinated except that it lacks fluorine atoms on its central benzene rings to complete the F-S-F interactions. As a consequence, it is the only new derivative reported here which exhibits a herringbone-like packing with edge-to-face interactions (at molecular termini). Its crystal plates were exceedingly thin, twinned and somewhat disordered, and therefore the precision of the reported structure is relatively low for a small molecule. However, the molecular structure and packing motif are unambiguous. Edge-to-edge close contacts (S-F and H-F) bridge adjacent oblique, rather than (nearly) parallel, molecular planes.



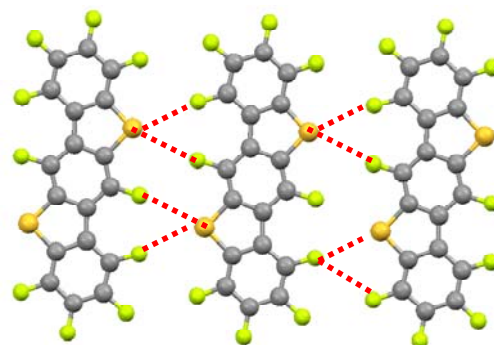
(a)



(b)



(c)



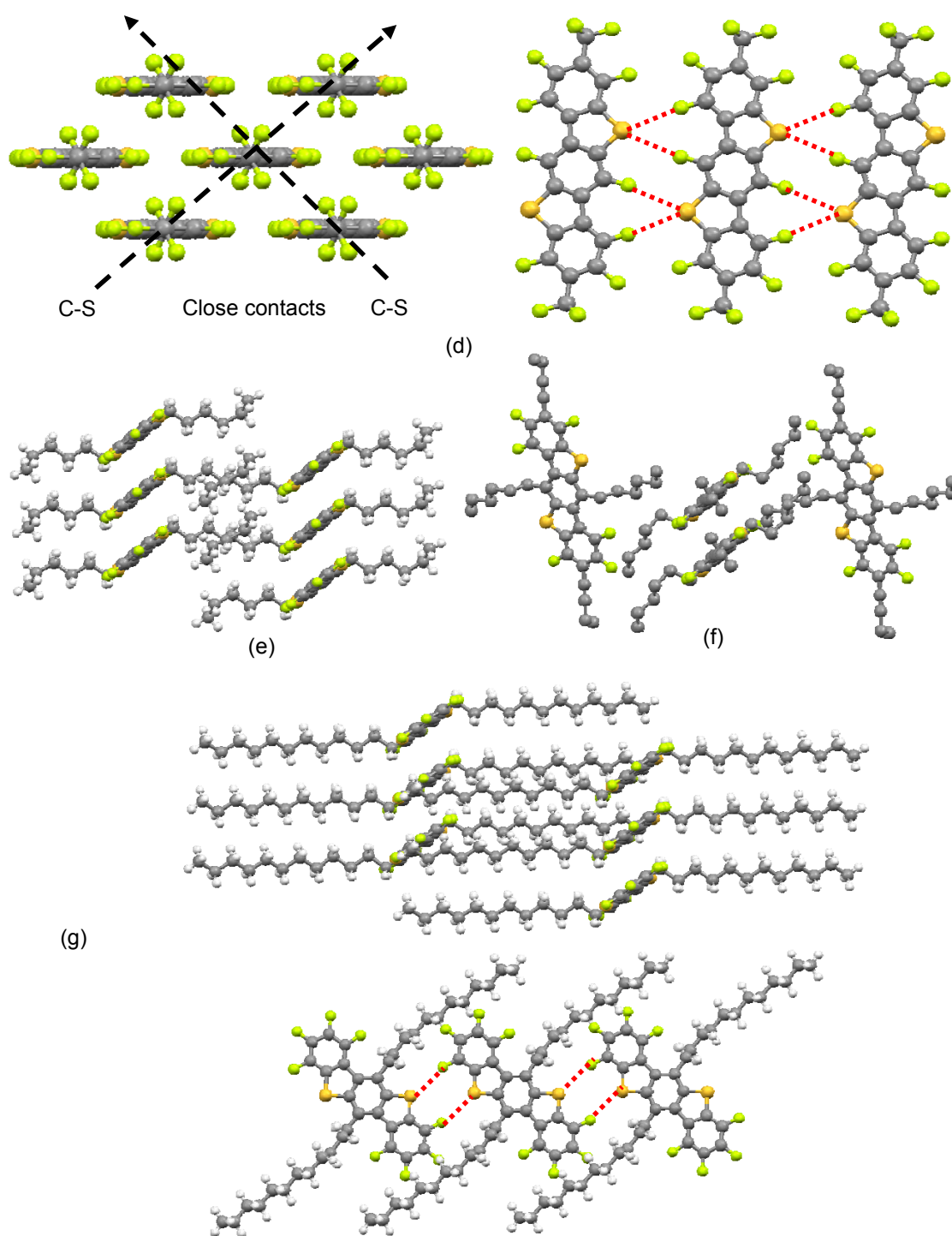


Figure 3. 11 Crystal packing diagrams for (a) **3-5**,¹⁶⁵ (b) **3-19**, (c) **3-15a**, (d) **3-15b**, (e) **3-24a**, (f) **3-25**, (g) **3-24b**. Red dashed lines: S-F close contacts. Blue dashed line: S-H close contacts.

3.4 UV-Vis spectra and cyclic voltammetry

Solution electrochemical measurements of **3-15a**, **3-15b** and **3-19** revealed reduction peaks at -1.99, -1.60 and -2.18 V (vs Fc/Fc⁺). From reduction wave onsets (**Table 3. 2** and **Figure 3. 12**), LUMO levels are estimated to be -2.81, -3.20 and -2.62 eV, respectively. These values can not be strictly compared with that reported from another laboratory for the parent **3-5** (LUMO = -2.50 eV)¹⁶⁵, but the effect of fluorination is clear. Greater fluorine substitution lowers the LUMO (**3-15a** vs **3-19**) and more electron-withdrawing CF₃ groups provide the largest effect.

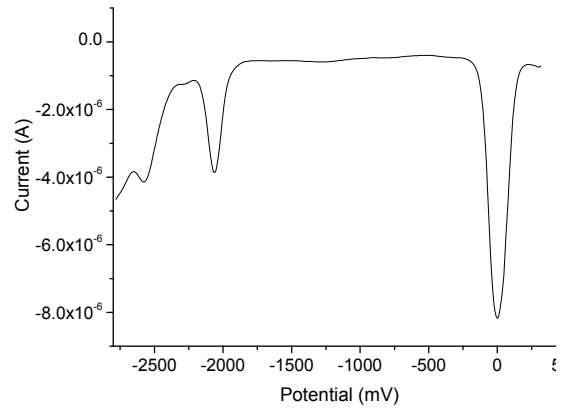
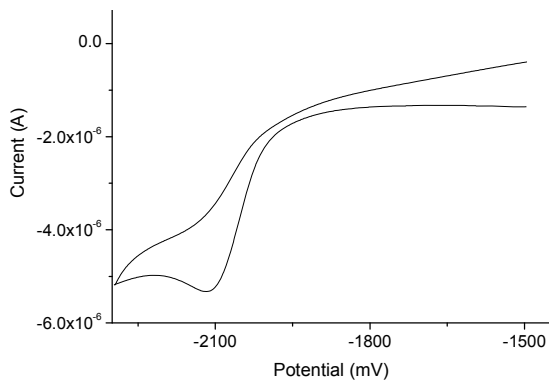
The UV-Vis spectra of **3-15a**, **3-15b** and **3-19** are shown in **Figure 3. 13** for comparison. Three absorption bands are observed for all of three compounds. The one with lowest intensity at longer wavelength is around 320-420 nm corresponding to the π - π^* transition of the conjugated cores (S₀-S₁), while the shorter wavelength band (280-320 nm) originates from the electronic transition from S₀ to S₂ and the shortest wavelength band (220nm-280nm) originates from the combination of electronic transitions from S₀ to S_n (n>2). Energy gaps E_g of the lowest allowed optical transitions (**Table 3. 2**) are 3.24 and 3.27 eV for **3-15a** and **3-19**, determined from the absorption edges of UV-Vis spectra. They are very similar to the unsubstituted compound **3-5** (3.26 eV),¹⁶⁵ while that for **3-15b** is significantly lower (2.98 eV). As previously demonstrated,^{184, 185} (even subtle) substitution effects can be well understood by quantum-chemical calculations, carried out at the DFT (density functional theory) level of theory, employing the B3LYP functional and the 6-311+G* basis set within the GAUSSIAN03 package.¹⁸⁶ According to the calculations performed by our collaborator Johannes Gierschner (**Table 3. 3**), the transition responsible for E_g is described mainly by the HOMO-LUMO transition. The small change in E_g when going from **3-5** to **3-15a** and **3-19** is due to a compensation of the hypsochromic shift induced by fluorination at the terminal positions (“R₂”) by the bathochromic shift due to fluorination in the lateral positions (“R₁”). (**Figure 3. 14**) Due to terminal CF₃ substituents, the S₀ → S₁ band of compound **3-15b** is significantly red-shifted compared to that of the per-fluorinated compound **3-15a**. The calculated overall shift is 0.33 eV, in reasonable agreement with the experimental value (0.26 eV). Simulated spectra relating the pure vertical transitions

($S_0 \rightarrow S_{1,2,3}$) are shown in **Figure 3. 15**.

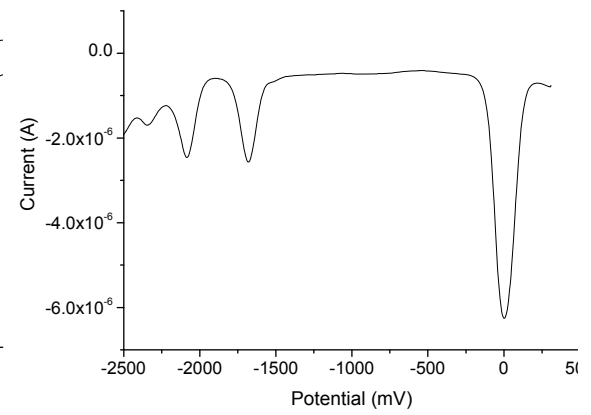
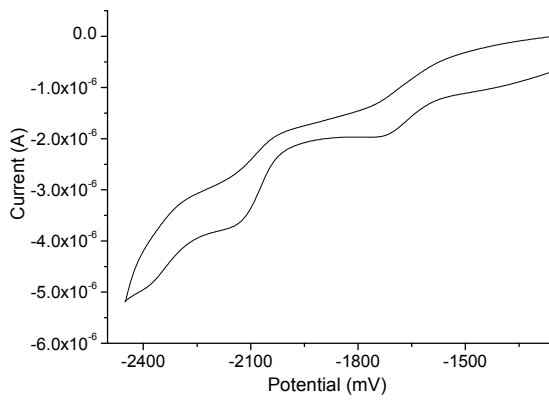
Table 3. 2 Electrochemical data , estimated HOMO and LUMO levels and UV-Vis Data of **3-15a**, **3-15b**, **3-19**, **3-24a**, **3-26** and **3-5**

	$E_{\text{red}}^{\text{a}}/\text{V}$ cathodic/onset	$\lambda_{\text{max}}^{\text{b}}/\text{nm}$ peak/edge	LUMO ^c /eV	$E_{\text{g}}^{\text{d}}/\text{eV}$	HOMO ^e /eV
3-15a	-2.13/-1.99	372/383	-2.81	3.24	-6.05
3-15b	-1.72/-1.60	400/416	-3.20	2.98	-6.18
3-19	-2.33/-2.18	366/379	-2.62	3.27	-5.89
3-24a	-2.42/-2.22	383/397	-2.58	3.12	-5.70
3-5^f		369/380	-2.50	3.26	-5.76
3-26	-2.04/-2.03	467/490	-2.77	2.53	-5.30

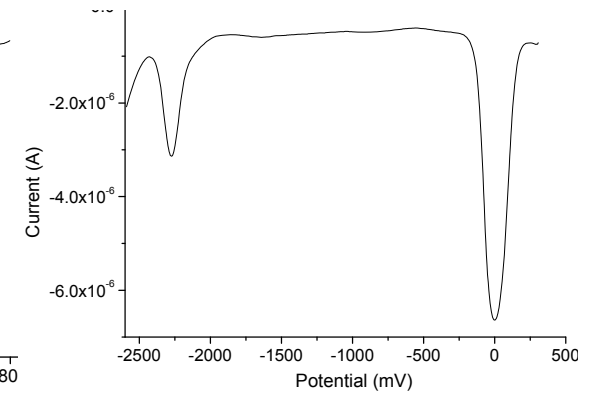
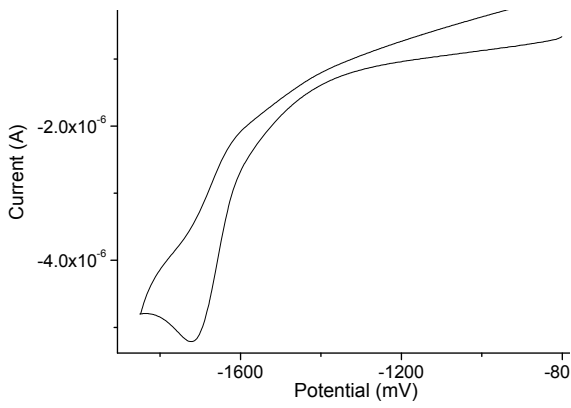
^a Versus Fc/Fc⁺ ($E_{1/2}$ =0.60V in this system). ^b Solution absorption spectra. ^c Estimated from reduction wave onset.(LUMO = $-E_{\text{red}} - 4.8$) ^d Determined from the absorption edge. ^e Estimated from HOMO = LUMO - E_{g} . ^f Reference ¹⁶⁵.



(a)



(b)



(c)

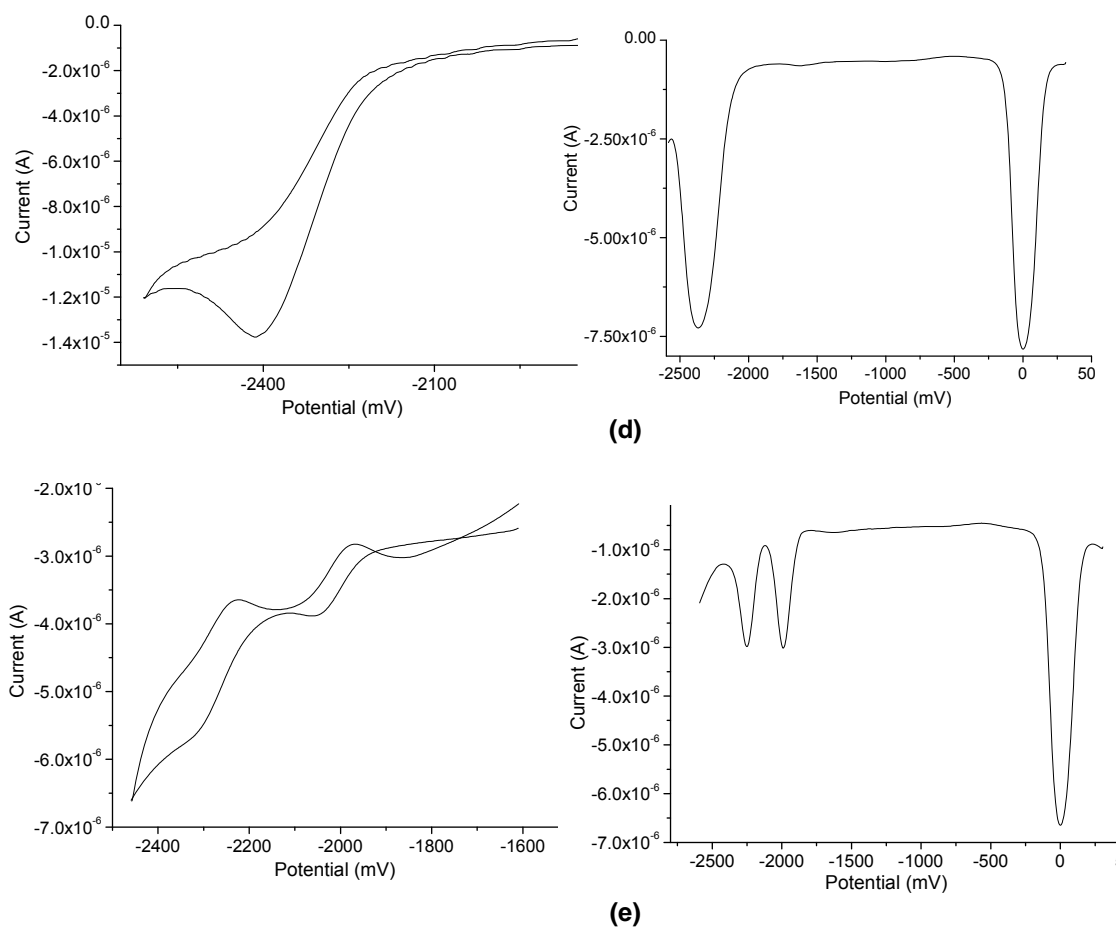


Figure 3. 12 Cyclic voltammograms (left, vs Fc/Fc^+) and Osteryoung square wave voltammograms (right, vs Fc/Fc^+ , $E_{1/2}=0.60$ V, which is the largest peak set to 0 mV) of compounds **3-15a** (a), **3-15b** (b), **3-19** (c), **3-24a** (d) and **3-26** (e). Conditions: 0.1M $(n\text{-Bu})_4\text{PF}_6$ in tetrahydrofuran; working electrode, Pt; counter electrode, Ag wire; reference electrode, Ag/AgCl; scanning rate, 50mV/s.

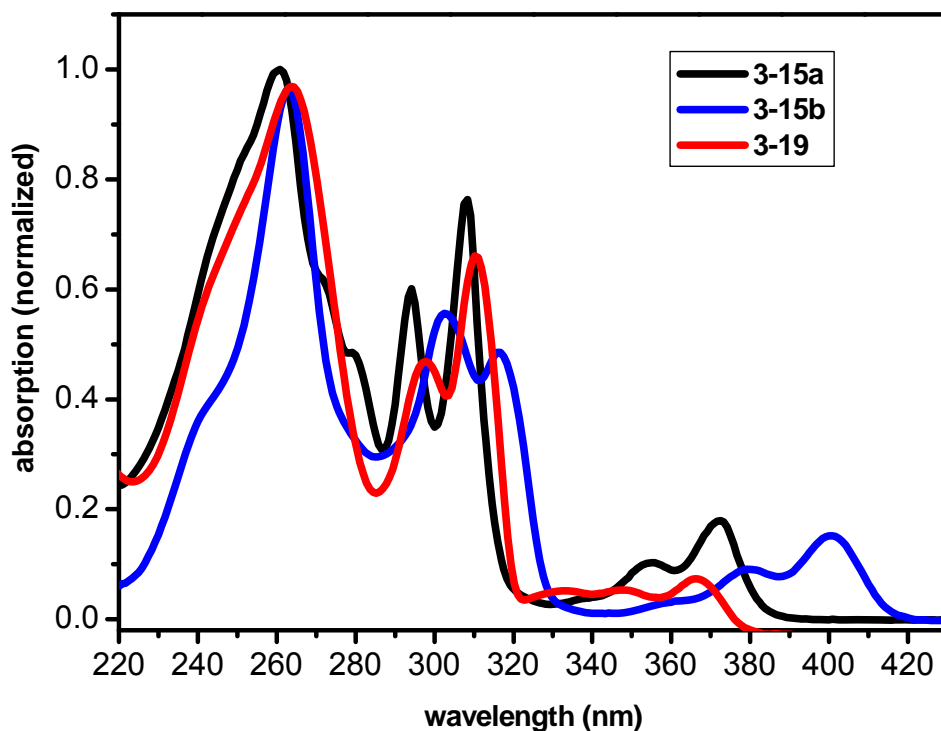


Figure 3. 13 Solution absorption spectra of compounds **3-15a**, **3-15b** and **3-19**. (10^{-6} M THF).

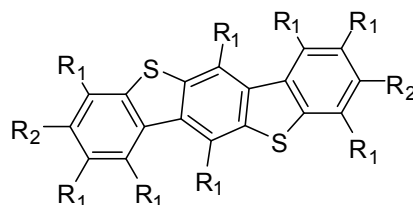


Figure 3. 14 Illustration of the different “lateral” and “terminal” positions considered during computational studies..

Table 3. 3 Energetic positions of the frontier orbitals, bandgap E_{H-L} , vertical transition energy $E_{vert}(S1)$ and oscillator strength $f(S1)$ of the lowest electronic transition.

R_1	R_2	E_{HOMO} (eV)	E_{LUMO} (eV)	ΔE_{H-L} (eV)	$E_{vert}(S1)$ (eV)	$f(S1)$
H	H	-5.823	-1.806	4.017	3.495	0.033
F	F	-6.739	-2.793	3.946	3.472	0.082

		(-0.916)	(-0.987)	(-0.071)	(-0.023)	
F	CF ₃	-6.930	-3.320	3.610	3.149	0.077
		(-1.107)	(-1.514)	(-0.407)	(-0.346)	
<i>H</i>	<i>F</i>	-6.105	-1.964	4.141		
<i>F</i>	<i>H</i>	-6.499	-2.709	3.790		

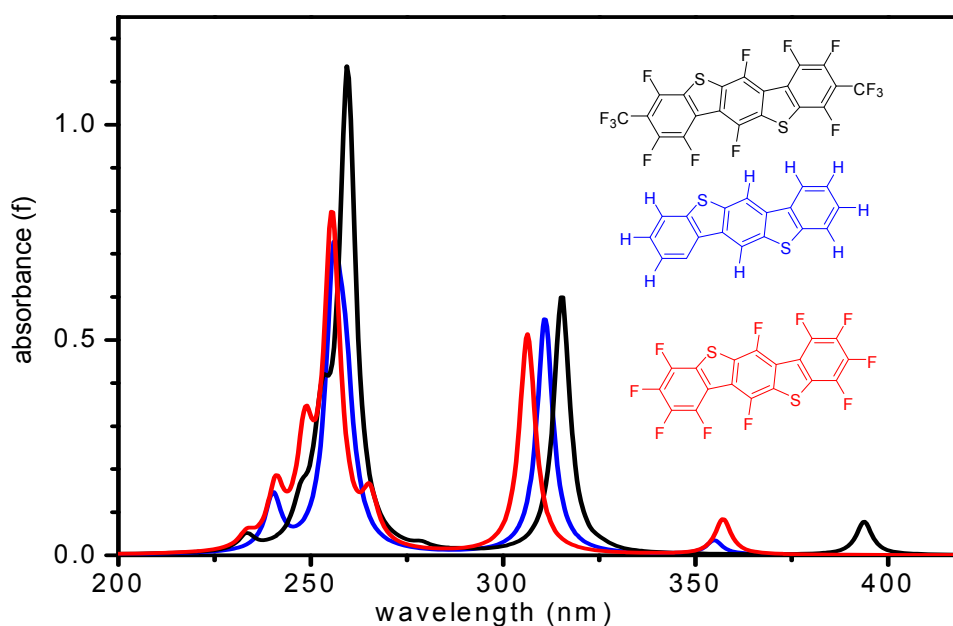


Figure 3. 15 Calculated absorption spectra (in units of oscillator strength) for **3-15a**, **3-15b** and **3-19**, representing the pure (vertical) electronic transitions, broadened by a Lorentzian.

3.5 Conclusion and outlook

In summary, an efficient route has been established, relying heavily on S_NAr reactions, to prepare regiopure fluorinated polycyclics **3-15a,b**, **3-19**, and **3-24a,b**. They are easily further functionalized with other substituents by post-synthesis S_NAr reactions. Experimental and computational estimates of the effects of substituents on the energy gap and frontier orbital energy levels are in accord: CF₃ substituents (**3-15b**) induce a bathochromic shift of the (optical) energy gap and decrease the LUMO level relative to the fluorine substituents of **3-15a**. Fluorine atoms attached to central benzene rings

decrease the LUMO energy level in comparison to protons at the same positions (**3-15a** vs **3-19**). Two antiparallel F-S-F units along each side of the lath-shaped molecules, likely together with face-to-face electrostatic attraction, preclude edge-to-face interactions. Two opposed S-F units are however insufficient to preclude edge-to-face arrangements, except when bulky alkyl chains are included. Crystallization to sheets of (nearly) parallel molecules coincides with assembly to 2D π -stacking motifs by BBBTs **3-15a** and **3-15b**, which may make them promising candidates for semiconductors.

Since 2-dimensional π -stacking occurs along the short axes of these molecules, and is not disrupted by terminal CF_3 substituents (**3-15b**), future work should involve derivatives carrying solubilizing groups such as long alkyl or alkynyl groups at the molecular termini (**3-27** and **3-28**) to increase the solution-processability. Compound **3-27** should be easily obtained by functionalizing **3-15a** with lithium acetylides by post-synthesis $\text{S}_{\text{N}}\text{Ar}$ reactions. The acetylenic bonds can be reduced by hydrogen to yield **3-28** with various alkyl substituents. (**Figure 3. 16**)

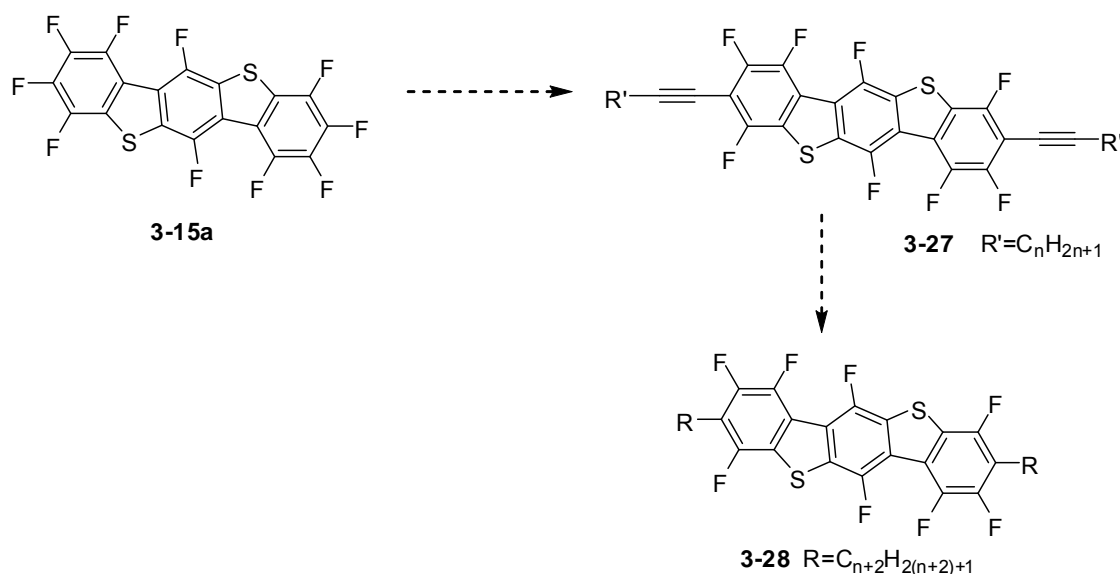


Figure 3. 16 Synthetic scheme of **3-27** and **3-28** with long alkyl solubilizing groups.

Chapter 4 Synthesis and characterization of benzodichalcogenophenes functionalized with fluorinated aromatics

4.1 Introduction

As described in **Chapter 3**, numerous studies have been focused on synthesis and characterization of π -extended heteroarenes containing chalcogenophenes (i.e., thiophene, selenophene, tellurophene) owing to their potential, and in some cases demonstrated, high performance as organic semiconductors within various optoelectronic devices.^{98, 160, 180, 182, 187, 188} (**Figure 4. 1**) 2,6-diphenylbenzo[1,2-b:4,5-b']diselenohene (**4-1**) showed OFET mobilities up to $0.17 \text{ cm}^2 \text{ V}^{-1}$ and on/off ratio of 10^5 .⁹⁸ Air stable OFETs can be fabricated from compound **4-2** ($\mu_{\text{FET}} = 2 \text{ cm}^2 \text{ V}^{-1} \text{ s}^{-1}$ and $I_{\text{on/off}}=10^8$)¹⁸⁷ and **4-3** ($\mu_{\text{FET}} = 2 \text{ cm}^2 \text{ V}^{-1} \text{ s}^{-1}$ and $I_{\text{on/off}}=10^7$)¹⁸⁸ respectively. Solution-processed OFETs with good performance have also been fabricated from soluble benzothienobenzothiophene (**4-4**) ($\mu_{\text{FET}} \geq 1 \text{ cm}^2 \text{ V}^{-1} \text{ s}^{-1}$ and $I_{\text{on/off}}=10^7$)¹⁸⁹ and TES-ADT (**4-6**) ($\mu_{\text{FET}} = 1 \text{ cm}^2 \text{ V}^{-1} \text{ s}^{-1}$).¹⁶¹ Mobility with $0.09 \text{ cm}^2 \text{ V}^{-1} \text{ s}^{-1}$ can be obtained for OFET fabricated from **4-5** based on the measurement of space-charge limited currents (SCLC).¹⁹⁰

As described earlier in this document n-type behavior has been observed after electron-withdrawing groups are introduced to the molecular termini of p-type materials.^{27, 28, 32, 33, 191} (**Figure 4. 2**) n-Type OFETs based on π -systems bearing terminal trifluoromethylphenyl groups have been prepared from **4-7** ($\mu_{\text{FET}} = 3.4 \times 10^{-3} \text{ cm}^2 \text{ V}^{-1} \text{ s}^{-1}$ and $I_{\text{on/off}}=10^4$), **4-10** ($\mu_{\text{FET}} = 0.26 \text{ cm}^2 \text{ V}^{-1} \text{ s}^{-1}$ and $I_{\text{on/off}}=10^6$)¹⁹¹ and **4-11** ($\mu_{\text{FET}} = 0.18 \text{ cm}^2 \text{ V}^{-1} \text{ s}^{-1}$ and $I_{\text{on/off}}=10^5$).¹⁹¹ Compound **4-12** lead to n-type OFETs with mobility of $0.08 \text{ cm}^2 \text{ V}^{-1} \text{ s}^{-1}$ and $I_{\text{on/off}} \geq 10^5$.²⁸ Most related to the new materials to be described in this chapter, Takimiya reported the series of benzodithiophene (selenophene) (BDT(Se)) derivatives **4-13**. Only derivative **4-13f** bearing CF_3 groups at its termini exhibited n-type transport in an FET, and its electron mobility was only $0.10 \text{ cm}^2 \text{ V}^{-1} \text{ s}^{-1}$.³³ This report was not accompanied by crystallographic studies relating performance to mode of self-assembly. The BDT scaffold building block, functionalized with various fluorinated arenes, might provide better performance if the electronic levels and supramolecular assembly are adjusted. Recall from the preceding chapters that face-to-face packing can

enhance semiconducting properties because intermolecular orbital overlap can be maximized to facilitate charge transport.¹⁵ Once again, face-to-face interactions and thus increasing orbital overlap can be driven by side chains or substituents around the conjugated core system which can preclude edge-to-edge interactions.^{64-66, 68, 69} In addition, arene-perfluoroarene interactions are effective to control molecular packing in face-to-face π - π packing motifs.^{28, 70, 141}

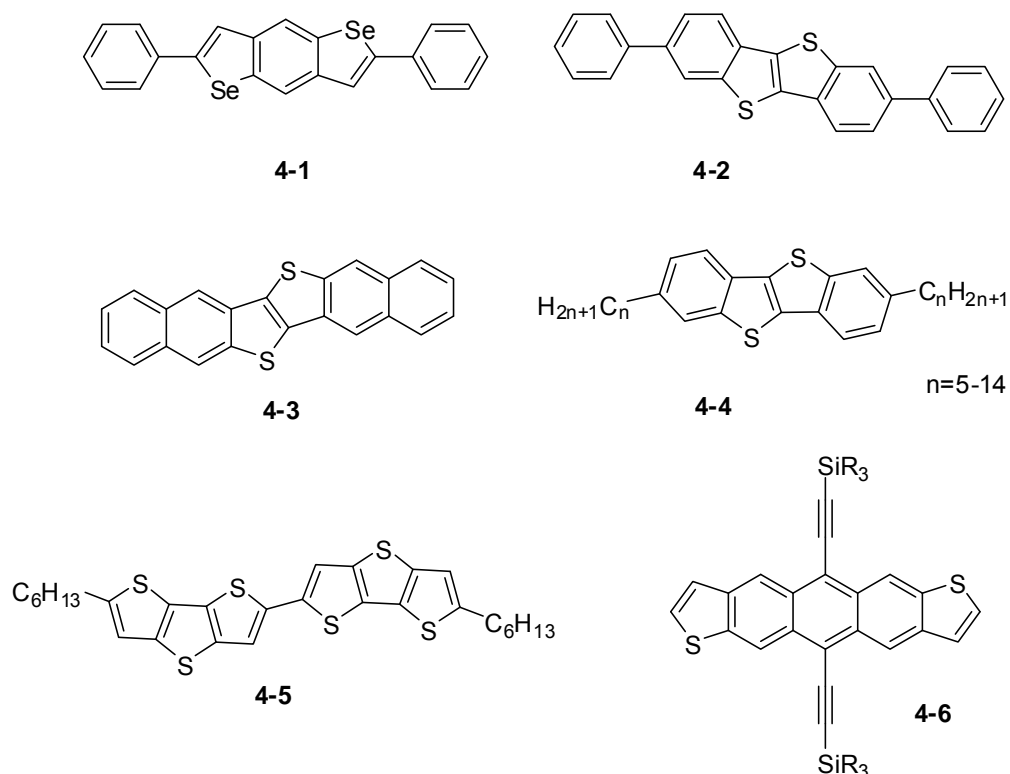


Figure 4. 1 Published π -extended heteroarenes containing chalcogenophenes.

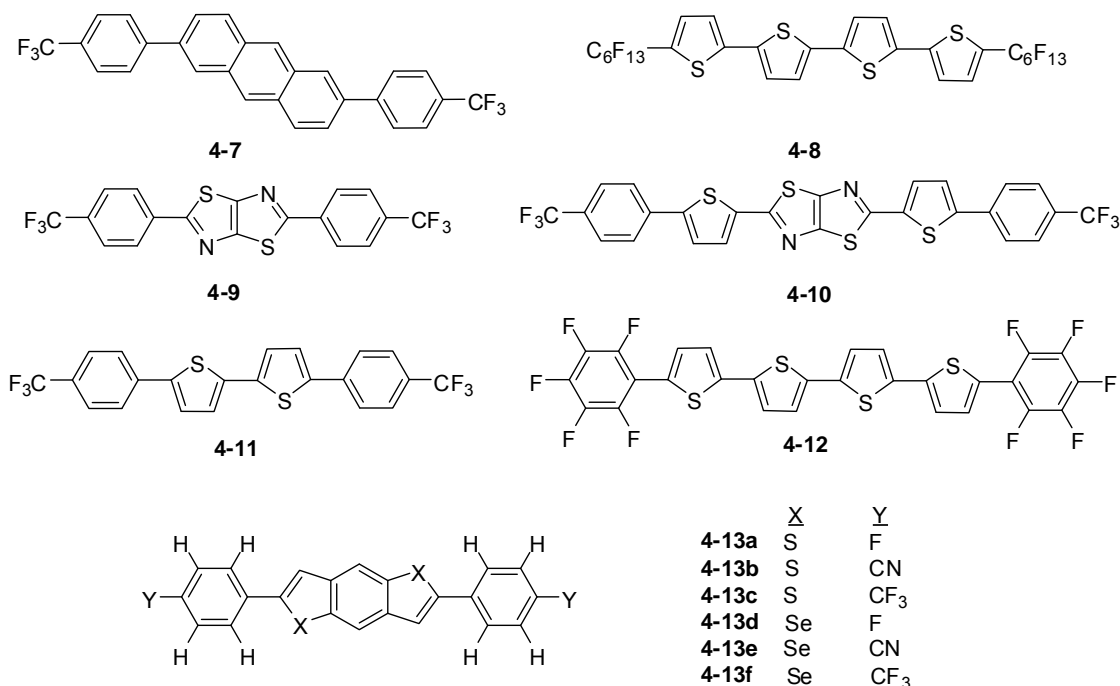


Figure 4. 2 Structures of some n-type materials with electron-withdrawing groups as terminal groups.

This chapter will describe synthetic efforts to attach electron-withdrawing groups (perfluoroarenes) to the benzodichalcogenophene core by nucleophilic replacement of fluoride from perfluoroarenes by metalated BDT(Se). Crystal packing and HOMO/LUMO energy levels were engineered by incorporating different substituents at the 4 and 8 positions of the benzodichalcogenophene core and various perfluoroarenes as the molecular termini.

4.2 Synthesis of perfluoroarene-substituted benzodichalcogenophene compounds

The syntheses of perfluoroarene-substituted benzodichalcogenophene derivatives are demonstrated in **Figure 4. 3**. Two different routes employing S_NAr reactions between metalated BDT(Se)s and perfluoroarenes are exploited to synthesize those derivatives. The first route for compounds **4-14** through **4-17** was to react silyl-functionalized (latent nucleophile) **4-26**, with perfluoroarenes, catalyzed by cesium fluoride and 18-crown-6 in toluene at 80°C overnight. These conditions are similar to those described in Chapter 2 for the preparation of conjugated thiophene-containing polymers. The yellow or light

yellow products **4-14** to **4-17** were obtained after purification by column chromatography or precipitation into methanol. The second route, employed for the synthesis of compounds **4-18** to **4-25**, relied on lithiation of compounds **4-27** to create nucleophiles, which were then reacted with excess perfluorarene. The pure compounds **4-18** to **4-25** with yellow or orange colors were obtained after purification by column chromatography or precipitation into methanol.

For the synthesis of **4-26**,¹⁹² 1,4-dibromo-2,5-bis(2-trimethylsilylethynyl)benzene (**4-28**), readily prepared from 1,4-dibromo-2,5-diiodobenzene and trimethylsilylacetylene (TMSA) via Sonogashira coupling catalyzed by Pd(PPh₃)₄, was lithiated by *t*-BuLi followed by adding chalcogen powder (sulfur or selenium). The reaction was finally quenched by ethanol. BDT **4-26a** and BDSe **4-26b** were obtained as colorless solids in 56% and 67% isolated yields after standard aqueous workup and column chromatography. Compound **4-26a** partially underwent proteodesilylation on exposure to chromatographic silica gel. Compounds **4-27a, b** bearing alkoxy groups were prepared by published procedures.¹⁹³ Compounds **4-27c, d** were prepared by the reaction of the Grignard reagents of silyl acetylenes with benzo[1,2-*b*:4,5-*b'*]dithiophene-4,8-dione (**4-29**) which was prepared from 3-bromothiophene via three steps.¹⁹⁴ The intermediate propargylic alkoxides were reduced (deoxygenated) with acidic aqueous solutions of SnCl₂·2H₂O at 60°C.⁶⁵ The workup with water and dichloromethane and purification by column chromatography yielded the solid products with 51% and 20% yields for the TIPS and TMS derivatives, respectively. The low yield for **4-27d** bearing TMS groups is attributed to some decomposition (protodesilylation) through silica gel.

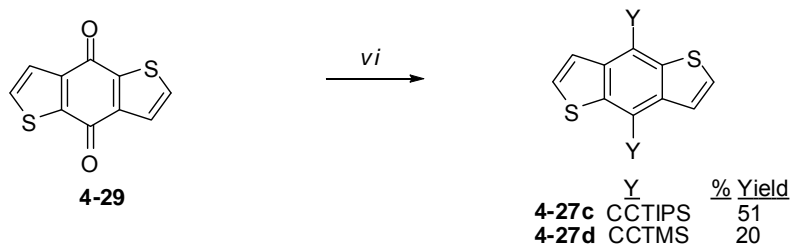
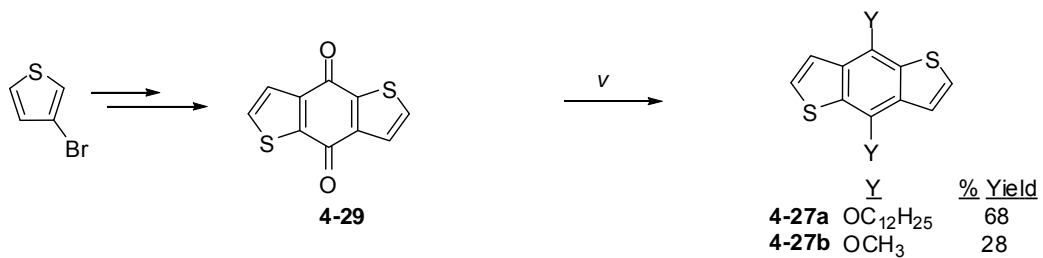
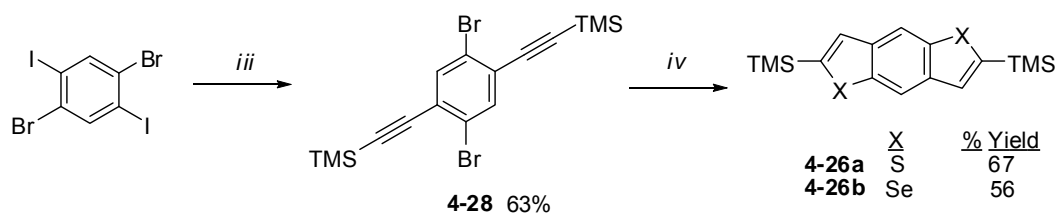
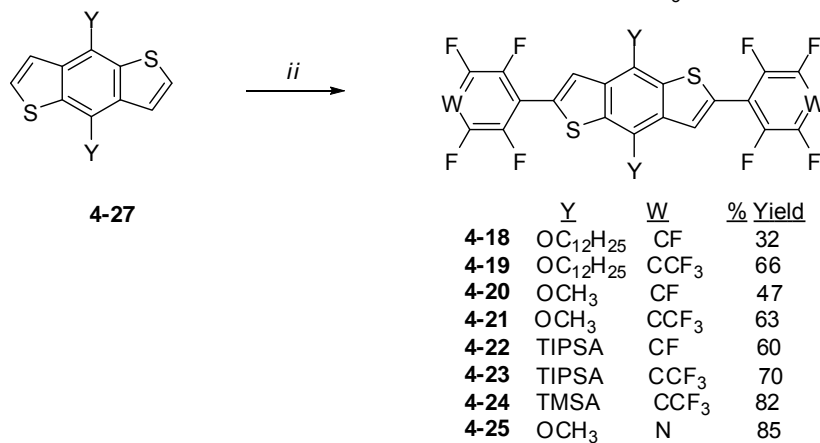
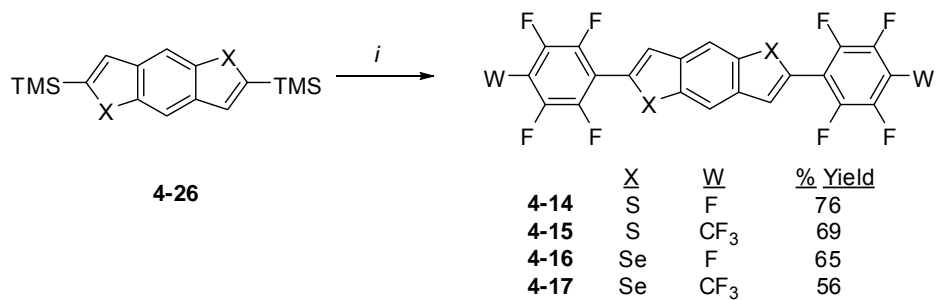


Figure 4.3 Synthetic schemes of compounds **4-14** – **4-25**. *i*: CsF, 18-crown-6, C₆F₆/C₇F₈,

Toluene, 80°C; *ii*: a). *n*-BuLi, TMEDA, THF, 0°C/-78°C, b). C₆F₆/C₇F₈/C₅F₅N; *iii*: TMSA, [Pd], DIPA, CuI, toluene, 80°C; *iv*: a). *t*-BuLi, b). S/Se, c). EtOH; *v*: a). Zn, EtOH, 20% NaOH, b). Ar-SO₃R; *vi*: a). RCCMgBr, THF, b). SnCl₂.

4.3 Crystal structures of compounds 4-14 through 4-25

Single-crystal X-ray analyses revealed, as predicted, that the ring systems of all BDT(Se) derivatives **4-14** through **4-25** are indeed coplanar, likely driven by intermolecular π - π F interactions with possibly some contribution from intramolecular S-F attraction. Compound **4-14** is the exception with a torsion angle of 50.31° between the central BDT unit and terminal pentafluorophenyl rings. This can be attributed to inclusion of solvent molecules (toluene) in the cocrystal. Interpolation of toluene obviously increases the distance between successive C₆F₅ rings within a π -stack. The BDT units must rotate out of the plane of the C₆F₅ units in order to accommodate the increased repeating distance. All derivatives excluding **4-14** form slip stacks with face-to-face orientation and with large pitch translation and small roll translation.⁵⁷ (**Table 4. 1**) See **Figure 1. 15** and the associated discussion in chapter 1 for definitions of pitch and roll. Partial packing diagrams are included in **Figure 4. 4** along with that of the published⁹⁸ nonfluorinated analogue **4-30** for comparison. Non-fluorinated analogue **4-30** packs in a typical herringbone arrangement with edge-to-face interactions along its long edges.

Table 4. 1 Pitch and roll angles (\angle P and \angle R) for BDT(Se) derivatives

	4-15	4-17	4-18	4-19	4-20	4-21	4-22	4-23	4-24	4-25		
\angle P(°)	56.6	58.2	40.0	45.6	68.4	73.2	43.9	64.8	76.0	66.2	57.9	45.1
\angle R(°)	8.0	11.6	20.6	20.6	23.2	20.0	21.2	1.7	49.9	3.0	20.2	14.4

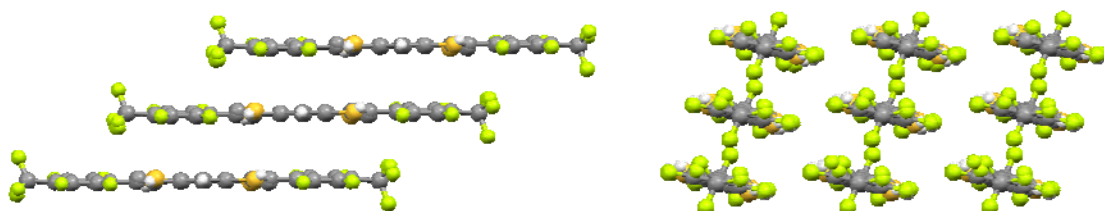
All of the compounds bearing CF₃ groups at their termini, regardless of the identity of substituents at the BDT 4, 8-positions such as H (**4-15**) or OC₁₂H₂₅ (**4-19**) or OCH₃ (**4-21**), or TIPSA (**4-23**) or TMSA (**4-24**), pack in a β motif with 1-D slipped stack

arrangement with face-to-face orientation where β motif is characterized by strong C-C (face-to-face π - π stacking) interactions without significant contribution from CH- π (edge-to-face) interactions. The average distances between π -faces are 3.47 Å (**4-15**), 3.37 Å (**4-19**), 3.48 Å (**4-21**), 3.33 Å (**4-23**) and 3.32 Å (**4-24**). Compound **4-18**, bearing C₆F₅ termini, also packed in a β motif forming slip stacks with face-to-face orientation with a π -stacking distance of 3.40 Å.

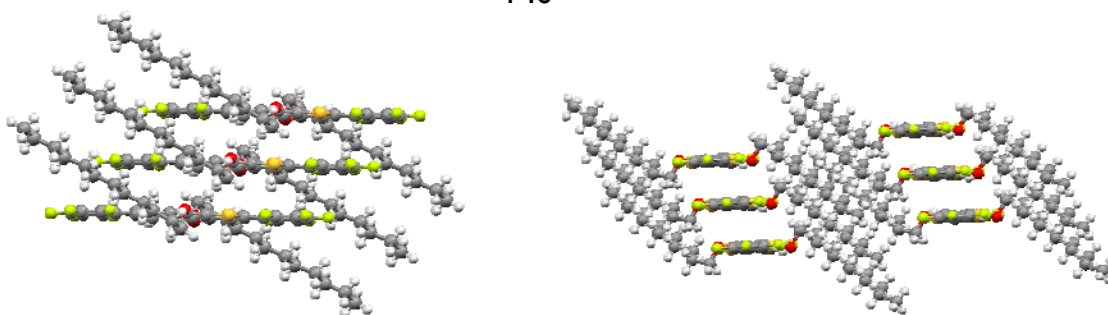
It is desirable in some cases to increase the dimensionality of π -stacking.^{28, 182, 195} The reasons for improvements in FET performance may be related to associated changes in band structure and likely differences in morphology and film-forming abilities. Compounds forming 2-D π -stacks may simply form better films. Compounds **4-20** with Y=OCH₃ and W=CF and **4-22** with Y=TIPSA and W=CF pack in a β motif with slip π -stacks along two dimensions resembling a brick wall when viewed along the short molecular axes. For **4-20**, one π -stacking axis is defined by four C-S close contacts per molecule and the other by four C-C close contacts. The average face-to-face (atom-to-plane) distance along one dimension is 3.33 Å and the distance along another dimension is 3.47 Å. For **4-22**, one π -stacking axis is defined by fourteen C-C close contacts per molecule and the other by four C-C close contacts. The average face-to-face (atom-to-plane) distance is 3.34 Å and the closest C-C contact is only 3.27 Å. The group of John Anthony has clearly established guidelines for establishing 2-D π -stacking in silylacetylene-functionalized (hetero)acenes.⁶⁵ The critical parameter is the ratio between the diameter of the silyl groups (balls) to the length of the acene (rod). These rules obviously do not apply to the systems described here whose self-assembly is also governed by π - π F interactions. Both **4-20** and **4-22** have identical rod lengths, but the size of the lateral substituents vary greatly: large TIPS versus small methoxy. However, both derivatives form 2D π -stacks.

Compound **4-25** exhibits a γ -motif packing (herringbone-like arrangement with molecules in adjacent stacks having opposing tilt angles) with π -stacking distance of 3.45 Å and tilting angle of 88.94° between neighboring stacks. The γ -motif is characterized by herringbone-like packing between neighboring stacks formed by strong C-C (face-to-face π - π stacking) interactions. Close contacts (N-F and C-F) bridge adjacent oblique molecular planes. There are four C-C close contacts and two C-S close

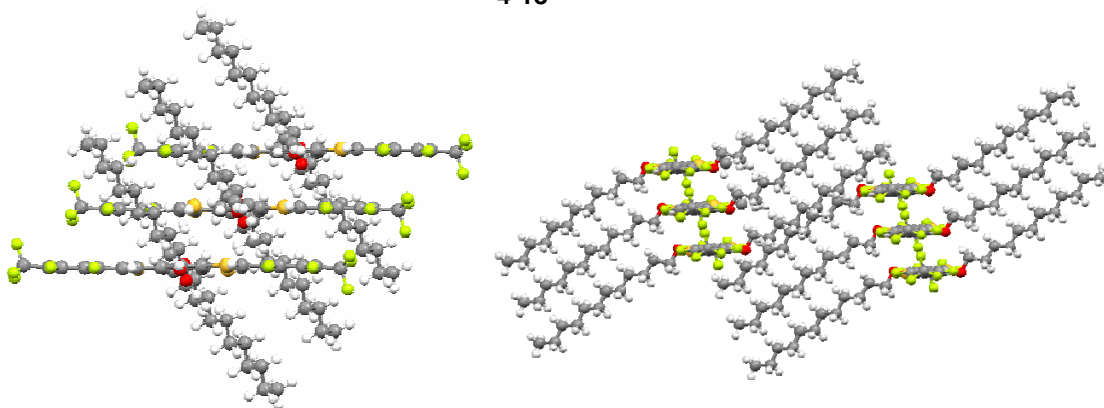
contacts per molecule, with the closest contact of only 3.21Å. Compound **4-17** packs in a γ -motif as well, with the average planar distance of 3.44Å and the titling angle of 62.24°.



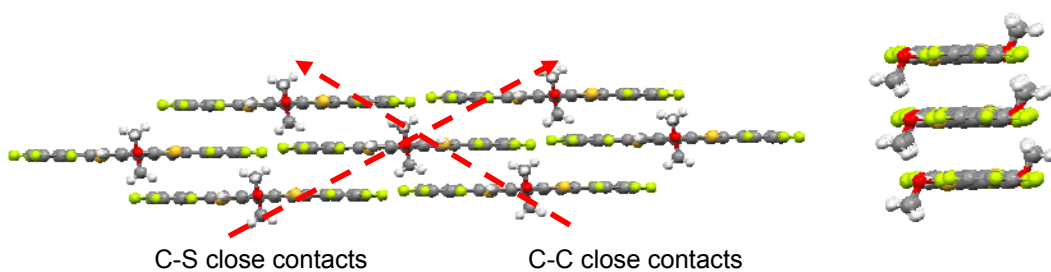
4-15



4-18



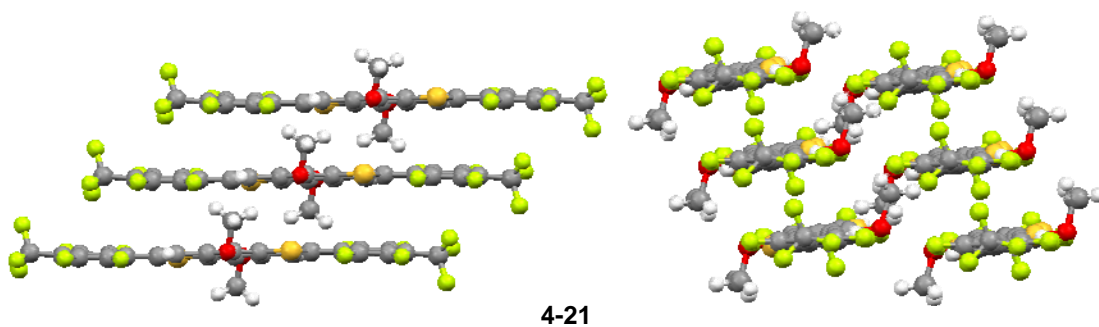
4-19



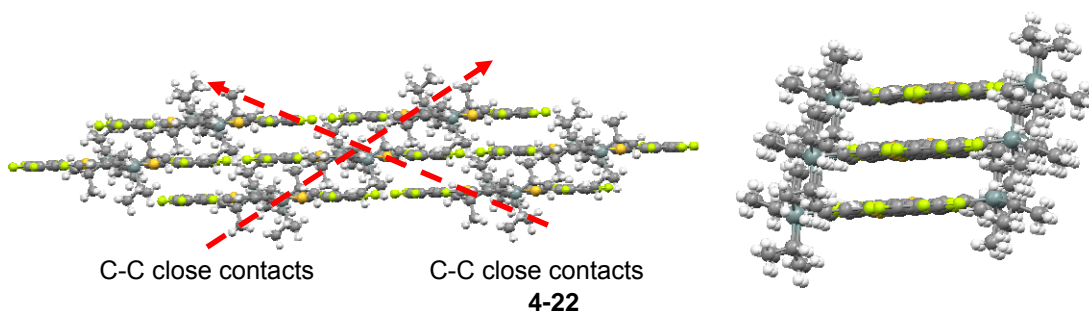
C-S close contacts

C-C close contacts

4-20



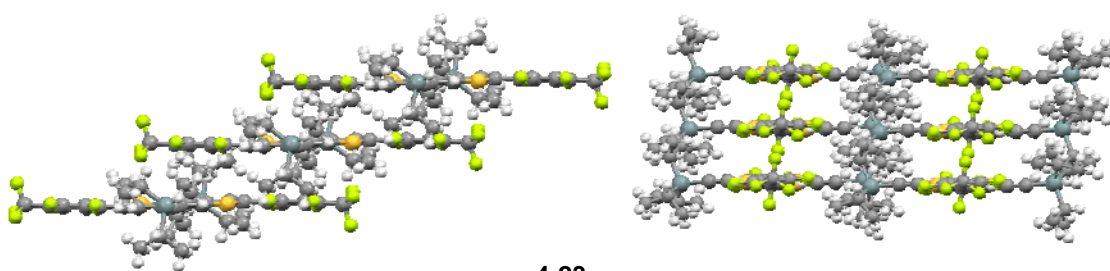
4-21



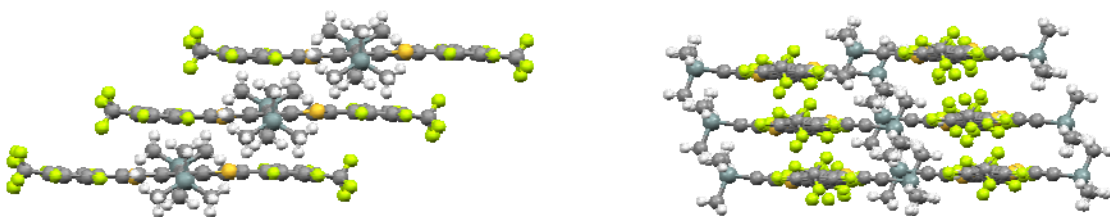
C-C close contacts

C-C close contacts

4-22



4-23



4-24

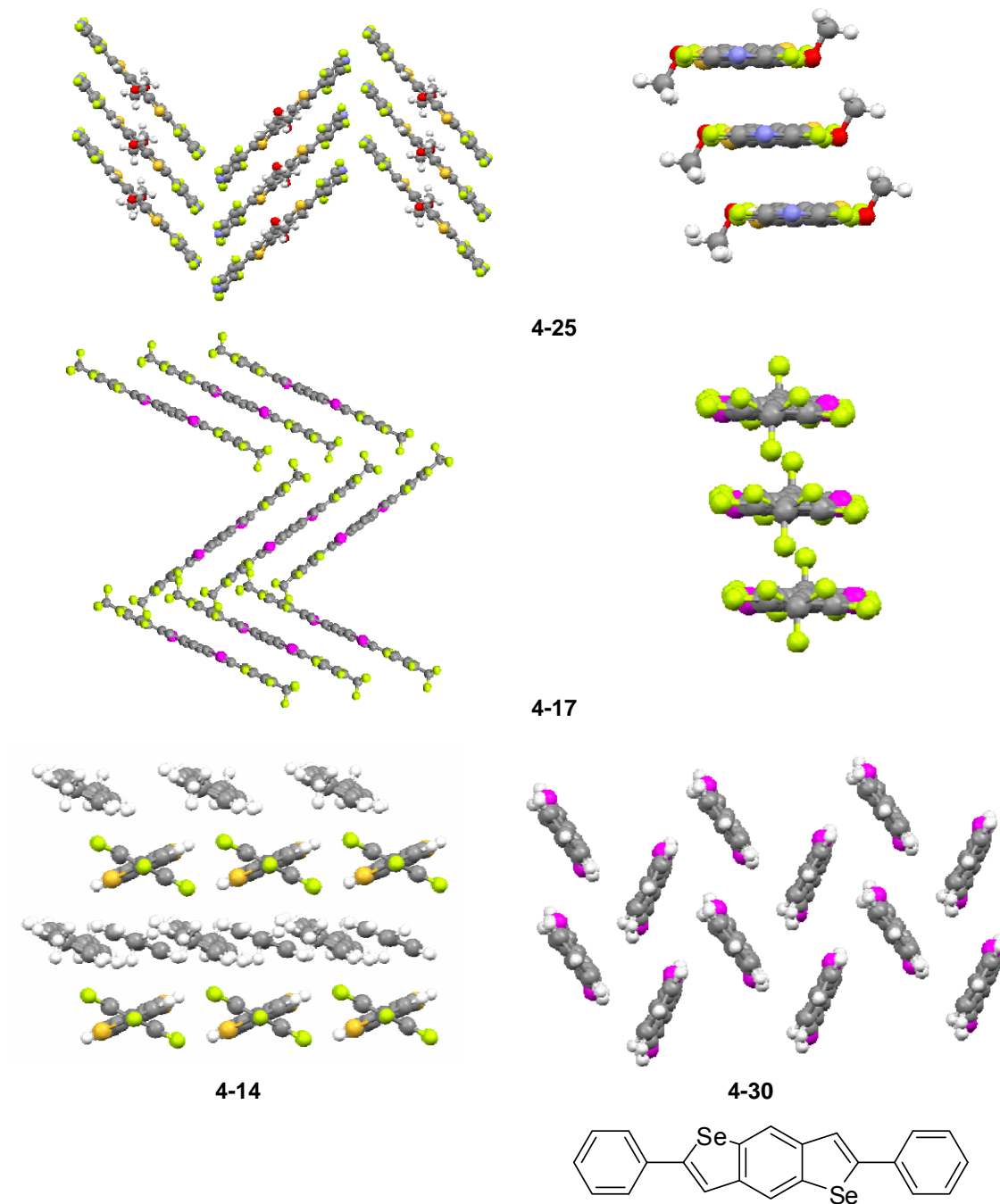
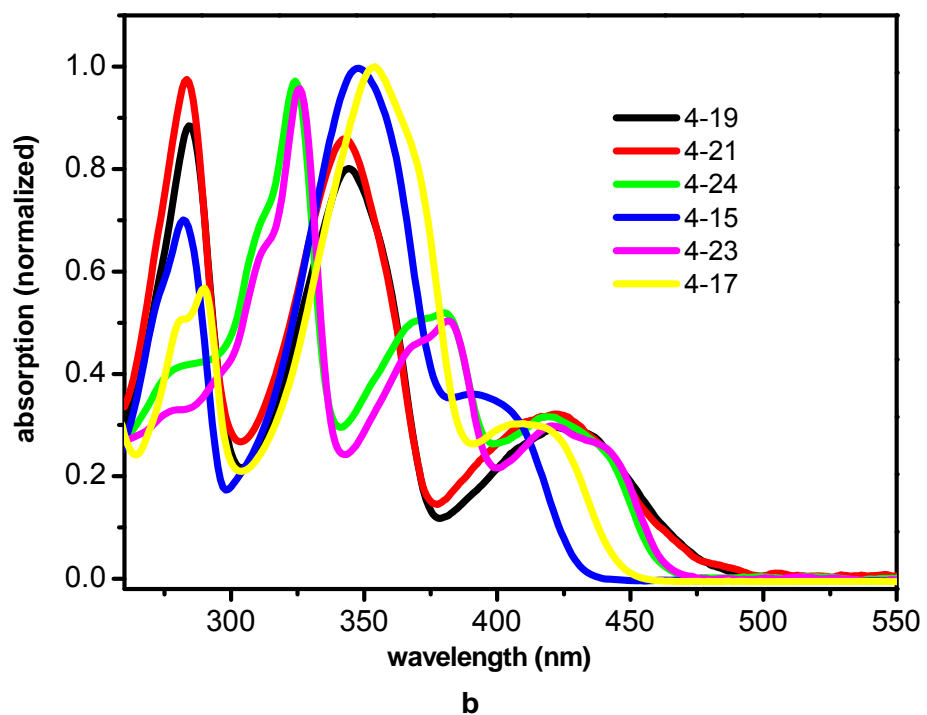
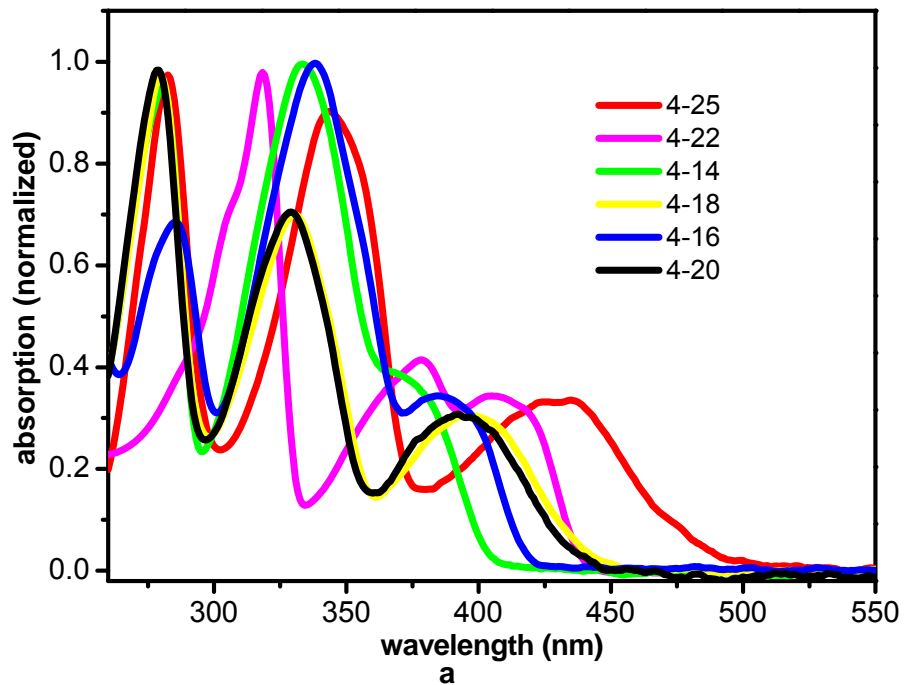
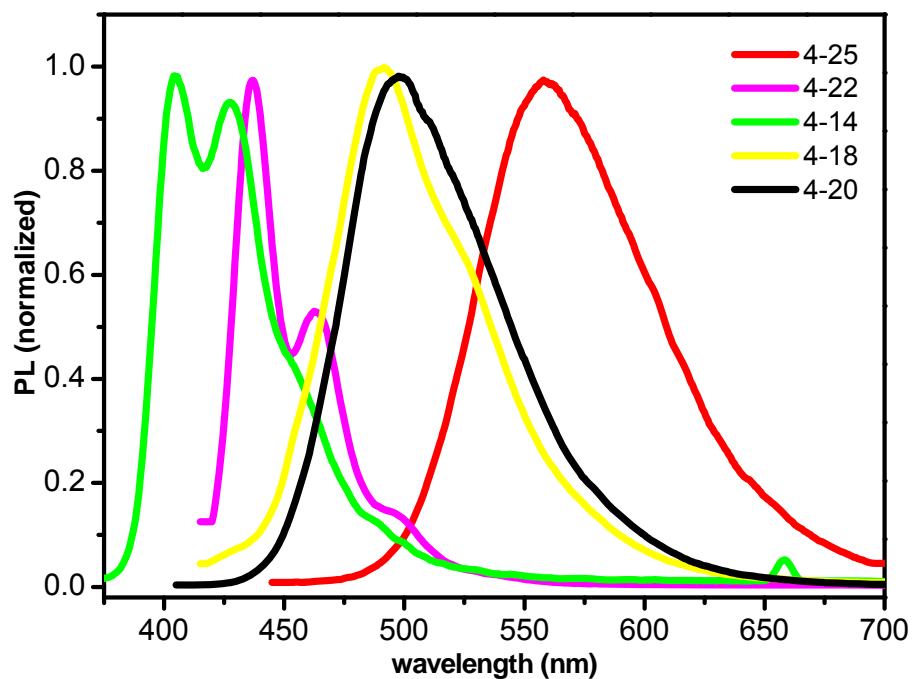


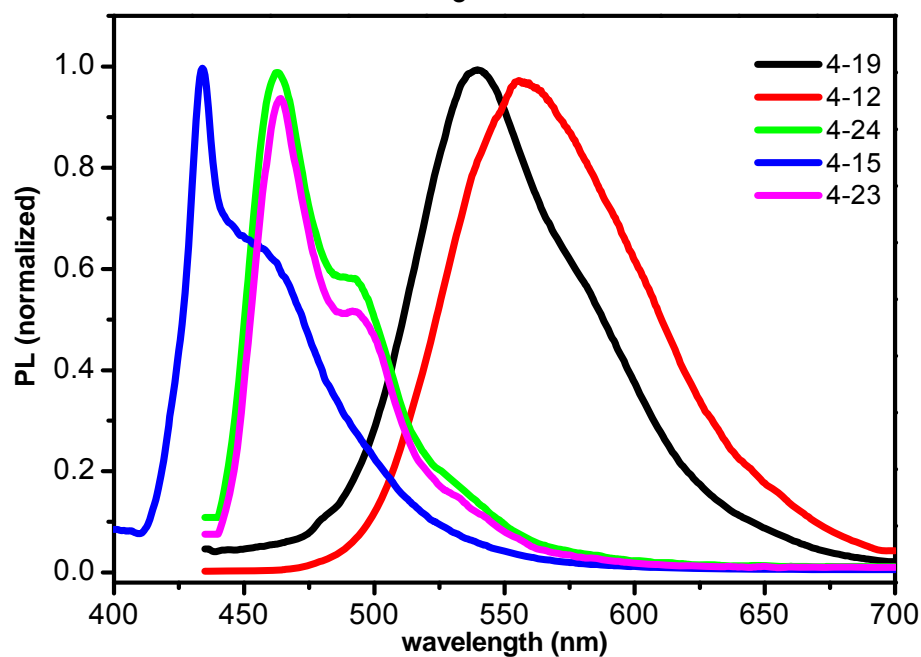
Figure 4. 4 Crystal packing diagrams. Left: view along short molecular axis; right: view along long molecular axis (except 4-14 and 4-30⁹⁸).

4.4 Optoelectronic properties of BDT(Se) derivatives





c



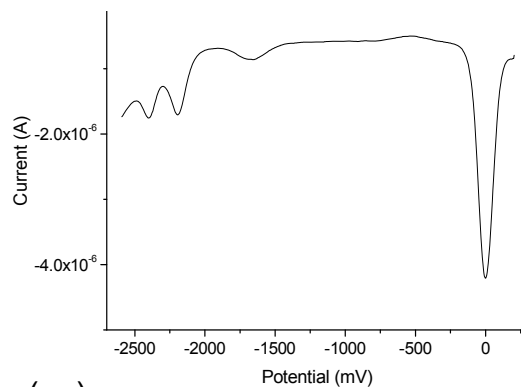
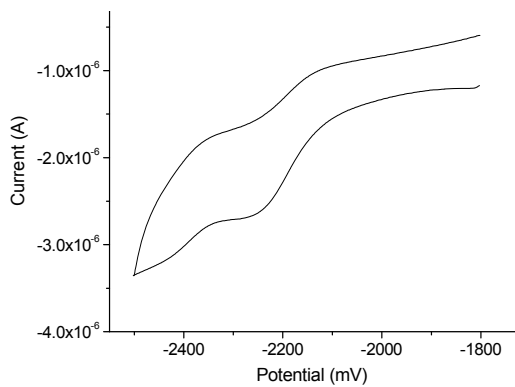
d

Figure 4. 5 Solution absorption (10^{-5} M THF) and photoluminescence (PL) (10^{-6} M, THF) spectra of compounds 4-14-4-25. a) absorption spectra of compounds with terminal C_6F_5 groups; b) absorption spectra of compounds with terminal C_7F_7 groups; c) emission spectra of compounds with terminal C_6F_5 groups; d) emission spectra of compounds with terminal C_7F_7 groups.

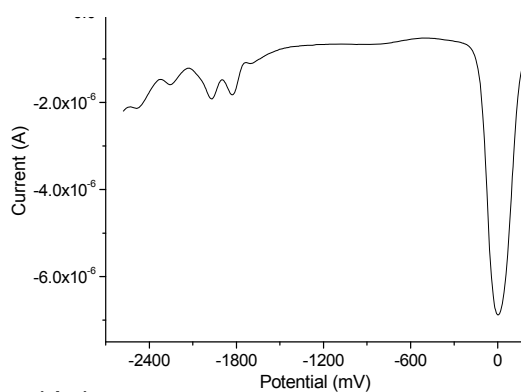
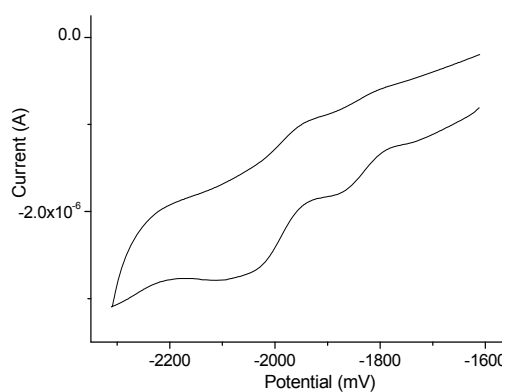
Table 4. 2 Electrochemical, UV-Vis and emission data for **4-14-4-25**

	λ_{\max}^a peak/edge (nm)	E_g^b (eV)	E_{red}^c onset (V)	LUMO ^d (eV)	HOMO ^e (eV)	λ_{\max}^f peak (nm)
4-14	375/405	3.06	-2.11	-2.33	-5.39	405, 427
4-15	400/430	2.88	-1.80	-2.64	-5.52	434, 459
4-16	390/418	2.97	-2.06	-2.38	-5.35	-
4-17	410/446	2.78	-1.75	-2.69	-5.47	-
4-18	400/442	2.81	-2.11	-2.33	-5.14	492
4-19	430/480	2.58	-1.78	-2.66	-5.24	539
4-20	400/440	2.82	-2.09	-2.35	-5.17	499
4-21	420/475	2.61	-1.77	-2.67	-5.28	557
4-22	410/440	2.82	-1.80	-2.64	-5.46	437, 464
4-23	420/465	2.67	-1.44	-3.00	-5.67	464, 491
4-24	420/462	2.68	-1.54	-2.90	-5.58	464, 491
4-25	430/485	2.56	-1.67	-2.77	-5.33	560

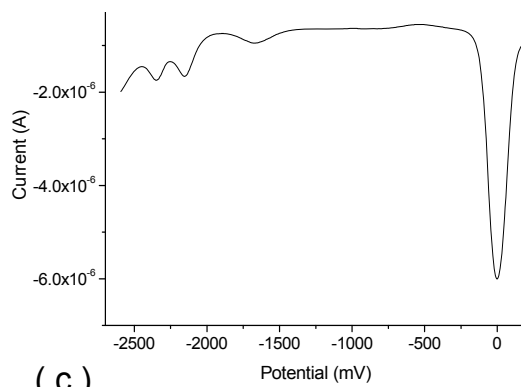
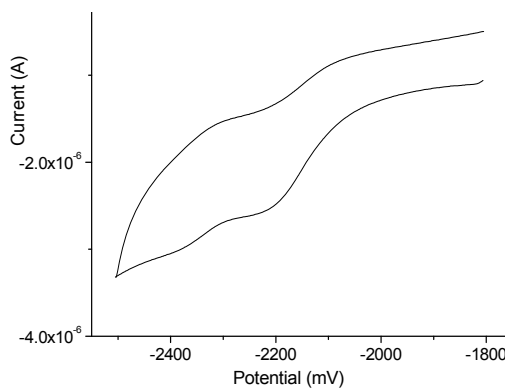
^a Solution absorption spectra. ^b Determined from the absorption edge. ^c Versus Fc/Fc⁺. ^d Estimated from reduction wave onset. (LUMO = -4.44 - E_{red})¹⁹⁶ ^e Estimated from HOMO = LUMO - E_g . ^f solution emission spectra.



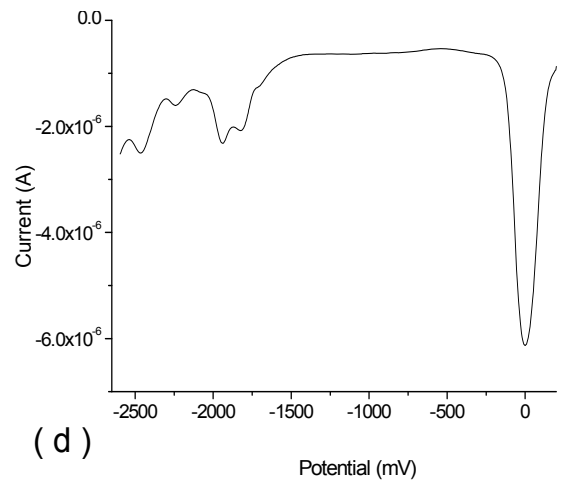
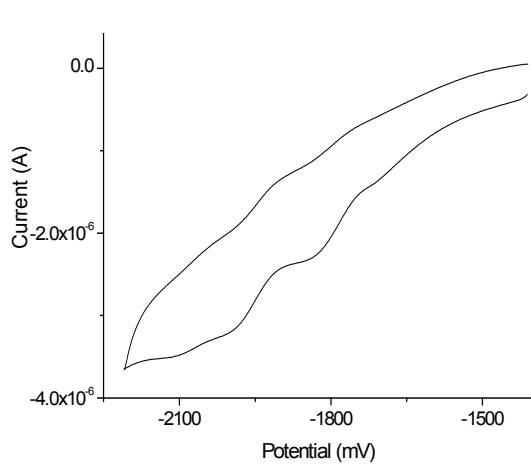
(a)



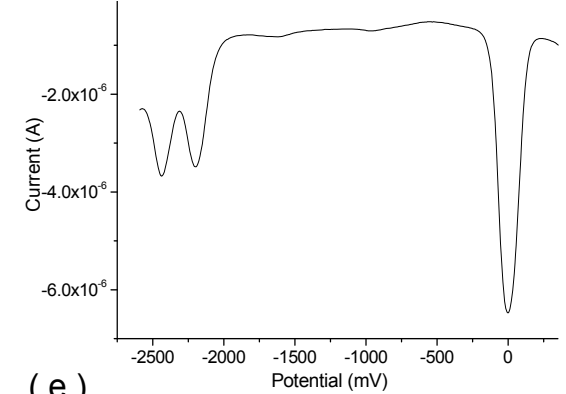
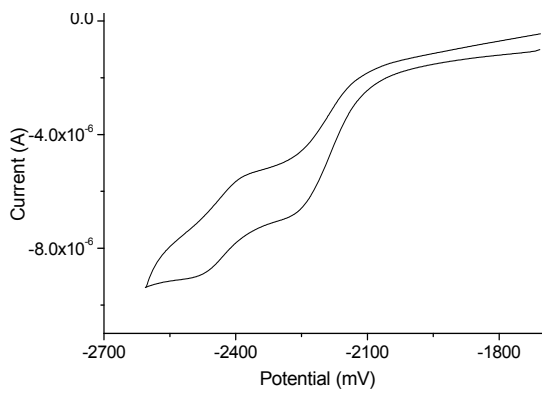
(b)



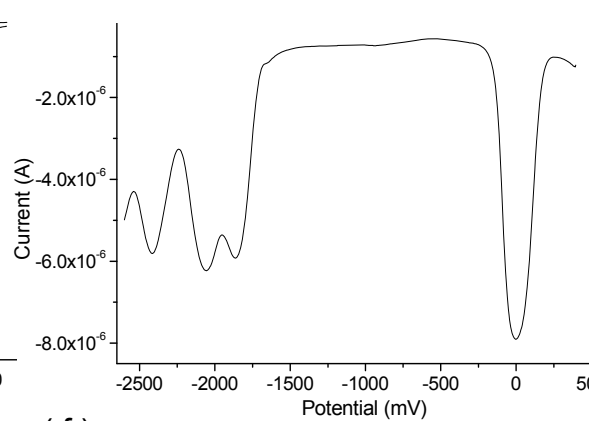
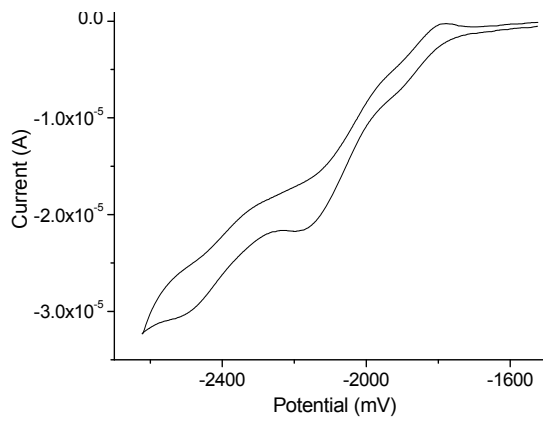
(c)



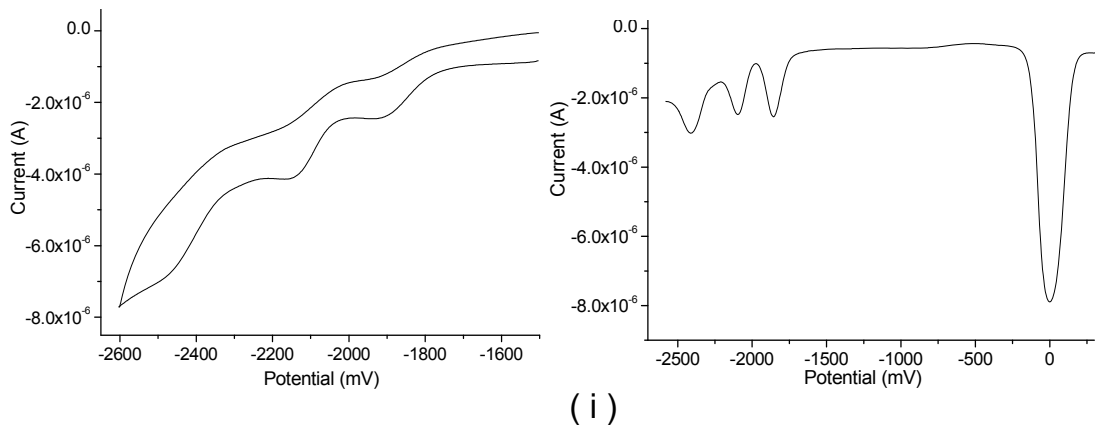
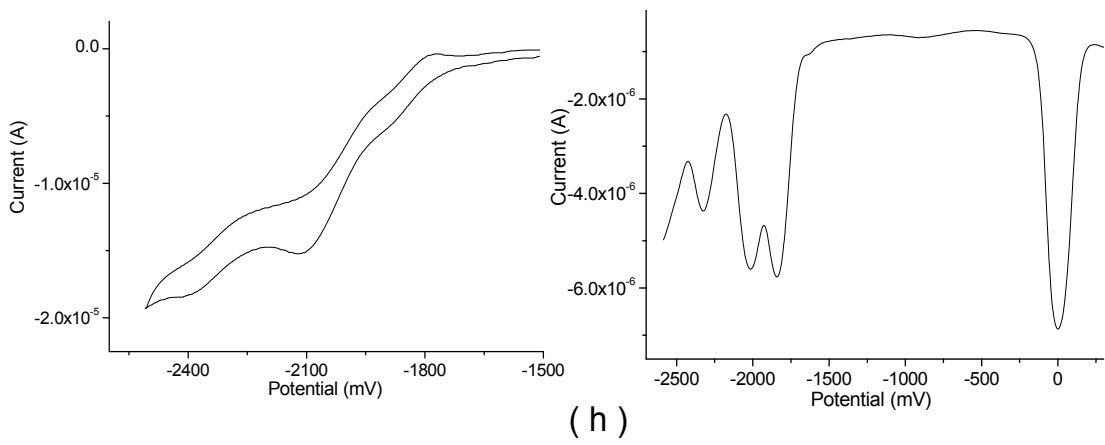
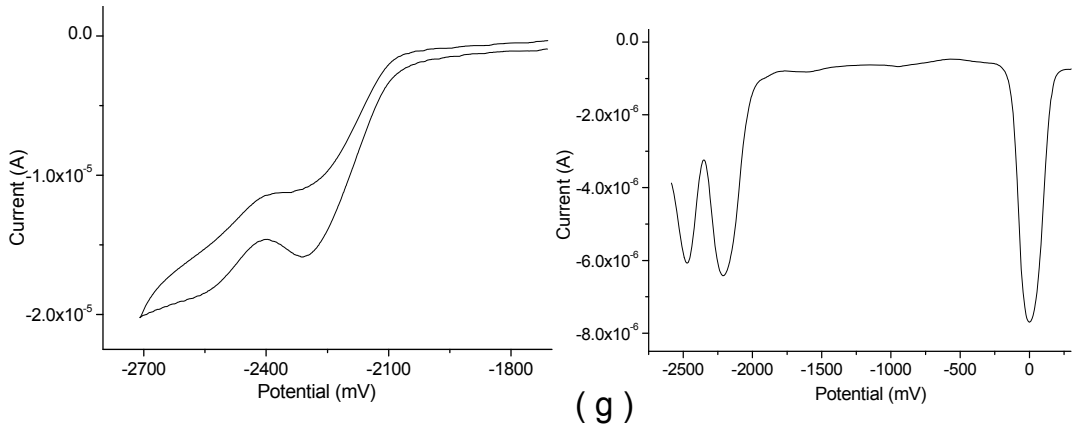
(d)



(e)



(f)



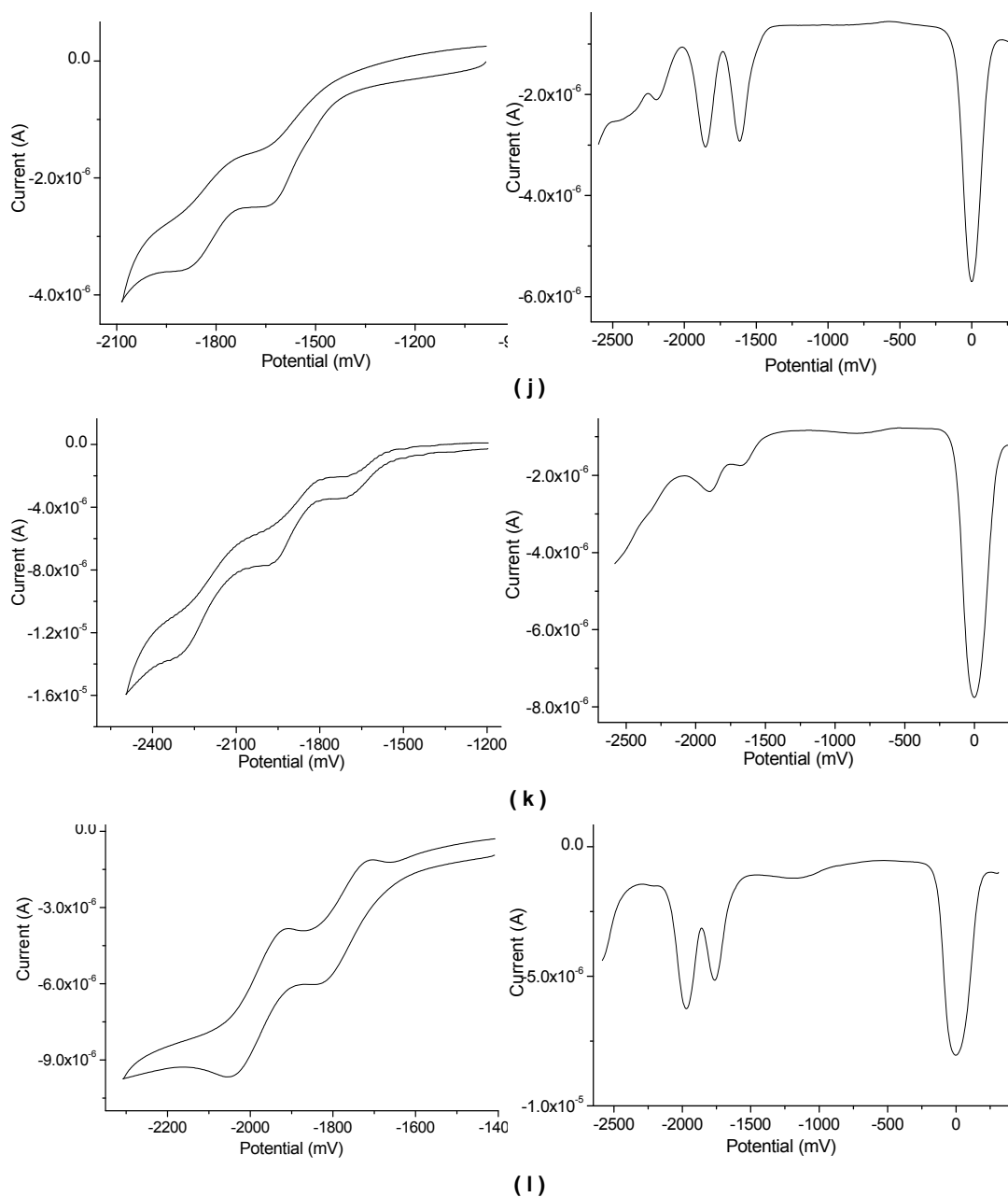


Figure 4. 6 Cyclic voltammograms (left, vs Fc/Fc^+) and Osteryoung square wave voltammograms (right, vs Fc/Fc^+ , large peak set to 0 V) of compounds **4-14** (a), **4-15** (b), **4-16** (c), **4-17** (d), **4-18** (e), **4-19** (f), **4-20** (g), **4-21** (h), **4-22** (i), **4-23** (j), **4-24** (k), **4-25** (l). Conditions: 0.1M $(n\text{-Bu})_4\text{PF}_6$ in tetrahydrofuran; working electrode, Pt; counter electrode, Ag wire; reference electrode, Ag/AgCl; scanning rate, 50 mV/s.

Solution absorption and emission spectra of **4-14** through **4-25** are shown in **Figure 4. 5** and the data are summarized in **Table 4. 2** along with the results of cyclic voltammetry. (**Figure 4. 6**) Energy gaps E_g of the lowest allowed optical transitions (**Figure 4. 5**), estimated from the absorption edges of UV-Vis spectra, range from 2.80eV to 3.10eV for compounds terminated with C_6F_5 groups. Compounds bearing C_7F_7 termini have E_g ranging from 2.55-2.90eV. The E_g s of C_7F_7 -capped compounds are smaller than the C_6F_5 -capped analogues by around 0.20eV, which can be ascribed to stronger interaction between the electron-rich BDT core (donor) with more electron-poor perfluorotolyl group (acceptor). The energy levels are displaced along the continuum between weak donor-acceptor interaction and true charge transfer. This trend is clear for compounds **4-20**, **4-21** and **4-25**, all bearing the more electron donating alkoxy substituents making the BDT core more electron rich. E_g in this series decreases with increasing electron-accepting ability of perfluoroarene termini from C_6F_5 (**4-20**) to C_7F_7 (**4-21**) to C_5F_4N (**4-25**). Changing the substituents at the 4 and 8 positions of the BDT core also clearly alters the optical properties. For example, E_g of compounds with electron-donating alkoxy substituents at the BDT 4 and 8 positions are smaller by around 0.30eV than those of compounds with hydrogens (**4-18/4-20** versus **4-14** = 2.81eV versus 3.06eV, **4-19/4-21** versus **4-15** = 2.60eV versus 2.88eV), where electron-donating alkoxy groups make the BDT core more electron-rich and thus increase the interaction between BDT donor and perfluoroarene acceptor and cause decreased E_g . The energy gap of compounds with TMS/TIPS acetylene groups at the BDT 4 and 8 positions are smaller than those of compounds with hydrogens (**4-22** versus **4-14** = 2.82eV versus 3.06eV, **4-23/4-24** versus **4-15** = 2.67eV versus 2.88eV). Computational studies comparing pentacene to 9,13-trialkylsilylacetylene-substituted pentacene are in accord.¹⁹⁷ The trialkylsilyl groups lower the acene's LUMO while leaving the HOMO essentially unaffected. Replacement of sulfur by selenium makes only relatively small changes in E_g (**4-16** versus **4-14** = 2.97eV versus 3.06eV, **4-17** versus **4-15** = 2.78eV versus 2.88eV), and the direction of the shift agrees with published studies.^{168, 192}

The larger Stokes shifts observed in compounds **4-18**, **4-19**, **4-20**, **4-21** and **4-25** (100-130nm) can be explained by considering that the geometry of those compounds mentioned above become more planar in the excited state due to strong interactions

between electron-rich BDT core and electron-poor perfluoroarenes. No detectable emission was observed for compounds **4-16** and **4-17** containing selenium. The Stokes shifts for other compounds (**4-14**, **4-15**, **4-22**, **4-23** and **4-24**) are around 30-40nm, indicating not significant change of geometry in the excited state relative to ground state. Unlike the other compounds, the emission spectra of compounds **4-14**, **4-15**, **4-22**, **4-23** and **4-24** are structured, indicating somewhat narrowed distributions in the thermal population of states. The reasons for this are not yet clear.

Solution electrochemical measurements of **4-14-4-25** (**Figure 4. 6** and **Table 4. 2**) revealed that (1): LUMO levels of compounds with C_7F_7 are 0.31-0.36eV lower relative to those with C_6F_5 . (2): LUMO levels are estimated to be -2.35, -2.67 and -2.77eV for **4-20**, **4-21** and **4-25**, respectively, which indicated the effect of C_5F_4N on the LUMO level is more significant than C_6F_5 and C_7F_7 . (3): LUMO levels of **4-14** and **4-16**, **4-15** and **4-17** are estimated to be almost the same, demonstrating the identity of the chalcogen atoms have little effect on LUMO.^{187, 192} (4): LUMO levels of compounds with acetylene groups at the 4, 8 positions of BDT can be decreased by around 0.3eV relating to compounds with H (**4-14** and **4-22**, **4-15** and **4-23**, **4-15** and **4-24**), which agrees with the published study described above comparing substituted and unsubstituted pentacene.¹⁹⁷ However, alkoxy groups at those positions do not affect the LUMO levels (**4-14** and **4-18/4-20**, **4-15** and **4-19/4-21**).

4.5 Thermal properties of BDT(Se) derivatives

Differential scanning calorimetry (DSC) was performed for all the compounds **4-14** through **4-25** and suggested (**Table 4. 3**) that the entire set of new compounds are thermally stable up to their melting points (no exothermic processes on heating indicating decomposition). It is observed that compounds capped with perfluorotoluene have higher melting point than those capped with perfluorobenzene except for the pair **4-22** and **4-23** where the relation is reversed. Though there are relatively few data points, it appears that substituents such as dodecyloxy and TIPS, which command a greater volume fraction of the entire molecule, lower the melting point of compounds (**4-18** and **4-19**, **4-22** and **4-23**).

Table 4. 3 Differential scanning calorimetry (DSC) data of compounds **4-14-4-25**

	T_m (°C) ^a	
	Heating cycle	Cooling cycle
4-14	287	272, 264
4-15	303	280
4-16	295	275, 295
4-17	314	295
4-18	98, 32	76, 24
4-19	133, 34	110,
4-20	218, 259	228, 193
4-21	252, 260	218, 245
4-22	67	62
4-23	43	33
4-24	377, 355	331
4-25	309	259

^a Peak values measured with differential scanning calorimetry (DSC) under N₂. The temperature ramp was 5-10 °C/min, and data were collected in the second scan cycle.

4.6 Conclusions

Benzodichalcogenophene cores may be easily functionalized with perfluoroarenes at their termini as a final synthetic step providing an expedient route to a library of different compounds with widely varying properties. CV and UV-Vis revealed that the positions and types of substituents govern the optical energy gap and LUMO energy levels in a predictable manner: (1) CF₃ substituents at the molecular termini can decrease the E_g of compounds by about 0.2eV and the LUMO level (0.3eV) relative to fluorine substituents at the same position. This is likely a consequence of the greater electron-withdrawing ability of the CF₃ group, without the opposing electron-donating property of fluorine atoms directly bonded to the π -system; (2) the introduction of silyl acetylene groups into the 4, 8 positions of BDT can decrease the LUMO energy level in comparison to H at the same positions while the introduction of OR has little effect; (3) choice of sulfur or selenium atoms has little effect on the LUMO; and (4) C₅F₄N molecular termini provide

the greatest reduction in energy gap and LUMO level relative to C₆F₅ or C₇F₇. The crystal packing also can be engineered by manipulating the types and positions of substituents: (1) All of compounds have coplanar ring systems arising from intramolecular S-F close contacts and intermolecular π - π F interactions; (2) Most compounds adopted 1D slipped π -stacked arrangement, while **4-17** and **4-25** packed in herrinbone-like motif and **4-20** and **4-22** form slip π -stacks along two dimensions, a feature which has been shown to improve FET performance.

Fabrication of n-type FETs with compounds **4-14-4-25** will be investigated in the future.

Chapter 5 Conclusion and outlook

5.1 Conclusion

In recent years organic electronics have been investigated so extensively in low-performance devices such as thin film transistors, light emitting diodes, photovoltaic cells etc. due to their easy processability (low temperature), light weight, flexibility and compatibility with flexible substrates compared to commercial amorphous silicon. Though many of the greatest advances have been brought on by physicists, theoreticians and engineers, materials chemists meet the challenges of designing new materials with improved properties. A lot of factors can determine the final device performance, including the chemical nature and purity (intrinsic and extrinsic), morphology, self-assembly, stability, orbital energy levels, geometry of device etc. The main directions of the work reported herein are synthetic method development, supramolecular engineering, and structure-property studies of fluorinated materials which can potentially function as the active components in organic electronic devices.

This dissertation was divided into three chapters describing the results of three independent but interrelated research projects centered on the synthesis, supramolecular engineering, and structure-property studies of 3 different classes of fluorinated organic electronic materials. These are thiophene-based conjugated copolymers (CPs, Chapter 2), highly fluorinated benzobisbenzothiophenes (BBBTs, Chapter 3) and functionalized benzodichalcogenophenes (BDT, BDSe) (Chapter 4). Common unifying themes are:

1. Synthetic methodology development exploiting S_NAr reactions of fluorinated aromatics to form the various conjugated frameworks;
2. Control of self-assembly via intermolecular interactions between fluorinated and non-fluorinated π -systems, inter- and intramolecular interactions between fluorine atoms and thienyl sulfur atoms, as well as in some cases space-filling demands of other substituents like alkyl side-chains;
3. Control over intrinsic molecular (opto) electronic properties through variation in substituents and in the bulk via control over self-assembly.

It is known that preparation of conjugated polymers using transition-metal-catalyzed coupling can leave behind residues that can detrimentally affect the device performance, therefore requiring extensive purification prior to application in organic electronic device. In Chapter 2 a new transition-metal-free methodology was described to synthesize commercially relevant thiophene-containing conjugated copolymers. The catalyst system of CsF and 18-crown-6 are facile to be removed by extraction and the sole side product is a gas, yielding polymers with high purity and high molecular weight. Some intrinsic polymer defects, possibly variations in regiochemistry of attachment to fluorinated benzenes or branching, are detectable by ^{19}F NMR. Only device studies comparing FETs fabricated from polymers prepared by this new route and traditional routes will reveal whether the new synthetic route provides superior or inferior materials.

Also the scope of this transition-metal-free polymer synthesis is likely to expand to a broad range of thiophene copolymers, based on the series of differing polymers prepared to date. Secondly, model reactions reveal that the relationship between degree of polymerization and comonomer stoichiometry for this type of polymerization should deviate from that predicted by Carothers equation. Thirdly, optical properties can be tuned by manipulating the structures of backbones and side chains of polymers. The UV-Vis spectra and solid colors demonstrated the trend of red shift when monomers are switched from 3,4-dibutoxythiophene to ProDOT(Hx)₂ to tetrabutoxybithiophene to 3,3'-dialkylbithiophene to 3,3'-dialkoxybithiophene. Polymer **2-33c** with bulkier 2-ethylhexyl side chain relative to polymers **2-33a,b** with dodecyl or 3,7-dimethyloctyl has significantly twisted backbone, leading to limited conjugation and thus yellow solid color. Fourthly, fluorination can lead to significant red-shifts of optical transitions in the solid state, which result from planarization and/or π -stacking in the solid state as clearly demonstrated by WAXD measurements. These changes in turn arise either from attractive intramolecular S-F, or intermolecular π - π F interactions. These results taken together show that head-to-head thiophenes may be forced into coplanarity with proper molecular design.

In Chapter 3, an efficient route, relying heavily on $\text{S}_{\text{N}}\text{Ar}$ reactions, has been established to prepare fluorinated polycyclics **3-15a,b**, **3-19**, and **3-24a,b**. They are easily further functionalized with other substituents by post-synthesis $\text{S}_{\text{N}}\text{Ar}$ reactions. Experimental and

computational estimates of the effects of substituents on the energy gap and frontier orbital energy levels are in accord: CF₃ substituents (**3-15b**) induce a bathochromic shift of the (optical) energy gap and decrease the LUMO level relative to the fluorine substituents of **3-15a**. Fluorine atoms attached to central benzene rings decrease the LUMO energy level in comparison to protons at the same positions (**3-15a** vs **3-19**).

The molecules were prepared to test the hypothesis that intermolecular interactions between thienyl sulfur and fluorine atoms could force edge-to-edge, and by default, face-to-face packing. Two antiparallel triangular arrangements of F-S-F units along each side of lath-shaped molecules, likely together with face-to-face electrostatic attraction, preclude edge-to-face interactions. Two S-F units are however insufficient to preclude edge-to-face arrangements, except when bulky alkyl chains are included. Comparison also with the published herringbone-like packing of the non-fluorinated parent compound further supports the hypothesis and conclusions. Crystallization to sheets of (nearly) parallel molecules coincides with assembly to 2D π -stacking motifs by BBTs **3-15a** and **3-15b**, which may make them promising candidates for semiconductors.

In Chapter 4 benzodichalcogenophene cores were easily functionalized with perfluoroarenes via S_NAr reactions at their termini as a final synthetic step, as an expedient route to a library of different compounds with widely varying properties. CV and UV-Vis revealed that the positions and types of substituents govern the optical energy gap and LUMO energy levels in a predictable manner: (1) CF₃ substituents at the molecular termini can decrease the E_g of compounds by about 0.2eV and the LUMO level (0.3eV) relative to fluorine substituents at the same position. This is likely a consequence of the greater electron-withdrawing ability of the CF₃ group, without the opposing electron-donating property of fluorine atoms directly bonded to the π -system; (2) the introduction of triple bond into the 4, 8 positions of BDT can decrease the LUMO energy level in comparison to H at the same positions while the introduction of OR has little effect; (3) choice of sulfur or selenium atoms has little effect on the LUMO; and (4) C₅F₄N molecular termini provides the greatest reduction in energy gap and LUMO level relative to C₆F₅ or C₇F₇. The crystal packing also can be engineered by manipulating the types and positions of substituents: (1) All compounds have coplanar ring systems arising from intramolecular S-F close contacts and intermolecular π - π F interactions; (2) Most

compounds adopted 1D slipped π -stacked arrangement (β -motif), while **4-17** and **4-25** packed in herringbone-like motif (γ -motif) and **4-20** and **4-22** form slip π -stacks along two dimensions, a feature which has been shown to improve FET performance.

5.2. Outlook

In the future OFETs will be fabricated to screen out those materials including thiophene-containing copolymers (Chapter 1), fluorinated fused polycyclics (Chapter 3) and functionalized benzodithiophene derivatives (Chapter 4).

Since the polymers prepared via the transition-metal-free route described herein are not completely defect-free, further work should focus on optimization of conditions. For example, more polar solvents may allow the $\text{S}_{\text{N}}\text{Ar}$ reaction to occur at lower temperatures which could increase selectivity. Other variables include fluoride source and fluoride salt solubilizing agent. Further studies should also be carried out to prepare more derivatives with varying side chains. Particularly the copolymers of bithiophene with C_6F_6 should be prepared with a variety of differing alkyl and alkoxy chains to optimize solid-state packing.

It was reported in Chapter 2 that thienyl monomers bearing triisopropylsilyl groups (TIPS) are unreactive towards hexafluorobenzene when the solvent is toluene, but reactive in THF. On the other hand, monomers bearing trimethylsilyl groups are reactive in both solvents. This selectivity should be exploited in the future for step-wise buildup of well-defined linear oligomers and dendrimers. An example is provided in **Figure 5. 1**, based on the terthiophene branching unit reported by Bauerle.¹⁹⁸ This route may be particularly suitable for solid-supported synthesis of dendrimers,¹⁹⁹ since each growth step only requires filtration and switching between solutions of the thienyl branching unit in toluene and C_6F_6 in THF. The dendrimers can be decorated at their peripheries (R) with solubilizing alkyl chains or functional units using functionalized pentafluorobenzenes in the last step. A variety of other structures can be prepared with differing branching agents and perfluoroarenes.

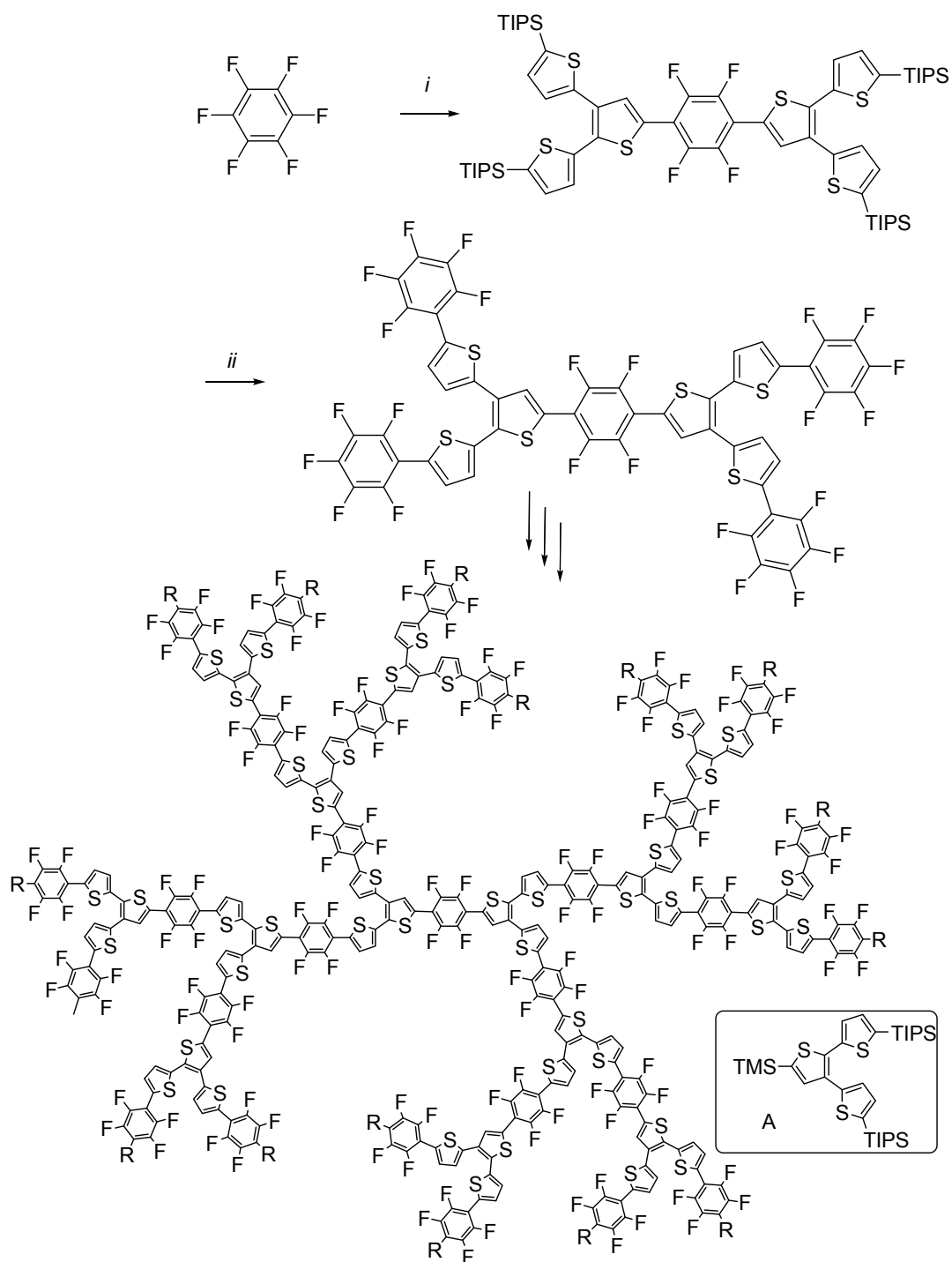


Figure 5. 1 Example proposed synthesis of dendrimers. *i*: compound “A”, toluene, CsF, 18-crown-6; *ii*: C₆F₆, THF.

Low band-gap polymers can be produced from fused heterocyclics like poly(isothianaphthene)²⁰⁰ and poly(thienothiophenes)^{201, 202}. The low band gaps have

been attributed in part to a substantial quinoidal character of the polymer backbones. It is proposed here that copolymers **B** and **C** containing thienothiophene units can be prepared via the transition-metal-free polymerization reported in chapter 2 (**Error! Reference source not found.**). Two regioregular forms **B** and **C** are shown. To get an initial idea of the possibility for backbone planarization, low level energy minimizations (MM2) of the repeat units were performed using Chem3D. The intramolecular H-F distances in structure “**B**” were estimated to be only 1.47 Å, which is so substantially shorter than the combined van der Waals radii (2.67 Å) that this polymer is unlikely to be fully planarized. The intramolecular S-F distances for “**C**” were estimated as 2.3 Å, which is also substantially less than the combined vdW radii (3.27 Å). However, crystallographic studies reported herein regular show similar intramolecular S-F contacts in planarized structures as short as 2.6 Å. The proposed polymers, together with crystallographic investigation of small-model model compounds, may let us know how far we can go with forcing planarization via S-F and π - π F interactions. The spacing between the side chains of the polymers might allow interdigitation of side-chains from neighboring polymer chains and thus greatly enhance order, device performance and stability.

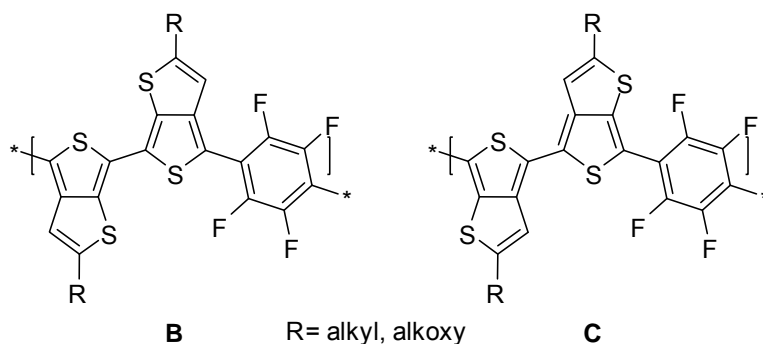


Figure 5. 2 Proposed regioregular copolymers of bithienothiophene copolymers **B** and **C**.

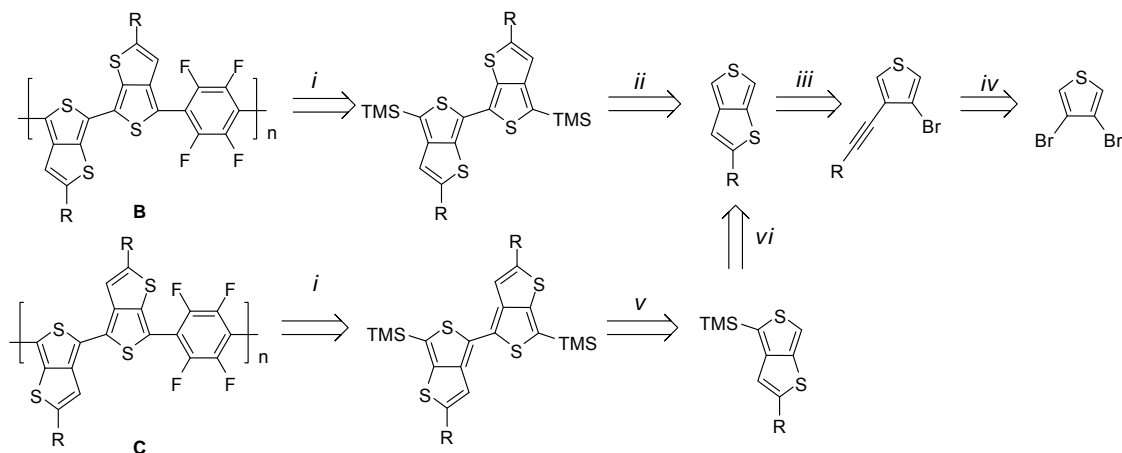
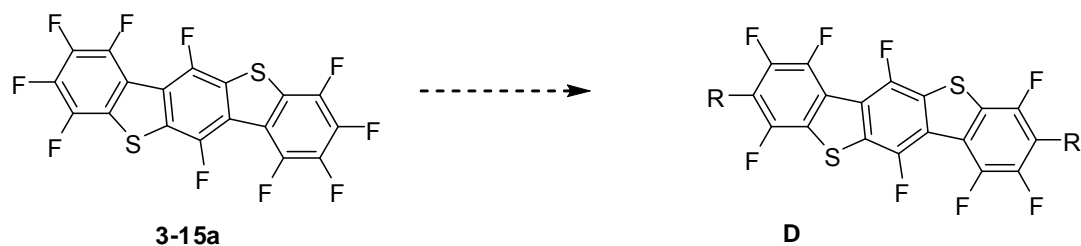


Figure 5. 3 Retrosynthesis of polymers **B** and **C** shown in **Figure 5. 1**. Steps *ii*, *v* and *vi* are based on published procedure²⁰² and steps *iii* and *iv* are based on literature procedure.²⁰³

Since 2-dimensional π -stacking occurs along the short axes of the BBTs described in Chapter 3, and is not disrupted by terminal CF_3 substituents (**3-15b**), it is proposed that solubilizing groups such as long alkyl, alkynyl, perfluoroalkyl, acyl, and perfluoroacyl groups should be introduced at the molecular termini (**D**) to increase the solution-processability. (**Figure 5. 4**) Fluorinated alkyl or alkynyl groups could dynamically prevent the permeation of O_2 and moisture and thus increase the device stability, in addition to further modifying energy levels.³⁴



R=long alkyl, alkynyl, perfluoroalkyl, acyl, and perfluoroacyl

Figure 5. 4 Synthetic scheme of **D** with different solubilizing groups.

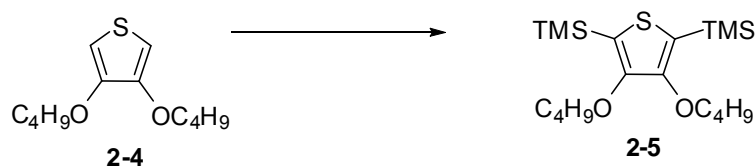
Chapter 6 Experimental section

6.1 Materials and methods

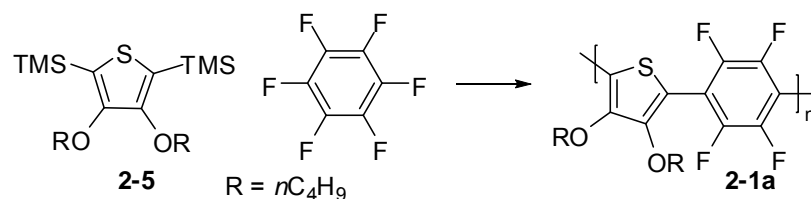
CsF and 18-crown-6 were each dried under reduced pressure ($< 10^{-3}$ mbar) at 180°C and 80°C, respectively and stored in an argon-filled glove box. C₆F₆, toluene, ether, DME, DMF, CHCl₃, DIPA and THF were distilled from appropriate drying agents and stored over molecular sieves under argon. Anhydrous copper chloride and zinc chloride beads were purchased from Aldrich and stored in an argon-filled glove box. AlCl₃ was quickly transferred from its shipping container to reaction vessels without weighing, and therefore the amounts reported are only rough estimates. All other materials were used as purchased. Unless otherwise stated, all manipulations and reactions were carried out under argon in a glove box or using standard Schlenk techniques. 3,4-dibutoxythiophene (**2-4**)²⁰⁴ and benzo[1,2-b: 4,5-b']dithiophene-4,8-dione (**2-23**)¹⁹³ were prepared via modified published procedures. Benzo[1,2-b: 4,5-b']dithiophene-4,8-dione **4-29** was prepared following the published procedure.¹⁹⁴ Dodecyl toluene-*p*-sulphonate **4-32a** was prepared based on published procedure.²⁰⁵ ¹H, ¹³C, and ¹⁹F NMR spectra were recorded on a Varian INOVA 400MHz spectrometer (purchased under the CRIF Program of the National Science Foundation, grant CHE-9974810). Chemical shifts were referenced to residual protio-solvent signals, except for ¹⁹F spectra, where CCl₃F was added as internal standard and set to $\delta = 0$ ppm. Relative molecular weight determinations were made using a Waters 600E HPLC system, driven by Waters Empower Software and equipped with two linear mixed-bed GPC columns (American Polymer Standards Corporation, AM Gel Linear/15) in series. Eluting polymers were detected with both refractive index and photodiode array detectors. The system was calibrated with 11 narrow PDI polystyrene samples in the range 580 - 2 x 10⁶ Da with THF or toluene at a flow rate of 1mL/min. Differential scanning calorimetry was performed using a Mettler 822^o under N₂. Melting points (T_m or MP) for small molecules are the peak values at a heating rate of 10 or 20°C/min. GC-MS data were collected from an Agilent technologies 6890N GC with 5973 MSD. UV-Vis data were recorded on a Varian CARY 1 UV-Visible spectrophotometer. Photoluminescence data were recorded on Fluorolog-3 fluorometer.

Elemental analysis was performed by Robertson Microlit laboratories. Electrochemical measurements were performed under nitrogen using a BAS-CV-50W voltammetric analyzer. The solvent (anhydrous THF) was thoroughly purged with N₂. 0.1M tetra-*n*-butylammonium hexafluorophosphate was used as supporting electrolyte. The scan rate was 50mVs⁻¹. A platinum working electrode, silver wire counter electrode, and Ag/AgCl reference electrode were employed. Ferrocene/ferrocenium (Fc/Fc⁺, $E_{1/2}$ =0.60V) was used as an internal reference for all measurements. The geometry and electronic structure of the molecules were calculated at the density-functional theory (DFT) level using the B3LYP functional and the 6-311+G* basis set. Vertical optical transition energies and oscillator strength were obtained by (time dependent) (TD-) DFT. All calculations were done within the Gaussian03 program package.

6.2 Syntheses

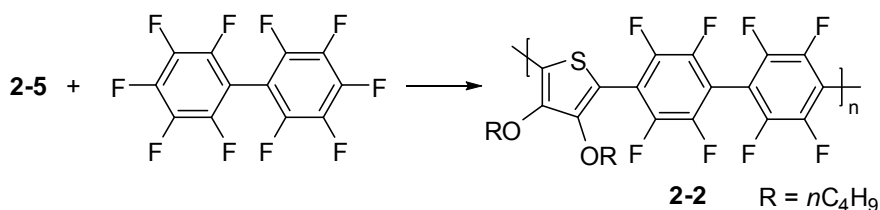


(3,4-dibutoxythiophene-2,5-diyl)bis(trimethylsilane) (2-5): *n*-BuLi (15.51mL, 1.6M hexanes, 4eq) was added drop-wise to a solution of 3,4-dibutoxythiophene **2-4** (1.42g, 6.22mmol) in 30mL hexanes:DME (2:1) maintained at 0°C. After stirring at room temperature for 30 minutes, then at reflux for 1 hr, TMSCl (3.14mL, 4eq) was added drop-wise into the suspension and the whole was stirred overnight at room temperature. The mixture was extracted with 10% HCl (aq) and deionized water, dried over MgSO₄, and concentrated via rotary evaporation. Monomer **2-5** was isolated after flash chromatography [silica gel, pentane:dichloromethane (3:1)] as a yellow solid (2.10g, 91%). ¹H NMR (CDCl₃) δ: 4.01 (t, 4H), 1.77 (m, 4H), 1.52 (m, 4H), 1.02 (t, 6H), 0.34 (s, 18H). ¹³C NMR (CDCl₃) δ: 156.85, 126.30, 72.94, 32.41, 19.35, 14.06, -0.39. GC-MS: *m/z*: 372 (C₁₈H₃₆O₂SSi₂⁺), 229 (100%).



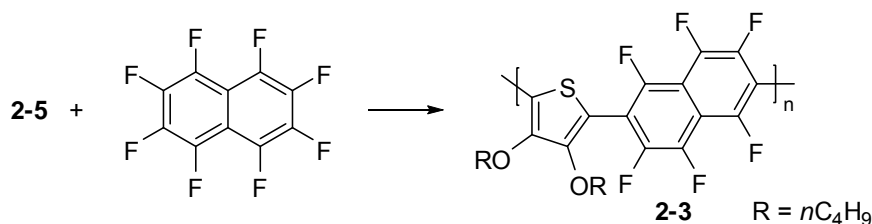
Polymer 2-1a (Method A, 80°C): In an argon-filled glove box, monomer **2-5** (145mg, 0.389mmol), C_6F_6 (53.95 μL , 1.2 eq), CsF (6.19mg, 0.1 eq), 18-crown-6 (20.56mg, 0.2 eq), and toluene (2mL) were combined in a vacuum flask containing a magnetic stir bar. The vessel was sealed and the contents stirred at 80°C for 5 days. The solution was extracted with deionized water twice and the polymer precipitated by pouring the solution in 50mL methanol. The polymer was re-dissolved in chloroform then precipitated again into methanol. After drying under reduced pressure, the polymer was obtained as a white solid (123 mg). ^1H NMR (CDCl_3) δ : 4.12 (m, 4H), 1.65 (m, 4H), 1.39 (m, 4H), 0.90 (m, 6H). ^{13}C NMR (CDCl_3) δ : 148.77, 144.32 (d of m), 112.37 (m), 110.75, 73.02, 31.90, 18.92, 13.72. ^{19}F NMR (CDCl_3) δ : -137.94 (m, 4 F), -138.81 (m, 147F), -153.41 (m, 2 F), -162.24 (m, 4 F). M_n (GPC) = 28 kDa (PDI = 2.7)

Polymer 2-1a (Method B, room temperature): Conducted exactly as in “Method A” above, except stoichiometry based upon 104mg monomer **2-5**, and entire reaction conducted at room temperature. Yield = 80mg. Spectroscopic data consistent with the above reaction at 80°C except for small differences in integral values in the ^{19}F NMR. M_n (GPC) = 23 kDa (PDI = 3.1)



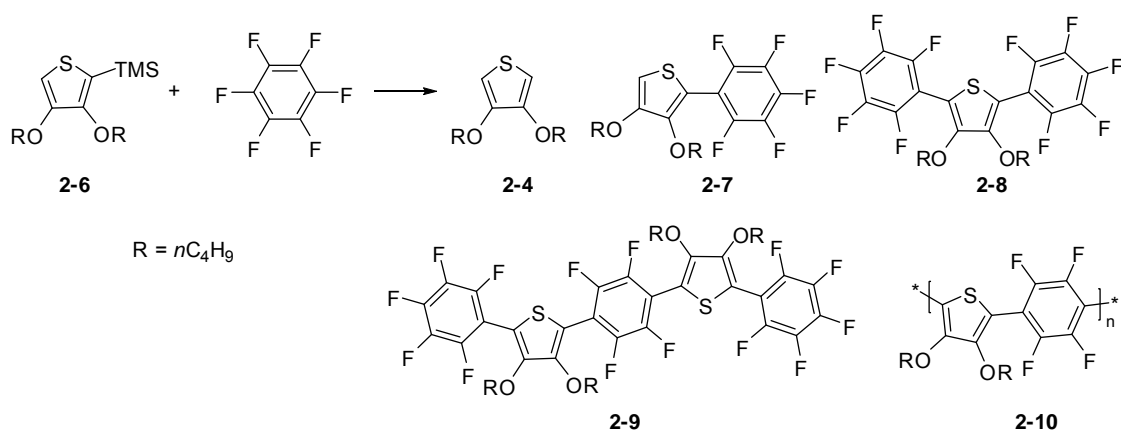
Polymer 2-2: In an argon-filled glove box, monomer **2-5** (106.7mg, 0.286mmol) decafluorobiphenyl (100.33mg, 1.05 eq), CsF (4.55mg, 0.1 eq), 18-crown-6 (15.12mg, 0.2 eq) and toluene (1mL) were combined in a vacuum flask containing a magnetic stir bar. The vessel was sealed and the contents stirred at 80°C for 7 days. The polymer was obtained as a white powder after purification as described above (148mg). ^1H NMR

(C₂D₂Cl₄) δ : 4.13 (t, 4H), 1.64 (m, 4H), 1.36 (m, 4H), 0.90 (t, 6H). ¹³C NMR (C₂D₂Cl₄) δ : 148.81, 144.08 (d of m), 113.98 (m), 110.57, 106.79 (m), 73.09, 31.67, 18.81, 13.59. ¹⁹F NMR (C₂D₂Cl₄) δ : -137.36 (m, 65F), -138.26 (m, 65F), -149.94 (m, 2F), -160.42 (m, 4F). M_n (GPC) = 17 kDa (PDI = 3.9)



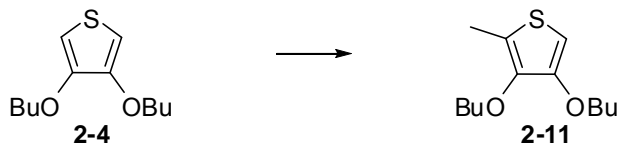
Polymer 2-3: In an argon-filled glove box, monomer **2-5** (105.6mg, 0.283mmol), octafluoronaphthalene (80.85mg, 1.05 eq), CsF (4.50mg, 0.1 eq), 18-crown-6 (14.96mg, 0.2 eq) and toluene (1mL) were combined in a vacuum flask containing a magnetic stir bar. The vessel was sealed and the contents stirred at 80°C for 7 days, during which time it precipitates. The polymer was obtained as a white powder after purification as described above (116 mg). ¹H NMR (C₂D₂Cl₄) δ : 4.12 (broad, 4H), 1.61 (broad, 4H), 1.35 (broad, 4H), 0.86 (broad, 6H). ¹³C NMR (C₂D₂Cl₄) δ : 149.67 (d of m), 148.83, 144.82 (d of m), 140.82 (d of m), 111.45 (m), 110.75, 72.94, 31.73, 18.79, 13.65. ¹⁹F NMR (C₂D₂Cl₄) δ : *Three signals with equivalent integrals: -116.46(m), -134.95(m), -147.15(m), Ten small ¹⁹F signals from nonregiospecific addition(3) and OFN end groups (7): -113.43(m), -115.77(m), -132.11(m), -133.65(m), -143.53(m), -146.09(m), -148.66(m), -149.18(m), -152.53(m), -155.10(m).* M_n (GPC) = 20 kDa (PDI = 3.4)

Small-Molecule Model Studies

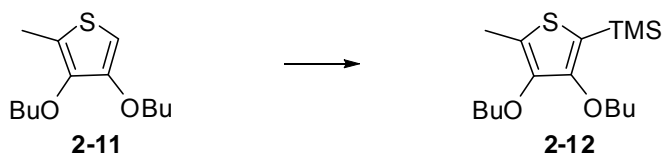


In an argon-filled glove box, **2-6** (518mg, 1.72 mmol), C_6F_6 (199 μL , 1eq), CsF (26.2mg, 0.24eq), 18-crown-6 (91.1mg, 0.2eq), and toluene (3mL) were combined in a vacuum flask containing a magnetic stir bar. The vessel was sealed and the contents stirred at 80°C for 7 days. The reaction mixture was concentrated under reduced pressure and subjected to flash chromatography on silica gel with pentane-dichloromethane (5:1, v/v) to give **2-4** as yellow liquid (172mg, 0.753mmol, 43.7%), **2-7** as a liquid (14mg, 0.035mmol, 2%), **2-8** (13mg, 0.023mmol, 1.3%), and **2-9** as a colorless solid (14mg, 0.015mmol, 1.7%). Purging the column with pure dichloromethane gave a waxy solid which was determined to be higher oligomers **2-10** (278mg, ~ 43 %). The total isolated yield based on **2-6** is 93%. **3,4-dibutoxythiophene (2-4)**: ^1H NMR (CDCl_3) δ : 6.18(s, 2H), 3.99(t, 4H), 1.82(m, 4H), 1.49(m, 4H), 0.99(t, 6H). ^{13}C NMR (CDCl_3) δ : 147.41, 96.67, 70.08, 30.98, 19.10, 13.75. GC-MS: m/z 228 ($\text{C}_{12}\text{H}_{20}\text{O}_2\text{S}^+$), 116 (100%). **3,4-dibutoxy-2-(perfluorophenyl)thiophene (2-7)**: ^1H NMR (CDCl_3) δ : 6.39(s, 1H), 4.08(t, 2H), 4.01(t, 2H), 1.81(m, 2H), 1.60-1.35(m, 4H), 1.33(m, 2H), 0.998(t, 3H), 0.878(t, 3H). ^{19}F NMR (CDCl_3) δ : -138.60(m, 2F), -154.75(m, 1F), -162.96(m, 2F). GC-MS: m/z 394 ($\text{C}_{18}\text{H}_{19}\text{F}_5\text{O}_2\text{S}^+$), 282 (100%). **3,4-dibutoxy-2,5-bis(perfluorophenyl)thiophene (2-8)**: ^1H NMR (CDCl_3) δ : 4.02(t, 4H), 1.60(m, 4H), 1.30(m, 4H), 0.89(t, 6H). ^{19}F NMR (CDCl_3) δ : -137.95(m, 4F), -153.32(m, 2F), -162.18(m, 4F). GC-MS: m/z 560, ($\text{C}_{24}\text{H}_{18}\text{F}_{10}\text{O}_2\text{S}^+$), 448 (100%). **5,5'-(perfluoro-1,4-phenylene)bis(3,4-dibutoxy-2-(perfluorophenyl)thiophene) (2-9)**: ^1H NMR (CDCl_3) δ : 4.07(t, 4H), 4.05(t, 4H), 1.61(m, 8H), 1.32(m, 8H), 0.89(t, 12H). ^{19}F NMR (CDCl_3) δ : -137.96(m, 4F), -138.63(s, 4F), -153.39(m, 2F), -162.22(m, 4F). MALDI: m/z : 934($\text{C}_{42}\text{H}_{36}\text{F}_{14}\text{O}_4\text{S}_2^+$), 710(100%)

Oligomers 2-10: See spectra below. M_n (GPC) = 4.3kDa.

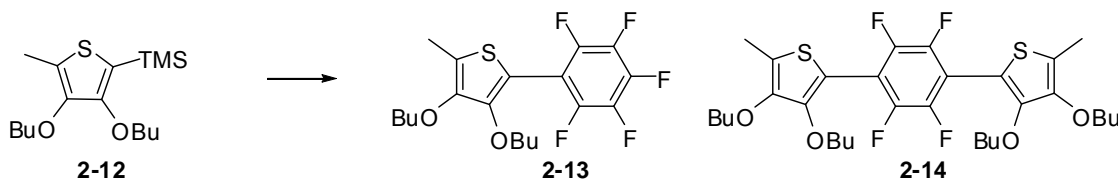


3,4-dibutoxy-2-methylthiophene (2-11): To a solution of **2-4** (1.12g, 4.90mmol) in THF (10mL) at 0°C was added a hexane solution of *n*-BuLi (2.5M, 2.06mL, 1.05eq.). The whole was stirred for 30 min, gradually warmed to room temperature, and then refluxed for 1 hour. After adding iodomethane (dried over CaH₂) (0.46mL, 1.5eq.) in one portion at 0°C, the mixture was stirred for 30 min, gradually warmed to room temperature, and left stirring overnight. The reaction mixture was diluted with CH₂Cl₂, extracted with 10% HCl (aq), dried over MgSO₄, and concentrated under reduced pressure. The residue was subjected to flash chromatography on silica gel with pentane-dichloromethane (2:1, v/v) to give **2-11** as a pale yellow liquid (520mg, 44%). ¹H NMR (CDCl₃) δ: 5.90(s, 1H), 3.98(t, 2H), 3.94(t, 2H), 2.28(s, 3H), 1.77(m, 2H), 1.69(m, 2H), 1.49(m, 4H), 0.98(t, 3H), 0.97(t, 3H). ¹³C NMR (CDCl₃) δ: 150.11, 142.97, 121.32, 91.69, 72.62, 69.38, 32.12, 31.19, 19.28, 19.11, 13.84, 13.78, 11.75. GC-MS: *m/z* 242 (C₁₃H₂₂O₂S⁺), 130 (100%).



(3,4-dibutoxy-5-methylthiophen-2-yl)trimethylsilane (2-12): To a solution of **2-11** (440mg, 1.82mmol) in THF (5mL) at 0°C was added a hexane solution of *n*-BuLi (2.5M, 0.80mL, 1.1eq.). The resulting mixture was stirred at the same temperature for 30 min, gradually warmed to room temperature, and then refluxed for 1 hour. After adding chlorotrimethylsilane (0.28mL, 1.2eq.) in one portion at 0°C, the mixture was stirred for 30 min, gradually warmed to room temperature and left stirring overnight. The reaction mixture was diluted with CH₂Cl₂, extracted with 10% HCl (aq), dried over MgSO₄, and concentrated under reduced pressure. The residue was subjected to flash chromatography on silica gel with pentane-dichloromethane (3:1, v/v) to give **2-12** as a pale yellow liquid (490mg, 86%). ¹H NMR (CDCl₃) δ: 3.98(t, 2H), 3.95(t, 2H), 2.30(s, 3H), 1.71(m, 4H),

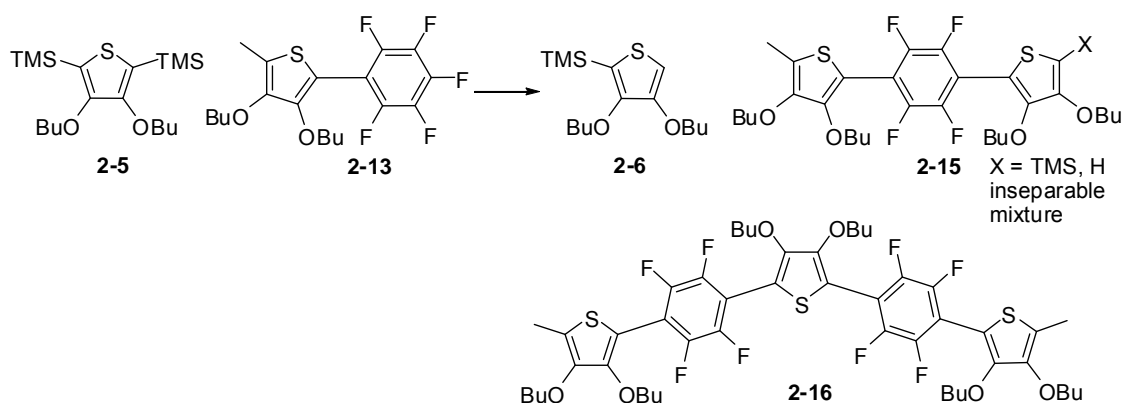
1.49(m, 4H), 0.984(t, 3H), 0.979(t, 3H), 0.29(s, 9H). ^{13}C NMR (CDCl_3) δ : 155.63, 147.03, 127.05, 115.12, 72.92, 32.33, 32.26, 19.29, 19.22, 14.00, 13.93, 12.33, -0.27. GC-MS: m/z 314 ($\text{C}_{16}\text{H}_{30}\text{O}_2\text{SSi}^+$), 187 (100%).



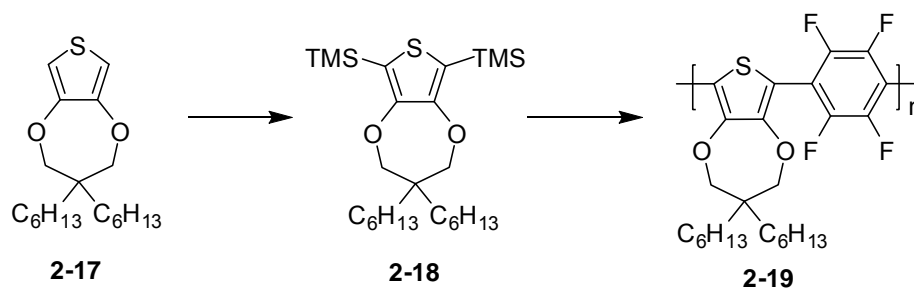
In an argon-filled glove box, **2-12** (380mg, 1.21mmol), C_6F_6 (140 μL , 1.2mmol), CsF (18.4mg, 0.1eq), 18-crown-6 (63.9 mg, 0.2eq), and toluene (2mL) were combined in a vacuum flask containing a magnetic stir bar. The vessel was sealed and the contents stirred at RT overnight after which GC-MS revealed essentially no reaction except a trace of **2-13**. After heating to 80 $^\circ\text{C}$ overnight, **2-12** was completely consumed (GC-MS). The reaction mixture was concentrated under reduced pressure to an oily residue, which was subjected to flash chromatography on silica gel with pentane-dichloromethane (3:1, v/v) to give **2-13** as a pale yellow liquid (217mg, 0.531mmol) and **2-14** as a colorless solid (183mg, 0.290mmol). The total isolated yield based on **2-12** was 92%.

3,4-dibutoxy-2-methyl-5-(perfluorophenyl)thiophene (2-13): ^1H NMR (CDCl_3) δ : 4.012(t, 2H), 4.009 (t, 2H), 2.36 (s, 3H), 1.74 (m, 2H), 1.57 (m, 4H), 1.33(m, 2H), 0.999(t, 3H), 0.879 (t, 3H). ^{19}F NMR (CDCl_3) δ : -138.76(m, 2F), -155.27(m, 1F), -163.09(m, 2F). ^{13}C NMR (CDCl_3) δ : 148.92, 145.68, 144.79 (d of m), 140.77 (d of m), 137.64(d of t), 124.72, 108.46 (m), 102.11, 73.29, 72.36, 32.17, 31.87, 19.19, 18.90, 13.82, 13.62, 11.91. GC-MS: m/z 408 ($\text{C}_{19}\text{H}_{21}\text{F}_5\text{O}_2\text{S}^+$), 296 (100%).

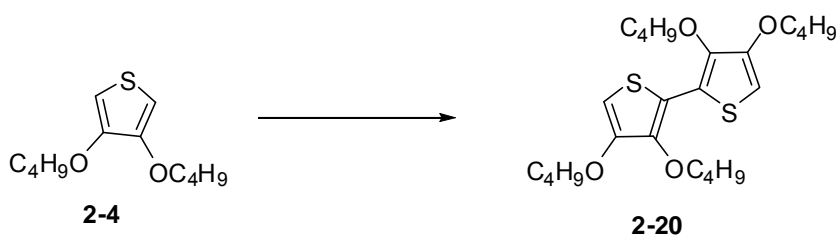
5,5'-(perfluoro-1,4-phenylene)bis(3,4-dibutoxy-2-methylthiophene) (2-14): ^1H NMR (CDCl_3) δ : 4.03(m, 8H), 2.37(s, 6H), 1.78(m, 4H), 1.57(m, 8H), 1.35(m, 4H), 1.002(t, 6H), 0.886(t, 6H). ^{19}F NMR (CDCl_3) δ : -140.24(s, 4F). ^{13}C NMR (CDCl_3) δ : 148.80, 145.66, 144.25 (d of m), 124.55, 112.44 (m), 103.46, 73.24, 72.33, 32.15, 31.88, 19.17, 18.89, 13.84, 13.66, 11.93. GC-MS: m/z 630 ($\text{C}_{32}\text{H}_{42}\text{F}_5\text{O}_4\text{S}_2^+$), 406(100%).



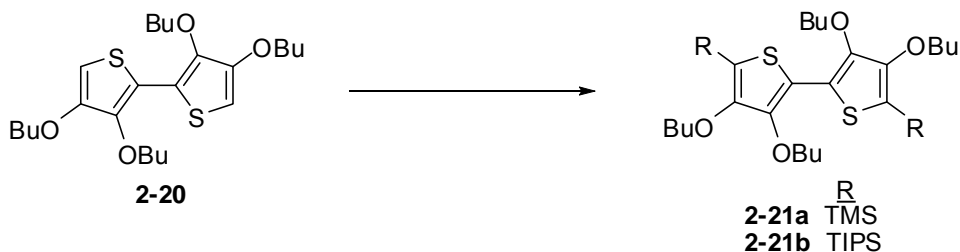
In an argon-filled glove box, **2-5** (100.2 mg, 0.269mmol), **2-13** (109.8mg, 0.269mmol), CsF (4.1mg, 0.1eq), 18-crown-6 (14.2 mg, 0.2eq), and toluene (1mL) were combined in a vacuum flask containing a magnetic stir bar. The vessel was sealed and the contents stirred at 80°C overnight. The reaction mixture was concentrated under reduced pressure to an oily residue, which was subjected to column chromatography on silica gel with pentane-dichloromethane (3:1, v/v) to give **2-5** (30mg, 30% recovered yield), **2-6** (20mg, 24.7% based on **2-5**) and **2-16** as a pale yellow liquid (100mg, 74% based on **2-13**). The remainder of products (**2-15**) resulting from reaction of **2-13** were obtained as an inseparable mixture (43 mg). The ^1H NMR spectrum of this mixture contained singlets corresponding to the methyls on the thiophene and TMS groups, as well as protons attached to the thiophene. **Compound 2-16**: ^1H NMR (CDCl_3) δ : 4.06 (overlapping triplets, 12H), 2.38 (s, 6H), 1.76-1.33 (overlapping multiplets, 24H), 1.00 (t, 6H), 0.90 (t, 6H), 0.89 (t, 6H). ^{19}F NMR (CDCl_3) δ : -139.59 (m). ^{13}C NMR (CDCl_3) δ : 148.98, 148.60, 145.73, 144.26 (d of m), 124.89, 113.45 (m), 111.43 (m), 110.70, 103.31, 73.31, 72.92, 72.40, 32.17, 31.92, 31.90, 19.19, 18.92, 18.90, 13.87, 13.70, 13.68, 12.00. MALDI: m/z : 1004($\text{C}_{50}\text{H}_{60}\text{F}_8\text{O}_6\text{S}_3^+$), 912(100%).



Polymer 2-19: Prepared similarly to polymer **2-1a**, starting from **2-18** (0.256mmol, 120.2mg), CsF (0.1 eq), 18-crown-6 (0.2 eq) and toluene at 110°C. Yield=120mg. ¹H NMR (CDCl₃) δ: 4.04 (m, 4H), 1.58-1.31 (overlapping multiplets, 20H), 0.90 (m, 6H). ¹³C NMR (CDCl₃) δ: 148.65, 143.81 (d of m), 111.69 (m), 108.38, 78.09, 44.11, 31.73, 31.67, 30.12, 22.73, 22.65, 14.07. ¹⁹F NMR (CDCl₃) δ: -138.42 (m, 4 F), -139.36 (m, 136F), -154.28 (m, 2 F), -162.40 (m, 4 F). M_n (GPC) = 10kDa (PDI = 2.1)

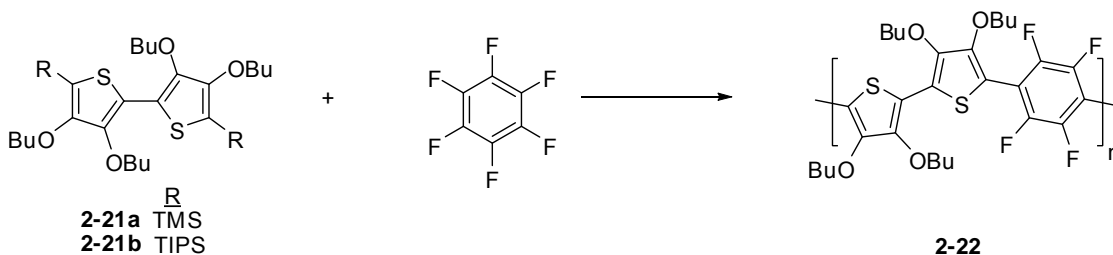


Compound 2-20: *n*-BuLi (21.78mL, 1.1eq, 2.0M) was added dropwise into 100mL of THF containing 3, 4-dibutoxythiophene **2-4** (9.05g, 39.60mmol) under argon atmosphere at -78°C temperature (isopropanol and dry ice). The mixture was stirred for 1.5h at -78°C. Subsequently, CuCl₂ (8.00g, 1.5eq) was added in one portion into the mixture at -78°C. Then the mixture was warmed up to room temperature and stirred overnight. The mixture was extracted with ether and deionized water. The ether layer was dried over anhydrous MgSO₄ and concentrated by rotary evaporation. The product was isolated after flash chromatography [silica gel, pentane:dichloromethane (2:1)] as a yellow solid (4.46g, 50%). ¹H NMR (400MHz, CDCl₃, r.t.) δ: 6.06 (s, 2H), 4.11 (t, 4H), 3.97 (t, 4H), 1.82 (m, 8H), 1.52 (m, 8H), 0.99 (t, 6H), 0.98 (t, 6H). ¹³C NMR (100MHz, CDCl₃, r.t.) δ: 149.63, 142.09, 117.85, 94.51, 72.38, 69.56, 32.19, 31.24, 19.30, 19.12, 13.88, 13.79. GC-MS: *m/z* 454 (C₂₄H₃₈O₄S₂⁺, 100%).



Compound 2-21a: All manipulations, including isolation, were carried out under argon using schlenk techniques. *n*-BuLi (10.1 mL, 3eq, 1.6M) was added dropwise into 50mL of THF containing compound **2-20** (2.45g, 5.39mmol) under argon atmosphere at -78°C (isopropanol and dry ice). The mixture was stirred for 1h at -78°C. Subsequently, TMSCl (2.4mL, 4eq) was added dropwise into the mixture at -78°C. Then the mixture was warmed up to room temperature and stirred overnight. The mixture was concentrated under reduced pressure. The residue was dissolved in 20mL hexane and 5mL dichloromethane. The solid was filtered through a cannula filter and the solution was concentrated under reduced pressure to yield **2-21a** as a yellow solid (3.23g, 100%). ¹H NMR (400MHz, CDCl₃, r.t.) δ: 4.06 (t, 4H), 3.99 (t, 4H), 1.82 (m, 8H), 1.52 (m, 8H), 0.98 (t, 12H), 0.32 (s, 18H). ¹³C NMR (100MHz, CDCl₃, r.t.) δ: 155.21, 146.24, 123.15, 117.85, 73.12, 72.69, 32.32, 19.30, 14.04, -0.36. HR-MS: 598.2996 +/- 0.0007 (1.1ppm) versus a calculated value of 598.2996, error is 0.0000 (0.1ppm). GC-MS: *m/z* 598 (C₃₀H₅₄O₄S₂Si₂⁺, 100%).

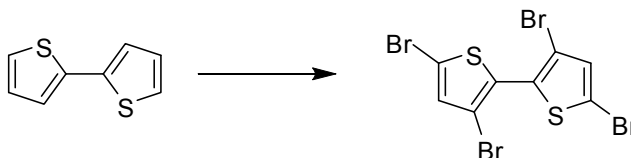
Compound 2-21b: Conducted exactly as in monomer **2-21a** above. ¹H NMR (400MHz, CDCl₃, r.t.) δ: 4.04 (m, 8H), 1.82 (m, 4H), 1.71 (m, 4H), 1.54-1.42 (m, 14H), 1.13 (d, 36H), 0.97 (m, 12H). ¹³C NMR (100MHz, CDCl₃, r.t.) δ: 155.51, 146.14, 123.69, 112.41, 72.70, 71.89, 32.38, 32.36, 19.41, 19.24, 18.86, 14.12, 14.05, 12.04. GC-MS: *m/z* 766 (C₄₂H₇₈O₄S₂Si₂⁺), 207 (100%).



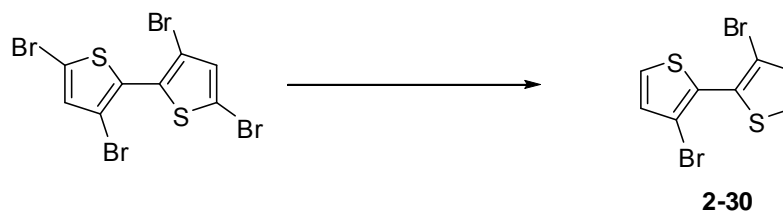
Polymer 2-22: In an argon-filled glove box, monomer **2-21a** (92.30mg, 0.154mmol), C₆F₆ (18.69μL, 1.05eq), CsF (2.34mg, 0.1eq), 18-crown-6 (8.14mg, 0.2eq), and toluene (1mL) were combined in a vacuum flask containing a magnetic stir bar. The vessel was sealed and the contents stirred at 80°C for 5 days. The solution was extracted with deionized water twice and the polymer precipitated by pouring the solution in 50mL

methanol. The polymer was re-dissolved in toluene then precipitated again into methanol. After drying under reduced pressure, the polymer was obtained as a yellow-green solid (65mg, 70%). ^1H NMR (CDCl_3 , 400MHz) δ : 4.20 (m, 4H), 4.06 (m, 4H), 1.89 (m, 4H), 1.63 (m, 4H), 1.54 (m, 4H), 1.38 (m, 4H), 1.01 (t, 6H), 0.90 (t, 6H). ^{19}F NMR (CDCl_3 , 376MHz) δ : -138.28 (m, 4F), -139.49 (s, 93F), -154.42 (m, 2F), -162.65 (m, 4F). M_n (GPC) = 20 kDa (PDI = 2.14).

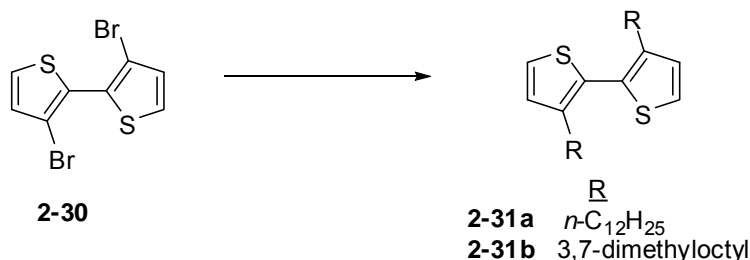
Polymer 2-22: In an argon-filled glove box, monomer **2-21b** (61.96mg, 0.0807mmol), C_6F_6 (9.79 μL , 1.05eq), CsF (0.1eq), 18-crown-6 (0.2eq), and THF (1mL) were combined in a vacuum flask containing a magnetic stir bar. The vessel was sealed and the contents stirred at 70°C for 5 days. The solution was extracted with deionized water twice and the polymer precipitated by pouring the solution in 50mL methanol. The polymer was re-dissolved in toluene then precipitated again into methanol. After drying under reduced pressure, the polymer was obtained as a yellow solid (35mg, 72%). ^1H NMR (400MHz, CDCl_3 , r.t.) δ : 4.19 (broad, 4H), 4.07 (broad, 4H), 1.90 (m, 4H), 1.64 (m, 8H), 1.37 (m, 4H), 1.02 (t, 6H), 0.91 (t, 6H). ^{19}F NMR (376MHz, CDCl_3 , r.t.) δ : -138.31 (m, 4F), -139.49 (m, 110F), -154.41 (m, 2F), -162.14 (m, 4F). M_n (GPC) = 15 kDa (PDI = 1.81).



3,3',5,5'-tetrabromo-2,2'-bithiophene: To a mixture of 2,2'-bithiophene (10g, 60.1mmol), acetic acid (200mL) and chloroform (150mL) was added bromine (12.35mL, 4eq) dropwise at 0°C over 40 min. The mixture was subsequently stirred at room temperature for 5 h and then under reflux at 90°C overnight. After cooling to room temperature, the reaction was quenched by addition of 50mL of 10% KOH (aq). After extraction with chloroform and water, the organic layer was dried over anhydrous MgSO_4 , filtered, and concentrated under reduced pressure. Recrystallization from ethanol afforded off-white crystals (7.00g, 78%). ^1H NMR (400MHz, CDCl_3 , r.t.) δ : 7.06 (s, 2H). ^{13}C NMR (100MHz, CDCl_3 , r.t.) δ : 132.98, 129.55, 114.81, 112.10. GC-MS: m/z 482 ($\text{C}_8\text{H}_2\text{Br}_4\text{S}_2^+$, 100%).



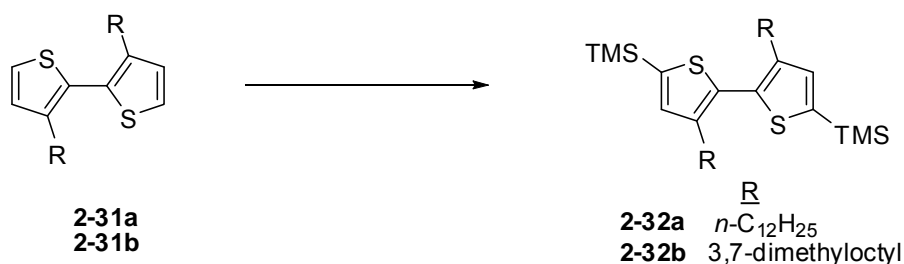
3,3'-dibromo-2,2'-bithiophene (2-30):²⁰⁶ A dispersion of zinc powder (2.16g, 4eq) in 40mL of ethanol containing 4mL of water, 10mL of glacial acetic acid, and 2mL of 10% HCl (aq) was heated at 80°C for 30min. 3,3',5,5'-tetrabromo-2,2'-bithiophene (4.00g, 8.30mol) was added into the above dispersion. After being refluxed at 100°C for an additional 2 h and then cooled to room temperature, the mixture was extracted with ether and the ether layer was treated with 10% KOH (aq). The ether layer was extracted by deionized water and dried over anhydrous MgSO₄ and filtered. The solvent was removed by rotary evaporation and the residue was recrystallized from hexane to give light-yellow crystals (1.10g, 41%). ¹H NMR (400MHz, CDCl₃, r.t.) δ: 7.42 (d, 2H), 7.09 (d, 2H). ¹³C NMR (100MHz, CDCl₃, r.t.) δ: 130.80, 128.87, 127.51, 112.63. GC-MS: *m/z* 324 (C₈H₄Br₂S₂⁺, 100%).



3,3'-didodecyl-2,2'-bithiophene (2-31a):²⁰⁷ A commercial solution of dodecylmagnesium bromide (13mL, 1M ether, 4eq) was degassed by argon sparge and then added dropwise to a suspension of 3,3'-dibromo-2,2'-bithiophene **2-30** (1.04g, 3.21mmol) and NiCl₂(dppp) (0.087g, 0.05eq) in 15mL of diethyl ether at r.t.. The resulting suspension was stirred for 24 h under reflux, and then cooled to room temperature. The mixture was extracted with ether and 10% HCl (aq). The ether layer was extracted by deionized water three times and dried over anhydrous MgSO₄ and filtered. The solvent was removed by rotary evaporation and the residue passed through a column of silica gel with pentane to yield a yellow oil (1.56g, 97%). ¹H NMR (400MHz,

CDCl₃, r.t.) δ : 7.29 (d, 2H), 6.97 (d, 2H), 2.51 (t, 4H), 1.55 (m, 4H), 1.24 (m, 36H), 0.89 (t, 6H). ¹³C NMR (100MHz, CDCl₃, r.t.) δ : 142.32, 128.72, 128.51, 125.19, 31.92, 30.71, 29.68, 29.66, 29.56, 29.43, 29.36, 28.78, 22.69, 14.11. GC-MS: m/z 502 (C₃₂H₅₄S₂⁺, 100%).

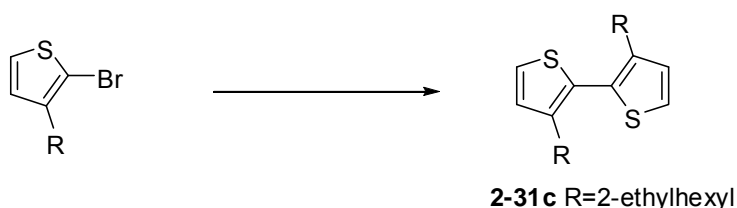
Compound 2-31b: Conducted exactly as in **2-31a** above, except the Grignard reagent was freshly prepared from 1-bromo-3,7-dimethyloctane (8.97g, 6eq) and Mg (1.30g, 8eq) in ether. This reagent solution was added dropwise to 3,3'-dibromo-2,2'-bithiophene (2.19g, 6.76mmol), NiCl₂(dppp) (0.183g, 0.05eq) and 35ml of ether. A light-yellow oil (2.69g, 89%) was obtained after purification through a column of silica gel with pentane. ¹H NMR (400MHz, CDCl₃, r.t.) δ : 7.29 (d, 2H), 6.98 (d, 2H), 2.53 (m, 4H), 1.59-1.09 (broad, 20H), 0.87 (d, 12H), 0.84 (d, 6H). ¹³C NMR (100MHz, CDCl₃, r.t.) δ : 142.44, 128.60, 128.55, 125.21, 39.30, 38.01, 37.03, 32.58, 27.96, 26.42, 24.62, 22.72, 22.62, 19.52. GC-MS: m/z 446 (C₂₈H₄₆S₂⁺, 100%)



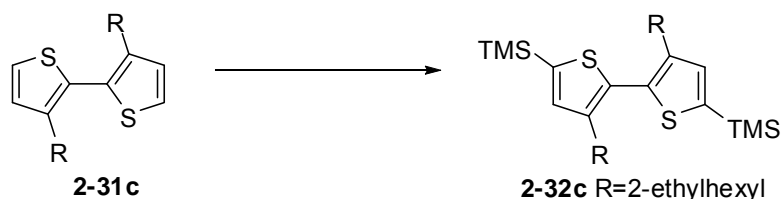
Compound 2-32a: *n*-BuLi (3.35mL, 1.6M hexanes, 2.02eq) was added dropwise into 10mL of hexane containing compound **2-31a** (1.34g, 2.66mmol) (dried at 50°C under reduced pressure for 20min) and 0.81mL of TMEDA (2.02eq) under argon atmosphere at room temperature. The mixture was stirred for 30min at r.t. and heated at 70°C for 2h. Subsequently, TMSCl (0.84mL, 2.5eq) was added dropwise into the mixture at 0°C. Then the mixture was warmed up to room temperature and stirred for 24h. The mixture was extracted with ether and 10% HCl (aq). The ether layer was extracted with deionized water three times and dried over anhydrous MgSO₄ and filtered. After removal of the solvent and purification through a column of silica gel with pentane, a yellow solid **2-32a** (1.66g, 96%) was obtained. ¹H NMR (400MHz, CDCl₃, r.t.) δ : 7.08 (s, 2H), 2.51 (t, 4H), 1.56 (m, 4H), 1.25 (m, 36H), 0.89 (t, 6H), 0.33 (s, 18H). ¹³C NMR (100MHz, CDCl₃, r.t.)

δ : 142.97, 139.94, 135.57, 134.59, 31.93, 30.85, 29.70, 29.67, 29.58, 29.53, 29.41, 29.37, 28.78, 22.69, 14.11, -0.057. Anal. calc. 70.51%, H 10.90%. Found C 72.35%, H 11.14%. HR-MS: 646.4465 +/- 0.0006 (0.9ppm) versus a calculated value of 646.4451, error is 0.0003(2.1ppm).

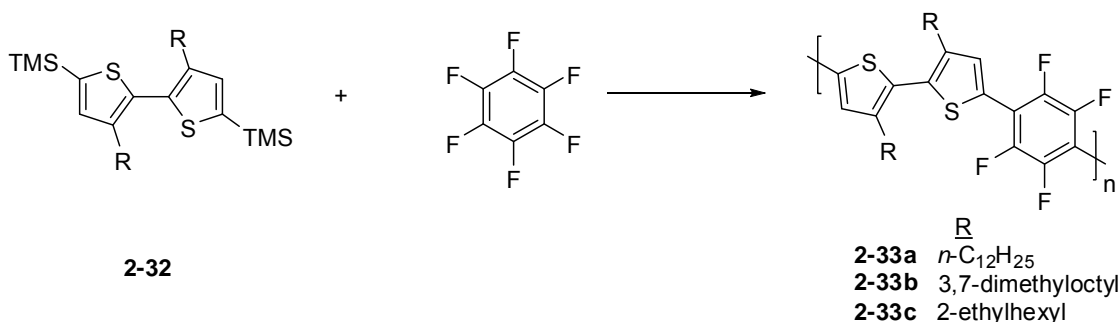
Compound 2-32b: Conducted exactly as in **2-32a** above. **2-31b** (2.5g, 5.60mmol), *n*-BuLi (4.7mL, 2.5M hexanes, 2.1eq), TMEDA (1.77mL, 2.1eq), TMSCl (1.77mL, 2.5eq) and 20mL of hexane. A light-yellow oil (3.00g, 91%) was obtained after purification through a column of silica gel with pentane. ^1H NMR (400MHz, CDCl_3 , r.t.) δ : 7.07 (s, 2H), 2.53 (m, 4H), 1.59-1.09 (broad, 20H), 0.88 (d, 12H), 0.85 (d, 6H), 0.33(s, 18H). ^{13}C NMR (100MHz, CDCl_3 , r.t.) δ :143.10, 139.88, 135.64, 134.48, 39.30, 38.20, 37.03, 32.76, 27.94, 26.46, 24.68, 22.72, 22.63, 19.57, -0.07. Anal. calc. 69.08%, H 10.57%. Found C 69.95%, H 11.70%. HR-MS: 590.3823 +/- 0.0006 (1.0ppm) versus a calculated value of 590.3825, error is -0.0003(-0.4ppm).



Compound 2-31c: A mixture of bis(1,5-cyclooctadienyl)nickel(0) (2.0g, 1.1eq), 2,2'-bipyridine (1.13g, 1.1eq), 1,5-cyclooctadiene (0.80mL, 6.54mmol), and 20mL of anhydrous DMF was maintained at 80°C for 1h under an argon atmosphere. To this solution, 2-bromo-3-(2-ethylhexyl)thiophene (1.80g, 6.54mmol) dissolved in 30mL of toluene, was added dropwise. The resulting solution was stirred at 80 °C overnight. The mixture was diluted with ether and extracted with 10% HCl (aq). The solution was dried with anhydrous magnesium sulfate, concentrated under reduced pressure, and the residue passed through a silica plug with hexane to yield **2-31c** (1.10g, 86%). ^1H NMR (400MHz, CDCl_3 , r.t.) δ : 7.29 (d, 2H), 6.94 (d, 2H), 2.45 (d, 4H), 1.54 (m, 2H), 1.23 (m, 16H), 0.86 (t, 6H), 0.78 (t, 6H). ^{13}C NMR (100MHz, CDCl_3 , r.t.) δ : 141.43, 129.43, 128.91, 125.01, 40.32, 33.00, 32.68, 28.80, 25.78, 22.98, 14.11, 10.76. GC-MS: m/z : 390 ($\text{C}_{24}\text{H}_{38}\text{S}_2^+$), 193 (100%).



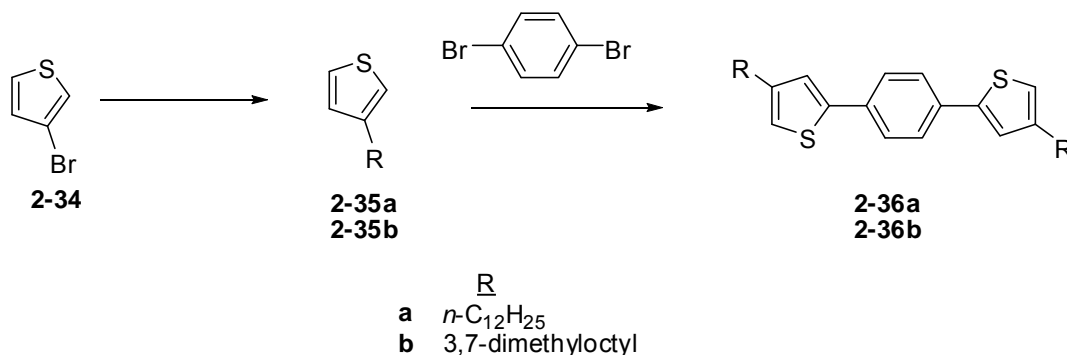
Compound 2-32c: Conducted exactly as for monomer **2-32a** above. Monomer **2-32c** was obtained as light-yellow oil (0.99g, 65%). ^1H NMR (400MHz, CDCl_3 , r.t.) δ : 7.03 (s, 2H), 2.45 (d, 4H), 1.51 (m, 2H), 1.22 (m, 16H), 0.84 (t, 6H), 0.77 (t, 6H), 0.33(s, 18H). ^{13}C NMR (100MHz, CDCl_3 , r.t.) δ : 142.09, 139.53, 136.08, 135.23, 40.36, 32.84, 32.62, 28.72, 25.87, 22.94, 14.12, 10.78, -0.087. Anal. calc. C 67.34%, H 10.17%. Found C 67.58%, H 10.06%.



Polymer 2-33a: In an argon-filled glove box, monomer **2-32a** (134.40mg, 0.208mmol), C_6F_6 (25.24 μL , 1.05eq), catalytic CsF, a few crystals of 18-crown-6 and toluene (1mL) were combined in a vacuum flask containing a magnetic stir bar. The vessel was sealed and the contents stirred at 80°C for 5 days. The solution was extracted with deionized water twice and the polymer precipitated by pouring the solution in 50mL methanol. The polymer was re-dissolved in chloroform at 80°C then precipitated again into methanol. Afterwards the polymer was stirred in hot hexane at 50°C for 8 hours to remove lower molecular-weight oligomers. After drying under reduced pressure, the polymer was obtained as a orange-red solid (116mg, 86%). ^1H NMR (400MHz, $\text{C}_2\text{D}_2\text{Cl}_4$, 75°C) δ : 7.63 (s, 2H), 2.68 (m, 4H), 1.69 (m, 4H), 1.30 (m, 36H), 0.93 (t, 6H). ^{19}F NMR (376MHz, $\text{C}_2\text{D}_2\text{Cl}_4$, 75°C) δ : -140.05 (m, 4F), -140.94 (s, 79F), -156.61 (m, 2F), -162.72 (m, 4F). M_n (GPC) = 22 kDa (PDI = 2.1)

Polymer 2-33b: Conducted exactly as for polymer **2-33a** above. Monomer **2-32b** (235.50mg, 0.398mmol), C₆F₆ (48.29μL, 1.05eq), catalytic CsF, a few crystals of 18-crown-6, and toluene (2mL). Polymer **2-33b** was obtained as an orange-red solid (147mg, 62%). ¹H NMR (400MHz, CDCl₃) δ: 7.60 (s, 2H), 2.68 (m, 4H), 1.29-1.13 (m and broad, 12H), 0.84 (m and broad, 18H). ¹³C NMR (CDCl₃) δ: 148.77, 144.32 (d of m), 112.37 (m), 110.75, 73.02, 31.90, 18.92, 13.72. ¹⁹F NMR (376MHz, CDCl₃) δ: -140.15 (m, 4F), -140.99 (s, 87F), -156.35 (m, 2F), -162.53 (m, 4F). M_n (GPC) = 20 kDa (PDI = 2.0).

Polymer 2-33c: Conducted exactly as fo polymer **2-33a** above. Polymer **2-33c** was obtained as a yellow solid (95mg, 65%). ¹H NMR (400MHz, CDCl₃) δ: 7.56 (s, 2H), 2.58 (d, 4H), 1.57 (m, 2H), 1.23 (m, 16H), 0.84 (m, 12H). ¹³C NMR (CDCl₃) δ: 148.77, 144.32 (d of m), 112.37 (m), 110.75, 73.02, 31.90, 18.92, 13.72. ¹⁹F NMR (376MHz, CDCl₃) δ: -140.23 (m, 4F), -141.09 (s, 72F), -156.43 (m, 2F), -162.58 (m, 4F). M_n (GPC) = 11 kDa (PDI = 2.1).

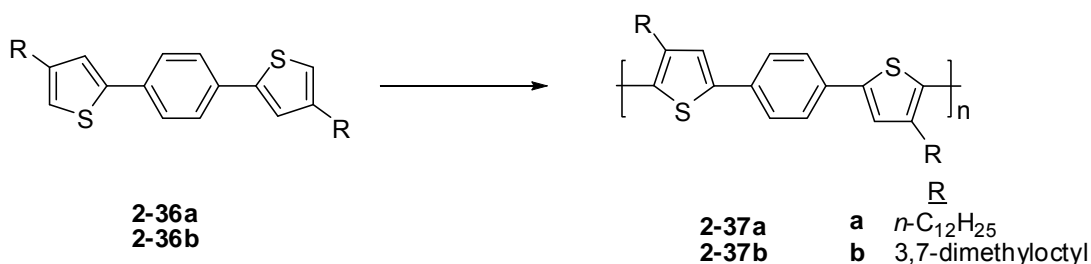


Compound 2-35a: Conducted exactly as for compound **2-31a** above, except using 3-bromothiophene replacing 3,3'-dibromo-2,2'-bithiophene. The title compound **2-35a** was obtained as yellow liquid (10.55g, 68%). ¹H NMR (400 MHz, CDCl₃, r.t.) δ: 7.30 (m, 1H), 6.99 (m, 2H), 2.71 (t, 2H), 1.70 (m, 2H), 1.36 (m, 18H), 0.98 (t, 3H). ¹³C NMR (50 MHz, CDCl₃, r.t.): δ: 143.33, 128.33, 125.05, 119.80, 31.92, 30.55, 30.27, 29.66, 29.47, 29.34, 22.66, 14.05. GC-MS: *m/z* 252 (C₁₆H₂₈S⁺), 98 (100%).

Compound 2-35b: Conducted exactly as for compound **2-31a** above, except using 3-bromothiophene replacing 3,3'-dibromo-2,2'-bithiophene and Grignard reagent made freshly from 1-bromo-3,7-dimethyloctane and Mg replacing dodecylmagnesium bromide. Compound **2-35b** was isolated as colorless liquid in 80% yield. ¹H NMR (400 MHz, CDCl₃, r.t.) δ: 7.26 (m, 1H), 6.97 (m, 2H), 2.67 (m, 2H), 1.69 (m, 2H), 1.38-1.60 (broad and m, 8H), 0.94 (d, 3H), 0.89 (d, 6H). ¹³C NMR (100 MHz, CDCl₃, r.t.): δ: 143.41, 128.26, 125.04, 119.60, 39.31, 37.80, 37.12, 32.46, 27.96, 27.84, 24.70, 22.71, 22.62, 19.57. GC-MS: *m/z* 224 (C₁₄H₂₄S⁺), 98 (100%).

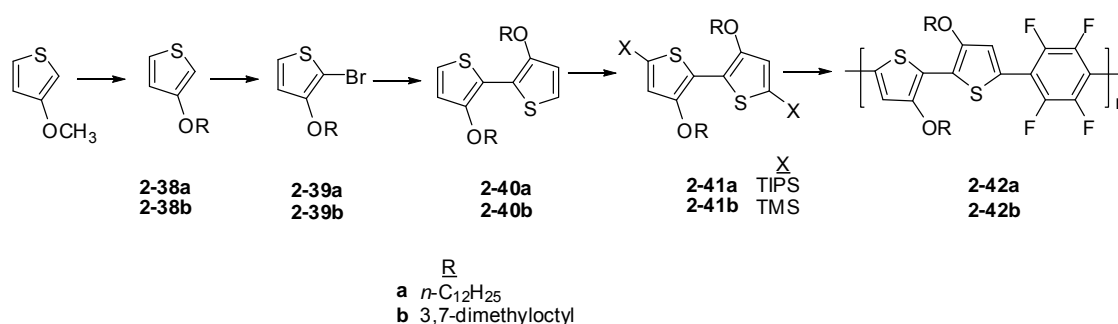
Compound 2-36a: *n*-BuLi (1.58mL, 2.5M solution in hexane, 3.96mmol) was added dropwise to a solution of diisopropylamine (0.56mL, 3.96mmol) in 6mL of dry THF at 0°C. After being stirred for 0.5 h at 0°C, the mixture was cooled to -78°C. 3-dodecylthiophene **2-35a** (1.00g, 3.96mmol) was added in one portion under nitrogen atmosphere. The mixture was stirred for 2 h at this temperature and a solution of anhydrous zinc chloride (0.65g, 4.75mmol) in 5mL of dry THF was added dropwise via syringe. The mixture was stirred for 1 h at -78°C and allowed to warm to room temperature for an additional hour. The mixture was transferred dropwise to a solution of 1, 4-dibromobenzene (0.374g, 1.58mmol) and Pd(PPh₃)₄ (92.4mg, 0.079mmol) in 10mL of dry THF. The resulting reaction mixture was stirred for 48h at 70°C. The solution was quenched by being poured into a saturated solution of ammonium chloride. The aqueous layer was extracted three times with hexane. The combined organic layers were dried over magnesium sulfate. The solvent was removed by rotary evaporation, and the residue was purified by flash chromatography (silica gel, pentane as eluent) to give **2-36a** as a white solid (284mg, yield: 50% based on consumed **2-35a**), recovered **2-35a** (500mg, 1.98mmol), 4-dodecyl-2-phenylthiophene (26mg, 0.079mmol). **2-36a:** ¹H NMR (400 MHz, CDCl₃, r.t.) δ: 7.59 (s, 4H), 7.19 (d, 2H), 6.88 (d, 2H), 2.63 (t, 4H), 1.67 (m, 4H), 1.29-1.35 (m, 36H), 0.91 (t, 6H). ¹³C NMR (100 MHz, CDCl₃, r.t.): 144.38, 143.36, 133.55, 125.94, 124.41, 119.50, 31.92, 30.63, 30.45, 29.68, 29.66, 29.61, 29.49, 29.37, 29.35, 22.69, 14.12. Anal. calc. 78.53%, H 10.23%. Found C 78.83%, H 10.10%. GC-MS: *m/z* 578 (C₃₈H₅₈S₂⁺, 100%).

Compound 2-36b: Prepared following the procedure similar to compound **2-36a**. **2-35b** (1.19g, 5.3mmol), 1,4-dibromobenzene (0.50g, 2.12mmol), *n*-BuLi (2.12mL, 5.3mmol), diisopropylamine (0.74mL, 5.3mmol), Pd(PPh₃)₄ (124mg, 0.106mmol) and anhydrous zinc chloride (0.87g, 6.36mmol). Product **2-36b** was isolated as a colorless solid (600mg, 70% based on consumed **2-35b**), recovered **2-35b** (451mg, 2.01mmol), 4-(3,7-dimethyloctyl)-2-phenylthiophene (21mg, 0.070mmol). **2-36b**: ¹H NMR (400 MHz, CDCl₃, r.t.) δ: 7.59 (s, 4H), 7.19 (d, 2H), 6.88 (d, 2H), 2.68-2.62 (m, 4H), 1.73-1.13 (m, 20H), 0.95 (d, 6H), 0.89 (d, 12H). ¹³C NMR (100 MHz, CDCl₃, r.t.): 144.55, 143.49, 133.55, 125.96, 124.42, 119.38, 39.32, 37.72, 37.13, 32.48, 28.21, 27.97, 24.71, 22.72, 22.63, 19.58. Anal. calc. 77.32%, H 9.71%. Found C 78.10%, H 9.64%. GC-MS: *m/z* 522 (C₃₄H₅₀S₂⁺), 270 (100%).



Polymer 2-37a: A solution of **2-36a** (120mg, 0.207mmol) in 3mL anhydrous chloroform was added dropwise into a solution of FeCl₃ (134.3mg, 1.08mmol) in 10mL anhydrous chloroform at r.t. The mixture was then heated at 50°C for 48h. The blue-black mixture was poured into 150mL methanol to generate a blue-green precipitate. The solid was collected by filtration and washed with methanol and water. The residue was dedoped by stirring with 80mL of a mixture of concentrated ammonium hydroxide and water (v:v=3:1) for 1.5h. The yellow solid was isolated by centrifugation and washed with methanol. The yellow polymer was dissolved in chloroform and precipitated into 100mL methanol. The resulting yellow polymer was stirred in 6mL hexane at 60°C for 6h to separate lower molecular-weight oligomers. After being centrifuged and dried, a yellow solid was obtained (37mg, 31%). ¹H NMR (400 MHz, CDCl₃, 55°C) δ: 7.67 (s, 4H), 7.28 (s, 2H), 2.65(m, 4H), 1.69-1.30 (m, 40H), 0.92 (t, 6H). ¹³C NMR (100 MHz, CDCl₃, 55°C): 143.70, 143.41, 133.55, 128.57, 126.01, 124.83, 31.96, 30.71, 29.72, 29.60, 29.48, 29.36, 29.24, 22.68, 14.03. *M_n* (GPC) = 30 kDa (PDI = 1.98).

Polymer 2-37b: The title compound was synthesized as described for polymer **2-37a**, substituting 50°C for r.t.. **Polymer 2-37b** was obtained as a yellow solid with 55% yield. ¹H NMR (400 MHz, C₂D₂Cl₄, 70°C) δ: 7.65 (s, 4H), 7.26 (s, 2H), 2.64(broad, 4H), 1.69-0.89 (broad and m, 38H). ¹³C NMR (100 MHz, C₂D₂Cl₄, r.t.): 144.52, 143.61, 133.86, 128.75, 126.36, 125.55, 39.87, 38.52, 37.57, 33.22, 28.54, 27.34, 25.24, 23.01, 22.92, 19.94. M_n (GPC) = 47 kDa (PDI = 1.62).



Compound 2-38a: A mixture of 3-methoxythiophene (3.00g, 26.30mmol), 1-dodecanol (11.77mL, 52.60mmol), *p*-toluenesulfonic acid monohydrate (0.50g, 0.10eq) and 30mL toluene was heated at 110°C for 2 days in a sealed vacuum flask under argon. After a dichloromethane/water extraction, the organic layer was dried over MgSO₄, concentrated and purified by column chromatography on silica gel with hexane-dichloromethane (3:1, v/v) to give **2-38a** as yellow liquid (4.18g, 60%). ¹H NMR (200MHz, CDCl₃, r.t.) δ: 7.14 (d of d, 1H), 6.73 (d of d, 1H), 6.20 (d of d, 1H), 3.92 (t, 2H), 1.75 (m, 2H), 1.25 (m, 18H), 0.86 (t, 3H). ¹³C NMR (50MHz, CDCl₃, r.t.) δ: 159.19, 124.52, 119.60, 97.06, 70.31, 31.86, 29.57, 29.53, 29.33, 29.28, 29.22, 25.99, 22.61, 14.01. GC-MS: *m/z*: 268 (C₁₆H₂₈OS⁺), 100 (100%).

Compound 2-38b: The title compound was synthesized as described for **2-38a**. The product was not pure after gradient column chromatography: hexane to hexane:DCM (5:1). **2-38b** was directly used for next step without further purification. GC-MS: *m/z*: 240 (C₁₄H₂₄OS⁺), 109 (100%).

Compound 2-39a: N-Bromosuccinimide (1.26g, 7.08mmol) was added in one portion to **2-38a** in 20mL DMF at 0°C. After being stirred for 1h at 0°C, the solution was warmed up to r.t. and stirred for 6h at r.t. The mixture was diluted with ether and treated with 10% HCl (aq). The organic layer was dried over MgSO₄, concentrated under reduced pressure, and the residue was purified by column chromatography (silica gel, hexane) to give **2-39a** as a yellow solid (2.00g, 77%). ¹H NMR (200MHz, CDCl₃, r.t.) δ: 7.16 (d, 1H), 6.72 (d, 1H), 4.01 (t, 2H), 1.73 (m, 2H), 1.25 (m, 18H), 0.86 (t, 3H). ¹³C NMR (50MHz, CDCl₃, r.t.) δ: 154.67, 124.11, 117.61, 91.68, 72.26, 31.84, 29.56, 29.49, 29.46, 29.42, 29.25, 25.73, 22.59, 13.99. GC-MS: *m/z*: 348 (C₁₆H₂₇BrOS⁺), 180 (100%).

Compound 2-39b: Synthesized and isolated as described for **2-39a**. The title compound **2-39b** was obtained as a yellow liquid (1.90g, 84%). ¹H NMR (400MHz, CDCl₃) δ: 7.20 (d, 1H), 6.76 (d, 1H), 4.08 (m, 2H), 1.83 (m, 1H), 1.70 (m, 1H), 1.56 (m, 2H), 1.38-1.14 (broad and m, 6H), 0.95 (d, 3H), 0.88 (d, 6H). ¹³C NMR (100MHz, CDCl₃) δ: 154.53, 124.10, 117.43, 91.51, 70.58, 39.18, 37.21, 36.37, 29.65, 27.95, 24.62, 22.69, 22.59, 19.66. GC-MS: *m/z*: 318 (C₁₄H₂₃BrOS⁺), 180 (100%).

Compound 2-40a: A mixture of bis(1,5-cyclooctadienyl)nickel(0) (1.78g, 1.5eq), 2,2'-dipyridyl (1.01g, 1.5eq), 1,5-cyclooctadiene (0.53mL, 4.32mmol), and 20mL of anhydrous DMF was maintained at 80°C for 1 h under an argon atmosphere. To this solution, **2-39a**, dissolved in 30mL of toluene, was added dropwise. The resulting solution was stirred at 80°C overnight. The mixture was diluted with DCM and extracted with 10% HCl (aq). The solution was dried with anhydrous magnesium sulfate and the volatiles were evaporated under reduced pressure. The residue was passed through a silica plug with hexane-dichloromethane (3:1, v/v) to yield **2-40a** (0.95g, 82%). ¹H NMR (400MHz, CDCl₃, r.t.) δ: 7.08 (d, 2H), 6.84 (d, 2H), 4.10 (t, 4H), 1.85 (m, 4H), 1.28 (m, 36H), 0.90 (t, 6H). ¹³C NMR (100MHz, CDCl₃, r.t.) δ: 151.91, 128.66, 121.56, 116.00, 71.95, 31.91, 29.69, 29.64, 29.59, 29.55, 29.35, 28.00, 26.03, 22.68, 14.11. GC-MS: *m/z*: 534 (C₃₂H₅₄O₂S₂⁺), 197 (100%).

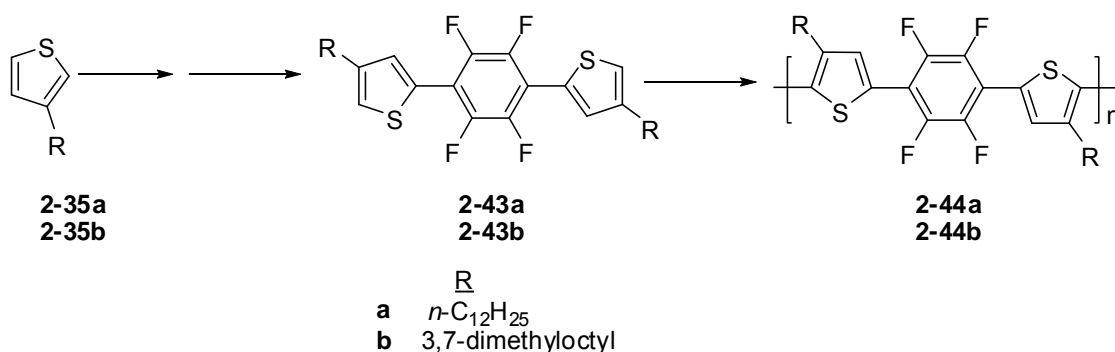
Compound 2-40b: Prepared and isolated as described above for **2-40a**. The title compound **2-40b** was obtained as a brown liquid (1.10g, 79%). ¹H NMR (400MHz, CDCl₃) δ: 7.09 (d, 2H), 6.86 (d, 2H), 4.15 (m, 4H), 1.83 (m, 2H), 1.70 (m, 2H), 1.56 (m, 4H), 1.38-1.14 (broad and m, 12H), 0.95 (d, 6H), 0.88 (d, 12H). ¹³C NMR (100MHz, CDCl₃) δ: 151.89, 121.54, 115.98, 114.09, 70.24, 39.20, 37.27, 36.66, 29.56, 27.96, 24.65, 22.70, 22.60, 19.63. GC-MS: *m/z*: 478 (C₂₈H₄₆O₂S₂⁺), 198 (100%).

Compound 2-41a: To a solution of **2-40a** (0.663mg, 1.24mmol) in THF (15mL) at 0°C was added a hexane solution of *n*-BuLi (2.5M, 1.49mL, 3eq.). The resulting mixture was stirred at the same temperature for 15 min, gradually warmed to room temperature, and then stirred at r.t. for 1 hour. After adding triisopropylsilylchloride (0.28mL, 1.2eq.) in one portion at 0°C, the mixture was gradually warmed to room temperature and left stirring overnight. The reaction mixture was diluted with ether, extracted with 10% HCl (aq), dried over MgSO₄, and concentrated under reduced pressure. The residue was subjected to flash chromatography on silica gel with hexane to give **2-41a** as a yellow solid (0.81mg, 77%). ¹H NMR (400MHz, CDCl₃, r.t.) δ: 6.94 (s, 2H), 4.13 (t, 4H), 1.85 (m, 4H), 1.60 (m, 6H), 1.32 (m, 36H), 1.13 (d, 36H), 0.89 (t, 6H). ¹³C NMR (100MHz, CDCl₃, r.t.) δ: 153.53, 129.39, 123.58, 119.59, 71.91, 31.90, 29.92, 29.73, 29.72, 29.69, 29.65, 29.35, 26.41, 22.67, 18.59, 14.10, 11.66. Anal. calc. 71.23%, H 12.25%. Found C 70.85%, H 11.18%.

Compound 2-41b: Prepared as described above for **2-41a**, with exception of using TMSCl instead of TIPSCl. The title compound **2-41b** was obtained as a brown liquid (1.10g, 79%). This monomer is highly susceptible to protodesilylation by acidic or basic aqueous solutions and silica gel. It was therefore not isolated.

Polymer 2-42a: Conducted exactly as for polymer **2-22** from **2-21b** above. Polymer **2-42a** was obtained as a deep purple solid (90%). The molecular weight of **2-42a** without optimizing reaction conditions is quite low, such that the actual molecular weights fell outside the calibration range of the employed GPC. A low molecular weight (≤3 kDa) was estimated from NMR end-group analysis.

Polymer 2-42b: Conducted exactly as for polymer **2-22** from **2-21a** above. Polymer **2-42b** was obtained as a deep purple solid (110mg, 100%). The molecular weight of **2-42b** without optimizing reaction conditions is quite low, such that its actual molecular weight fell outside the calibration range of the employed GPC. Low molecular weight (≤ 3 kDa) estimated from NMR end-group analysis.

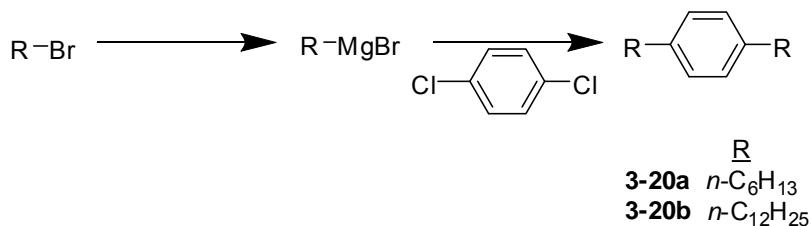


Compound 2-43a: Prepared similarly to **2-36a**, starting from **2-35a** (1.00g, 3.96mmol), 1,4-dibromo-2,3,5,6-tetrafluorobenzene (0.488g, 1.58mmol), *n*-BuLi (1.58mL, 3.96mmol, 2.5M), DIPA (0.611mL, 4.36mmol), ZnCl₂ (0.648g, 4.75mmol), THF (25mL), Pd(PPh₃)₄ [freshly prepared from Pd₂(dba)₃ (91mg, 0.10mmol) and PPh₃ (208mg, 0.79mmol)]. Yield (0.506g, 49%). ¹H NMR (CDCl₃, 400MHz) δ : 7.50 (s, 2H), 7.15 (d, 2H), 2.67 (t, 4H), 1.68 (m, 4H), 1.38-1.27 (m and broad, 36H), 0.89 (t, 6H). ¹⁹F NMR (CDCl₃, 376MHz) δ : -141.59 (s, 4F). GC-MS: m/z : 650 (C₃₈H₅₄F₄S₂⁺), 341 (100%).

Compound 2-43b: Prepared similarly to **2-36a**, starting from **2-35b** (1.46g, 6.50mmol), 1,4-dibromo-2,3,5,6-tetrafluorobenzene (0.80g, 2.60mmol), *n*-BuLi (2.60mL, 6.50mmol, 2.5M), DIPA (1.00mL, 7.15mmol), ZnCl₂ (1.06g, 7.80mmol), THF (25mL), Pd(PPh₃)₄ [freshly prepared from Pd₂(dba)₃ (148mg, 0.163mmol) and PPh₃ (341mg, 1.30mmol)]. Yield (0.815g, 53%). ¹H NMR (CDCl₃, 400MHz) δ : 7.50 (s, 2H), 7.15 (d, 2H), 2.68 (m, 4H), 1.70 (m, 2H), 1.50 (m, 6H), 1.36-1.13 (m and broad, 12H), 0.95 (d, 12H), 0.88 (d, 6H). ¹⁹F NMR (CDCl₃, 376MHz) δ : -141.58 (s, 4F). GC-MS: m/z : 594 (C₃₄H₄₆F₄S₂⁺), 342 (100%).

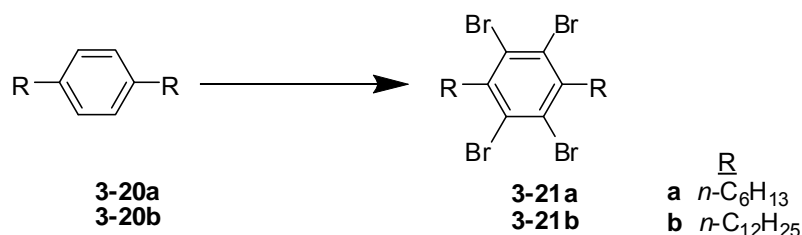
Polymer 2-44a: Prepared similarly to polymer **2-37a**, starting from compound **2-43a** (100mg, 0.154mmol), FeCl₃ (100mg, 4eq), and CHCl₃ (20mL). Isolated as a dark brown solid (68mg, 67%). ¹H NMR (400 MHz, C₂D₂Cl₄, 75°C) δ: 7.63 (s, 2H), 2.70 (m, 4H), 1.69-1.30 (m, 40H), 0.92 (t, 6H). ¹⁹F NMR (376MHz, C₂D₂Cl₄, 75°C) δ: -140.80 (m, 4F), -140.95 (s, 42F), -141.55 (m, 4F). M_n (GPC) = 14kDa (PDI = 2.55).

Polymer 2-44b: Prepared similarly to polymer **2-37a**, starting from compound **2-43b** (100mg, 0.168mmol), FeCl₃ (109mg, 4eq), and CHCl₃ (20mL). Isolated as an orange-red solid (49mg, 49%). ¹H NMR (400 MHz, C₂D₂Cl₄, 75°C) δ: 7.64 (s, 2H), 2.68 (m, 4H), 1.70 (m, 2H), 1.50 (m, 6H), 1.36-1.13 (m and broad, 12H), 0.95 (d, 12H), 0.88 (d, 6H).. ¹⁹F NMR (376MHz, C₂D₂Cl₄, 75°C) δ: -140.80 (m, 4F), -140.98 (s, 77F), -141.55 (m, 4F). M_n (GPC) = 22kDa (PDI = 2.78).



1,4-dihexylbenzene (3-20a): In an oven-dried Schlenk flask, freshly ground magnesium turnings (3.20g, 0.132mol), 80mL dry ether and a single iodine crystal were combined. 1-bromohexane (19.76g, 0.120mol) was added drop-wise to the flask after which reflux was maintained for 1 hr. In a separate oven-dried three-neck round bottom flask equipped with a condenser and addition funnel, 1,4-dichlorobenzene (8.00g, 0.054mol), NiCl₂[dppp] (0.147g, 0.5 mol %) and 30mL dry ether were combined and sparged with argon. The hexyl Grignard reagent was transferred into the addition funnel and added drop-wise into the three-neck flask, after which the whole was refluxed for 12 hr. The mixture was treated with 10% HCl (aq), 10% KOH (aq), dried over anhydrous MgSO₄, and concentrated via rotary evaporation. Compound **3-20a** was isolated via column chromatography (silica gel, pentane) as a colorless oil (8.77g, 65%). ¹H NMR (400MHz, CDCl₃) δ: 7.17 (s, 4H), 2.65 (t, 4H), 1.68 (m, 4H), 1.40 (m, 12H), 0.97 (t, 6H). ¹³C NMR (100MHz, CDCl₃) δ: 140.04, 128.20, 35.58, 31.77, 31.58, 29.08, 22.63, 14.09.

1,4-didodecylbenzene (3-20b): Prepared and isolated as described above for **3-20a** from 1,4-dichlorobenzene (35.00g, 0.238mol), 1-bromododecane (171.2mL, 0.714mol), magnesium (18.23g, 0.714mol), yield (94.50g, 95.7%). ¹H NMR (400MHz, CDCl₃) δ: 7.13 (s, 4H), 2.61(t, 4H), 1.64 (m, 4H), 1.31 (m, 36H), 0.93 (t, 6H). ¹³C NMR (400MHz, CDCl₃) δ: 140.05, 128.21, 35.59, 31.95, 31.61, 29.70, 29.63, 29.57, 29.41, 29.38, 22.71, 14.12.

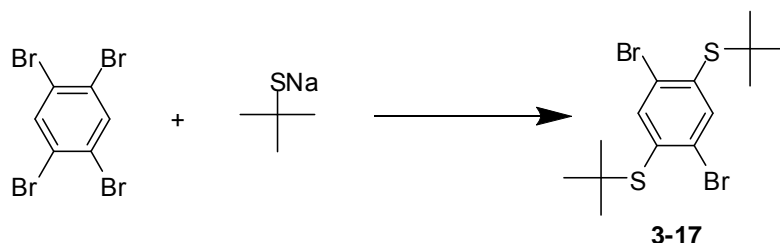


Compound 3-21a: Bromine (17.72mL, 0.345mol) and a catalytic amount of iodine were combined in a 3-neck round bottom flask, fitted with thermometer and gas bubbler, and cooled in an ice bath. Compound **3-20a** (8.50g, 0.0345mol) was added drop-wise, with protection from light. After stirring for 20 hr, the reaction mixture was diluted with ether and treated with 20% KOH (aq). The organic layer was concentrated via rotary evaporation and the residue was recrystallized from boiling ethanol to yield **3-21a** as colorless needles (14.12g, 76%). ¹H NMR (400MHz, CDCl₃) δ: 3.18 (t, 4H), 1.46 (m, 16H), 0.92 (t, 6H). ¹³C NMR (100MHz, CDCl₃) δ: 143.16, 127.49, 41.86, 31.40, 29.34, 27.57, 22.60, 14.07. MP: 94°C.

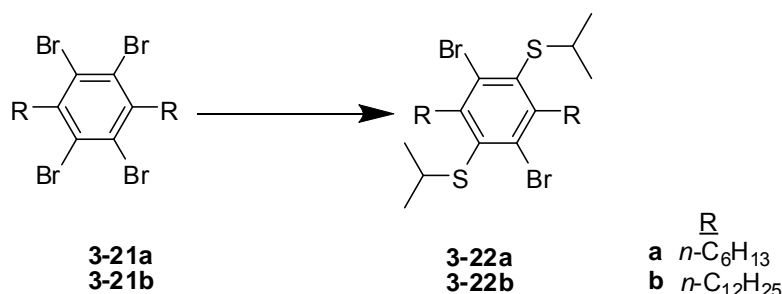
Compound 3-21b: Prepared and isolated as described above for **3-21a**. Title compound was isolated as colorless crystals (80%). ¹H NMR (400MHz, CDCl₃) δ: 3.17 (m, 4H), 1.55 (m, 4H), 1.44 (m, 4H), 1.32 (m, 32H), 0.90 (t, 6H). ¹³C NMR (400MHz, CDCl₃) δ: 143.16, 127.50, 41.87, 31.93, 29.70, 29.66, 29.57, 29.37, 27.60, 22.71, 14.14.

Compound 3-13: Isolated as a byproduct during preparation, for other purposes, of 1,2,4,5-tetrakis(tert-butylthio)benzene from 1,2,4,5-tetrafluorobenzene. ¹H NMR (400MHz, CDCl₃) δ: 7.30 (t, 2H), 1.34 (s, 18H). ¹⁹F NMR (376MHz, CDCl₃) δ: -111.03

(t, 2F). ^{13}C NMR (100MHz, CDCl_3) δ : 159.12 (d), 125.67 (m), 122.93 (m), 48.19, 30.98. GC-MS: m/z : 290($\text{C}_{14}\text{H}_{20}\text{F}_2\text{S}_2^+$), 178(100%). MP: 101°C.



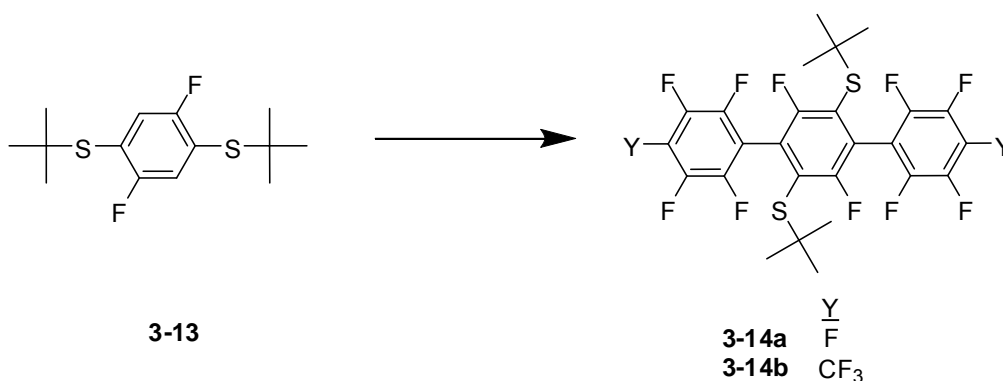
Compound 3-17: In an oven-dried Schlenk flask, sodium 2-methyl-2-propanethiolate (3.12g, 2.1eq) was added to a solution of 1,2,4,5-tetrabromobenzene (5.00g, 12.3mmol) in DMF (35mL) and the solution was stirred at 50°C for 5 hours. The contents of the vessel were diluted with ether, treated with 20% KOH, and dried over anhydrous magnesium sulfate. After concentration via rotary evaporation, the yellow residue was sonicated with MeOH to obtain a colorless solid (3.78g, 74%). ^1H NMR (400MHz, CDCl_3) δ : 7.95 (s, 2H), 1.39 (s, 18H). ^{13}C NMR (100MHz, CDCl_3) δ : 141.89, 136.73, 130.00, 49.43, 31.04. GC-MS: m/z : 412 ($\text{C}_{14}\text{H}_{20}\text{Br}_2\text{S}_2^+$), 300(100%).



Compound 3-22a: 2-propanethiol (2.98mL, 0.032mol) was added drop-wise into an oven-dried Schlenk flask containing sodium hydride (0.897g, 0.022mol) and anhydrous DMF (30mL). After stirring for 30min, compound **3-21a** (6.00g, 0.0107mol) was added and the whole was sparged with argon and then stirred at 50°C overnight. The whole was diluted with pentane, treated with 10% KOH, and dried over anhydrous magnesium sulfate, and concentrated via rotary evaporation to yield compound **3-22a** as a pale yellow solid (5.91g, 100%). ^1H NMR (400MHz, CDCl_3) δ : 3.52 (m, 2H), 3.29 (t, 4H),

1.43 (m, 16H), 1.25 (d, 12H), 0.91 (t, 6H). ^{13}C NMR (100MHz, CDCl_3) δ : 147.82, 137.89, 135.01, 40.76, 39.84, 31.80, 29.85, 29.82, 23.28, 22.93, 14.41. MP: 73°C.

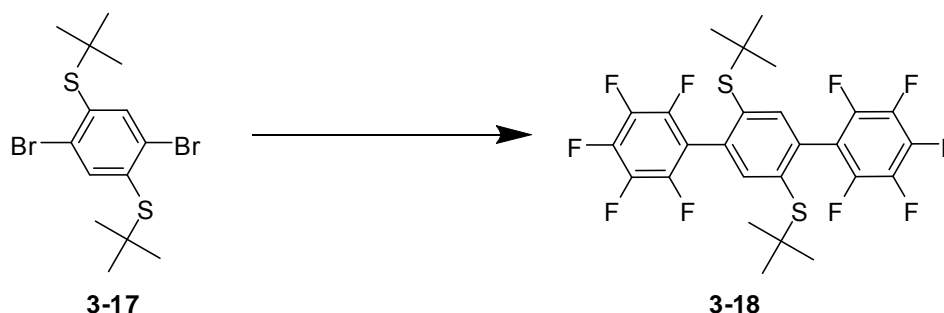
Compound 3-22b: Prepared and isolated as described above for compound **3-22a** from compound **3-21b** (2.00g, 2.738mmol), sodium hydride (0.23g, 5.75mmol), 2-propylthiol (0.625g, 8.21mmol). Yield (1.88g, 95.2%). ^1H NMR (400MHz, CDCl_3) δ : 3.52 (m, 2H), 3.29 (t, 4H), 1.52- 1.24 (broad, 52H), 0.89 (t, 6H). ^{13}C NMR (100MHz, CDCl_3) δ : 147.51, 137.58, 134.71, 40.45, 39.52, 31.93, 29.82, 29.68, 29.66, 29.58, 29.55, 29.36, 29.29, 22.97, 22.70, 14.12.



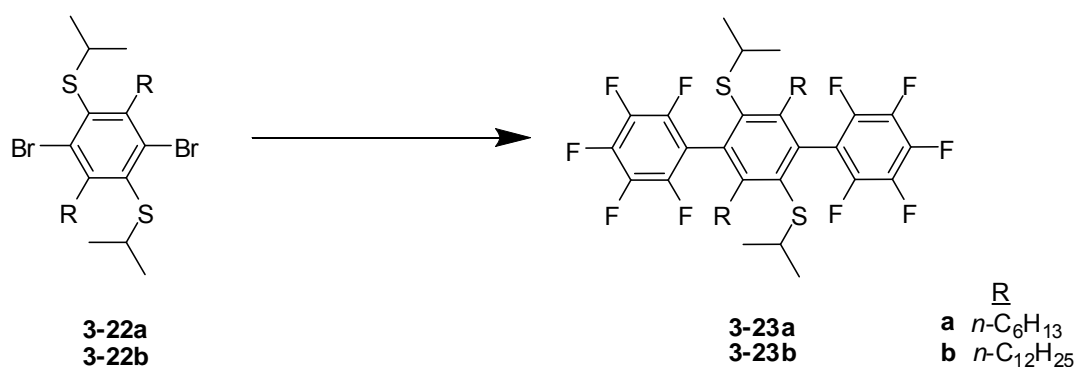
Compound 3-14a: A solution of LDA [3eq, freshly prepared from *n*-BuLi (8.26mL, 2.5 M hexanes) and diisopropylamine (3.19mL) in 10mL THF] was added drop-wise to a solution of **3-13** (2.00g, 6.886mmol) in 50mL anhydrous THF which was cooled in an acetone/ CO_2 bath. After stirring for 6 hours, excess anhydrous C_6F_6 (15.91mL, 20eq.) was added in one portion at -78°C. The reaction mixture was allowed to warm to room temperature overnight, then concentrated via rotary evaporation. The residue was diluted with ether, treated with 10% HCl, dried over anhydrous magnesium sulfate and concentrated via rotary evaporation. Compound **3-14a** was obtained as an off-white solid after sonication of the residue with MeOH (3.10g, 72%). ^1H NMR (400MHz, CDCl_3) δ : 1.19 (s, 18H). ^{19}F NMR (376MHz, CDCl_3) δ : -98.41 (s, 2F), -137.26 (m, 4F), -152.44 (m, 2F), 162.20 (m, 4F). GC-MS: m/z : 622 ($\text{C}_{26}\text{H}_{18}\text{F}_{12}\text{S}_2^+$), 57 (100%). MP: 236°C.

Compound 3-14b: Prepared and isolated as described for **3-14a**, but from **3-13** (2.00g, 6.886mmol), anhydrous THF (50mL), LDA (3eq.), anhydrous C_7F_8 (5.85mL, 6eq.).

Isolated as a colorless solid (4.3g, 86%). ^1H NMR (400MHz, CDCl_3) δ : 1.21 (s, 18H). ^{19}F NMR (376MHz, CDCl_3) δ : -56.71 (t, 6F), -98.26 (s, 2F), -135.36 (m, 4F), -140.55 (m, 4F). GC-MS: m/z : 722 ($\text{C}_{28}\text{H}_{18}\text{F}_{16}\text{S}_2^+$), 57 (100%). MP: 240°C.



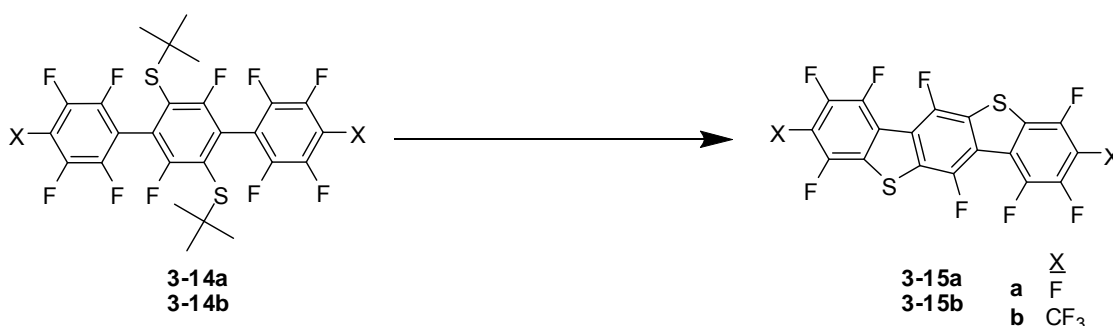
Compound 3-18: *n*-BuLi (1.0mL of a 2.1M solution in hexanes, 2.54mmol) was slowly added via syringe to compound **3-17** (0.50g, 1.21mmol) in 10mL dry ether at 0°C. After allowing the suspension to slowly warm to room temperature over 1 hr, C_6F_6 (2.80mL, 20eq) was added in one portion at 0°C and the vessel was sealed. After stirring overnight, the mixture was treated with 10% HCl, dried over anhydrous magnesium sulfate, and concentrated via rotary evaporation. The residue was sonicated with methanol to yield a colorless solid (0.29g, 41%). ^1H NMR (400MHz, CDCl_3) δ : 7.72 (s, 2H), 1.21 (s, 18H). ^{19}F NMR (376MHz, CDCl_3) δ : -139.3 (m, 4F), -154.39 (t, 2F), -162.61 (m, 4F). GC-MS: m/z : 586 ($\text{C}_{26}\text{H}_{20}\text{F}_{10}\text{S}_2^+$), 474 (100%). MP: 227°C.



Compound 3-23a: *t*-BuLi (12.78mL, 1.65M hexanes, 21.72mmol) was slowly added via syringe to compound **3-22a** (3.00g, 5.43mmol) in 100mL dry ether, while maintaining the temperature below -78°C. After allowing the solution to slowly warm to room temperature over 1 hr, C_6F_6 (12.55mL, 20eq) and 15mL DME were added in rapid

succession and the vessel was sealed. After stirring overnight, the mixture was treated with 10% HCl then 10% KOH, dried over anhydrous magnesium sulfate and concentrated via rotary evaporation. Compound **3-23a** was isolated via column chromatography (silica gel, pentane) as a colorless oil (2.00g, 51%). ^{19}F NMR (376MHz, CDCl_3) δ : -138.85 (d, 4F), -155.38 (t, 2F), -162.75 (m, 4F).

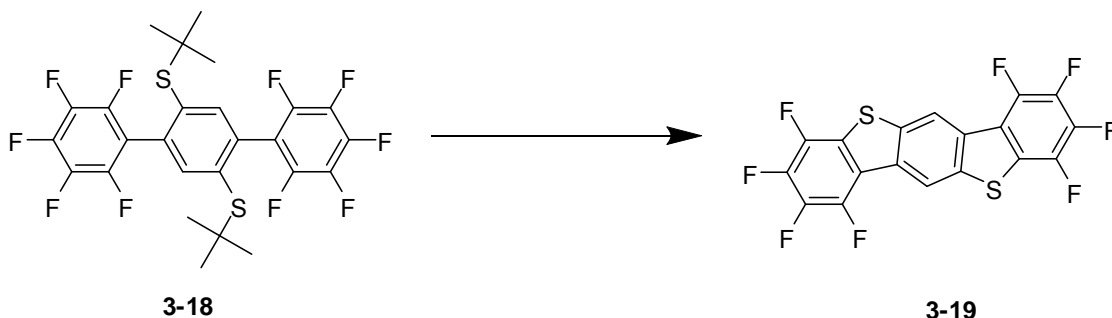
Compound 3-23b: Prepared and isolated as described above for **3-23a**. Yield: 56%. ^{19}F NMR (376MHz, CDCl_3) δ : -138.87 (d, 4F), -155.26 (t, 2F), -162.65 (m, 4F).



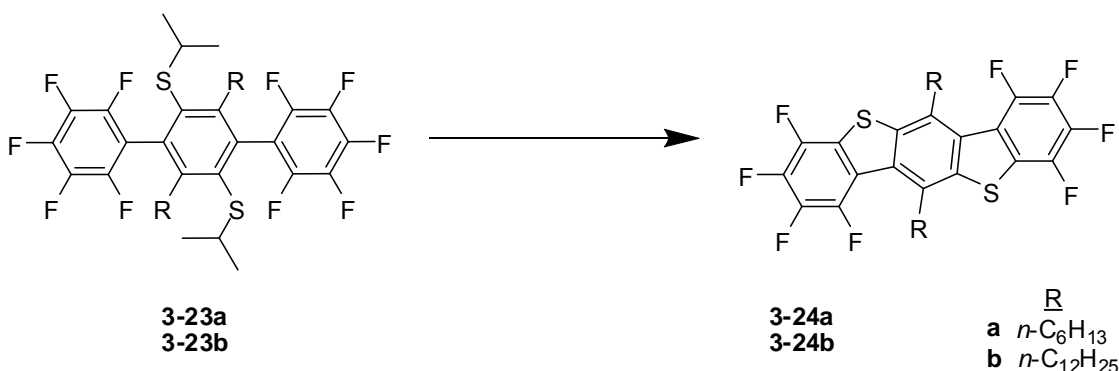
Compound 3-15a: Compound **3-14a** (0.20g, 0.32mmol) was dissolved in 5mL anhydrous toluene at 110°C. After cooling to room temperature, $\text{HBF}_4 \cdot \text{ether}$ (0.176mL, 4eq.) was added to the solution. The tube was placed in oil bath at 110°C for 12 hours. A large excess of freshly ground KOH and a spatula tip of 18-crown-6 were added to the brown solution and the whole was stirred at 110°C for 12 hours. The vessel contents were concentrated under reduced pressure and the residue was stirred with 10% HCl and aqueous layer was discarded. The obtained solid was sonicated three times with fresh methanol. Compound **3-15a** was obtained as a pale yellow solid after recrystallization from boiling toluene (86mg, 57%). ^1H NMR (400MHz, $\text{C}_2\text{D}_2\text{Cl}_4$, 130°C): no signals. ^{19}F NMR (376MHz, $\text{C}_2\text{D}_2\text{Cl}_4$, 130°C) δ : -111.17 (m, 2F), -132.41 (m, 2F), -139.90 (m, 2F), -153.81 (s, 2F), -157.38 (s, 2F). Anal. calcd. C 45.97%. Found: C 45.78%. HR-MS: 469.9273 +/- 0.0006 (1.2ppm) versus a calculated value of 469.9276, error is -0.0003 (-0.6ppm). MP: 279°C.

Compound 3-15b: Prepared as above for **3-15a** but from compound **3-14b** (0.40g, 0.55mmol), $\text{HBF}_4 \cdot \text{ether}$ (0.30mL, 4eq.), KOH (124mg, 4eq.), 18-crown-6, toluene (10mL). Compound **3-15b** was obtained as a yellow solid after Soxhlet extraction

(toluene) (292mg, 93%). ^1H NMR (400MHz, CDCl_3 , 75°C): no signals. ^{19}F NMR (376MHz, CDCl_3 , 75°C) δ : -56.82 (t, 6F), -109.14 (m, 2F), -115.73 (m, 2F), -133.36 (m, 2F), -137.97 (m, 2F). Anal. calcd. C 42.12%. Found: C 42.27%. GC-MS: m/z : 570 ($\text{C}_{20}\text{F}_{14}\text{S}_2^+$, 100%). MP: 270°C .



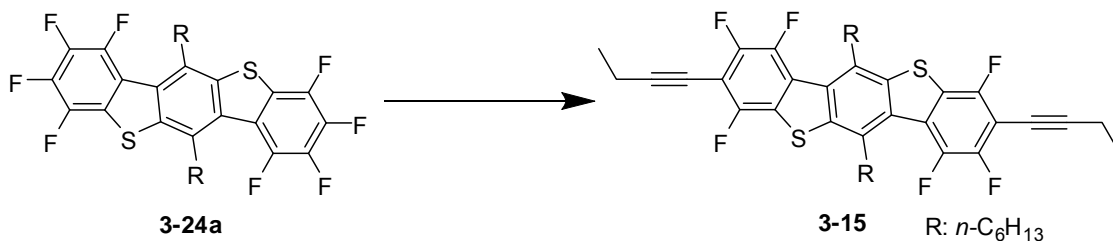
Compound 3-19: AlCl_3 (~ 0.1eq) was added to **3-18** (88mg, 0.15mmol) in 1mL dry deoxygenated toluene in an oven-dried schlenk flask. After stirring overnight, freshly ground KOH powder (33.6mg, 4eq) and 18-crown-6 (7.93mg, 0.2eq) were added in rapid succession. The whole was stirred at room temperature for 12 hours. The yellow residue obtained after concentration by rotary evaporation was stirred with 10% HCl (aq) and then sonicated with methanol. The remaining solid was passed through a short pad of silica (hexane:dichloromethane 3:1). The solvent was removed by rotary evaporation and the residue was sonicated with methanol to yield an off-white solid (20mg, 31%). ^1H NMR (400MHz, CDCl_3) δ : 8.80 (s, 2H). ^{19}F NMR (376MHz, CDCl_3) δ : -140.30 (dd, 1F), -144.36 (m, 1F), -155.85 (td, 1F), -159.30 (t, 1F). GC-MS: m/z : 434 ($\text{C}_{18}\text{H}_2\text{F}_8\text{S}_2^+$, 100%). MP: 295°C .



Compound 3-24a: AlCl_3 (~ 0.1eq) was added to **3-23a** (580mg, 0.798mmol) in 15mL dry deoxygenated toluene in an oven-dried schlenk flask. After stirring overnight, freshly

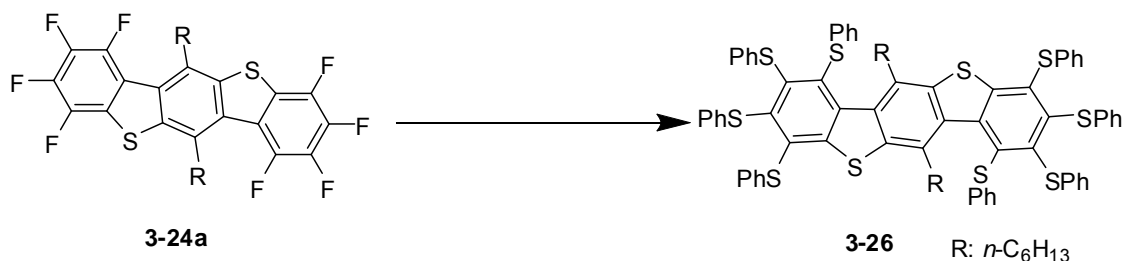
ground KOH powder (0.358g, 8eq) and 18-crown-6 (42.19mg, 0.2eq) were added in rapid succession. After stirring for 12 hours, the reaction mixture was treated with 10% HCl (aq), dilute NaHCO₃ (aq), and then concentrated by rotary evaporation. Compound **3-24a** was obtained after dissolution in hot CHCl₃ and precipitation into MeOH (300mg, 62%). ¹H NMR (400MHz, CDCl₃, 50°C) δ: 3.42 (m, 4H), 1.81 (m, 4H), 1.56 (m, 4H), 1.37 (m, 8H), 0.92 (t, 6H). ¹⁹F NMR (376MHz, CDCl₃, 50°C) δ: -131.51 (t, 1F), -140.34 (m, 1F), -156.48 (m, 1F), -159.08 (t, 1F). ¹³C NMR (100MHz, CDCl₃, 55°C) δ: 144.51 (m), 142.66 (m), 141.95 (m), 140.64, 140.26 (m), 137.71 (m), 132.41, 130.57, 124.16 (m), 120.09 (m), 36.85, 31.63, 30.13, 29.63, 22.61, 13.95. GC-MS: *m/z*: 602 (C₃₀H₂₆F₈S₂⁺, 100%). MP: 210°C.

Compound 3-24b: Prepared similarly to **3-24a**, starting from **3-23b** (60mg, 0.067mmol). Yield (40mg, 77%). ¹H NMR (400MHz, CDCl₃) δ: 3.39 (m, 4H), 1.80 (m, 4H), 1.58 (m, 4H), 1.33 (m, 32H), 0.92 (t, 6H). ¹⁹F NMR (376MHz, CDCl₃) δ: -131.44 (t, 1F), -140.36 (m, 1F), -156.50 (m, 1F), -159.05 (t, 1F). MP: 138°C.

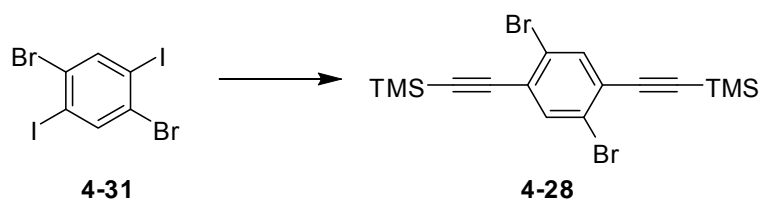


Compound 3-25: In a nitrogen-filled glove box, **3-24a** (50mg, 0.083mmol), 1mL dry DME, 3mL dry THF and butynyllithium (11mg, 2.2eq) were combined in a vacuum flask with rotary valve. After 40 hours, the reaction mixture was treated with 10% HCl (aq) then dried over anhydrous magnesium sulfate. The organic phase was concentrated by rotary evaporation and the residue passed through a column of silica gel with pentane to yield a pale yellow solid (17mg, 30.5%). The isolated yield is not representative as a significant portion of the product was accidentally spilled during isolation. ¹H NMR (400MHz, CDCl₃, 55°C) δ: 3.39 (broad, 4H), 2.60(t, 4H), 1.80 (broad, 4H), 1.58 (broad, 4H), 1.37 (m, 14H), 0.94 (t, 6H). ¹⁹F NMR (376MHz, CDCl₃, 55°C) δ: -115.17 (m, 2F), -135.29 (m, 2F), -137.02 (m, 2F). ¹³C NMR (100MHz, CDCl₃, 55°C) δ: 153.63, 151.17,

150.12 (m), 147.70 (m), 143.93 (m), 141.47 (m), 141.08, 132.47, 131.12, 124.19 (m), 123.20 (m), 105.08, 102.44 (m), 66.25, 36.56, 31.64, 30.13, 29.64, 22.60, 13.97, 13.70, 13.45. GC-MS: m/z : 670 ($C_{38}H_{36}F_6S_2^+$), 207 (100%).

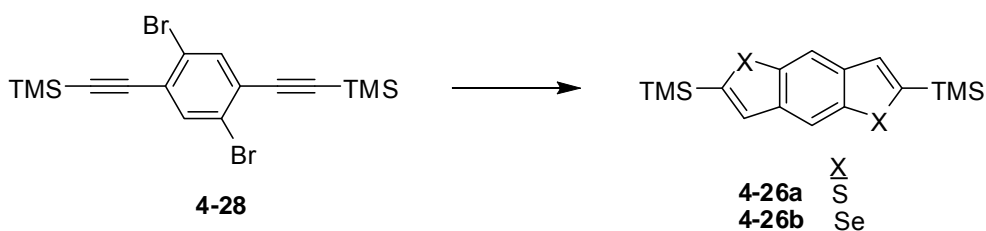


Compound 3-26: In an oven-dried Schlenk flask, benzenethiol (0.22mL, 16eq) was added drop-wise to sodium hydride (64mg, 12eq) in anhydrous DMF (2mL). After stirring for 30min, compound **3-24a** (80mg, 0.133mmol) was added and the solution was sparged with argon and stirred at 80°C overnight. The reaction mixture was treated with 10% KOH, 10% HCl, then brine, and dried over anhydrous magnesium sulfate. The organic phase was concentrated via rotary evaporation and the residue passed through a column of silica gel with toluene to yield a yellow solid (93mg, 52.8%). 1H NMR (400MHz, $CDCl_3$) δ : 7.2-6.4 (br and m, 40H), 3.14 (t, 4H), 1.26 (m, 4H), 0.98 (m, 12H), 0.66 (t, 6H). ^{13}C NMR (100MHz, $CDCl_3$) δ : 150.83, 143.44, 141.48, 139.97, 138.71, 138.58, 138.12, 137.94, 136.39, 135.83, 134.07, 131.85, 131.76, 128.96, 128.86, 128.79, 128.57, 128.30, 128.23, 127.93, 127.35, 126.46, 126.23, 125.84, 125.78, 35.36, 31.31, 28.88, 28.68, 22.43, 13.93. MS (LD): m/z : 1322 ($C_{78}H_{66}S_{10}^+$), 1073, 1263, 1251, 1213, 1104 etc. MP: 58°C.



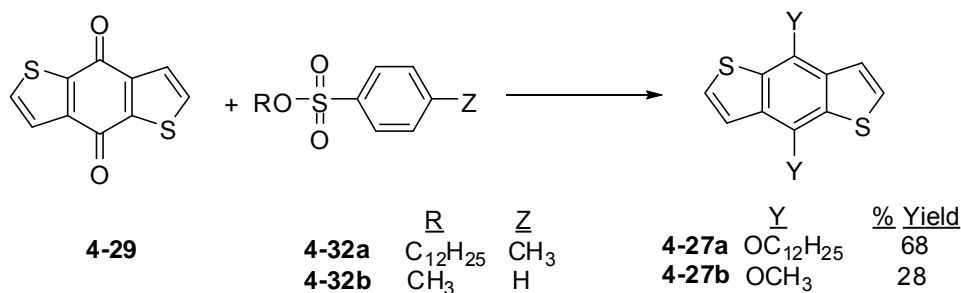
(2,5-dibromo-1,4-phenylene)bis(ethyne-2,1-diyl)bis(trimethylsilane) (4-28):¹⁹² In a nitrogen-filled glove box, 1,4-Dibromo-2,5-diiodo-benzene **4-31** (5.00g, 10.30mmol), trimethylsilylacetylene (2.84mL, 1.95eq), CuI (118mg, 0.60eq), $Pd(PPh_3)_4$ [(0.5eq, freshly prepared from $Pd_2(dba)_3$ and PPh_3 in toluene)], toluene (50mL) and diisopropylamine (30mL) were combined in a Schlenk flask containing a magnetic stir

bar. The vessel was sealed and the contents stirred at 80°C for 3 days. The reaction mixture was diluted with ether, extracted with 10% HCl (aq), dried over MgSO₄, and concentrated under reduced pressure. Compound **4-28** was isolated via column chromatography (silica gel, hexane) as a colorless solid (2.80g, 65%). ¹H NMR (400MHz, CDCl₃, r.t.) δ: 7.68 (s, 2H), 0.28 (s, 18H). ¹³C NMR (100MHz, CDCl₃, r.t.) δ: 136.40, 126.41, 123.69, 103.05, 101.34, -0.34. GC-MS: *m/z*: 428 (C₁₆H₂₀Br₂Si₂⁺), 413 (100%).



2,6-Bis(trimethylsilyl)benzo[1,2-*b*:4,5-*b'*]dithiophene (4-26a):¹⁹² *t*-BuLi (2.20mL, 4eq) was added dropwise into 15mL of hexane containing **4-28** (0.40g, 0.93mmol) under argon atmosphere at -78°C (dry ice and isopropanol). After stirring for 15 min at -78°C, warming to r.t. and stirring for 2h, sulfur powder (0.06g, 2eq) was added in one portion into the mixture. Then the mixture stirred for 15 min. After addition of 20mL ethanol, the mixture was stirred for 1h and then diluted with chloroform, extracted with 10% HCl (aq) dried over anhydrous MgSO₄, and concentrated via rotary evaporation. Compound **4-26a** was isolated via column chromatography (silica gel, hexane) as a colorless solid (2.80g, 65%). ¹H NMR (200MHz, CDCl₃, r.t.) δ: 8.25 (s, 2H), 7.44 (s, 2H), 0.37 (s, 18H). GC-MS: *m/z*: 334 (C₁₆H₂₂S₂Si₂⁺, 100%).

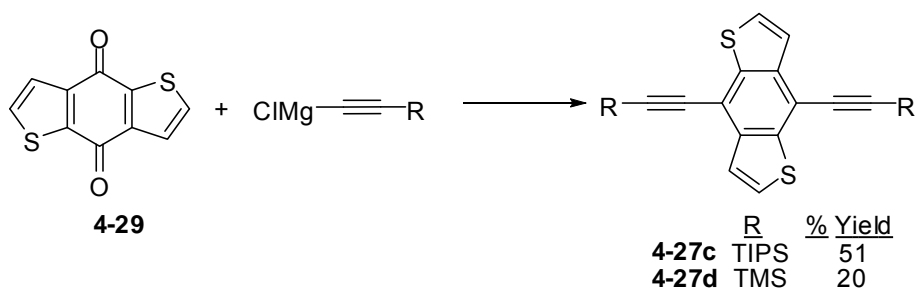
2,6-Bis-(trimethylsilyl)benzo[1,2-*b*:4,5-*b'*]diselenophene (4-26b): Prepared as above for **4-26a** but from compound **4-28** (0.50g, 1.17mmol), *t*-BuLi (2.75mL, 4eq), selenium powder (0.18g, 2eq), ether (20mL). Compound **4-26b** was isolated via column chromatography (silica gel, hexane) as a colorless solid (0.28g, 56%). ¹H NMR (400MHz, CDCl₃, r.t.) δ: 8.34 (s, 2H), 7.74 (s, 2H), 0.41 (s, 18H). ¹³C NMR (100MHz, CDCl₃, r.t.) δ: 148.04, 141.58, 140.77, 133.56, 121.48, -0.026. GC-MS: *m/z*: 670 (C₁₆H₂₂Se₂Si₂⁺, 100%)



4,8-dimethoxybenzo[1,2b:4,5-b']dithiophene(4-27b):¹⁹³

Benzo[1,2-b:4,5-b']dithiophene-4,8-dione **4-29** (1.00g, 4.54mmol) and zinc dust (0.89g, 3eq) were combined in a reaction flask with 4mL of ethanol and 5mL of 20% NaOH. After refluxing overnight, methyl benzenesulfonate **4-32b** (1.80mL, 3eq) was added. Then the reaction mixture refluxed for 3 days. The resulting precipitate was filtered and washed with Na₂S₂O₅ for three times. The resulting solid was dissolved in hot toluene and the zinc residue was filtered. The yellow solid (0.32g, 28%) was obtained via rotary evaporation. ¹H NMR (400MHz, CDCl₃) δ: 7.52 (d, 2H), 7.41 (d, 2H), 4.15 (s, 6H). ¹³C NMR (100MHz, CDCl₃) δ: 145.33, 131.26, 129.79, 126.27, 120.08, 61.01. GC-MS: *m/z*: 250 (C₁₂H₁₀O₂S₂⁺), 235(100%).

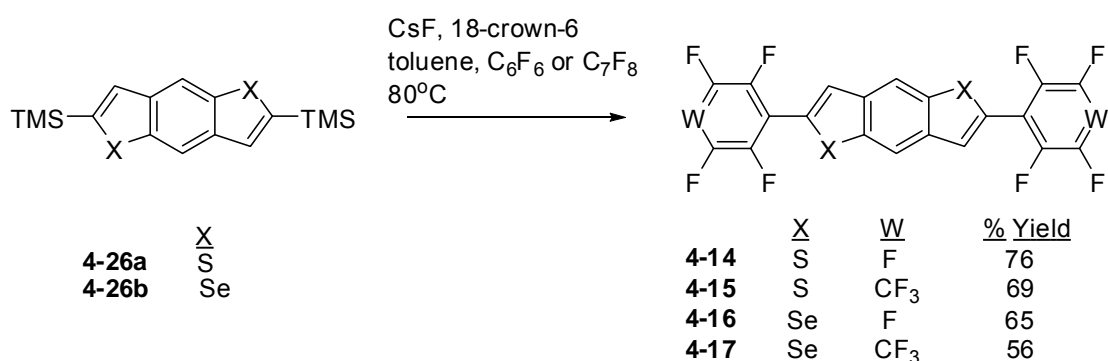
Compound 4-27a: Prepared as above for **4-27b** but from compound **4-29** (0.50g, 2.20mol), zinc dust (0.44g, 3eq), 20% NaOH (8mL), ethanol (2mL), **4-32a** (2.32g, 3eq). Compound **4-27a** was isolated via column chromatography [silica gel, petroleum ether: dichloromethane (3:1)] as a yellow solid (0.87g, 70%). ¹H NMR (400MHz, CDCl₃) δ: 7.49 (d, 2H), 7.37 (d, 2H), 4.29 (t, 4H), 1.89 (m, 4H), 1.58 (m, 4H), 1.29 (m, 32H), 0.89 (t, 6H). ¹³C NMR (100MHz, CDCl₃) δ: 144.52, 131.59, 131.59, 125.94, 120.30, 73.94, 31.93, 30.53, 29.62, 29.46, 29.36, 26.07, 22.69, 14.13. GC-MS: *m/z*: 558 (C₃₄H₅₄O₂S₂⁺), 222(100%).



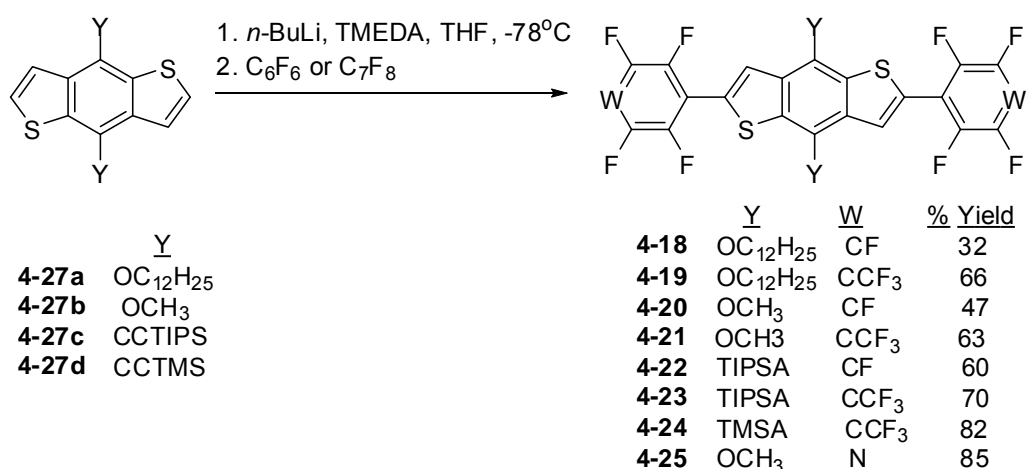
Compound 4-27c:⁶⁵ Isopropyl magnesium chloride (4.08mL, 2.0M in THF, 3eq) was added drop-wise to a solution of ethynyltriisopropylsilane (2.20mL, 7.2eq.) in 10mL THF in an oven-dried Schlenk flask at r.t.. Afterwards the solution was heated at 60°C for 3h. When the solution cooled down to r.t., compound **4-29** (0.3g, 1.36mmol) was added in one portion and the whole was stirred overnight at 60°C. After the flask was allowed to cool, a solution of 10mL 10% aqueous HCl saturated with SnCl₂ (3g) was added carefully to the flask. The flask was heated at 60°C with vigorously stirring for 9hr. The reaction mixture was diluted with chloroform, extracted with 10% HCl (aq), dried over MgSO₄, and concentrated via rotary evaporation. Compound **4-27c** was isolated via column chromatography (silica gel, pentane) as a colorless solid (0.39g, 51%). ¹H NMR (400MHz, CDCl₃) δ: 7.61 (d, 2H), 7.56 (d, 2H), 1.23 (m, 42H). ¹³C NMR (100MHz, CDCl₃) δ: 140.83, 138.48, 128.26, 123.12, 112.15, 102.59, 101.59, 18.75, 11.29. GC-MS: *m/z*: 551 (C₃₂H₄₆S₂Si₂⁺), 169 (100%).

Compound 4-27d: Prepared as above for **4-27c** but from compound **4-29** (0.40g, 1.82mmol), ethynyltrimethylsilane (2.31mL, 9eq), isopropyl magnesium chloride (5.46mL, 2.0M in THF, 3eq), THF (15mL) and a solution of SnCl₂ (3.0g) in 4mL 10% HCl. Compound **4-27d** was isolated via column chromatography [silica gel, hexane: dichloromethane (3:1)] as a yellowish green solid (0.14g, 20%). Desilylation through the column caused the low yield. ¹H NMR (400MHz, CDCl₃) δ: 7.60 (d, 2H), 7.55 (d, 2H), 0.37 (s, 18H). ¹³C NMR (100MHz, CDCl₃) δ: 140.60, 138.40, 128.19, 123.15, 111.96, 105.13, 100.62, 0.004. GC-MS: *m/z*: 382 (C₂₀H₂₂S₂Si₂⁺), 367(100%).

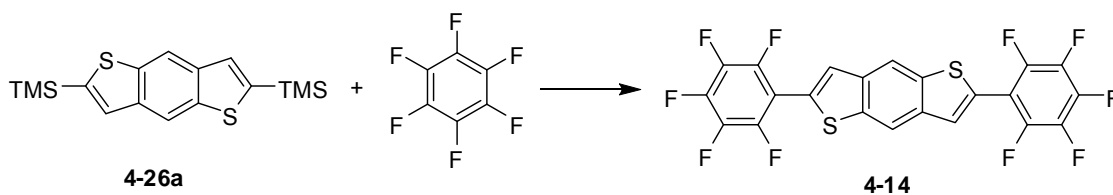
General procedures for compounds 4-14 through 4-25:



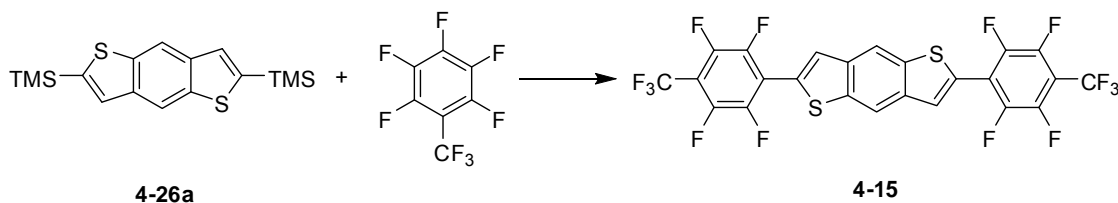
Method A: (4-14 through 4-17) In a nitrogen-filled glove box, compound **4-26a** (or **4-26b**), CsF (0.10eq), 18-crown-6 (0.20eq), perfluorotoluene (or perfluorobenzene) and toluene were combined in an oven-dried Schlenk flask containing a magnetic stir bar. The vessel was sealed and the contents stirred at 80°C for 12-24 hrs. The product mixture was added dropwise into 50mL MeOH, and the resulting solid precipitate collected after centrifugation. The solid was sonicated with 10% HCl and MeOH, then dried under reduced pressure.



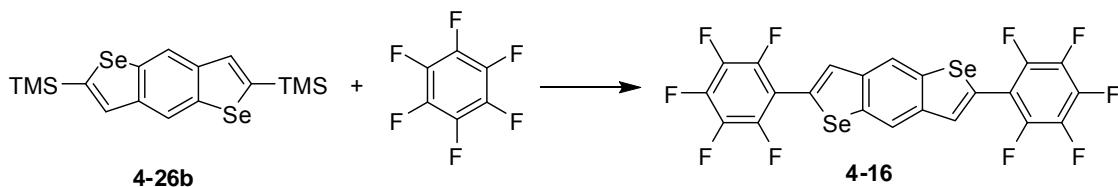
Method B: (4-18 through 4-25) *n*-BuLi (2.5M hexanes, 3eq) was added drop-wise via syringe to compound **4-27** in the solvent mixture of THF and TMEDA (3eq.) which was cooled at 0°C or -78°C. After stirring at low temperature for 30 minutes, excess C₆F₆ (or C₇F₈ or C₅F₅N) was added in one portion and the vessel was sealed. The reaction mixture was allowed to warm to room temperature overnight, then concentrated via rotary evaporation. The residue was diluted with ether (or chloroform), extracted with 10% HCl (aq), dried over magnesium sulfate, and concentrated via rotary evaporation. Compounds **4-18-4-25** isolated as solids after column chromatography (silica gel).



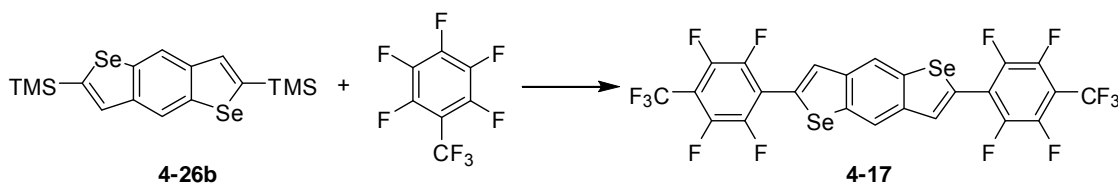
Compound 4-14 (Method A): 4-26a (50mg, 0.15mmol), CsF (0.10eq), 18-crown-6 (0.20eq), perfluorobenzene (0.34mL, 20eq) and toluene (2mL). Compound 4-14 was isolated as a light yellow solid (59mg, 76%). ¹H NMR (400MHz, C₂D₂Cl₄, 120°C) δ: 8.43 (s, 2H), 7.81 (s, 2H). ¹⁹F NMR (376MHz, C₂D₂Cl₄, 120°C) δ: -139.39 (m, 4F), -154.51 (t, 2F), -162.32 (m, 4F). GC-MS: *m/z*: 522 (C₂₂H₄F₁₀S₂⁺, 100%).



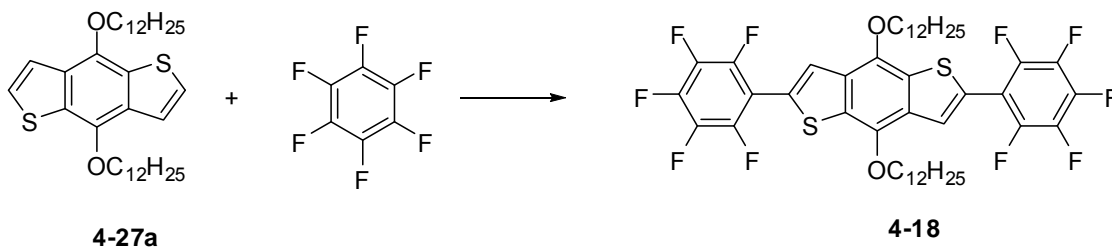
Compound 4-15 (Method A): 4-26a (50mg, 0.15mmol), CsF (0.10eq), 18-crown-6 (0.20eq), perfluorotoluene (0.064mL, 3eq) and toluene (2mL). Compound 4-15 isolated as a yellow solid (64mg, 69%). ¹H NMR (400MHz, C₂D₂Cl₄, 120°C) δ: 8.50 (s, 2H), 8.00 (s, 2H). ¹⁹F NMR (376MHz, C₂D₂Cl₄, 120°C) δ: -57.01 (t, 6F), -137.84 (m, 4F), -140.84 (m, 4F). GC-MS: *m/z*: 622 (C₂₄H₄F₁₄S₂⁺, 100%).



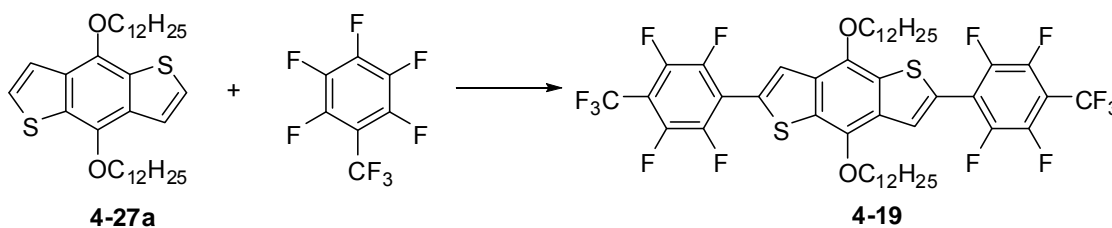
Compound 4-16 (Method A): 4-26b (50mg, 0.12mmol), CsF (0.10eq), 18-crown-6 (0.20eq), perfluorobenzene (0.27mL, 20eq) and toluene (2mL). Compound 4-16 isolated as a light yellow solid (47mg, 65%). ¹H NMR (400MHz, C₂D₂Cl₄, 120°C) δ: 8.47 (s, 2H), 8.02 (s, 2H). ¹⁹F NMR (376MHz, C₂D₂Cl₄, 120°C) δ: -139.70 (d, 4F), -154.88 (t, 2F), -162.42 (m, 4F). GC-MS: *m/z*: 616 (C₂₂H₄F₁₀Se₂⁺, 100%).



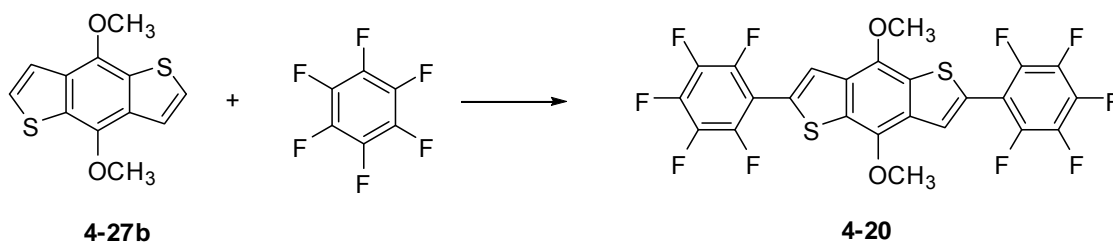
Compound 4-17 (Method A): 4-26b (50mg, 0.12mmol), CsF (0.10eq), 18-crown-6 (0.20eq), perfluorotoluene (0.050mL, 3eq) and toluene (2mL). Compound 4-17 isolated as a yellow solid (47mg, 56%). ¹H NMR (400MHz, C₂D₂Cl₄, 120°C) δ: 8.54 (s, 2H), 8.21 (s, 2H). ¹⁹F NMR (376MHz, C₂D₂Cl₄, 120°C) δ: -56.98 (t, 6F), -138.31 (m, 4F), -140.97 (m, 4F). GC-MS: *m/z*: 718 (C₂₄H₄F₁₄Se₂⁺, 100%).



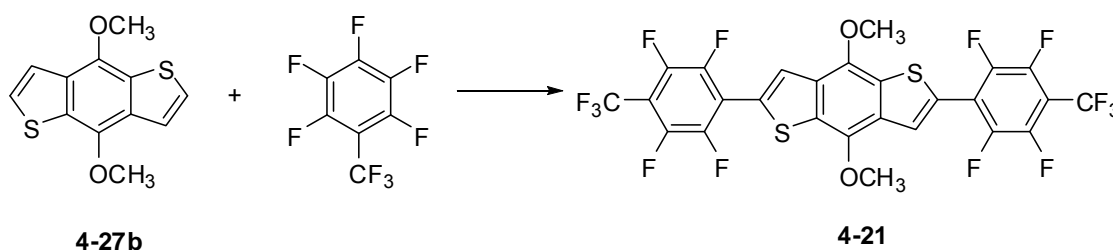
Compound 4-18 (Method B): 4-27a (0.127g, 0.23mmol), THF (5mL), *n*-BuLi (0.27mL, 2.5M hexanes, 3eq), TMEDA (0.103mL, 3eq.), C₆F₆ (0.53mL, 20eq). Compound 4-18 was isolated as a yellow-green solid via column chromatography [silica gel, hexane : dichloromethane (3:1)] as a yellow solid (0.065g, 32%). ¹H NMR (400MHz, CDCl₃) δ: 7.89 (s, 2H), 4.34 (t, 4H), 1.91 (m, 4H), 1.59 (m, 4H), 1.34 (m, 32H), 0.88 (t, 6H). ¹⁹F NMR (376MHz, CDCl₃) δ: -139.19 (m, 4F), -154.17 (t, 2F), -161.94 (m, 4F). MALDI-TOF MS (neat): *m/z*: 890 (M⁺, 100%). Calculated for C₄₆H₅₂F₁₀O₂S₂: 891.02.



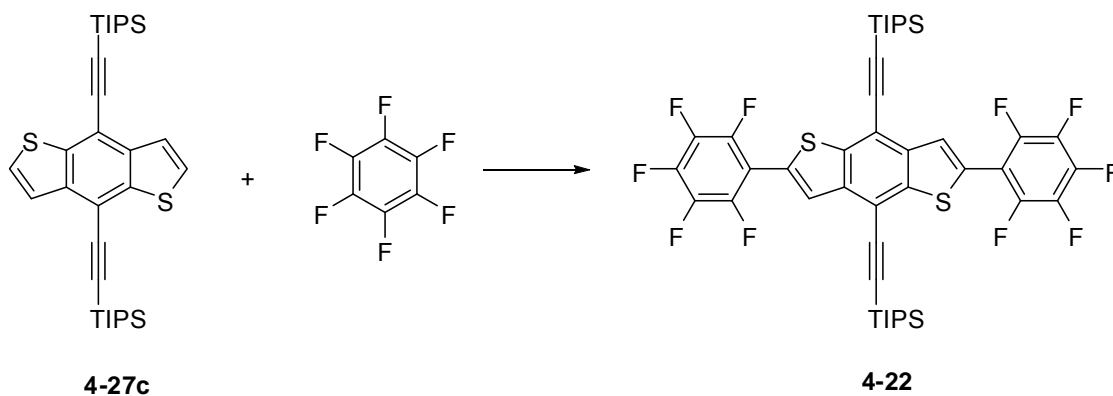
Compound 4-19 (Method B): 4-27a (0.123g, 0.22mmol), THF (5mL), *n*-BuLi (0.26mL, 2.5M hexanes, 3eq), TMEDA (0.10mL, 3eq.), C₇F₈ (0.094mL, 3eq). Compound 4-19 was isolated via column chromatography [silica gel, hexane : dichloromethane (3:1)] as an orange solid (0.143g, 66%). ¹H NMR (400MHz, CDCl₃) δ: 8.09 (s, 2H), 4.36 (t, 4H), 1.92 (m, 4H), 1.59 (m, 4H), 1.34 (m, 32H), 0.88 (t, 6H). ¹⁹F NMR (376MHz, CDCl₃) δ: -56.70 (t, 6F), -137.61 (m, 4F), -140.68 (m, 4F). MS (LD): *m/z*: 990 (M⁺, 100%). Calculated for C₄₈H₅₂F₁₄O₂S₂: 991.03.



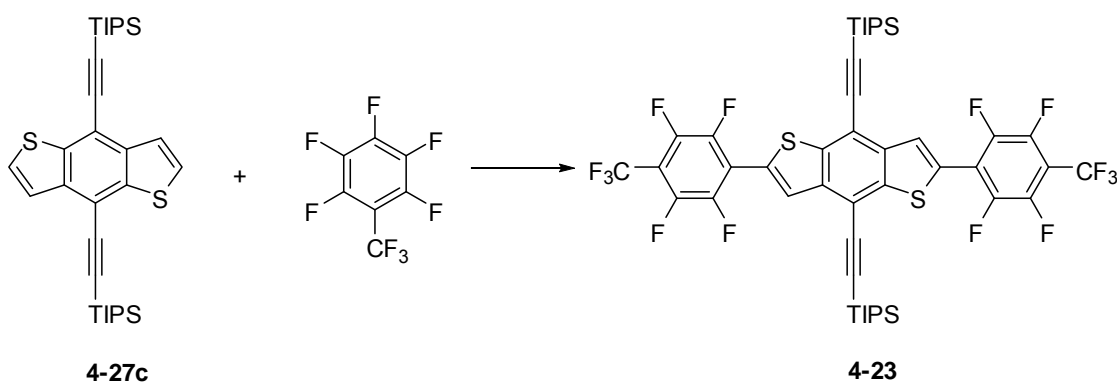
Compound 4-20 (Method B): **4-27b** (50mg, 0.20mmol), THF (2mL), *n*-BuLi (0.24mL, 2.5M hexanes, 3eq), TMEDA (0.09mL, 3eq.), C₆F₆ (0.92mL, 40eq). Compound **4-20** was isolated via column chromatography [silica gel, hexane : dichloromethane (1:1)] as a yellow solid (0.055g, 47%). ¹H NMR (400Hz, CDCl₃) δ: 7.92 (s, 2H), 4.20 (s, 6H). ¹⁹F NMR (376MHz, CDCl₃) δ: -139.25 (m, 4F), -153.98 (t, 2F), -161.86 (m, 4F). GC-MS: *m/z*: 582 (C₂₄H₈F₁₀O₂S₂⁺), 567 (100%).



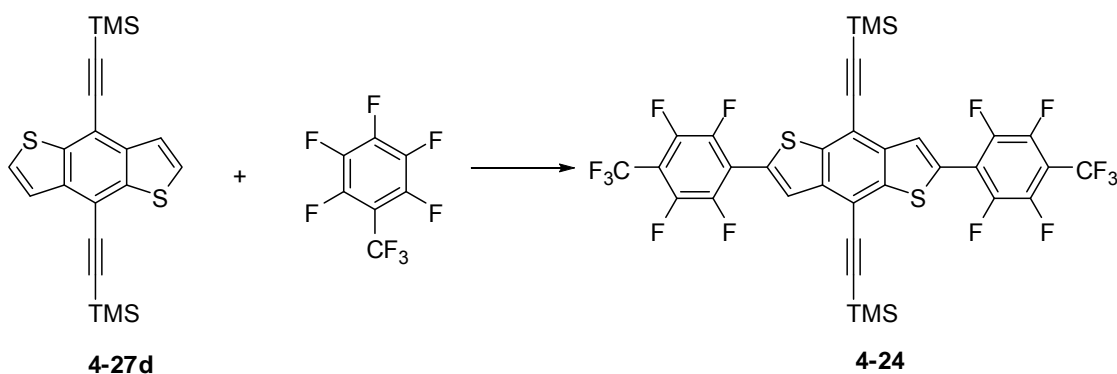
Compound 4-21 (Method B): **4-27b** (50mg, 0.20mmol), THF (2mL), *n*-BuLi (0.24mL, 2.5M hexanes, 3eq), TMEDA (0.09mL, 3eq.), C₇F₈ (0.11mL, 4eq). Compound **4-21** was isolated as a light orange solid (86mg, 63%). ¹H NMR (400MHz, CDCl₃) δ: 8.12 (s, 2H), 4.23 (s, 6H). ¹⁹F NMR (376MHz, CDCl₃) δ: -56.71 (t, 6F), -137.57 (m, 4F), -140.64 (m, 4F). GC-MS: *m/z*: 682 (C₂₆H₈F₁₄O₂S₂⁺), 667 (100%).



Compound 4-22 (Method B): 4-27c (80mg, 0.15mmol), THF (2mL), *n*-BuLi (0.17mL, 2.5M hexanes, 3eq), TMEDA (0.066mL, 3eq.), C₆F₆ (0.67mL, 40eq). Compound 4-22 was isolated via column chromatography (silica gel, hexane) and recrystallization from hexane as a yellow solid (51mg, 40%). ¹H NMR (400MHz, CDCl₃) δ: 8.03 (s, 2H), 1.24 (m, 42H). ¹⁹F NMR (376MHz, CDCl₃) δ: -138.97 (m, 4F), -53.82 (t, 2F), -161.75 (m, 4F). MALDI-TOF MS (DHB): *m/z*: 882 (M⁺), 846 (100%). Calculated for C₄₄H₄₄F₁₀S₂Si₂: 883.

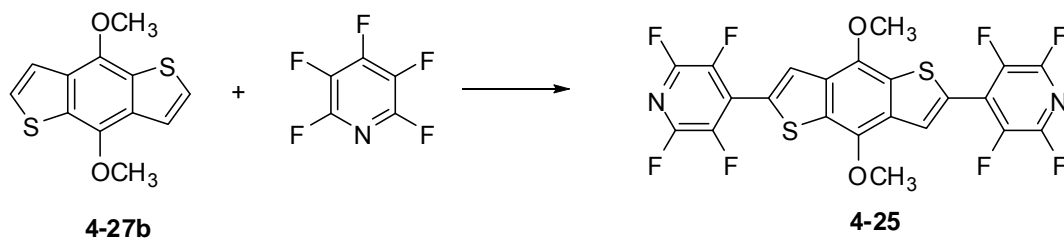


Compound 4-23 (Method B): 4-27c (50mg, 0.09mmol), THF (2mL), *n*-BuLi (0.11mL, 2.5M hexanes, 3eq), TMEDA (0.041mL, 3eq.), C₇F₈ (0.077mL, 6eq). Compound 4-23 was isolated via column chromatography (silica gel, hexane) as a yellow solid (61mg, 70%). ¹H NMR (400MHz, CDCl₃) δ: 8.22 (s, 2H), 1.24 (m, 42H). ¹⁹F NMR (376MHz, CDCl₃) δ: -56.72 (t, 6F), -137.43 (m, 4F), -140.54 (m, 4F). MALDI-TOF MS (DHB): *m/z*: 982 (M⁺, 100%), 963, 946. Calculated for C₄₆H₄₄F₁₄S₂Si₂: 983.12.



Compound 4-24 (Method B): 4-27d (50mg, 0.13mmol), THF (2mL), *n*-BuLi (0.16mL, 2.5M hexanes, 3eq), TMEDA (0.059mL, 3eq.), C₇F₈ (0.11mL, 6eq). Compound 4-24 was

isolated by dropping solution into methanol as a yellow solid (87mg, 82%). ^1H NMR (400MHz, $\text{C}_2\text{D}_2\text{Cl}_4$, 120°C) δ : 8.19 (s, 2H), 0.47 (s, 18H). ^{19}F NMR (376MHz, $\text{C}_2\text{D}_2\text{Cl}_4$, 120°C) δ : -57.02 (t, 6F), -137.58 (m, 4F), -140.70 (m, 4F). LD-MS (neat): m/z : 814 (M^+ , 100%). Calculated for $\text{C}_{34}\text{H}_{20}\text{F}_{14}\text{S}_2\text{Si}_2$: 814.8.



Compound 4-25 (Method B): 4-27b (50mg, 0.20mmol), THF (2mL), *n*-BuLi (0.24mL, 2.5M hexanes, 3eq), TMEDA (0.09mL, 3eq.), $\text{C}_5\text{F}_5\text{N}$ (0.44mL, 20eq). Compound 4-25 was isolated by dropping solution into methanol as a dark orange solid (93mg, 85%). ^1H NMR (400MHz, $\text{C}_2\text{D}_2\text{Cl}_4$, 100°C) δ : 8.28 (s, 2H), 4.31 (s, 6H). ^{19}F NMR (376MHz, $\text{C}_2\text{D}_2\text{Cl}_4$, 100°C) δ : -90.81 (m, 4F), -141.25 (m, 4F). GC-MS: m/z : 548($\text{C}_{22}\text{H}_8\text{F}_8\text{N}_2\text{O}_2\text{S}_2^+$), 533(100%).

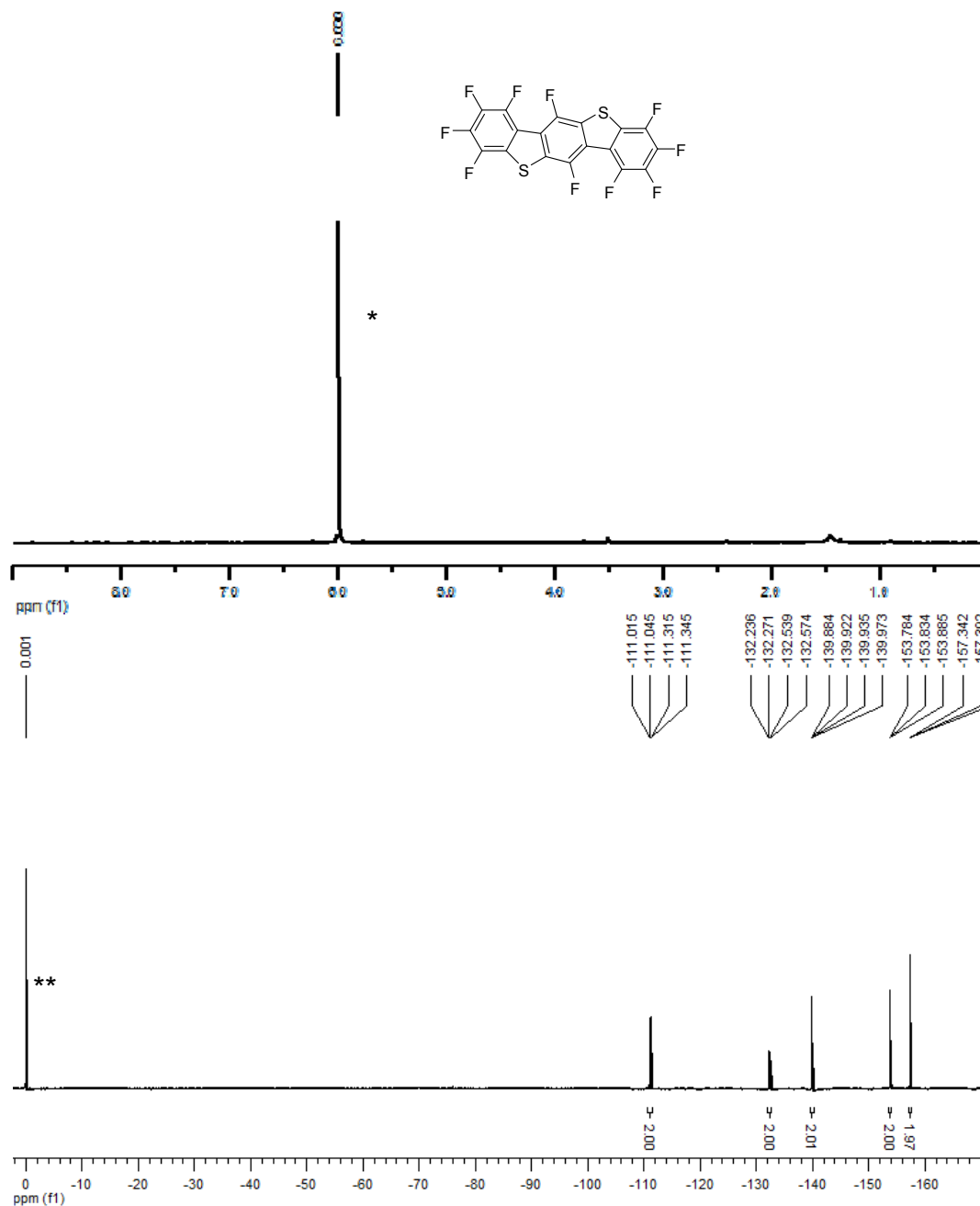


Figure 6. 1 ¹H (top) and ¹⁹F (bottom) NMR (130°C, C₂D₂Cl₄) spectra of compound 3-15a. (*solvent, **CCl₃F)

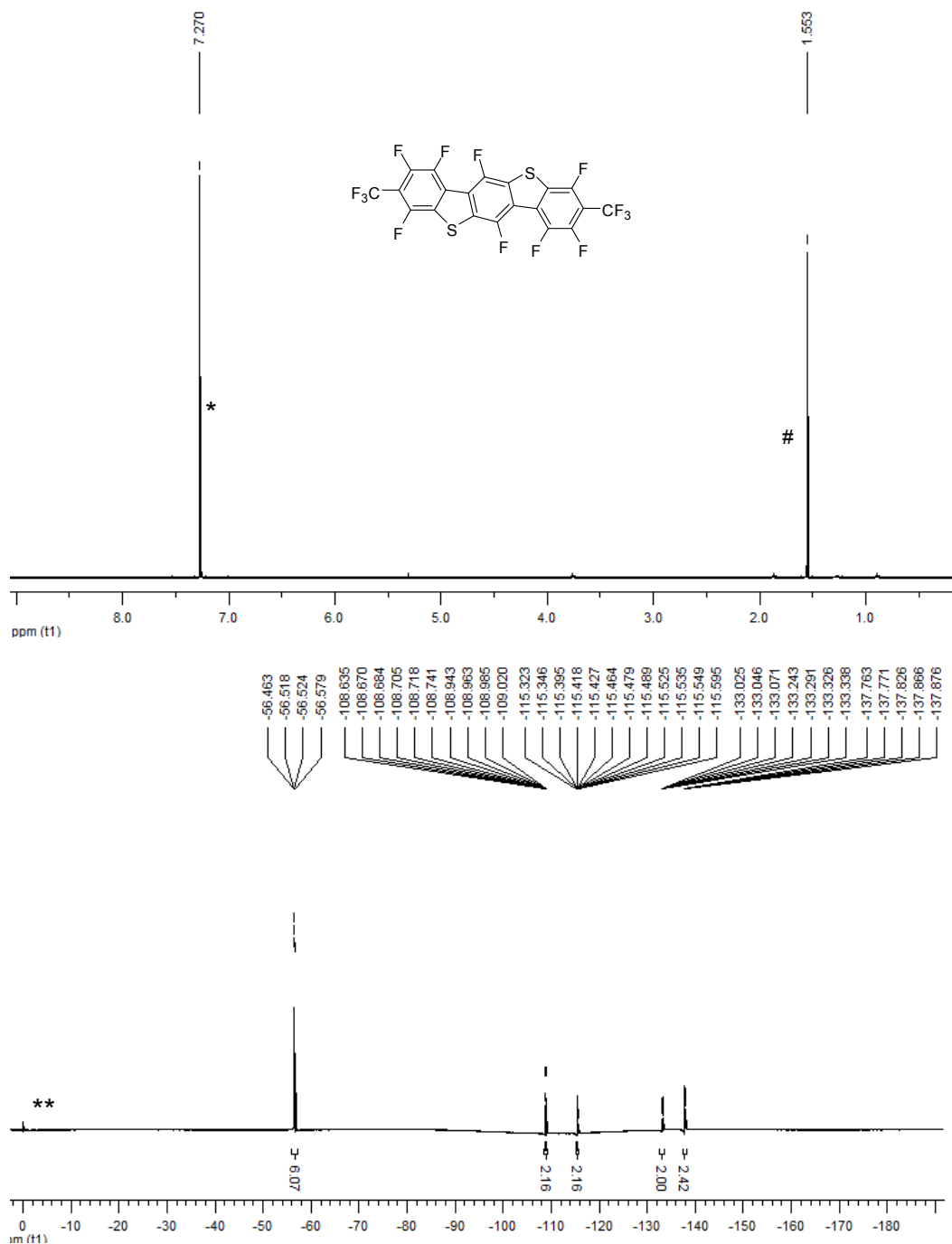


Figure 6.2 ¹H (top) and ¹⁹F (bottom) NMR (75°C, CDCl₃) spectra of compound 3-15b. (*solvent, **CCl₃F, #H₂O)

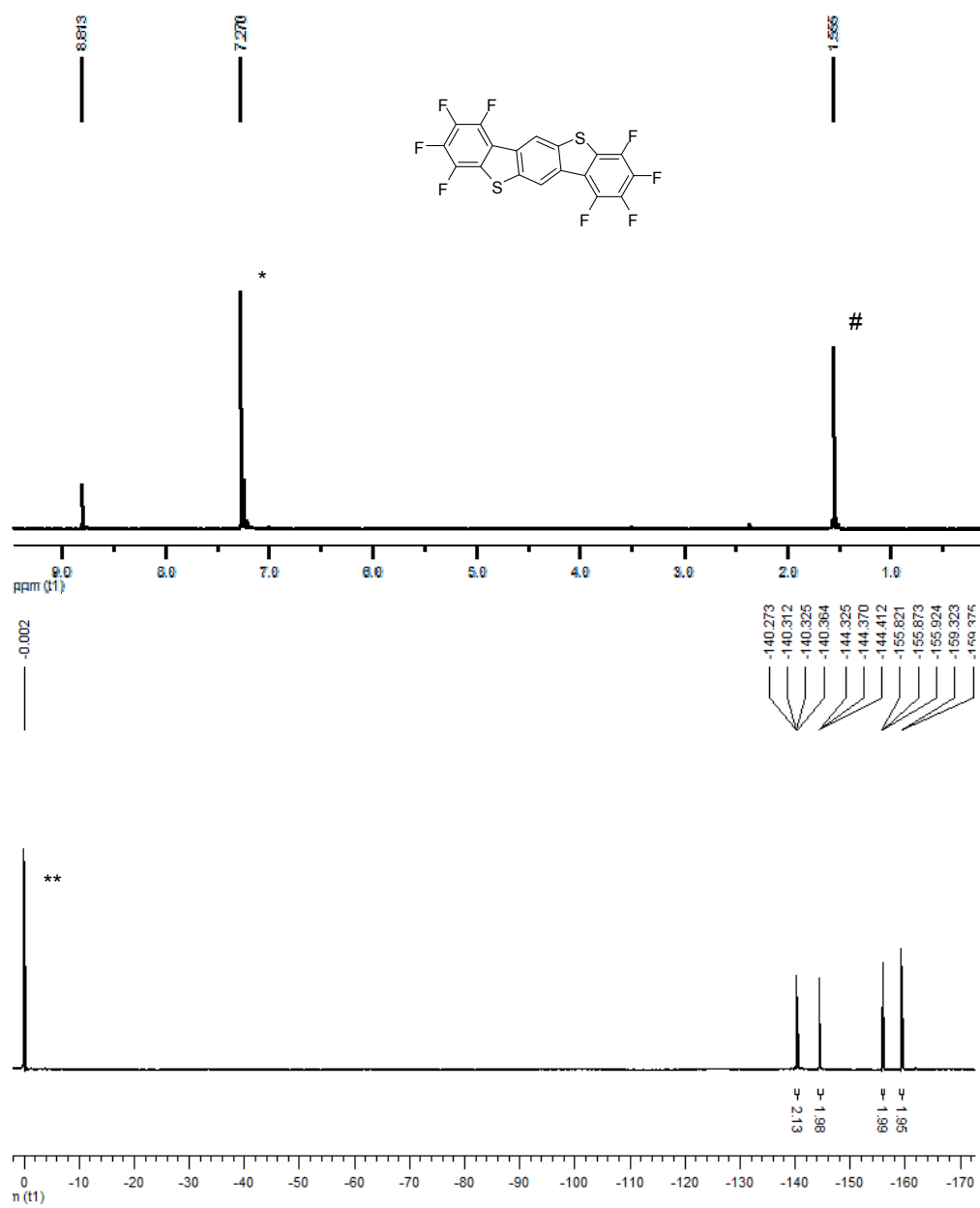


Figure 6. 3 ¹H (top) and ¹⁹F (bottom) NMR (r.t., CDCl₃) spectra of compound 3-19. (*solvent, **CCl₃F, # H₂O)

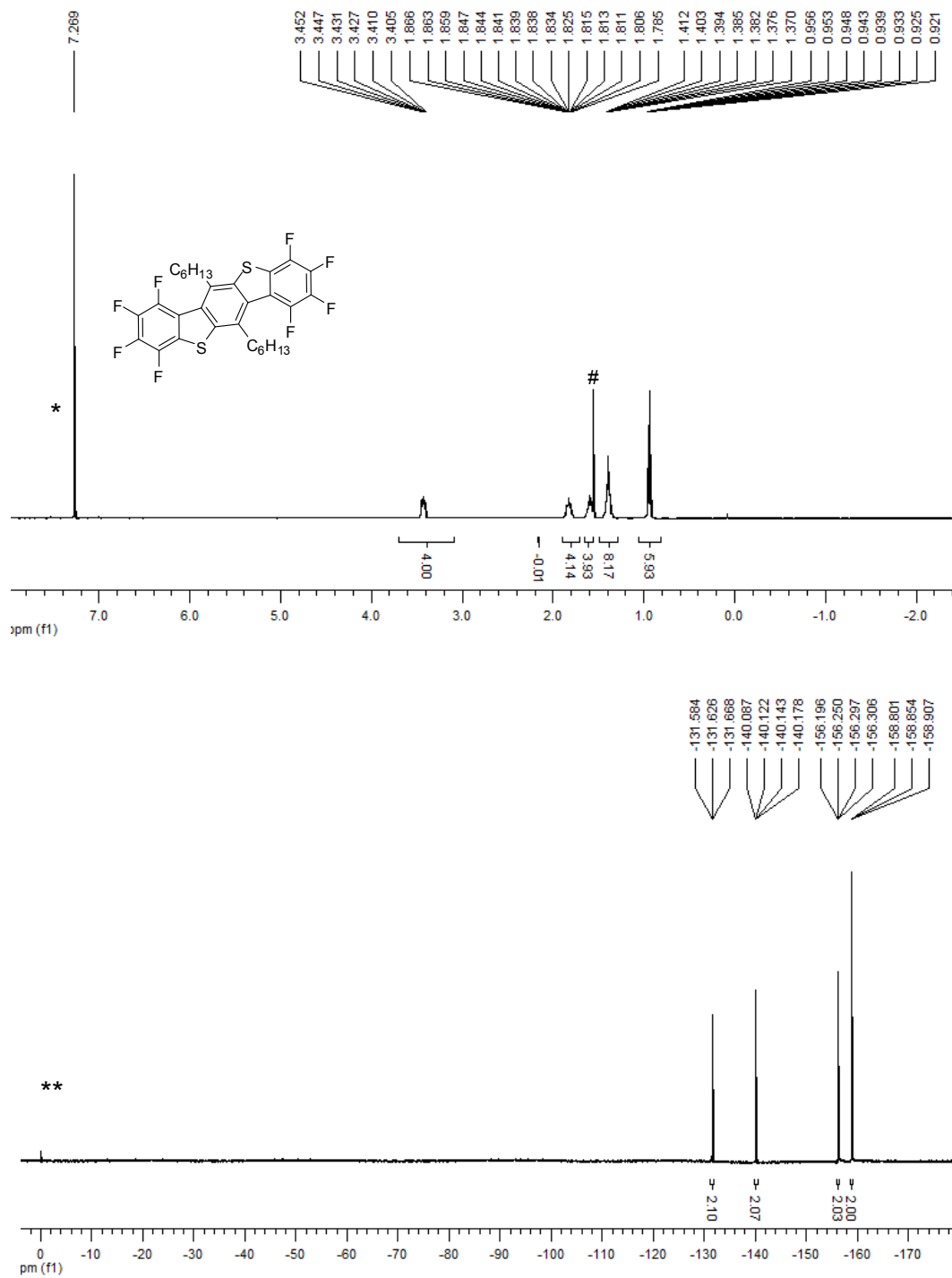


Figure 6. 4 ¹H (top) and ¹⁹F (bottom) NMR (50°C, CDCl₃) spectra of compound **3-24a**. (*solvent, **CCl₃F, #H₂O)

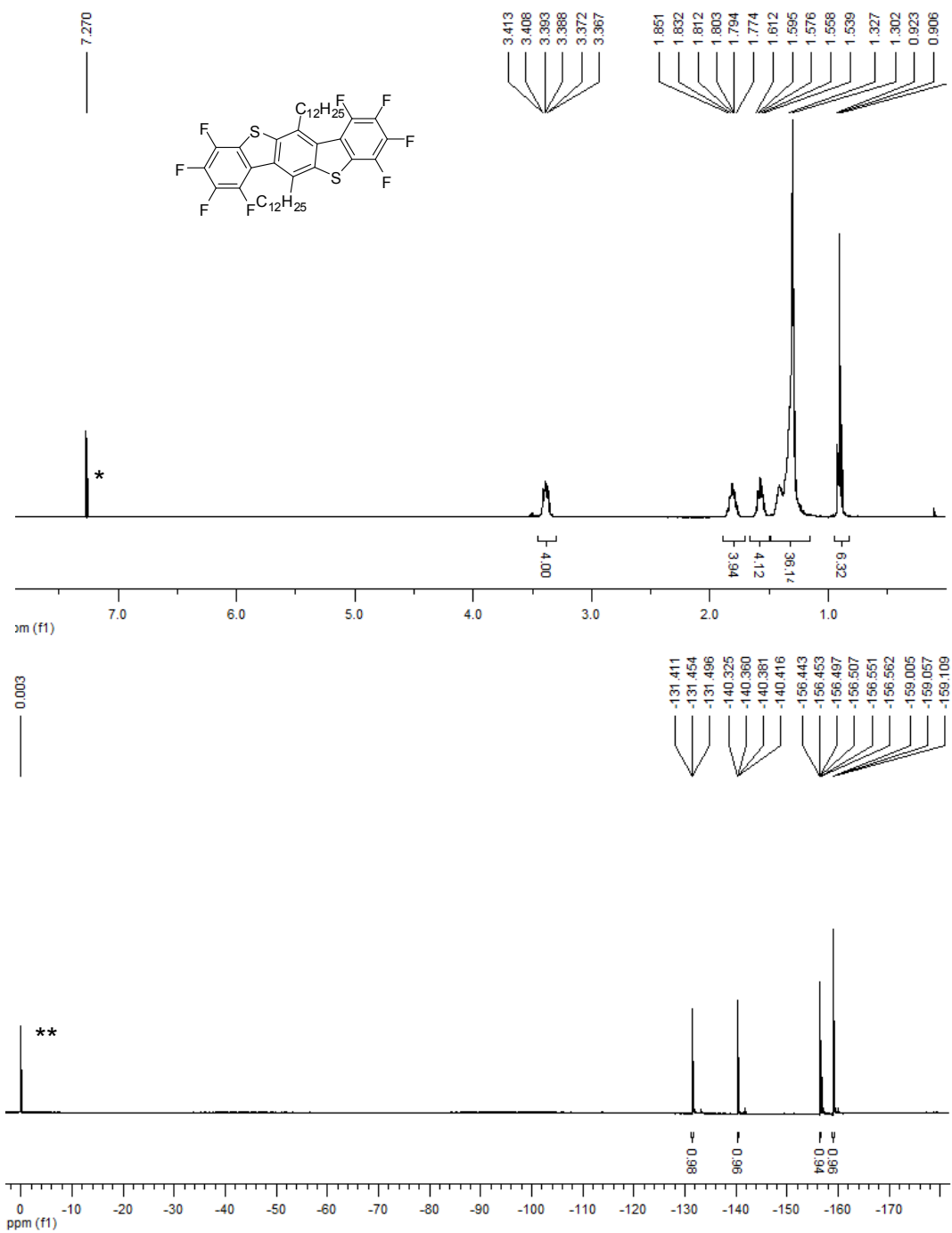


Figure 6. 5 ¹H (top) and ¹⁹F (bottom) NMR (r.t., CDCl₃) spectra of compound **3-24b**. (*solvent, **CCl₃F)

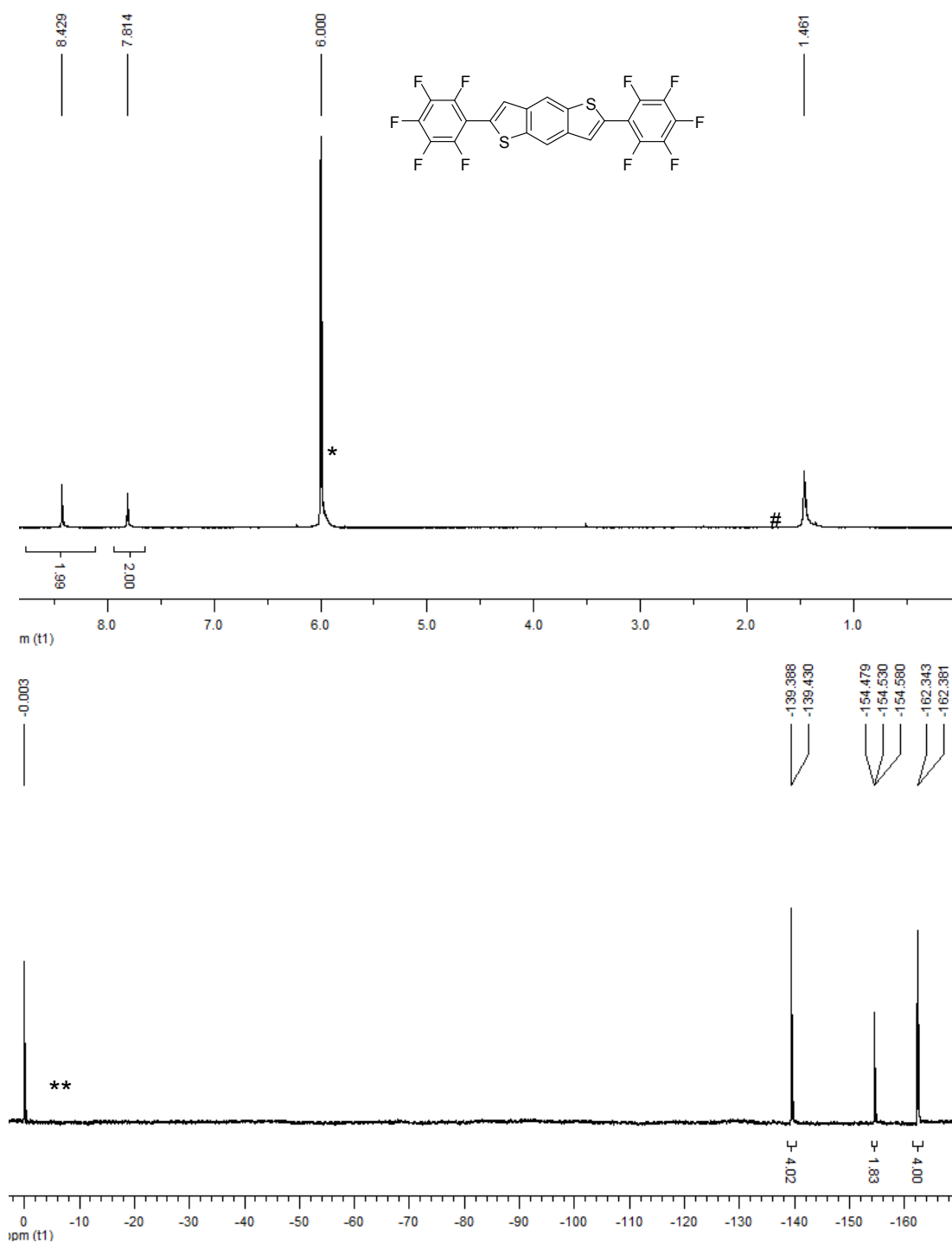


Figure 6.6 ^1H (top) and ^{19}F (bottom) NMR (120°C, $\text{C}_2\text{D}_2\text{Cl}_4$) spectra of compound **4-14**. (*solvent, ** CCl_3F , # H_2O)

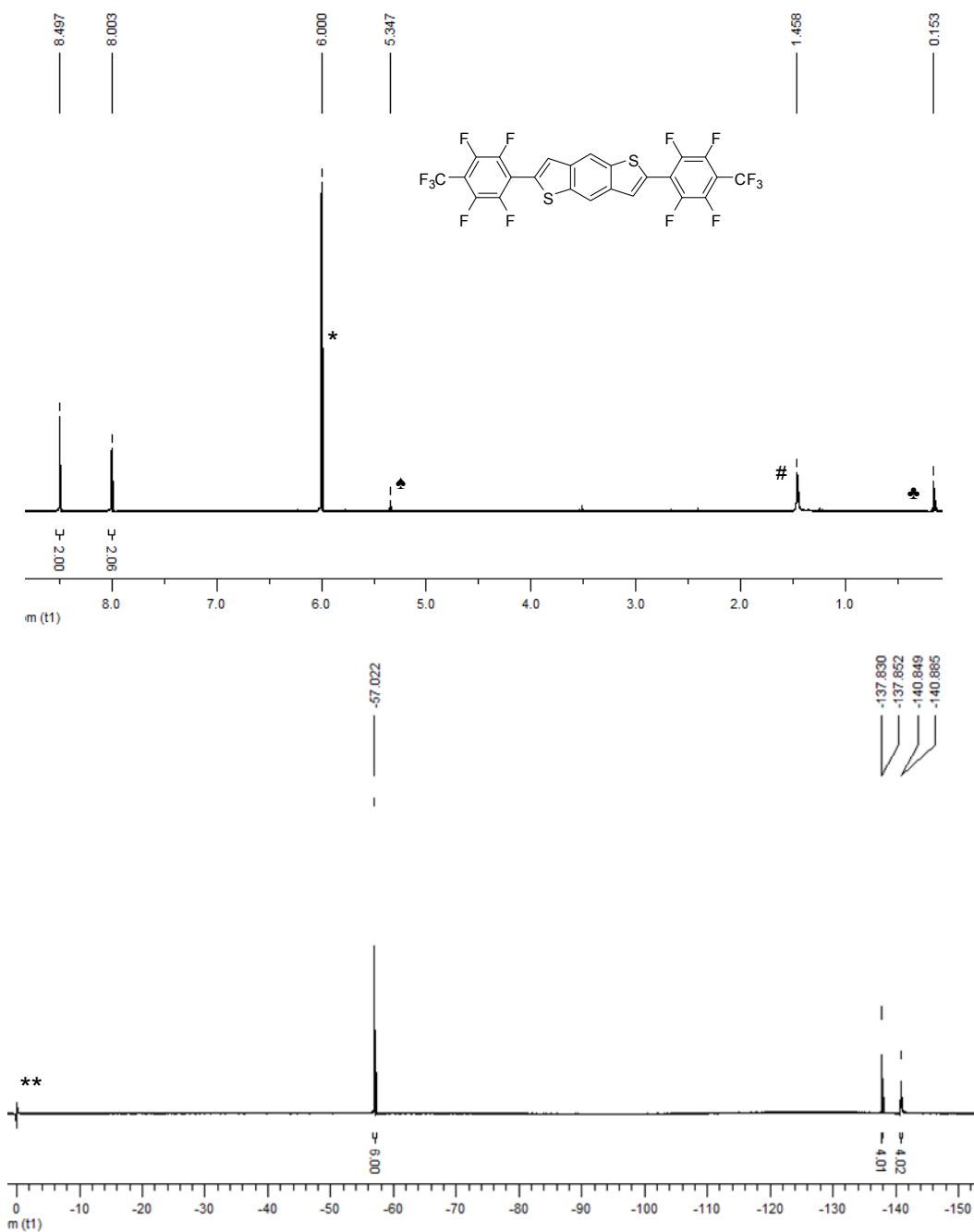


Figure 6. 7 ¹H (top) and ¹⁹F (bottom) NMR (120°C, C₂D₂Cl₄) spectra of compound **4-15**. (*solvent, **CCl₃F, #H₂O, ♠CH₂Cl₂, ♣grease)

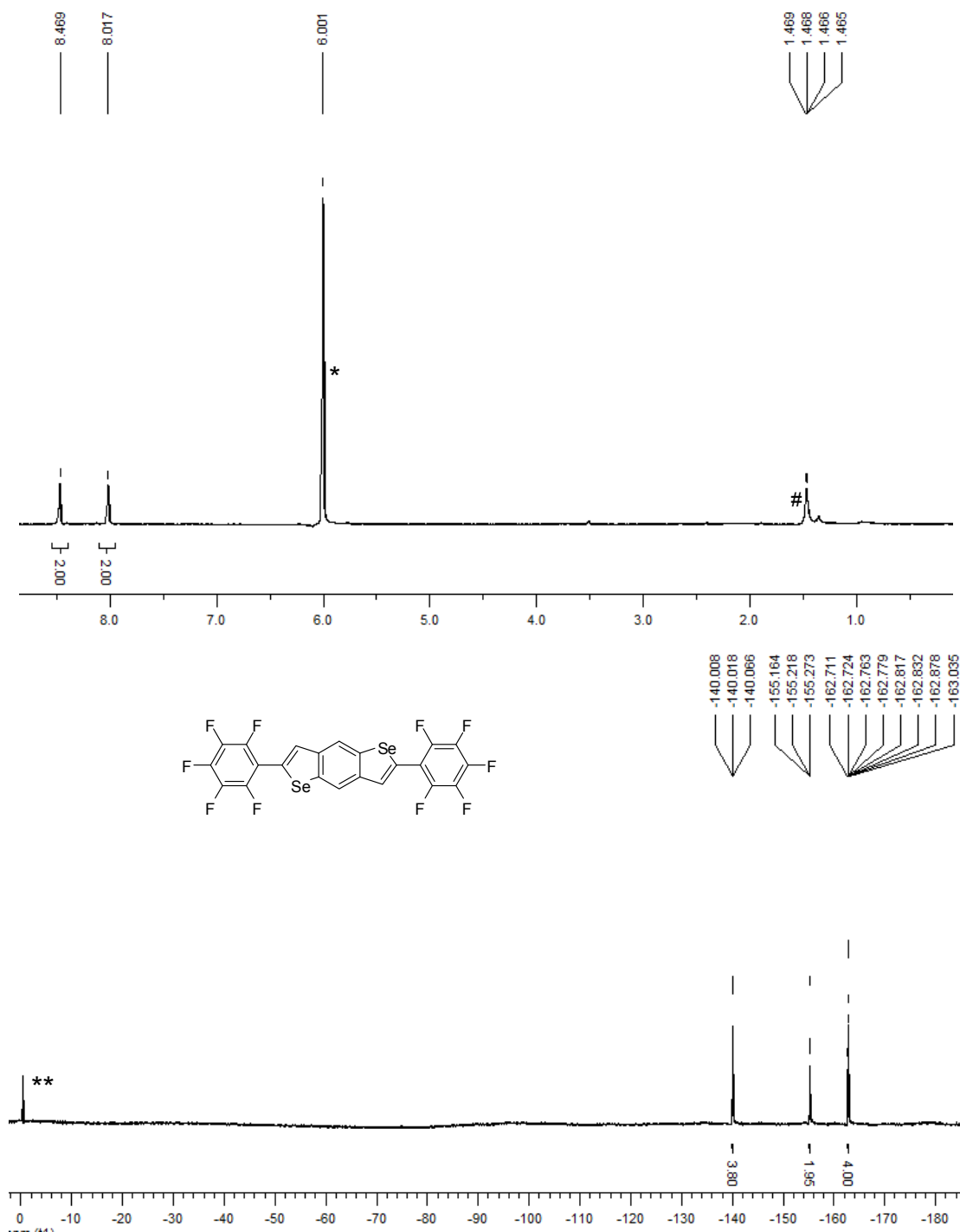


Figure 6. 8 ^1H (top) and ^{19}F (bottom) NMR (120°C, $\text{C}_2\text{D}_2\text{Cl}_4$) spectra of compound 4-16. (*solvent, ** CCl_3F , # H_2O)

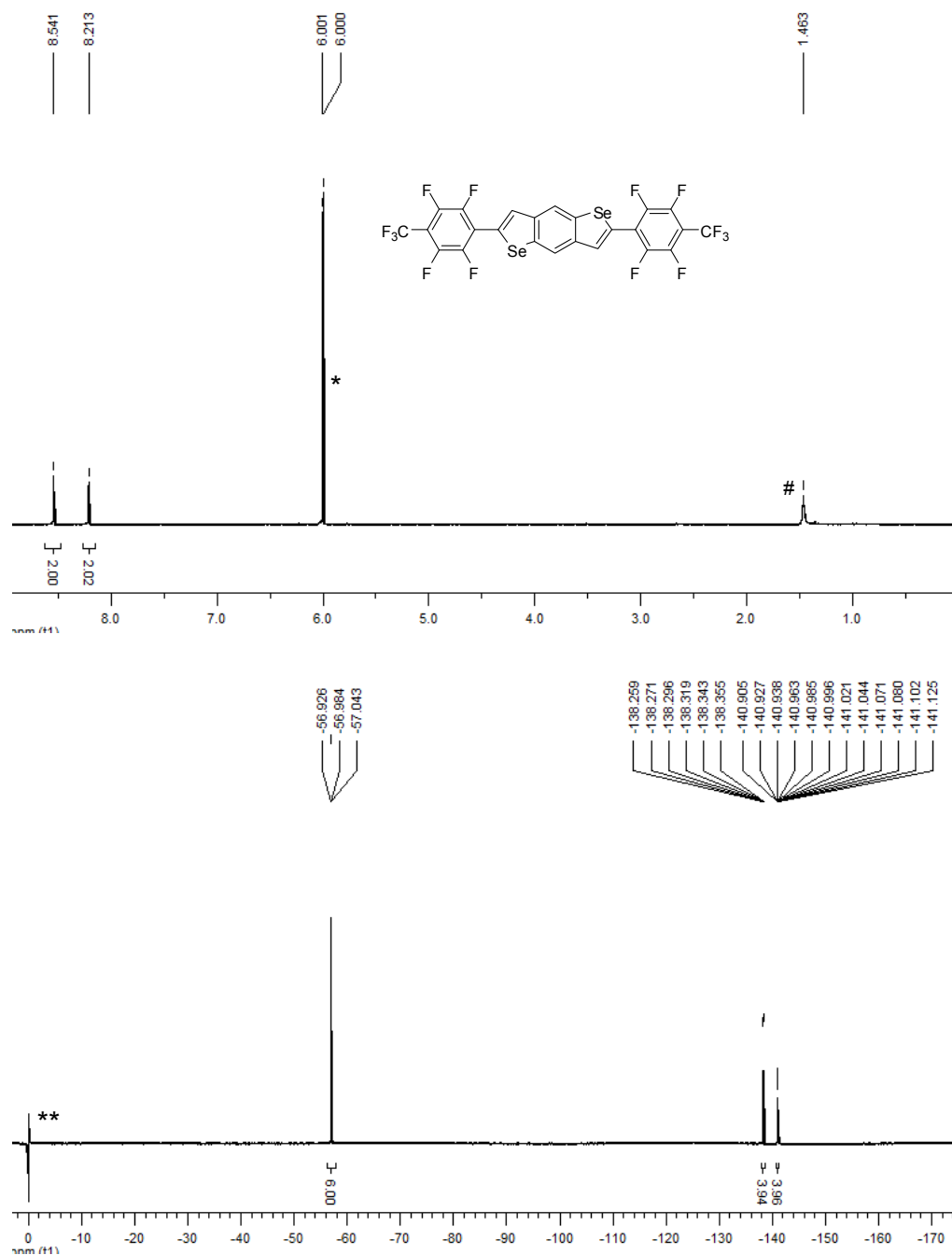


Figure 6.9 ¹H (top) and ¹⁹F (bottom) NMR (120°C, C₂D₂Cl₄) spectra of compound 4-17. (*solvent, **CCl₃F, #H₂O)

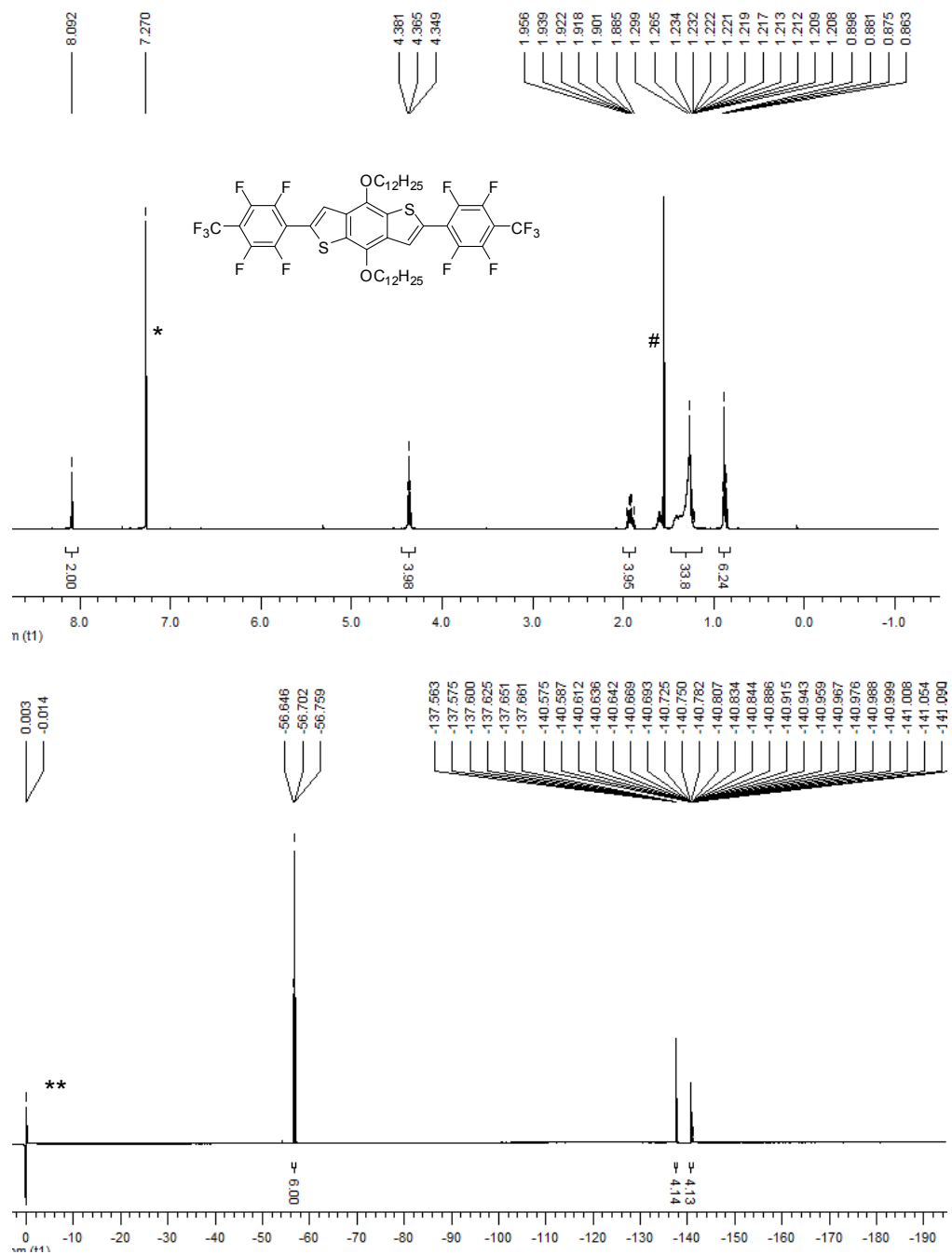


Figure 6. 11 ¹H (top) and ¹⁹F (bottom) NMR (r.t., CDCl₃) spectra of compound **4-19**. (*solvent, **CCl₃F, #H₂O)

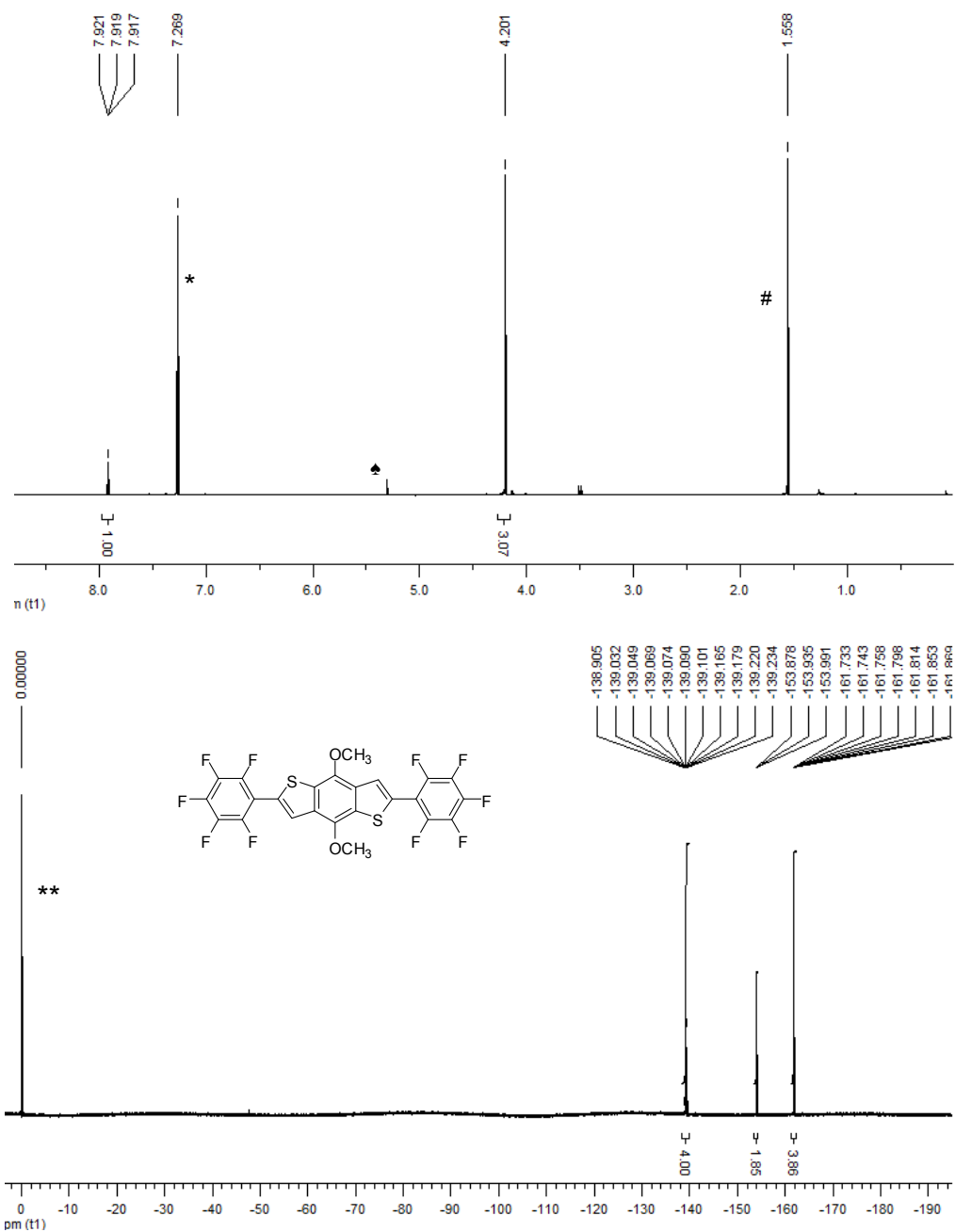


Figure 6. 12 ^1H (top) and ^{19}F (bottom) NMR (r.t., CDCl_3) spectra of compound 4-20. (*solvent, ** CCl_3F , # H_2O , ♣ CH_2Cl_2)

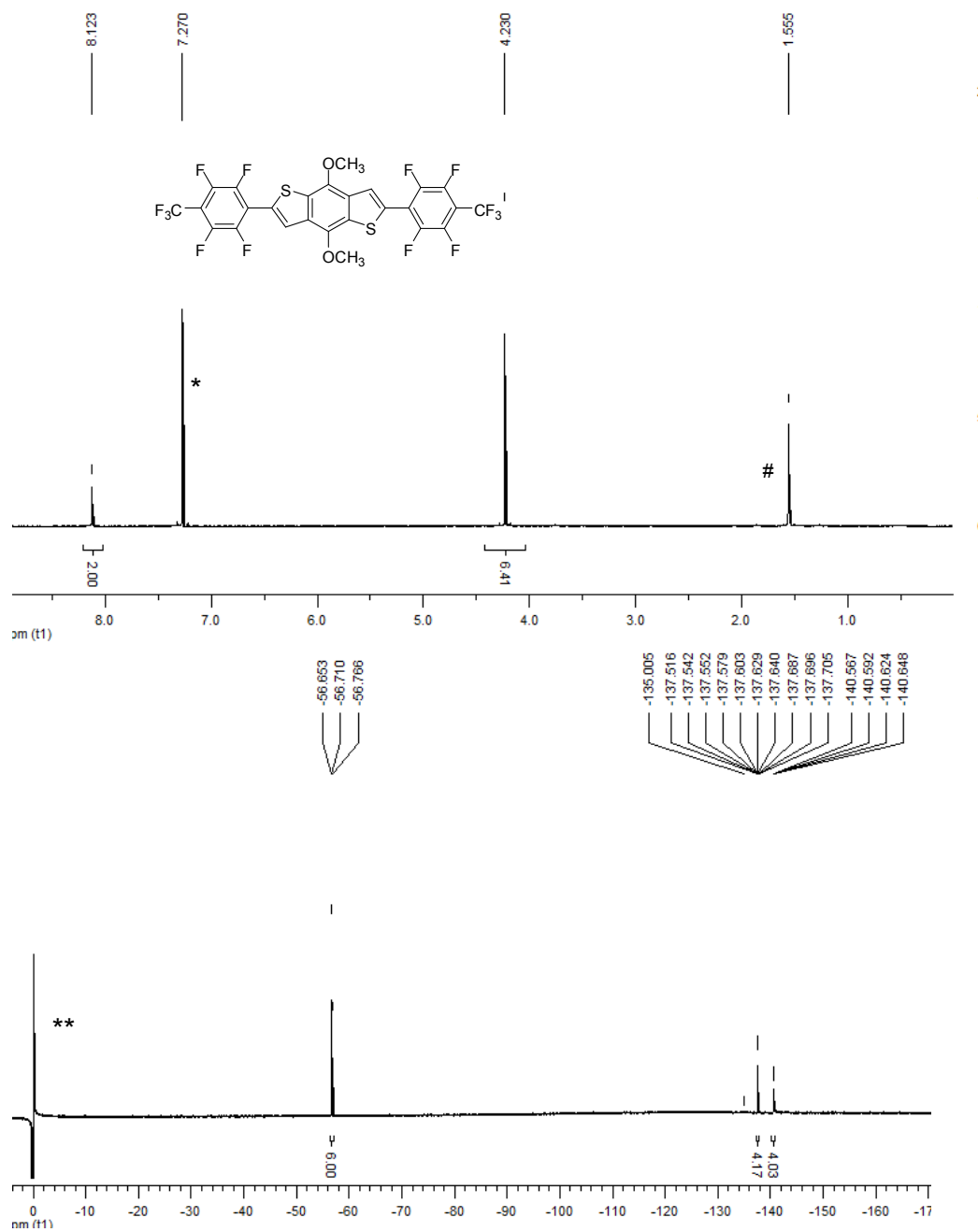


Figure 6. 13 ¹H (top) and ¹⁹F (bottom) NMR (r.t., CDCl₃) spectra of compound **4-21**. (*solvent, **CCl₃F, #H₂O)

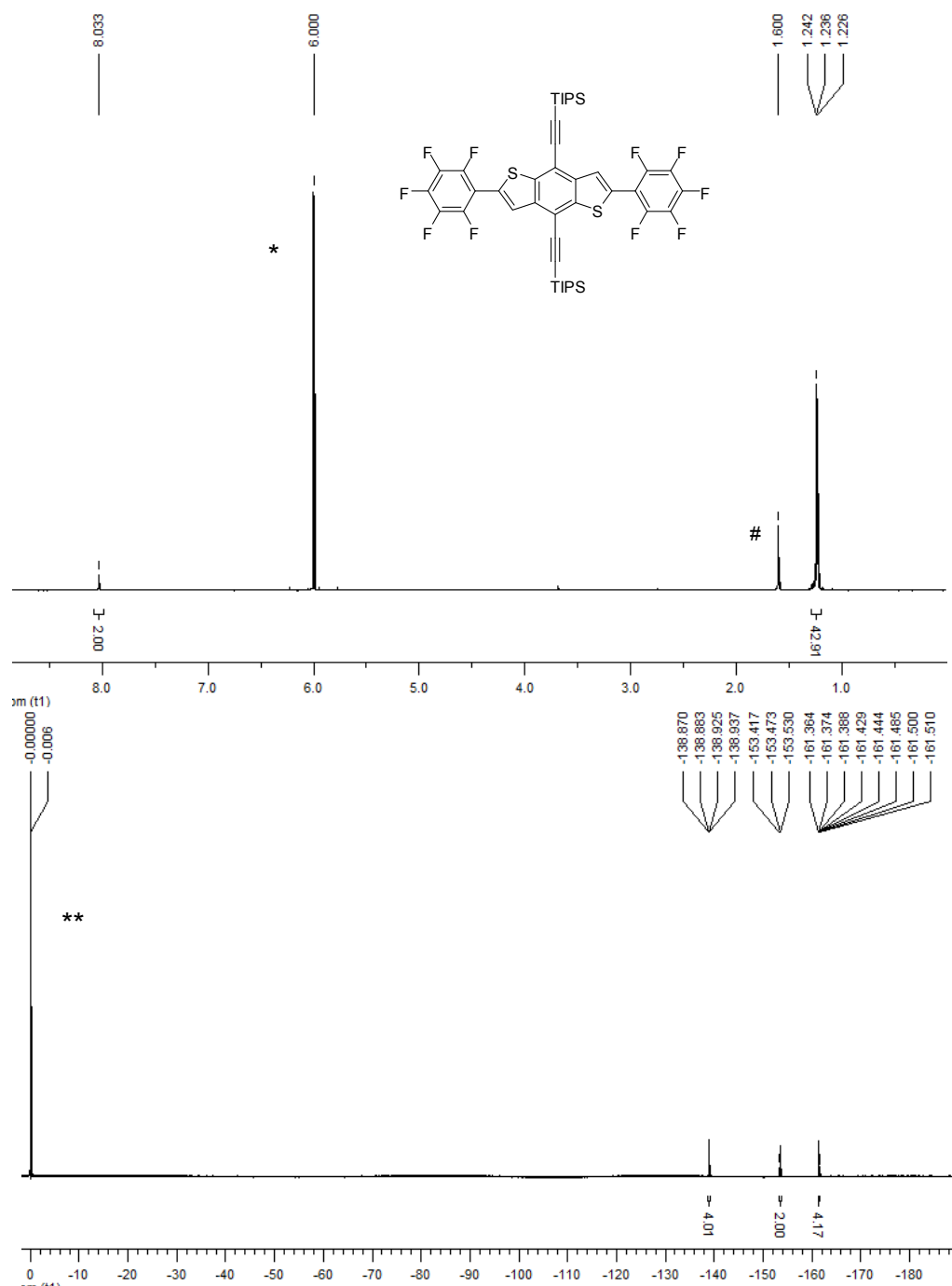


Figure 6. 14 ¹H (top) and ¹⁹F (bottom) NMR (r.t., C₂D₂Cl₄) spectra of compound **4-22**. (*solvent, **CCl₃F, #H₂O)

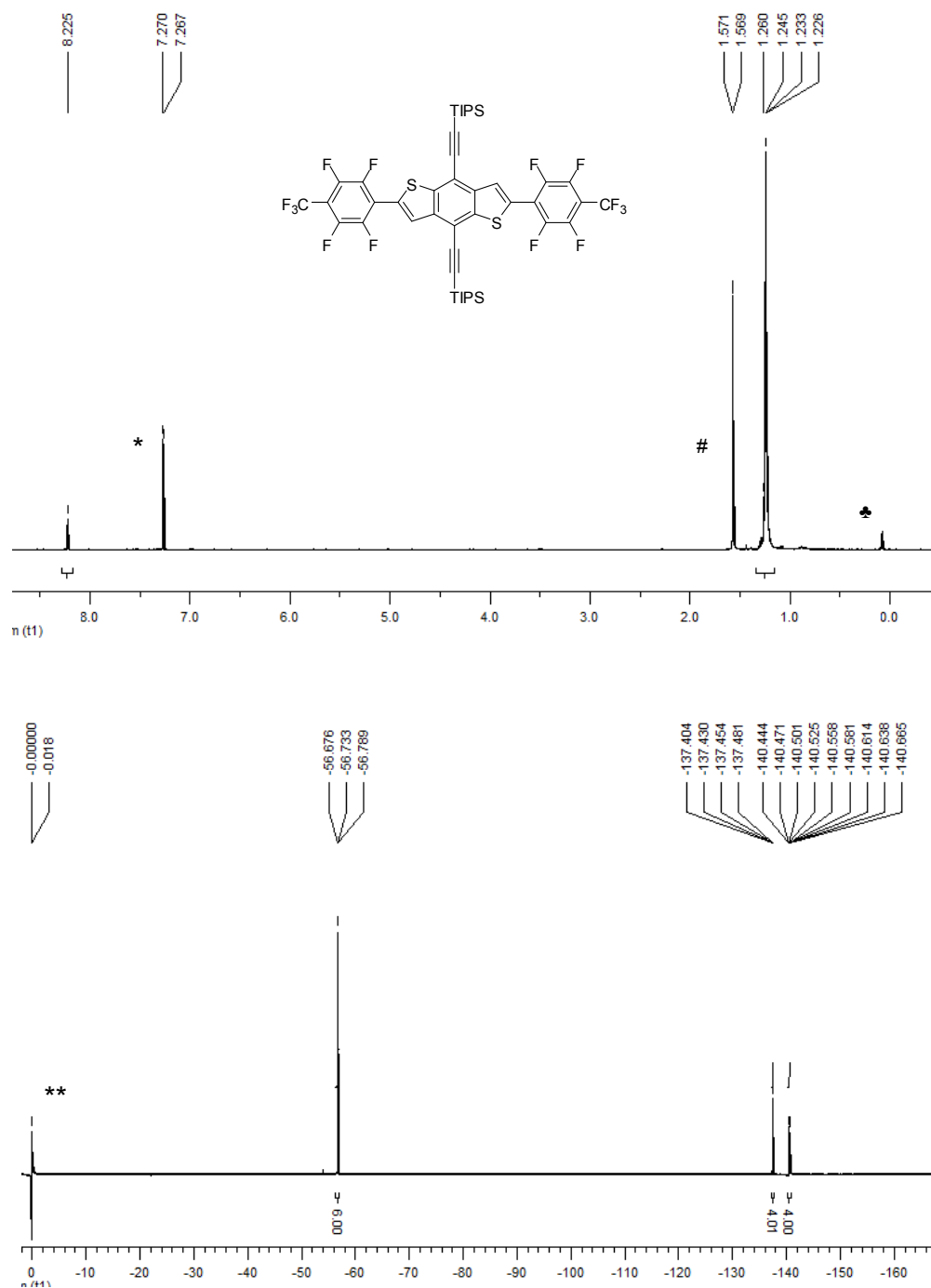


Figure 6. 15 ¹H (top) and ¹⁹F (bottom) NMR (r.t., CDCl₃) spectra of compound **4-23**. (*solvent, **CCl₃F, #H₂O, ♣grease)

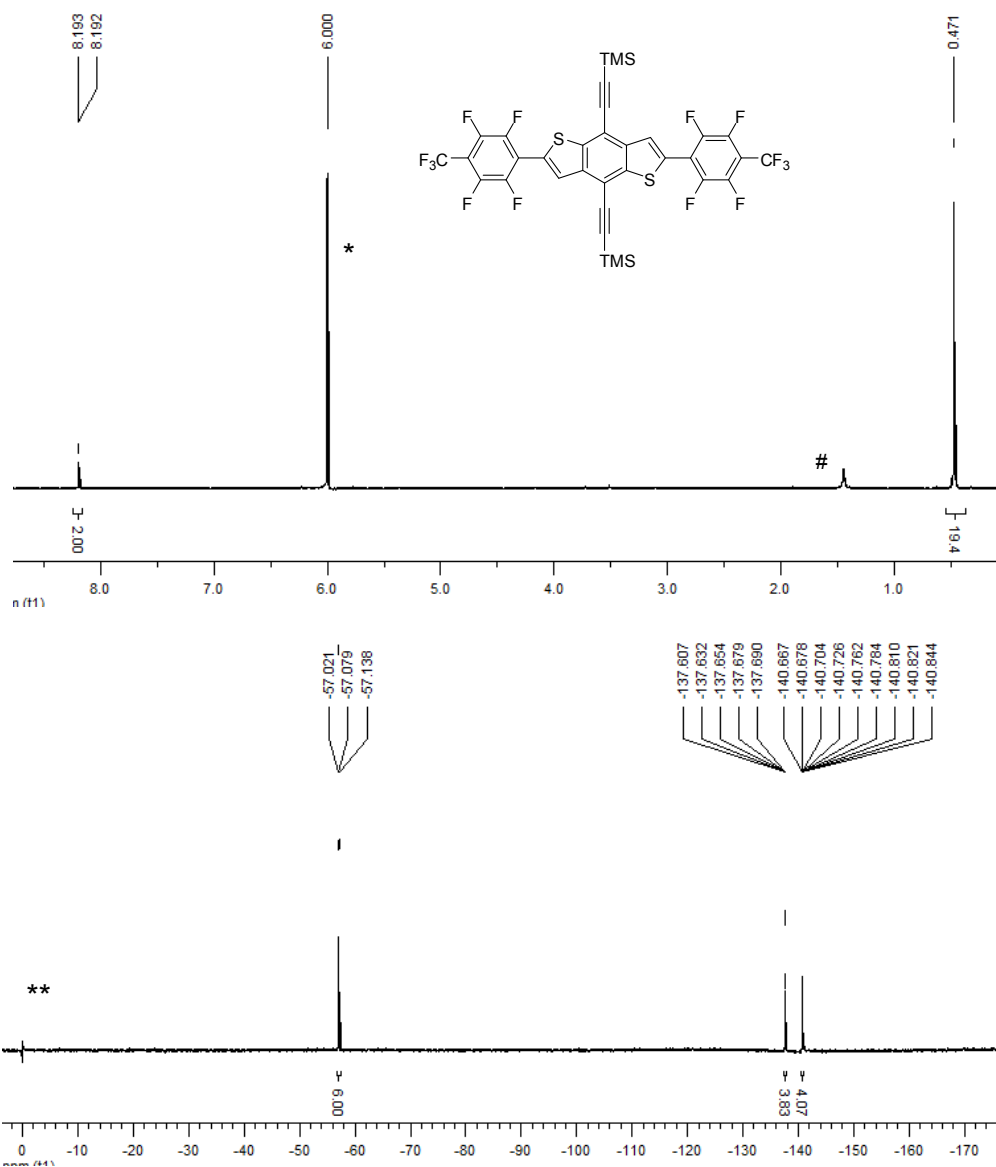
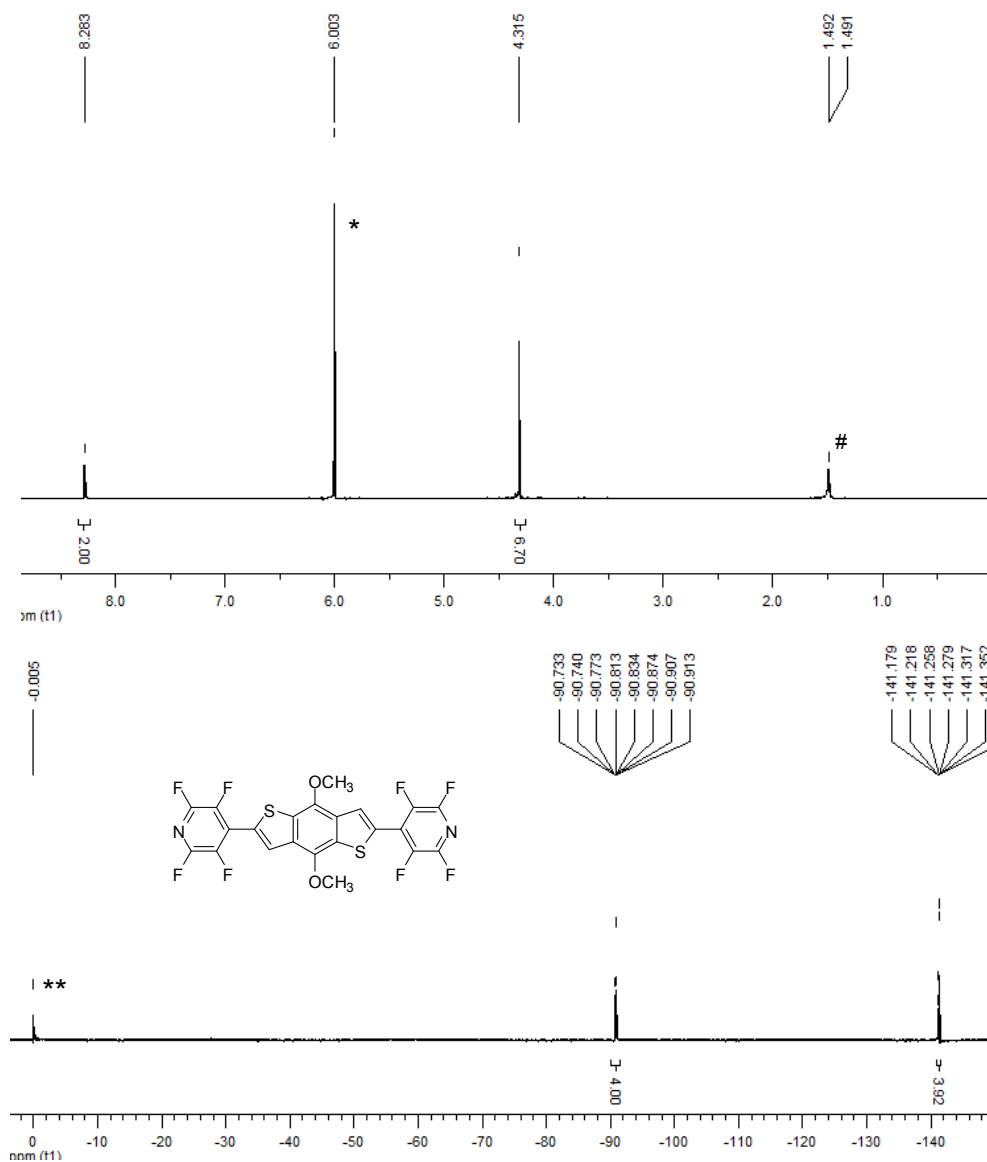


Figure 6. 16 ^1H (top) and ^{19}F (bottom) NMR (130°C, $\text{C}_2\text{D}_2\text{Cl}_4$) spectra of compound 4-24. (*solvent, ** CCl_3F , # H_2O)



Copyright © Yongfeng Wang 2008

References

1. Tsumura, A.; Koezuka, H.; Ando, T., Macromolecular Electronic Device - Field-Effect Transistor with a Polythiophene Thin-Film. *Applied Physics Letters* **1986**, 49, (18), 1210-1212.
2. Kudo, K.; Yamashina, M.; Moriizumi, T., Field-Effect Measurement of Organic-Dye Films. *Japanese Journal of Applied Physics Part 1-Regular Papers Short Notes & Review Papers* **1984**, 23, (1), 130-130.
3. Rotzoll, R.; Mohapatra, S.; Olariu, V.; Wenz, R.; Grigas, M.; Dimmler, K.; Shchekin, O.; Dodabalapur, A., Radio frequency rectifiers based on organic thin-film transistors. *Applied Physics Letters* **2006**, 88, (12).
4. Baude, P. F.; Ender, D. A.; Haase, M. A.; Kelley, T. W.; Muyres, D. V.; Theiss, S. D., Pentacene-based radio-frequency identification circuitry. *Applied Physics Letters* **2003**, 82, (22), 3964-3966.
5. Dodabalapur, A.; Bao, Z.; Makhija, A.; Laquindanum, J. G.; Raju, V. R.; Feng, Y.; Katz, H. E.; Rogers, J., Organic smart pixels. *Applied Physics Letters* **1998**, 73, (2), 142-144.
6. Sheraw, C. D.; Zhou, L.; Huang, J. R.; Gundlach, D. J.; Jackson, T. N.; Kane, M. G.; Hill, I. G.; Hammond, M. S.; Campi, J.; Greening, B. K.; Francl, J.; West, J., Organic thin-film transistor-driven polymer-dispersed liquid crystal displays on flexible polymeric substrates. *Applied Physics Letters* **2002**, 80, (6), 1088-1090.
7. Cornil, J.; Bredas, J. L.; Zaumseil, J.; Sirringhaus, H., Ambipolar transport in organic conjugated material. *Advanced Materials* **2007**, 19, (14), 1791-1799.
8. Karl, N.; Kraft, K. H.; Marktanner, J.; Munch, M.; Schatz, F.; Stehle, R.; Uhde, H. M., Fast electronic transport in organic molecular solids? *Journal of Vacuum Science & Technology A* **1999**, 17, (4), 2318-2328.
9. Chua, L. L.; Zaumseil, J.; Chang, J. F.; Ou, E. C. W.; Ho, P. K. H.; Sirringhaus, H.; Friend, R. H., General observation of n-type field-effect behaviour in organic semiconductors. *Nature* **2005**, 434, (7030), 194-199.
10. Yasuda, T.; Fujita, K.; Tsutsui, T., Emergence of n-type characteristic of conjugated polymer field-effect transistors with calcium source-drain electrodes. *Japanese Journal of Applied Physics Part 1-Regular Papers Short Notes & Review Papers* **2004**, 43, (11A), 7731-7732.
11. Yasuda, T.; Goto, T.; Fujita, K.; Tsutsui, T., Ambipolar pentacene field-effect transistors with calcium source-drain electrodes. *Applied Physics Letters* **2004**, 85, (11), 2098-2100.
12. deLeeuw, D. M.; Simenon, M. M. J.; Brown, A. R.; Einerhand, R. E. F., Stability of n-type doped conducting polymers and consequences for polymeric microelectronic devices. *Synthetic Metals* **1997**, 87, (1), 53-59.
13. Zaumseil, J.; Sirringhaus, H., Electron and ambipolar transport in organic field-effect transistors. *Chemical Reviews* **2007**, 107, (4), 1296-1323.
14. Yoon, M. H.; Kim, C.; Facchetti, A.; Marks, T. J., Gate dielectric chemical structure-organic field-effect transistor performance correlations for electron, hole, and ambipolar organic semiconductors. *Journal of the American Chemical Society* **2006**, 128, (39), 12851-12869.

15. Newman, C. R.; Frisbie, C. D.; da Silva, D. A.; Bredas, J. L.; Ewbank, P. C.; Mann, K. R., Introduction to organic thin film transistors and design of n-channel organic semiconductors. *Chemistry of Materials* **2004**, 16, (23), 4436-4451.
16. Guillaud, G.; Alsadoun, M.; Maitrot, M.; Simon, J.; Bouvet, M., Field-Effect Transistors Based on Intrinsic Molecular Semiconductors. *Chemical Physics Letters* **1990**, 167, (6), 503-506.
17. Bao, Z. A.; Lovinger, A. J.; Brown, J., New air-stable n-channel organic thin film transistors. *Journal of the American Chemical Society* **1998**, 120, (1), 207-208.
18. Haddon, R. C.; Perel, A. S.; Morris, R. C.; Palstra, T. T. M.; Hebard, A. F.; Fleming, R. M., C-60 Thin-Film Transistors. *Applied Physics Letters* **1995**, 67, (1), 121-123.
19. Frankevich, E.; Maruyama, Y.; Ogata, H., Mobility of Charge-Carriers in Vapor-Phase Grown C-60 Single-Crystal. *Chemical Physics Letters* **1993**, 214, (1), 39-44.
20. Kobayashi, S.; Takenobu, T.; Mori, S.; Fujiwara, A.; Iwasa, Y., Fabrication and characterization of C-60 thin-film transistors with high field-effect mobility. *Applied Physics Letters* **2003**, 82, (25), 4581-4583.
21. Horiuchi, K.; Nakada, K.; Uchino, S.; Hashii, S.; Hashimoto, A.; Aoki, N.; Ochiai, Y.; Shimizu, M., Passivation effects of alumina insulating layer on C-60 thin-film field-effect transistors. *Applied Physics Letters* **2002**, 81, (10), 1911-1912.
22. Brown, A. R.; Deleeuw, D. M.; Lous, E. J.; Havinga, E. E., Organic N-Type Field-Effect Transistor. *Synthetic Metals* **1994**, 66, (3), 257-261.
23. Laquindanum, J. G.; Katz, H. E.; Dodabalapur, A.; Lovinger, A. J., n-channel organic transistor materials based on naphthalene frameworks. *Journal of the American Chemical Society* **1996**, 118, (45), 11331-11332.
24. Pappenfus, T. M.; Chesterfield, R. J.; Frisbie, C. D.; Mann, K. R.; Casado, J.; Raff, J. D.; Miller, L. L., A pi-stacking terthiophene-based quinodimethane is an n-channel conductor in a thin film transistor. *Journal of the American Chemical Society* **2002**, 124, (16), 4184-4185.
25. Chesterfield, R. J.; Newman, C. R.; Pappenfus, T. M.; Ewbank, P. C.; Haukaas, M. H.; Mann, K. R.; Miller, L. L.; Frisbie, C. D., High electron mobility and ambipolar transport in organic thin-film transistors based on a pi-stacking quinoidal terthiophene. *Advanced Materials* **2003**, 15, (15), 1278-+.
26. Facchetti, A.; Deng, Y.; Wang, A. C.; Koide, Y.; Sirringhaus, H.; Marks, T. J.; Friend, R. H., Tuning the semiconducting properties of sexithiophene by alpha,omega-substitution - alpha,omega-diperfluorohexylsexithiophene: The first n-type sexithiophene for thin-film transistors. *Angewandte Chemie-International Edition* **2000**, 39, (24), 4547-+.
27. Facchetti, A.; Mushrush, M.; Yoon, M. H.; Hutchison, G. R.; Ratner, M. A.; Marks, T. J., Building blocks for n-type molecular and polymeric electronics. Perfluoroalkyl-versus alkyl-functionalized oligothiophenes (nT; n=2-6). Systematics of thin film microstructure, semiconductor performance, and modeling of majority charge injection in field-effect transistors. *Journal of the American Chemical Society* **2004**, 126, (42), 13859-13874.
28. Facchetti, A.; Yoon, M. H.; Stern, C. L.; Katz, H. E.; Marks, T. J., Building blocks for n-type organic electronics: Regiochemically modulated inversion of majority carrier

- sign in perfluoroarene-modified polythiophene semiconductors. *Angewandte Chemie-International Edition* **2003**, 42, (33), 3900-3903.
29. Yoon, M. H.; DiBenedetto, S. A.; Facchetti, A.; Marks, T. J., Organic thin-film transistors based on carbonyl-functionalized quaterthiophenes: High mobility N-channel semiconductors and ambipolar transport. *Journal of the American Chemical Society* **2005**, 127, (5), 1348-1349.
30. Sakamoto, Y.; Suzuki, T.; Kobayashi, M.; Gao, Y.; Fukai, Y.; Inoue, Y.; Sato, F.; Tokito, S., Perfluoropentacene: High-performance p-n junctions and complementary circuits with pentacene. *Journal of the American Chemical Society* **2004**, 126, (26), 8138-8140.
31. Inoue, Y.; Sakamoto, Y.; Suzuki, T.; Kobayashi, M.; Gao, Y.; Tokito, S., Organic thin-film transistors with high electron mobility based on perfluoropentacene. *Japanese Journal of Applied Physics Part 1-Regular Papers Short Notes & Review Papers* **2005**, 44, (6A), 3663-3668.
32. Ando, S.; Nishida, J.; Fujiwara, E.; Tada, H.; Inoue, Y.; Tokito, S.; Yamashita, Y., Novel p- and n-type organic semiconductors with an anthracene unit. *Chemistry of Materials* **2005**, 17, (6), 1261-+.
33. Takimiya, K.; Kunugi, Y.; Ebata, H.; Otsubo, T., Molecular modification of 2,6-diphenylbenzo[1,2-b : 4,5-b']dichalcogenophenes by introduction of strong electron-withdrawing groups: Conversion from p- to n-channel OFET materials. *Chemistry Letters* **2006**, 35, (10), 1200-1201.
34. Katz, H. E.; Lovinger, A. J.; Johnson, J.; Kloc, C.; Siegrist, T.; Li, W.; Lin, Y. Y.; Dodabalapur, A., A soluble and air-stable organic semiconductor with high electron mobility. *Nature* **2000**, 404, (6777), 478-481.
35. Jones, B. A.; Facchetti, A.; Wasielewski, M. R.; Marks, T. J., Tuning orbital energetics in arylene diimide semiconductors. Materials design for ambient stability of n-type charge transport. *Journal of the American Chemical Society* **2007**, 129, (49), 15259-15278.
36. Ostrick, J. R.; Dodabalapur, A.; Torsi, L.; Lovinger, A. J.; Kwock, E. W.; Miller, T. M.; Galvin, M.; Berggren, M.; Katz, H. E., Conductivity-type anisotropy in molecular solids. *Journal of Applied Physics* **1997**, 81, (10), 6804-6808.
37. Struijk, C. W.; Sieval, A. B.; Dakhorst, J. E. J.; van Dijk, M.; Kimkes, P.; Koehorst, R. B. M.; Donker, H.; Schaafsma, T. J.; Picken, S. J.; van de Craats, A. M.; Warman, J. M.; Zuilhof, H.; Sudholter, E. J. R., Liquid crystalline perylene diimides: Architecture and charge carrier mobilities. *Journal of the American Chemical Society* **2000**, 122, (45), 11057-11066.
38. Malenfant, P. R. L.; Dimitrakopoulos, C. D.; Gelorme, J. D.; Kosbar, L. L.; Graham, T. O.; Curioni, A.; Andreoni, W., N-type organic thin-film transistor with high field-effect mobility based on a N,N'-dialkyl-3,4,9,10-perylene tetracarboxylic diimide derivative. *Applied Physics Letters* **2002**, 80, (14), 2517-2519.
39. Jones, B. A.; Ahrens, M. J.; Yoon, M. H.; Facchetti, A.; Marks, T. J.; Wasielewski, M. R., High-mobility air-stable n-type semiconductors with processing versatility: Dicyanoperylene-3,4 : 9,10-bis(dicarboximides). *Angewandte Chemie-International Edition* **2004**, 43, (46), 6363-6366.

40. Chiang, C. K.; Fincher, C. R.; Park, Y. W.; Heeger, A. J.; Shirakawa, H.; Louis, E. J.; Gau, S. C.; Macdiarmid, A. G., Electrical-Conductivity in Doped Polyacetylene. *Physical Review Letters* **1977**, 39, (17), 1098-1101.
41. Shirakawa, H.; Louis, E. J.; Macdiarmid, A. G.; Chiang, C. K.; Heeger, A. J., Synthesis of Electrically Conducting Organic Polymers - Halogen Derivatives of Polyacetylene, (Ch)X. *Journal of the Chemical Society-Chemical Communications* **1977**, (16), 578-580.
42. Roncali, J., Conjugated Poly(Thiophenes) - Synthesis, Functionalization, and Applications. *Chemical Reviews* **1992**, 92, (4), 711-738.
43. Mao, H. Y.; Holdcroft, S., Grignard Synthesis of Pi-Conjugated Poly(3-Alkylthiophenes) - Controlling Molecular-Weights and the Nature of Terminal Units. *Macromolecules* **1992**, 25, (2), 554-558.
44. Kobayashi, M.; Chen, J.; Chung, T. C.; Moraes, F.; Heeger, A. J.; Wudl, F., Synthesis and Properties of Chemically Coupled Poly(Thiophene). *Synthetic Metals* **1984**, 9, (1), 77-86.
45. Yamamoto, T.; Morita, A.; Miyazaki, Y.; Maruyama, T.; Wakayama, H.; Zhou, Z.; Nakamura, Y.; Kanbara, T.; Sasaki, S.; Kubota, K., Preparation of Pi-Conjugated Poly(Thiophene-2,5-Diyl), Poly(Para-Phenylene), and Related Polymers Using Zero Valent Nickel-Complexes - Linear Structure and Properties of the Pi-Conjugated Polymers. *Macromolecules* **1992**, 25, (4), 1214-1223.
46. Yamamoto, T.; Maruyama, T.; Zhou, Z. H.; Miyazaki, Y.; Kanbara, T.; Sanechika, K., New Method Using Nickel(0) Complex for Preparation of Poly(Para-Phenylene), Poly(2,5-Thienylene) and Related Pi-Conjugated Polymers. *Synthetic Metals* **1991**, 41, (1-2), 345-348.
47. Pomerantz, M.; Tseng, J. J.; Zhu, H.; Sproull, S. J.; Reynolds, J. R.; Uitz, R.; Arnott, H. J.; Haider, M. I., Processable Polymers and Copolymers of 3-Alkylthiophenes and Their Blends. *Synthetic Metals* **1991**, 41, (3), 825-830.
48. Niemi, V. M.; Knuutila, P.; Osterholm, J. E.; Korvola, J., Polymerization of 3-Alkylthiophenes with FeCl₃. *Polymer* **1992**, 33, (7), 1559-1562.
49. Abdou, M. S. A.; Lu, X. T.; Xie, Z. W.; Orfino, F.; Deen, M. J.; Holdcroft, S., Nature of Impurities in Pi-Conjugated Polymers Prepared by Ferric-Chloride and Their Effect on the Electrical-Properties of Metal-Insulator-Semiconductor Structures. *Chemistry of Materials* **1995**, 7, (4), 631-641.
50. McCullough, R. D.; Lowe, R. D.; Jayaraman, M.; Anderson, D. L., Design, Synthesis, and Control of Conducting Polymer Architectures - Structurally Homogeneous Poly(3-Alkylthiophenes). *Journal of Organic Chemistry* **1993**, 58, (4), 904-912.
51. Chen, T. A.; Rieke, R. D., The 1st Regioregular Head-to-Tail Poly(3-Hexylthiophene-2,5-Diyl) and a Regiorandom Isopolymer - Ni Vs Pd Catalysis of 2(5)-Bromo-5(2)-(Bromozincio)-3-Hexylthiophene Polymerization. *Journal of the American Chemical Society* **1992**, 114, (25), 10087-10088.
52. Chen, T. A.; Wu, X. M.; Rieke, R. D., Regiocontrolled Synthesis of Poly(3-Alkylthiophenes) Mediated by Rieke Zinc - Their Characterization and Solid-State Properties. *Journal of the American Chemical Society* **1995**, 117, (1), 233-244.

53. Maior, R. M. S.; Hinkelmann, K.; Eckert, H.; Wudl, F., Synthesis and Characterization of 2 Regiochemically Defined Poly(Dialkylbithiophenes) - a Comparative-Study. *Macromolecules* **1990**, 23, (5), 1268-1279.
54. Pang, Y.; Li, J.; Barton, T. J., Processible poly[(p-phenyleneethynylene)-alt-(2,5-thienyleneethynylene)]s of high luminescence: their synthesis and physical properties. *Journal of Materials Chemistry* **1998**, 8, (8), 1687-1690.
55. Donat-Bouillud, A.; Levesque, I.; Tao, Y.; D'Iorio, M.; Beaupre, S.; Blondin, P.; Ranger, M.; Bouchard, J.; Leclerc, M., Light-emitting diodes from fluorene-based pi-conjugated polymers. *Chemistry of Materials* **2000**, 12, (7), 1931-1936.
56. Bao, Z. N.; Chan, W. K.; Yu, L. P., Exploration of the Stille coupling reaction for the syntheses of functional polymers. *Journal of the American Chemical Society* **1995**, 117, (50), 12426-12435.
57. Curtis, M. D.; Cao, J.; Kampf, J. W., Solid-state packing of conjugated oligomers: from pi-stacks to the herringbone structure. *Journal of the American Chemical Society* **2004**, 126, (13), 4318-4328.
58. Anthony, J. E.; Brooks, J. S.; Eaton, D. L.; Parkin, S. R., Functionalized pentacene: Improved electronic properties from control of solid-state order. *Journal of the American Chemical Society* **2001**, 123, (38), 9482-9483.
59. Budzianowski, A.; Katrusiak, A., Pressure-frozen benzene I revisited. *Acta Crystallographica Section B-Structural Science* **2006**, 62, 94-101.
60. Siegrist, T.; Kloc, C.; Schon, J. H.; Batlogg, B.; Haddon, R. C.; Berg, S.; Thomas, G. A., Enhanced physical properties in a pentacene polymorph. *Angewandte Chemie-International Edition* **2001**, 40, (9), 1732-1736.
61. Haddon, R. C.; Chi, X.; Itkis, M. E.; Anthony, J. E.; Eaton, D. L.; Siegrist, T.; Matheus, C. C.; Palstra, T. T. M., Band electronic structure of one- and two-dimensional pentacene molecular crystals. *Journal of Physical Chemistry B* **2002**, 106, (33), 8288-8292.
62. Coropceanu, V.; Cornil, J.; da Silva, D. A.; Olivier, Y.; Silbey, R.; Bredas, J. L., Charge transport in organic semiconductors (vol 107, pg 926, 2007). *Chemical Reviews* **2007**, 107, (5), 2165-2165.
63. Sarma, J. A. R. P.; Desiraju, G. R., The Role of Cl=Cl and C-H=O Interactions in the Crystal Engineering of 4-a Short-Axis Structures. *Accounts of Chemical Research* **1986**, 19, (7), 222-228.
64. Moon, H.; Zeis, R.; Borkent, E. J.; Besnard, C.; Lovinger, A. J.; Siegrist, T.; Kloc, C.; Bao, Z. N., Synthesis, crystal structure, and transistor performance of tetracene derivatives. *Journal of the American Chemical Society* **2004**, 126, (47), 15322-15323.
65. Anthony, J. E.; Eaton, D. L.; Parkin, S. R., A road map to stable, soluble, easily crystallized pentacene derivatives. *Organic Letters* **2002**, 4, (1), 15-18.
66. Kobayashi, K.; Masu, H.; Shuto, A.; Yamaguchi, K., Control of face-to-face pi-pi stacked packing arrangement of anthracene rings via chalcogen-chalcogen interaction: 9,10-bis(methylchalcogeno)anthracenes. *Chemistry of Materials* **2005**, 17, (26), 6666-6673.
67. Zeis, R.; Besnard, C.; Siegrist, T.; Schlockermann, C.; Chi, X. L.; Kloc, C., Field effect studies on rubrene and impurities of rubrene. *Chemistry of Materials* **2006**, 18, (2), 244-248.

68. Podzorov, V.; Menard, E.; Borissov, A.; Kiryukhin, V.; Rogers, J. A.; Gershenson, M. E., Intrinsic charge transport on the surface of organic semiconductors. *Physical Review Letters* **2004**, 93, (8).
69. Sundar, V. C.; Zaumseil, J.; Podzorov, V.; Menard, E.; Willett, R. L.; Someya, T.; Gershenson, M. E.; Rogers, J. A., Elastomeric transistor stamps: Reversible probing of charge transport in organic crystals. *Science* **2004**, 303, (5664), 1644-1646.
70. Patrick, C. R.; Prosser, G. S., Molecular Complex of Benzene and Hexafluorobenzene. *Nature* **1960**, 187, (4742), 1021-1021.
71. Coates, G. W.; Dunn, A. R.; Henling, L. M.; Ziller, J. W.; Lobkovsky, E. B.; Grubbs, R. H., Phenyl-perfluorophenyl stacking interactions: Topochemical[2+2] photodimerization and photopolymerization of olefinic compounds. *Journal of the American Chemical Society* **1998**, 120, (15), 3641-3649.
72. Watt, S. W.; Dai, C.; Scott, A. J.; Burke, J. M.; Thomas, R. L.; Collings, J. C.; Viney, C.; Clegg, W.; Marder, T. B., Structure and phase behavior of a 2 : 1 complex between arene- and fluoroarene-based conjugated rigid rods. *Angewandte Chemie-International Edition* **2004**, 43, (23), 3061-3063.
73. Wang, Z. H.; Dotz, F.; Enkelmann, V.; Mullen, K., "Double-Concave" graphene: Permethoxylated hexa-peri-hexabenzocoronene and its cocrystals with hexafluorobenzene and fullerene. *Angewandte Chemie-International Edition* **2005**, 44, (8), 1247-1250.
74. Ong, B. S.; Wu, Y. L.; Liu, P.; Gardner, S., High-performance semiconducting polythiophenes for organic thin-film transistors. *Journal of the American Chemical Society* **2004**, 126, (11), 3378-3379.
75. McCulloch, I.; Heeney, M.; Bailey, C.; Genevicius, K.; Macdonald, I.; Shkunov, M.; Sparrowe, D.; Tierney, S.; Wagner, R.; Zhang, W. M.; Chabinyc, M. L.; Kline, R. J.; McGehee, M. D.; Toney, M. F., Liquid-crystalline semiconducting polymers with high charge-carrier mobility. *Nature Materials* **2006**, 5, (4), 328-333.
76. Sirringhaus, H.; Brown, P. J.; Friend, R. H.; Nielsen, M. M.; Bechgaard, K.; Langeveld-Voss, B. M. W.; Spiering, A. J. H.; Janssen, R. A. J.; Meijer, E. W.; Herwig, P.; de Leeuw, D. M., Two-dimensional charge transport in self-organized, high-mobility conjugated polymers. *Nature* **1999**, 401, (6754), 685-688.
77. Lo, S. C.; Burn, P. L., Development of dendrimers: Macromolecules for use in organic light-emitting diodes and solar cells. *Chemical Reviews* **2007**, 107, (4), 1097-1116.
78. Barbarella, G.; Zambianchi, M.; Bongini, A.; Antolini, L., Crystal-Structure of 4,4',3'',4'''-Tetramethyl-2,2'/5',5'-5'',2'''-Tetrathiophene - a Comparison with the Conformation in Solution. *Advanced Materials* **1992**, 4, (4), 282-285.
79. Barbarella, G.; Zambianchi, M.; Antolini, L.; Ostojica, P.; Maccagnani, P.; Bongini, A.; Marseglia, E. A.; Tedesco, E.; Gigli, G.; Cingolani, R., Solid-state conformation, molecular packing, and electrical and optical properties of processable beta-methylated sexithiophenes. *Journal of the American Chemical Society* **1999**, 121, (38), 8920-8926.
80. Paulus, E. F.; Dammel, R.; Kämpf, G.; Wegener, P.; Siam, K.; Wolinski, K.; Schäfer, L., Structure of 3,3'-dimethoxy-2,2'-bithiophene and comparison with quantum-mechanical calculations. *Acta Crystallographica. Section B: Structural science* **1988**, 44, 509-512.

81. Pomerantz, M.; Amarasekara, A. S.; Dias, H. V. R., Synthesis and solid-state structures of dimethyl 2,2'-bithiophenedicarboxylates. *Journal of Organic Chemistry* **2002**, *67*, (20), 6931-6937.
82. Crouch, D. J.; Skabara, P. J.; Lohr, J. E.; McDouall, J. J. W.; Heeney, M.; McCulloch, I.; Sparrowe, D.; Shkunov, M.; Coles, S. J.; Horton, P. N.; Hursthouse, M. B., Thiophene and selenophene copolymers incorporating fluorinated phenylene units in the main chain: Synthesis, characterization, and application in organic field-effect transistors. *Chemistry of Materials* **2005**, *17*, (26), 6567-6578.
83. Zhu, Y.; Champion, R. D.; Jenekhe, S. A., Conjugated donor-acceptor copolymer semiconductors with large intramolecular charge transfer: Synthesis, optical properties, electrochemistry, and field effect carrier mobility of thienopyrazine-based copolymers. *Macromolecules* **2006**, *39*, (25), 8712-8719.
84. Yasuda, T.; Imase, T.; Nakamura, Y.; Yamamoto, T., New alternative donor-acceptor arranged poly(aryleneethynylene)s and their related compounds composed of five-membered electron-accepting 1,3,4-thiadiazole, 1,2,4-triazole, or 3,4-dinitrothiophene units: Synthesis, packing structure, and optical properties. *Macromolecules* **2005**, *38*, (11), 4687-4697.
85. Prosa, T. J.; Winokur, M. J.; McCullough, R. D., Evidence of a novel side chain structure in regioregular poly(3-alkylthiophenes). *Macromolecules* **1996**, *29*, (10), 3654-3656.
86. Prosa, T. J.; Winokur, M. J.; Moulton, J.; Smith, P.; Heeger, A. J., X-Ray Structural Studies of Poly(3-Alkylthiophenes) - an Example of an Inverse Comb. *Macromolecules* **1992**, *25*, (17), 4364-4372.
87. Tashiro, K.; Kobayashi, M.; Kawai, T.; Yoshino, K., Crystal structural change in poly(3-alkyl thiophene)s induced by iodine doping as studied by an organized combination of X-ray diffraction, infrared/Raman spectroscopy and computer simulation techniques. *Polymer* **1997**, *38*, (12), 2867-2879.
88. Brooke, G. M., The preparation and properties of polyfluoro aromatic and heteroaromatic compounds. *Journal of Fluorine Chemistry* **1997**, *86*, (1), 1-76.
89. Chambers, R. D.; Close, D.; Williams, D. L. H., Mechanisms for Reactions of Halogenated Compounds .3. Variation in Activating Influence of Halogen Substituents in Nucleophilic Aromatic-Substitution. *Journal of the Chemical Society-Perkin Transactions 2* **1980**, (5), 778-780.
90. Chambers, R. D.; Musgrave, W. K.; Waterhouse, J.; Williams, D. L.; Burdon, J.; Hollyhe, W.; Tatlow, J. C., Orientation and Reactivity in Nucleophilic Replacement in Polyfluoro-Benzenes and Polyfluoro-Pyridines. *Journal of the Chemical Society-Chemical Communications* **1974**, (6), 239-240.
91. Chambers, R. D.; Waterhouse, J. S.; Williams, D. L. H., Mechanisms for Reactions of Halogenated Compounds .1. Activating Effects of Fluorine in Polyfluoropyridines in Reactions with Ammonia. *Journal of the Chemical Society-Perkin Transactions 2* **1977**, (5), 585-588.
92. Chambers, R. D.; Seabury, M. J.; Williams, D. L. H.; Hughes, N., Mechanisms for Reactions of Halogenated Compounds .5. Orientating Effects of Fluorine Substituents on Nucleophilic-Substitution in Naphthalene and Other Polycyclic Systems. *Journal of the Chemical Society-Perkin Transactions 1* **1988**, (2), 251-254.

93. Brooke, G. M.; Burdon, J.; Stacey, M.; Tatlow, J. C., Aromatic Polyfluoro-Compounds .4. The Reaction of Aromatic Polyfluoro-Compounds with Nitrogen-Containing Bases. *Journal of the Chemical Society* **1960**, (Apr), 1768-1771.
94. Burdon, J.; Hollyhea, Wb; Tatlow, J. C., Aromatic Polyfluoro-Compounds .25. Nucleophilic Replacement Reactions of Pentafluoro-Toluene-Anisole and -Phenol. *Journal of the Chemical Society* **1965**, (Oct), 5152-&.
95. Chambers, R. D.; Martin, P. A.; Waterhouse, J. S.; Williams, D. L. H.; Anderson, B., Mechanisms for Reactions of Halogenated Compounds .4. Activating Influences of Ring-Nitrogen and Trifluoromethyl in Nucleophilic Aromatic-Substitution. *Journal of Fluorine Chemistry* **1982**, 20, (4), 507-514.
96. Zhang, Q. T.; Tour, J. M., Alternating donor/acceptor repeat units in polythiophenes. Intramolecular charge transfer for reducing band gaps in fully substituted conjugated polymers. *Journal of the American Chemical Society* **1998**, 120, (22), 5355-5362.
97. Dong, X. Y. M.; Tyson, J. C.; Collard, D. M., Controlling the macromolecular architecture of poly(3-alkylthiophene)s by alternating alkyl and fluoroalkyl substituents. *Macromolecules* **2000**, 33, (10), 3502-3504.
98. Takimiya, K.; Kunugi, Y.; Konda, Y.; Niihara, N.; Otsubo, T., 2,6-diphenylbenzo[1,2-b : 4,5-b 'd]dichalcogenophenes: a new class of high-performance semiconductors for organic field-effect transistors. *Journal of the American Chemical Society* **2004**, 126, (16), 5084-5085.
99. Loewe, R. S.; Ewbank, P. C.; Liu, J. S.; Zhai, L.; McCullough, R. D., Regioregular, head-to-tail coupled poly(3-alkylthiophenes) made easy by the GRIM method: Investigation of the reaction and the origin of regioselectivity. *Macromolecules* **2001**, 34, (13), 4324-4333.
100. Welsh, D. M.; Kloeppner, L. J.; Madrigal, L.; Pinto, M. R.; Thompson, B. C.; Schanze, K. S.; Abboud, K. A.; Powell, D.; Reynolds, J. R., Regiosymmetric dibutyl-substituted poly(3,4-propylenedioxythiophene)s as highly electron-rich electroactive and luminescent polymers. *Macromolecules* **2002**, 35, (17), 6517-6525.
101. Caras-Quintero, D.; Bauerle, P., Synthesis of the first enantiomerically pure and chiral, disubstituted 3,4-ethylenedioxythiophenes (EDOTs) and corresponding stereo- and regioregular PEDOTs. *Chemical Communications* **2004**, (8), 926-927.
102. Zhang, W.; Moore, J. S., Synthesis of poly(2,5-thienyleneethynylene)s by alkyne metathesis. *Macromolecules* **2004**, 37, (11), 3973-3975.
103. Babudri, F.; Farinola, G. M.; Naso, F., Synthesis of conjugated oligomers and polymers: the organometallic way. *Journal of Materials Chemistry* **2004**, 14, (1), 11-34.
104. Killian, J. G.; Gofer, Y.; Sarker, H.; Poehler, T. O.; Searson, P. C., Electrochemical synthesis and characterization of a series of fluoro-substituted phenylene-2-thienyl polymers. *Chemistry of Materials* **1999**, 11, (4), 1075-1082.
105. Nielsen, K. T.; Bechgaard, K.; Krebs, F. C., Removal of palladium nanoparticles from polymer materials. *Macromolecules* **2005**, 38, (3), 658-659.
106. Krebs, F. C.; Nyberg, R. B.; Jorgensen, M., Influence of residual catalyst on the properties of conjugated polyphenylenevinylene materials: Palladium nanoparticles and poor electrical performance. *Chemistry of Materials* **2004**, 16, (7), 1313-1318.
107. Budd, P. M.; Ghanem, B. S.; Makhseed, S.; McKeown, N. B.; Msayib, K. J.; Tattershall, C. E., Polymers of intrinsic microporosity (PIMs): robust,

- solution-processable, organic nanoporous materials. *Chemical Communications* **2004**, (2), 230-231.
108. Kim, J. P.; Kang, J. W.; Kim, J. J.; Lee, J. S., Fluorinated poly(arylene ether sulfone)s for polymeric optical waveguide devices. *Polymer* **2003**, 44, (15), 4189-4195.
109. Ding, J. F.; Day, M., Novel highly fluorinated poly(arylene ether-1,3,4-oxadiazole)s, their preparation, and sensory properties to fluoride anion. *Macromolecules* **2006**, 39, (18), 6054-6062.
110. Deck, P. A.; Lane, M. J.; Montgomery, J. L.; Slobodnick, C.; Fronczek, F. R., Synthesis and structural trends in pentafluorophenyl-substituted ferrocenes, 1,4-tetrafluorophenylene-linked diferrocenes, and 1,1'-ferrocenylene-1,4-tetrafluorophenylene co-oligomers. *Organometallics* **2000**, 19, (6), 1013-1024.
111. Deck, P. A.; Maiorana, C. R., Step-growth polymers derived from indene and decafluorobiphenyl. A new polymerization mode for indene. *Macromolecules* **2001**, 34, (1), 9-13.
112. Nitschke, J. R.; Tilley, T. D., Efficient, high-yield route to long, functionalized p-phenylene oligomers containing perfluorinated segments, and their cyclodimerizations by zirconocene coupling. *Journal of the American Chemical Society* **2001**, 123, (42), 10183-10190.
113. Geramita, K.; McBee, J.; Shen, Y. L.; Radu, N.; Tilley, T. D., Synthesis and characterization of perfluoroaryl-substituted siloles and thiophenes: A series of electron-deficient blue light emitting materials. *Chemistry of Materials* **2006**, 18, (14), 3261-3269.
114. Krumm, B.; Vij, A.; Kirchmeier, R. L.; Shreeve, J. M., Studies on the reactivity of tetrafluoro- and pentafluorophenyl trimethylsilyl ether with pentafluorobenzenes. Chemistry and X-ray structural investigations of polyfluorodiphenyl ethers. *Inorganic Chemistry* **1997**, 36, (3), 366-381.
115. Patel, N. R.; Chen, J. G.; Zhang, Y. F.; Kirchmeier, R. L.; Shreeve, J. M., Synthesis and Chemistry of Acyclic Monosiloxanes and Disiloxanes - Useful Precursors to Per- and Polyfluoroethers. *Inorganic Chemistry* **1994**, 33, (24), 5463-5470.
116. Chen, J. G.; Kirchmeier, R. L.; Shreeve, J. M., Synthesis and properties of fluorinated ethers with fluorobenzene rings. *Inorganic Chemistry* **1996**, 35, (6), 1718-&.
117. Prakash, G. K. S.; Yudin, A. K., Perfluoroalkylation with organosilicon reagents. *Chemical Reviews* **1997**, 97, (3), 757-786.
118. Omotowa, B. A.; Shreeve, J. M., Difluoroorganometalate-assisted generation of perfluorocarbanions from trimethylsilyl synthons and their interactions with perfluoroaryl compounds. *Organometallics* **2000**, 19, (14), 2664-2670.
119. Zeidan, T. A.; Kovalenko, S. V.; Manoharan, M.; Clark, R. J.; Ghiviriga, I.; Alabugin, I. V., Triplet acetylenes as synthetic equivalents of 1,2-bicarbenes: Phantom n,π^* state controls reactivity in triplet photocycloaddition. *Journal of the American Chemical Society* **2005**, 127, (12), 4270-4285.
120. Wilson, J. N.; Waybright, S. M.; McAlpine, K.; Bunz, U. H. F., Acetylene gas: A reagent in the synthesis of high molecular weight poly(p-phenyleneethynylene)s utilizing very low catalyst loadings. *Macromolecules* **2002**, 35, (10), 3799-3800.

121. Kihara, N.; Komatsu, S.; Takata, T.; Endo, T., Significance of stoichiometric imbalance in step polymerization via reactive intermediate. *Macromolecules* **1999**, *32*, (15), 4776-4783.
122. Albertin, L.; Bertarelli, C.; Gallazzi, M. C.; Meille, S. V.; Capelli, S. C., Synthesis and characterisation of 1,2-difluoro-1,2-bis(5-trimethylsilyl-2-thienyl) ethenes. A new family of conjugated monomers for oxidative polymerisation. *Journal of the Chemical Society-Perkin Transactions 2* **2002**, (10), 1752-1759.
123. Hiyama, T., How I came across the silicon-based cross-coupling reaction. *Journal of Organometallic Chemistry* **2002**, *653*, (1-2), 58-61.
124. Denmark, S. E.; Ober, M. H., Organosilicon reagents: Synthesis and application to palladium-catalyzed cross-coupling reactions. *Aldrichimica Acta* **2003**, *36*, (3), 75-85.
125. Groenendaal, B. L.; Jonas, F.; Freitag, D.; Pielartzik, H.; Reynolds, J. R., Poly(3,4-ethylenedioxythiophene) and its derivatives: Past, present, and future. *Advanced Materials* **2000**, *12*, (7), 481-494.
126. Sotzing, G. A.; Reynolds, J. R.; Steel, P. J., Poly(3,4-ethylenedioxythiophene) (PEDOT) prepared via electrochemical polymerization of EDOT, 2,2'-bis(3,4-ethylenedioxythiophene) (BiEDOT), and their TMS derivatives. *Advanced Materials* **1997**, *9*, (10), 795-&.
127. Pron, A.; Louarn, G.; Lapkowski, M.; Zagorska, M.; Glowczykzubek, J.; Lefrant, S., In-Situ Raman Spectroelectrochemical Studies of Poly(3,3'-Dibutoxy-2,2'-Bithiophene). *Macromolecules* **1995**, *28*, (13), 4644-4649.
128. Wakamiya, A.; Yamazaki, D.; Nishinaga, T.; Kitagawa, T.; Komatsu, K., Synthesis and properties of novel oligothiophenes surrounded by bicyclo[2.2.2]octene frameworks. *Journal of Organic Chemistry* **2003**, *68*, (22), 8305-8314.
129. Kobashi, M.; Takeuchi, H., Inhomogeneity of spin-coated and cast non-regioregular poly(3-hexylthiophene) films. Structures and electrical and photophysical properties. *Macromolecules* **1998**, *31*, (21), 7273-7278.
130. Shiraishi, K.; Yamamoto, T., New pi-conjugated polymers constituted of dialkoxybenzodithiophene units: synthesis and electronic properties. *Synthetic Metals* **2002**, *130*, (2), 139-147.
131. Katz, H. E.; Bao, Z. N.; Gilat, S. L., Synthetic chemistry for ultrapure, processable, and high-mobility organic transistor semiconductors. *Accounts of Chemical Research* **2001**, *34*, (5), 359-369.
132. Laquindanum, J. G.; Katz, H. E.; Lovinger, A. J.; Dodabalapur, A., Benzodithiophene rings as semiconductor building blocks. *Advanced Materials* **1997**, *9*, (1), 36-&.
133. Buschel, M.; Helldobler, M.; Daub, J., Electronic coupling in 6,6"-donor-substituted terpyridines: tuning of the mixed valence state by proton and metal ion complexation. *Chemical Communications* **2002**, (13), 1338-1339.
134. Hoeben, F. J. M.; Jonkheijm, P.; Meijer, E. W.; Schenning, A., About supramolecular assemblies of pi-conjugated systems. *Chemical Reviews* **2005**, *105*, (4), 1491-1546.
135. O'Neill, M.; Kelly, S. M., Liquid crystals for charge transport, luminescence, and photonics. *Advanced Materials* **2003**, *15*, (14), 1135-1146.

136. Watson, M. D.; Fechtenkotter, A.; Mullen, K., Big is beautiful - "Aromaticity" revisited from the viewpoint of macromolecular and supramolecular benzene chemistry. *Chemical Reviews* **2001**, 101, (5), 1267-1300.
137. Lee, B. L.; Yamamoto, T., Syntheses of new alternating CT-Type copolymers of thiophene and pyrido[3,4-b]pyrazine units: Their optical and electrochemical properties in comparison with similar CT copolymers of thiophene with pyridine and quinoxaline. *Macromolecules* **1999**, 32, (5), 1375-1382.
138. Yamamoto, T.; Zhou, Z. H.; Kanbara, T.; Shimura, M.; Kizu, K.; Maruyama, T.; Nakamura, Y.; Fukuda, T.; Lee, B. L.; Ooba, N.; Tomaru, S.; Kurihara, T.; Kaino, T.; Kubota, K.; Sasaki, S., pi-conjugated donor-acceptor copolymers constituted of pi-excessive and pi-deficient arylene units. Optical and electrochemical properties in relation to CT structure of the polymer. *Journal of the American Chemical Society* **1996**, 118, (43), 10389-10399.
139. Ballardini, R.; Balzani, V.; Credi, A.; Brown, C. L.; Gillard, R. E.; Montalti, M.; Philp, D.; Stoddart, J. F.; Venturi, M.; White, A. J. P.; Williams, B. J.; Williams, D. J., Controlling catenations, properties and relative ring-component movements in catenanes with aromatic fluorine substituents. *Journal of the American Chemical Society* **1997**, 119, (51), 12503-12513.
140. Ponzini, F.; Zaghera, R.; Hardcastle, K.; Siegel, J. S., Phenyl/pentafluorophenyl interactions and the generation of ordered mixed crystals: sym-triphenethynylbenzene and sym-tris(perfluorophenethynyl)benzene. *Angewandte Chemie-International Edition* **2000**, 39, (13), 2323-2325.
141. Dai, C. Y.; Nguyen, P.; Marder, T. B.; Scott, A. J.; Clegg, W.; Viney, C., Control of single crystal structure and liquid crystal phase behaviour via arene-perfluoroarene interactions. *Chemical Communications* **1999**, (24), 2493-2494.
142. Bunz, U. H. F.; Enkelmann, V., Structure elucidation, packing, and solid-state behavior of the Eglinton-Galbraith dimer. *Chemistry-a European Journal* **1999**, 5, (1), 263-266.
143. McCulloch, L.; Bailey, C.; Giles, M.; Heeney, M.; Love, I.; Shkunov, M.; Sparrowe, D.; Tierney, S., Influence of molecular design on the field-effect transistor characteristics of terthiophene polymers. *Chemistry of Materials* **2005**, 17, (6), 1381-1385.
144. Jayakannan, M.; Van Hal, P. A.; Janssen, R. A. J., Synthesis and structure-property relationship of new donor-acceptor-type conjugated monomers and polymers on the basis of thiophene and benzothiadiazole. *Journal of Polymer Science Part a-Polymer Chemistry* **2002**, 40, (2), 251-261.
145. Crouch, D. J.; Skabara, P. J.; Heeney, M.; McCulloch, I.; Coles, S. J.; Hursthouse, M. B., Hexyl-substituted oligothiophenes with a central tetrafluorophenylene unit: crystal engineering of planar structures for p-type organic semiconductors. *Chemical Communications* **2005**, (11), 1465-1467.
146. Demanze, F.; Yassar, A.; Garnier, F., Alternating donor-acceptor substitutions in conjugated polythiophenes. *Macromolecules* **1996**, 29, (12), 4267-4273.
147. Thomas, C. A.; Zong, K. W.; Abboud, K. A.; Steel, P. J.; Reynolds, J. R., Donor-mediated band gap reduction in a homologous series of conjugated polymers. *Journal of the American Chemical Society* **2004**, 126, (50), 16440-16450.

148. Zhang, Q. T.; Tour, J. M., Low optical bandgap polythiophenes by an alternating donor/acceptor repeat unit strategy. *Journal of the American Chemical Society* **1997**, 119, (21), 5065-5066.
149. Daoust, G.; Leclerc, M., Structure Property Relationships in Alkoxy-Substituted Polythiophenes. *Macromolecules* **1991**, 24, (2), 455-459.
150. Zotti, G.; Gallazzi, M. C.; Zerbi, G.; Meille, S. V., Conducting Polymers from Anodic Coupling of Some Regiochemically Defined Dialkoxy-Substituted Thiophene Oligomers. *Synthetic Metals* **1995**, 73, (3), 217-225.
151. Meille, S. V.; Farina, A.; Bezziccheri, F.; Gallazzi, M. C., The Influence of Alkoxy Side-Chains on the Conformational Flexibility of Oligothiophenes and Polythiophenes. *Advanced Materials* **1994**, 6, (11), 848-851.
152. Pelletier, M.; Brisse, F.; Cloutier, R.; Leclerc, M., 3,3'-Bis(Octyloxy)-2,2'-Bithiophene at 195 K. *Acta Crystallographica Section C-Crystal Structure Communications* **1995**, 51, 1394-1397.
153. Gallazzi, M. C.; Toscano, F.; Paganuzzi, D.; Bertarelli, C.; Farina, A.; Zotti, G., Polythiophenes with unusual electrical and optical properties based on donor acceptor alternance strategy. *Macromolecular Chemistry and Physics* **2001**, 202, (10), 2074-2085.
154. Marsella, M. J.; Carroll, P. J.; Swager, T. M., Design of Chemoresistive Sensory Materials - Polythiophene-Based Pseudopolyrotaxanes. *Journal of the American Chemical Society* **1995**, 117, (39), 9832-9841.
155. Pomerantz, M., Planar 2,2'-bithiophenes with 3,3'- and 3,3',4,4'-substituents. A computational study. *Tetrahedron Letters* **2003**, 44, (8), 1563-1565.
156. Woody, K. B.; Bullock, J. E.; Parkin, S. R.; Watson, M. D., Alternating arene-perfluoroarene poly(phenylene ethynyls). *Macromolecules* **2007**, 40, (13), 4470-4473.
157. Siringhaus, H.; Friend, R. H.; Wang, C.; Leuninger, J.; Muellen, K., Dibenzothienobisbenzothiophene-a novel fused-ring oligomer with high field-effect mobility. *Journal of Materials Chemistry* **1999**, 9, 2095-2101.
158. Wex, B.; Kaafarani, B. R.; Kirschbaum, K.; Neckers, D. C., Synthesis of the anti and syn isomers of thieno[ff']bis[1]benzothiophene. Comparison of the optical and electrochemical properties of the anti and syn isomers. *Journal of Organic Chemistry* **2005**, 70, (11), 4502-4505.
159. Wex, B.; Kaafarani, B. R.; Neckers, D. C., Efficient isomer-pure synthesis of a benzo[b]thiophene analogue of pentacene. *Journal of Organic Chemistry* **2004**, 69, (6), 2197-2199.
160. Wex, B.; Kaafarani, B. R.; Schroeder, R.; Majewski, L. A.; Burckel, P.; Grell, M.; Neckers, D. C., New organic semiconductors and their device performance as a function of thiophene orientation. *Journal of Materials Chemistry* **2006**, 16, (12), 1121-1124.
161. Kuo, C. C.; Payne, M. M.; Anthony, J. E.; Jackson, T. N. In *TES anthradithiophene solution-processed OTFTs with 1cm²/Vs mobility*, Tech. Digest-International Electronic Devices Meeting 2004; 2004.
162. Lloyd, M. T.; Mayer, A. C.; Subramanian, S.; Mourey, D. A.; Herman, D. J.; Bapat, A. V.; Anthony, J. E.; Malliaras, G. G., Efficient solution-processed photovoltaic cells based on an anthradithiophene/fullerene blend. *Journal of the American Chemical Society* **2007**, 129, (29), 9144-9149.

163. Okamoto, T.; Kudoh, K.; Wakamiya, A.; Yamaguchi, S., General synthesis of thiophene and selenophene-based heteroacenes. *Organic Letters* **2005**, *7*, (23), 5301-5304.
164. Yamada, K.; Okamoto, T.; Kudoh, K.; Wakamiya, A.; Yamaguchi, S.; Takeya, J., Single-crystal field-effect transistors of benzoannulated fused oligothiophenes and oligoselenophenes. *Applied Physics Letters* **2007**, *90*, (7), -.
165. Ebata, H.; Miyazaki, E.; Yamamoto, T.; Takimiya, K., Synthesis, properties, and structures of benzo[1,2-b : 4,5-b']bis[b]benzothiophene and benzo[1,2-b : 4,5-b']bis[b]benzoselenophene. *Organic Letters* **2007**, *9*, (22), 4499-4502.
166. Irvin, J. A.; Schwendeman, I.; Lee, Y.; Abboud, K. A.; Reynolds, J. R., Low-oxidation-potential conducting polymers derived from 3,4-ethylenedioxythiophene and dialkoxybenzenes. *Journal of Polymer Science Part a-Polymer Chemistry* **2001**, *39*, (13), 2164-2178.
167. Sotzing, G. A.; Reynolds, J. R.; Steel, P. J., Electrochromic conducting polymers via electrochemical polymerization of bis(2-(3,4-ethylenedioxy)thienyl) monomers. *Chemistry of Materials* **1996**, *8*, (4), 882-889.
168. Yamashita, Y.; Ono, K.; Tomura, M.; Tanaka, S., Synthesis and properties of benzobis(thiadiazole)s with nonclassical pi-electron ring systems. *Tetrahedron* **1997**, *53*, (29), 10169-10178.
169. Cho, D. M.; Parkin, S. R.; Watson, M. D., Partial fluorination overcomes herringbone crystal packing in small polycyclic aromatics. *Organic Letters* **2005**, *7*, (6), 1067-1068.
170. Bruno, G.; Randaccio, L., A Refinement of the Benzoic-Acid Structure at Room-Temperature. *Acta Crystallographica Section B-Structural Science* **1980**, *36*, (Jul), 1711-1712.
171. Cozzolino, A. F.; Vargas-Baca, I.; Mansour, S.; Mahmoudkhani, A. H., The nature of the supramolecular association of 1,2,5-chalcogenadiazoles. *Journal of the American Chemical Society* **2005**, *127*, (9), 3184-3190.
172. Jones, J. B.; Brown, D. S.; Massey, A. G., The Crystal and Molecular-Structure of Octafluorodibenzothiophene. *Phosphorus Sulfur and Silicon and the Related Elements* **1988**, *35*, (1-2), 67-70.
173. Kongprakaiwoot, N.; Luck, R. L.; Urnezis, E., New synthetic route to polyphosphine ligands bearing 1,2,4,5-tetrakis(phosphino)benzene framework: structural characterizations of 1,4-(PPh₂)₂-2,5-(PR₂)₂-C₆F₂ (R = Ph, Pr-i, Et). *Journal of Organometallic Chemistry* **2004**, *689*, (21), 3350-3356.
174. Bridges, A. J.; Lee, A.; Maduakor, E. C.; Schwartz, C. E., Fluorine as an Orthodirecting Group in Aromatic Metalation - Generality of the Reaction and the High Position of Fluorine in the Dir-Met Potency Scale. *Tetrahedron Letters* **1992**, *33*, (49), 7495-7498.
175. Reddy, T. J.; Iwama, T.; Halpern, H. J.; Rawal, V. H., General synthesis of persistent trityl radicals for EPR imaging of biological systems. *Journal of Organic Chemistry* **2002**, *67*, (14), 4635-4639.
176. Arai, I.; Yamaguchi, T.; Hida, Y. process for preparation of aromatic sulfur compounds. US 6376716 B1, 2002.

177. Chambers, R. D.; Spring, D. J., Polyfluoroaryl Organometallic Compounds .12. Nucleophilic Substitution in Octafluorodibenzothiophen, and Related Compounds. *Tetrahedron* **1971**, 27, (3), 669-&.
178. Mayor, M.; Buschel, M.; Fromm, K. M.; Lehn, J. M.; Daub, J., Electron transfer through bridging molecular structures. In *Molecular Electronics II*, 2002; Vol. 960, pp 16-28.
179. Tucker, J. H. R.; Gingras, M.; Brand, H.; Lehn, J. M., Redox properties of polythiaarene derivatives. A novel class of electron acceptors. *Journal of the Chemical Society-Perkin Transactions 2* **1997**, (7), 1303-1307.
180. Takimiya, K.; Kunugi, Y.; Konda, Y.; Ebata, H.; Toyoshima, Y.; Otsubo, T., 2,7-diphenyl[1]benzoselenopheno[3,2-b][1]benzoselenophene as a stable organic semiconductor for a high-performance field-effect transistor. *Journal of the American Chemical Society* **2006**, 128, (9), 3044-3050.
181. Yoon, M. H.; Facchetti, A.; Stern, C. E.; Marks, T. J., Fluorocarbon-modified organic semiconductors: Molecular architecture, electronic, and crystal structure tuning of arene-versus fluoroarene-thiophene oligomer thin-film properties. *Journal of the American Chemical Society* **2006**, 128, (17), 5792-5801.
182. Payne, M. M.; Parkin, S. R.; Anthony, J. E.; Kuo, C. C.; Jackson, T. N., Organic field-effect transistors from solution-deposited functionalized acenes with mobilities as high as 1 cm²/V-s. *Journal of the American Chemical Society* **2005**, 127, (14), 4986-4987.
183. Laudise, R. A.; Kloc, C.; Simpkins, P. G.; Siegrist, T., Physical vapor growth of organic semiconductors. *Journal of Crystal Growth* **1998**, 187, (3-4), 449-454.
184. Anthony, J. E.; Gierschner, J.; Landis, C. A.; Parkin, S. R.; Sherman, J. B.; Bakus, R. C., A new functionalization strategy for pentacene. *Chemical Communications* **2007**, (45), 4746-4748.
185. Medina, B. M.; Beljonne, D.; Egelhaaf, H. J.; Gierschner, J., Effect of fluorination on the electronic structure and optical excitations of pi-conjugated molecules. *Journal of Chemical Physics* **2007**, 126, (11), -.
186. Frisch, M. J.; Trucks, G. W.; Schlegel, H. B.; Scuseria, G. E.; Robb, M. A.; Cheeseman, J. R.; Montgomery, J. A.; Vreven, J. T.; Kudin, K. N.; Burant, J. C.; Millam, J. M.; Iyengar, S. S.; Tomasi, J.; Barone, V.; Mennucci, B.; Cossi, M.; Scalmani, G.; Rega, N.; Petersson, G. A.; Nakatsuji, H.; Hada, M.; Ehara, M.; Toyota, K.; Fukuda, R.; Hasegawa, J.; Ishida, M.; Nakajima, T.; Honda, Y.; Kitao, O.; Nakai, H.; Klene, M.; Li, X.; Knox, J. E.; Hratchian, H. P.; Cross, J. B.; Bakken, V.; Adamo, C.; Jaramillo, J.; Gomperts, R.; Stratmann, R. E.; Yazyev, O.; Austin, A. J.; Cammi, R.; Pomelli, C.; Ochterski, J.; Ayala, P. Y.; Morokuma, K.; Voth, G. A.; Salvador, P.; Dannenberg, J. J.; Zakrzewski, V. G.; Dapprich, S.; Daniels, A. D.; Strain, M. C.; Farkas, O.; Malick, D. K.; Rabuck, A. D.; Raghavachari, K.; Foresman, J. B.; Ortiz, J. V.; Cui, Q.; Baboul, A. G.; Clifford, S.; Cioslowski, J.; Stefanov, B. B.; Liu, G.; Liashenko, A.; Piskorz, P.; Komaromi, I.; Martin, R. L.; Fox, D. J.; Keith, T.; Al-Laham, M. A.; Peng, C. Y.; Nanayakkara, A.; Challacombe, M.; Gill, P. M. W.; Johnson, B. G.; Chen, W.; Wong, M. W.; Gonzalez, C.; Pople, J. A. *GAUSSIAN 03*, (Revision C.02); Gaussian, Inc.: Wallingford, CT, 2004.
187. Takimiya, K.; Ebata, H.; Sakamoto, K.; Izawa, T.; Otsubo, T.; Kunugi, Y., 2,7-Diphenyl[1]benzothieno[3,2-b]benzothiophene, a new organic semiconductor for

- air-stable organic field-effect transistors with mobilities up to $2.0 \text{ cm}^2 \text{ V}^{-1} \text{ s}^{-1}$. *Journal of the American Chemical Society* **2006**, 128, (39), 12604-12605.
188. Yamamoto, T.; Takimiya, K., Facile synthesis of highly pi-extended heteroarenes, dinaphtho[2,3-b : 2',3'-f]chalcogenopheno[3,2-b]chalcogenophenes, and their application to field-effect transistors. *Journal of the American Chemical Society* **2007**, 129, (8), 2224-+.
189. Ebata, H.; Izawa, T.; Miyazaki, E.; Takimiya, K.; Ikeda, M.; Kuwabara, H.; Yui, T., Highly soluble [1]benzothieno[3,2-b]benzothiophene (BTBT) derivatives for high-performance, solution-processed organic field-effect transistors. *Journal of the American Chemical Society* **2007**, 129, (51), 15732-+.
190. Hunziker, C.; Zhan, X.; Losio, P. A.; Figi, H.; Kwon, O. P.; Barlow, S.; Guenter, P.; Marder, S. R., Highly ordered thin films of a bis(dithienothiophene) derivative. *Journal of Materials Chemistry* **2007**, 17, (47), 4972-4979.
191. Ando, S.; Nishida, J. I.; Tada, H.; Inoue, Y.; Tokito, S.; Yamashita, Y., High performance n-type organic field-effect transistors based on pi-electronic systems with trifluoromethylphenyl groups. *Journal of the American Chemical Society* **2005**, 127, (15), 5336-5337.
192. Takimiya, K.; Konda, Y.; Ebata, H.; Niihara, N.; Otsubo, T., Facile synthesis, structure, and properties of benzo[1,2-b : 4,5-b']dichalcogenophenes. *Journal of Organic Chemistry* **2005**, 70, (25), 10569-10571.
193. Beimling, P.; Kobmehl, G., Synthesis of Benzo[1,2-b:4,5-b']dithiophene and its 4,8-Dimethoxy and 4,8-Dimethyl Derivatives. *Chem. Ber.* **1986**, 119, 3198-3203.
194. Slocum, D. W.; Gierer, P. L., Directed Metalation Reactions .8. Directed Metalation of 3-Mono-Disubstituted and 2,5-Disubstituted Thiophenes. *Journal of Organic Chemistry* **1976**, 41, (23), 3668-3673.
195. Sheraw, C. D.; Jackson, T. N.; Eaton, D. L.; Anthony, J. E., Functionalized pentacene active layer organic thin-film transistors. *Advanced Materials* **2003**, 15, (23), 2009-2011.
196. Meng, H.; Zheng, J.; Lovinger, A. J.; Wang, B. C.; Van Patten, P. G.; Bao, Z. N., Oligofluorene-thiophene derivatives as high-performance semiconductors for organic thin film transistors. *Chemistry of Materials* **2003**, 15, (9), 1778-1787.
197. Maliakal, A.; Raghavachari, K.; Katz, H.; Chandross, E.; Siegrist, T., Photochemical stability of pentacene and a substituted pentacene in solution and in thin films. *Chemistry of Materials* **2004**, 16, (24), 4980-4986.
198. Ma, C. Q.; Mena-Osteritz, E.; Debaerdemaeker, T.; Wienk, M. M.; Janssen, R. A. J.; Bauerle, P., Functionalized 3D oligothiophene dendrons and dendrimers - Novel macromolecules for organic electronics. *Angewandte Chemie-International Edition* **2007**, 46, (10), 1679-1683.
199. Kehat, T.; Goren, K.; Portnoy, M., Dendrons on insoluble supports: synthesis and applications. *New Journal of Chemistry* **2007**, 31, (7), 1218-1242.
200. Wudl, F.; Kobayashi, M.; Heeger, A. J., Poly(Isothianaphthene). *Journal of Organic Chemistry* **1984**, 49, (18), 3382-3384.
201. Pomerantz, M.; Gu, X. M.; Zhang, S. X., Poly(2-decylthieno[3,4-b]thiophene-4,6-diyl). A new low band gap conducting polymer. *Macromolecules* **2001**, 34, (6), 1817-1822.

202. Lee, B.; Yavuz, M. S.; Sotzing, G. A., Poly(thieno[3,4-b]thiophene)s from three symmetrical thieno[3,4-b]thiophene dimers. *Macromolecules* **2006**, 39, (9), 3118-3124.
203. Sotzing, G. A.; Lee, K. H., Poly(thieno[3,4-b]thiophene): A p- and n-dopable polythiophene exhibiting high optical transparency in the semiconducting state. *Macromolecules* **2002**, 35, (19), 7281-7286.
204. Agarwal, N.; Mishra, S. P.; Kumar, A.; Hung, C. H.; Ravikanth, M., *Chemical Communications* **2002**, (22), 2642-2643.
205. Furniss, B.; Hannaford, A.; Smith, P.; Tatchell, A., *Vogel's textbook of practical organic chemistry*. Fifth ed.; 1989; p 887.
206. Yu, W. L.; Meng, H.; Pei, J.; Huang, W.; Li, Y. F.; Heeger, A. J., Synthesis and characterization of a new p-n diblock light-emitting copolymer. *Macromolecules* **1998**, 31, (15), 4838-4844.
207. Khor, E.; Siu, C. N.; Hwee, C. L.; Chai, S., Selective Functionalization of 2,2'-Bithiophenes. *Heterocycles* **1991**, 32, (9), 1805-1812.

Vita

PERSONAL INFORMATION

Name	Yongfeng Wang
Date of birth	02/18/1978
Place of birth	Rongcheng, Shandong
Nationality	China

EDUCATION

Ph.D. candidate, Organic Chemistry, University of Kentucky, 2003-present
M.S., Polymer physics and chemistry, Nanjing University, 2000-2003
B.S., Polymer science and engineering, Nanjing University of Science and Technology, 1996-2000

TEACHING AND SERVICE

2007	Chemistry and physics demonstration at the Second Annual STLP State Championship (Kentucky)
2007	Voluntary judge for the Regional Undergraduate Poster Symposium (University of Kentucky).
2007	Chemistry and physics demonstrations for K-8 students at local children's museum.
2004-05	Teaching Assistant: Organic Chemistry Lab, Dept of Chemistry, Univ. of Kentucky, USA. (2 semesters)
2002	Grader for Jiangsu Province National Matriculation Test (chemistry), CHINA.
2001	Teaching Assistant, Organic Chemistry Lab, Dept of Chemistry, Nanjing University, CHINA.

HONORS AND AWARDS

Kentucky Opportunity Fellowship, University of Kentucky, 2007

Student Travel Award, University of Kentucky, 2007
Excellent Bachelor Thesis, Nanjing University of Science and Technology, 2003
Excellent Graduate, Nanjing University of Science and Technology, 2003
University Scholarship, Nanjing University of Science and Technology, 1997, 1999
Outstanding Student, Nanjing University of Science and Technology, 1997, 1998,
1999
Freshman Scholarship, Nanjing University of Science and Technology, 1996

PUBLICATIONS

1. Wang, Y.; Watson, M. D. Tuning the properties of alternating copolymers from perfluorobenzene and thiophene derivatives. *Polymer Preprints*, **2007**, *48*, 127.
2. Wang, Y.; Watson, M. D. Synthesis and characterization of alternating thiophene-perfluoroarene copolymers and fully/partially fluorinated small-molecule polycyclics. *PMSE Preprints*, **2007**, *96*, 182.
3. Wang, Y.; Watson, M. D. Transition-Metal-Free Synthesis of Alternating Thiophene-Perfluoroarene copolymers. *J. Am. Chem. Soc.* **2006**, *128*, 8, 2536-37.
4. Zhu, Z.; Wang, Y.; Lu, Y. Time-Dependent Density Functional Theory study on polyazopyrrole and polyazothiophene. *Macromolecules*, **2003**, *36*(25), 9585-9593.
5. Wang, Y.; Parkin, S. R.; Watson, M. D. Highly fluorinated Benzobisbenzothiophenes. *Submitted*.
6. Wang, Y.; Watson, M. D. Controlling intrachain torsion in copolymers of head-to-head 3,3'-dialkyl bithiophene copolymers. *in preparation*.
7. Wang, Y.; Parkin, S. R.; Watson, M. D. Synthesis and engineering of self-assembly and optical property of fluorinated benzodithiophene (BDT) derivatives. *in preparation*.

PRESENTATIONS

1. Wang, Y.; Watson, M. D. Tuning the properties of alternating copolymers from perfluorobenzene and thiophene Derivatives. *234th National Meeting of the American Chemical Society*, Boston, MA, August 2007. (Poster)

2. Wang, Y.; Watson, M. D. Preparation and supramolecular engineering of alternating thiophene-perfluoroarene copolymers and fully/partially fluorinated heteroacenes. *2007 National Graduate Polymer Research Conference*, Knoxville, TN. June 2007. (Oral)
3. Wang, Y.; Watson, M. D. Engineering of molecular packing of thiophene-perfluoroarene copolymers and fluorinated heteroacenes. *39th Central Regional Meeting of the American Chemical Society*, Covington, KY, May 2007. (Poster)
4. Wang, Y.; Cho, D. M.; Guo, X.; Watson, M. D. Materials chemistry: molecular design, synthesis and structure-properties studies. *2007 Naff symposium on chemistry and molecular biology*, University of Kentucky, KY, April 2007. (Poster)
5. Wang, Y.; Watson, M. D. Synthesis and characterization of alternating thiophene-perfluoroarene copolymers and fully/partially fluorinated small-molecule polycyclics. *233rd National Meeting of the American Chemical Society*, Chicago, IL, March 2007. (Oral)
6. Wang, Y. Synthesis and structure-property studies of organic materials containing fluorinated and non-fluorinated pi-systems. Eastern Kentucky University, KY, September 2006. (Oral) *Invited*.

Yongfeng Wang
03/21/2008